



Investigating routes toward
metallointercalator-tethered gold
nanoparticles

By

Samuel Joseph Ashworth

A thesis submitted for the degree of Doctor of Philosophy

September 2018

Department of Chemistry

“Results! Why, man, I have gotten a lot of results! I have found several
thousand things that won’t work”

Thomas Edison

Abstract

Gold nanoparticles surface coated with Ru (II) polypyridyl complexes have recently attracted interest as novel probes for cellular imaging. To date, most research has focussed on relatively simple complexes; this project aimed to extend the scope of these system by incorporating more complicated structures, based on an achiral DNA “light-switch” complex, $[\text{Ru}(\text{tpm})(\text{dppz})(\text{Cl})]^{2+}$. Initial synthetic routes explored functionalisation of this complex with extended pyridine ligands bearing a pendant thiol group, however, for a variety of reasons, these were unsuccessful. Later synthetic routes involved co-ordination of simpler pyridines, and synthesis of reactive linkers that could be pre-attached to the nanoparticles. A proposed system based on an amide linkage is presented. The free complex was studied was shown to bind to DNA by intercalation, and displayed the expected “light-switch” effect on binding to DNA.

Additionally, several new intercalating complexes were investigated. A series of complexes bearing the shorter pzp ligand and various functionalised pyridines were synthesised. They were found to behave in a similar fashion to their dppz analogues, mostly binding to DNA through intercalation, albeit with reduced affinity due to the shorter aromatic ligand. As in the dppz system, the complex bearing 4-aminopyridine groove bound at higher temperatures, and displayed temperature dependent binding. Routes towards two other intercalating complexes, bearing ligands that are longer or wider than dppz, were also developed.

Declaration

Except where specific references have been made to other sources, the work in this thesis is the original work of the author. It has not been submitted, in whole or in part, for any other degree. Certain results have already been published in peer review journals.

Samuel Joseph Ashworth

Sept 2018

Acknowledgements

It's always difficult to start writing stuff like those, so I'll just dive right in. First and foremost, I'd like to thank my supervisor, Prof. Jim Thomas, for his support, boundless enthusiasm, and constant ability to help come up with Plan Z, even when A-Y have come up short. I'd also like to thank my secondary supervisor, Dr Fred Claeysens for his ideas through the start of the project.

I'd also like to thank all the people around the department who've helped me throughout the four years: Prof. Anthony Meijer for the computational work; Dr Craig Robertson for crystallography; Dr Sandra van Meurs for help with NMR; Simon and Sharon down in mass spec; Nick, Pete and Phil in stores; and Denise and Louise in accounts. Also, thanks to Prof. Beining Chen and Dr Jenn Dick for giving me the opportunity to spend a few months working at Biofordrug in Bari, and thanks to everyone over in Bari for their help in exploring the many coffee shops and restaurants.

To all the members of the Thomas group, past and present, it's been great. Thanks for all the help, guidance, ideas and discussions, I couldn't have done it without you. Cheers to Mike, Stu, Simon, Hiwa, Kirsty, Rachel, Fliss, Charlotte, Sasha, Caroline, Sree, Paul, Hawazin and Shahryar (I don't think I've missed anyone!). Special mention to Tom for joining me on our exciting adventure through all the ways we tried (and failed) to stick ruthenium to nanoparticles/surfaces.

In the wider department, there are loads more people who've helped to made the past four years all the fun it's been. To the "Quiz and Games Night Super Fun Club", in

particular, Charlie, Matt, Jenna, Rheanna, Rosie, Shannon, Joe, Alec, Chris, Ester; past and present members of “Exeter Gently” (most of whom have already been mentioned); all the regular attendees of Friday Interval (too many to mention) – thanks to all.

Outside of chemistry, massive thanks to the Weak Clique, I quite literally could not have done it without you guys. Speedy, Ben, Calum, Carla, Dave, Dawn, Ed, Fran, Harry, Jamie, Matt, other Matt, Micki, Olga, Pete, Ruairidh, Sarah, Shaun, Tim, Tom, other Tom, Ellie, Felicity and Milena (listed in that order because that’s the order you were on the group chat!), thanks for all the climbing, drinking, parties, and fun over the past 1-8 years. Here’s to loads more trips in the future!

Last, and very much not least, thank you to my family, for their love and support, not only during the past few years, but throughout my entire life.

Sam

P.S. Anyone who feels they’ve been unjustly missed off any of the lists here, it probably wasn’t deliberate.

P.P.S. I would also be remiss if I did not credit Dr Dennis Upper for his help in confronting a blank sheet of paper. (D. Upper, *J. Appli. Behav. Anal.*, 1974, **7**, 497).

Table of Contents

Abstract.....	ii
Declaration.....	iii
Acknowledgements.....	iv
Table of Contents	vi
List of Abbreviations.....	xv
1 Introduction.....	2
1.1 What is DNA?	2
1.2 The Structure of DNA.....	3
1.3 DNA binding	4
1.3.1 Irreversible Binding	5
1.3.2 Electrostatic Binding	7
1.3.3 Groove Binding	8
1.3.4 Intercalation.....	9
1.4 Transition Metal Complexes	10
1.4.1 Metallo-intercalation.....	10
1.4.2 Structural derivatives of the prototype “light-switch” complex.....	17

1.5	Gold Nanoparticles	23
1.5.1	Overview	23
1.5.2	Therapeutic applications	24
1.5.3	Sensing applications	26
1.5.4	Imaging applications.....	30
1.5.5	Ru-AuNP adducts.....	31
1.6	Aim	33
1.7	References	36
2	Attempted routes towards tether moieties	2
2.1	Introduction	2
2.2	Parent Complex	2
2.2.1	Design	2
2.2.2	Synthesis of [Ru(tpm)(dppz)Cl] ⁺	8
2.3	Design of linking ligand.....	11
2.4	“All-in-one” method	14
2.4.1	Gunnlaugsson Route.....	14
2.4.2	Acid Chloride Route	15
2.4.3	Copper-catalysed Azide-Alkyne Click Reaction	17
2.4.4	Suzuki-Miyaura Route.....	18
2.4.5	Oligoethylene glycol route.....	20

2.5	“Two-halves” method.....	23
2.5.1	Amide route.....	24
2.5.2	Reductive amination route	27
2.5.3	Copper catalysed azide-alkyne click route.....	30
2.5.4	Second amide route	33
2.6	Characterisation.....	38
2.6.1	Crystallographic studies.....	38
2.6.2	UV-visible absorption.....	39
2.6.3	Luminescence.....	41
2.6.4	Relative viscosity.....	42
2.6.5	DNA binding affinity.....	43
2.7	Conclusions and Future Work.....	48
2.8	References.....	50
3	Tuning DNA binding affinity of metallointercalators through modulation of hydrogen bonding and steric interactions	55
3.1	Introduction.....	55
3.1.1	General.....	55
3.1.2	Previous Work.....	56
3.1.3	This work – aims	58
3.2	Pzp complexes	60

3.2.1	Synthesis	60
3.2.2	UV-vis.....	66
3.2.3	Luminescence.....	72
3.2.4	Computational Studies.....	73
3.2.5	Relative Viscosity.....	76
3.2.6	DNA binding titrations	79
3.3	Towards other Ru complexes	88
3.3.1	Synthesis – ligands	88
3.3.2	Synthesis of chloride complexes	89
3.4	Conclusions and future work.....	93
	References	95
4	Conclusions and Future Work	99
4.1	Conclusions	99
4.2	Future work.....	103
4.3	References.....	105
5	Experimental	107
5.1	Materials and Equipment	107
5.1.1	Chemicals.....	107
5.1.2	Nuclear Magnetic Resonance (NMR) Spectra.....	107
5.1.3	Mass spectrometry.....	107

5.1.4	Infrared spectroscopy (IR)	107
5.1.5	UV-visible spectroscopy	107
5.1.6	Luminescence spectroscopy	108
5.1.7	Anion metathesis	108
5.2	Extinction coefficients	108
5.3	X-ray crystallography	108
5.4	Computational Studies	109
5.5	DNA Binding Studies	110
5.5.1	Buffer preparation	110
5.5.2	DNA preparation	110
5.5.3	DNA binding titrations	111
5.5.4	Relative Viscometry	111
5.5.5	Continuous Variation Analysis	111
5.6	Synthesis	112
5.6.1	Tris(1-pyrazole)methane (tpm)	112
5.6.2	1,10-phenanthroline-5,6-dione (dpq).....	113
5.6.3	Dipyridophenazine (dppz).....	113
5.6.4	Pyrazinophenanthroline (pzp)	114
5.6.5	5-Nitro-1,10-phenanthroline	114
5.6.6	5-nitro-6-amino-1,10-phenanthroline	115

5.6.7	5,6-diamino-1,10-phenanthroline	115
5.6.8	4,5,9,18-Tetraazaphenanthrenetriphenylene (taptp).....	116
5.6.9	Benzimidazol-2-one.....	116
5.6.10	5,6-dinitrobenzimidazol-2-one	117
5.6.11	5,6-diaminobenzimidazol-2-one	117
5.6.12	Dipyridophenazineimidazolone (dppz-izdo).....	118
5.6.13	[(tpm)RuCl ₃].....	118
5.6.14	[Ru(tpm)(dppz)Cl][PF ₆].....	119
5.6.15	Attempted synthesis of 11-mercapto-N-(pyridine-4-yl)undecamide 119	
5.6.16	Attempted synthesis of 11-mercapto-N-(pyridine-3-yl)undecamide 120	
5.6.17	11-azidoundec-1-ene	120
5.6.18	Attempted synthesis of Undec-10-en-1-amine	121
5.6.19	3-(1-(undec-10-en-1-yl)-1H-1,2,3-triazol-4-yl)pyridine.....	121
5.6.20	Attempted synthesis of S-(11-(4-(pyridin-3-yl)-1H-1,2,3-triazol-1-yl)undecyl) ethanethioate.....	122
5.6.21	S-(11-chloroundecyl) ethanethioate	123
5.6.22	Attempted synthesis of S-(11-azidoundecyl) ethanethioate.....	123
5.6.23	Attempted synthesis of 4-(pyridine-3-yl)phenol.....	124
5.6.24	Triethylene glycol monotosylate	124

5.6.25	1-(3-Pyridyloxy)-3,6-dioxaoctane-8-ol.....	126
5.6.26	Lipoic acid 1-(4-Pyridyloxy)-3,6-dioxaoctane-8-yl ester (3Py-O ₃ -LA) 126	
5.6.27	Attempted synthesis of [Ru(tpm)(dppz)(3Py-O ₃ -LA)][PF ₆] ₂	127
5.6.28	2-(2-(2-azidoethoxy)ethoxy)ethan-1-ol.....	128
5.6.29	2-(2-(2-azidoethoxy)ethoxy)ethyl 4-tosylate.....	128
5.6.30	S-(2-(2-(2-azidoethoxy)ethoxy)ethyl) ethanethioate	129
5.6.31	Attempted synthesis of 2-(2-(2-aminoethoxy)ethoxy)ethane-1-thiol 129	
5.6.32	Attempted synthesis of [Ru(tpm)(dppz)(4-Py-MeCOOH)][PF ₆] ₂	130
5.6.33	Attempted synthesis of [Ru(tpm)(dppz)(3-Py-MeCOOH)][PF ₆] ₂	130
5.6.34	[Ru(tpm)(dppz)(4-CHOPy)][PF ₆] ₂	131
5.6.35	[Ru(tpm)(dppz)(3-CHOPy)][PF ₆] ₂	132
5.6.36	Attempted synthesis of [Ru(tpm)(dppz)(3-≡-Py)][PF ₆] ₂	133
5.6.37	Attempted synthesis of [Ru(tpm)(dppz)(4-≡-Py)][PF ₆] ₂	133
5.6.38	4-((Trimethylsilyl)ethynyl)pyridine	134
5.6.39	Attempted synthesis of [Ru(tpm)(dppz)(4-TMS-≡-Py)][PF ₆] ₂ (a)	134
5.6.40	Attempted synthesis of [Ru(tpm)(dppz)(4-TMS-≡-Py)][PF ₆] ₂ (b)	135
5.6.41	2-(2-(2-chloroethoxy)ethoxy)acetic acid.....	135
5.6.42	2-(2-(2-(acetylthio)ethoxy)ethoxy)acetic acid.....	136

5.6.43	2-(2-(2-mercaptoethoxy)ethoxy)acetic acid	137
5.6.44	[Ru(tpm)(dppz)(3-NH ₂ MePy)][PF ₆] ₂	137
5.6.45	Thiol terminated [Ru(tpm)(dppz)(3-NH ₂ MePy)][PF ₆] ₂	138
5.6.46	[Ru(tpm)(pzp)Cl][PF ₆]	138
5.6.47	[Ru(tpm)(pzp)(nic)][PF ₆] ₂	139
5.6.48	[Ru(tpm)(pzp)(isonic)][PF ₆] ₂	140
5.6.49	[Ru(tpm)(pzp)(3-NH ₂ Py)][PF ₆] ₂	141
5.6.50	[Ru(tpm)(pzp)(4-NH ₂ Py)][PF ₆] ₂	142
5.6.51	[Ru(tpm)(pzp)(3-pic)][PF ₆] ₂	143
5.6.52	[Ru(tpm)(pzp)(4-pic)][PF ₆] ₂	144
5.6.53	Attempted synthesis of [Ru(tpm)(pzp)(3-CHOPy)][PF ₆] ₂	145
5.6.54	Attempted synthesis of [Ru(tpm)(pzp)(4-CHOPy)][PF ₆] ₂	146
5.6.55	Attempted synthesis of [Ru(tpm)(tapt)(Cl)][PF ₆].....	146
5.6.56	Attempted synthesis of [Ru(tpm)(dppz-izdo)(Cl)][PF ₆]	147
5.6.57	Attempted synthesis of [Ru(tpm)(dpq)(Cl)][PF ₆].....	147
5.6.58	[Ru(DMSO) ₄ Cl ₂].....	147
5.6.59	Attempted synthesis of [Ru(tapt)(DMSO) ₂ Cl ₂].....	148
5.6.60	Attempted synthesis of [Ru(dppz-izdo)(DMSO) ₂ Cl ₂]	148
5.6.61	[Ru(dpq)(DMSO) ₂ Cl ₂]	148
5.6.62	[Ru(tpm)(dpq)(Cl)][PF ₆]	149

5.6.63	[Ru(tpm)(taptp)(Cl)][PF ₆]	149
5.6.64	[Ru(tpm)(dppz-izdo)(Cl)][PF ₆]	150
References		151
6	Appendix	155
6.1	X-ray Crystallographic Data	155
6.2	Example extinction coefficient calculation	157

List of Abbreviations

A	Adenine
AIBN	Azobisisobutyronitrile
AuNP	Gold Nanoparticles
bpy	2,2'-bipyridine
C	Cytosine
CD	Circular Dichroism
CT	Computed Tomography
ct-DNA	Calf Thymus DNA
CuAAC	Copper-catalysed azide-alkyne cycloaddition
DAPI	4',6-diamidino-2-phenylindole
DFT	Density Functional Theory
DIP	4,7-diphenyl-1,10-phenanthroline
DLS	Dynamic Light Scattering
dmb	4,4'-dimethyl-2,2'-bipyridine
dmp	2,9-dimethyl-1,10-phenanthroline
DNA	Deoxyribonucleic Acid
dppn	Benzo[i]dipyrido[3,2-a:2'3'-c]phenazine
dppz	Dipyrido[3,2-a:2',3'-c]phenazine
dppz-izdo	11,13-dihydro-12H-imidazo[4,5-i]dipyrido[3,2-a:2',3'-c]phenazin-12-one
dpq	1,10-phenanthroline-5,6-dione
ECD/EDCI	1-ethyl-3-(3-dimethylaminopropyl)carbodiimide
EPR	Enhanced Permeability and Retention
ESI-MS	Electrospray Ionisation Mass Spectrometry
FRET	Förster Resonance Energy Transfer
G	Guanine
HATU	Hexafluorophosphate Azabenzotriazole Tetramethyl Uronium

HPLC	High Performance Liquid Chromatography
IR	Infrared
Isonic	Isonicotinamide
ITC	Isothermal Titration Calorimetry
LC-MS	Liquid Chromatography-Mass Spectrometry
LD	Linear Dichroism
MGP	4-(guanidylmethyl)-1,10-phenanthroline
MLCT	Metal-to-ligand Charge Transfer
MMR	Mismatch Repair
mRNA	Messenger Ribonucleic Acid
Nic	Nicotinamide
NIR	Near Infrared
NMR	Nuclear Magnetic Resonance
ORTEP	Oak Ridge Thermal-Ellipsoid Plot
PDT	Photodynamic Therapy
PEG	Polyethylene Glycol
phen	1,10-phenanthroline
phi	Phenanthrene-9,10-diimine
PTT	Photothermal Therapy
py	Pyridine
pzp	pyrazino-1,10-phenanthroline
RNA	Ribonucleic Acid
SPR	Surface Plasmon Resonance
SP-Sephadex	Sulfopropyl-Sephadex
T	Thymine
TAP	1,4,5,8-tetraazaphenanthrene
taptp	dibenzo[a,c]dipyrido[3,2-h:2',3'-j]phenazine
TBAI	Tetra-n-butylammonium Iodide
TCCA	Trichloroisocyanuric acid

TEM	Transmission Electron Microscopy
TEMPO	2,2,6,6-tetramethyl-1-piperidinyloxy
terpy	2,2':6',2''-terpyridine
TMS	Trimethylsilane
TOAB	Tetra-n-octylammonium Bromide
Tp	Tris(1-pyrazole)borate
tpm	Tris(1-pyrazole)methane
tpphz	tetrapyrido[3,2-a:2',3'-c:3'',2''-h:2''',3''''-j]phenazine

Chapter One

1 Introduction

1.1 What is DNA?

Nucleic acids are molecules capable of storing and expressing information through chemical bonds. All life, from simple, single-celled organisms such as bacteria, through to complex multi-cellular organisms use deoxyribonucleic acid (DNA) to store genetic information. DNA stores information through a linear code of base pairs. Self-replication of this code allows propagation of genetic information between generations by cellular processes, such as mitosis. This linear code can be expressed through transcription onto ribonucleic acid (RNA), which can then be translated into a protein sequence by ribosomes. Transcription can happen in reverse, whereby RNA can be used to alter the DNA sequence. This method is used by viruses to inject their genetic code into healthy cells. The relationship between DNA, RNA and proteins was described by Crick as the “central dogma of molecular biology”,¹ and is shown in figure 1.1.

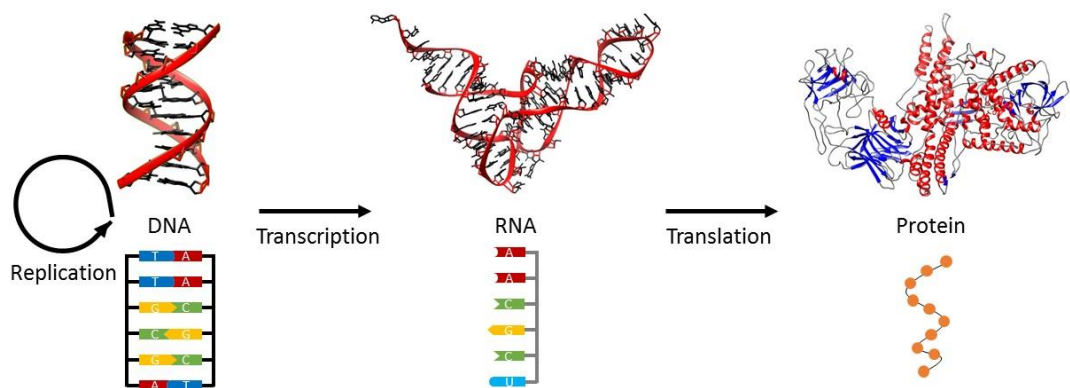


Figure 1.1 The central dogma of molecular biology. Genetic information is stored on DNA, which can self-replicate. The information on DNA can be translated onto RNA, which can then interact with ribosomes to allow a specific protein sequence to be generated. (PDB ID: 1KB1, 4TNA, 3BTA)²⁻⁴

1.2 The Structure of DNA

DNA is composed of nucleotides. Each nucleotide consists of three units – a nucleobase, a deoxyribose sugar, and a phosphate group. The sugar acts as a central scaffold for the nucleotide, with the phosphate group linking between nucleotides. The nucleobases then act as molecular recognition units, to either form the secondary structure, or interact with proteins to allow transcription to RNA to occur. In DNA, there are four nucleobases used – the purines, adenosine (**A**) and guanine (**G**), and the pyrimidines, thymine (**T**) and cytosine (**C**). These are shown in figure 1.2. DNA has a directionality imparted through the deoxyribose sugar. As DNA synthesis occurs from the 5' end to the 3' end, this is also how sequences are normally read.

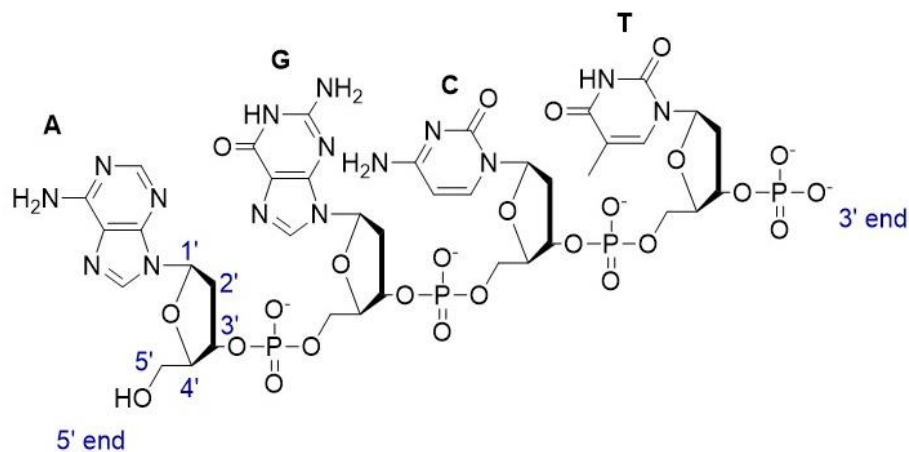


Figure 1.2 A short DNA oligomer showing each nucleotide base – adenosine (**A**), guanine (**G**), cytosine (**C**) and thymine (**T**).

DNA secondary structures occur due to specific interactions between the nucleobases. The lowest energy, and most biologically relevant structure is B-DNA, which consists of two anti-parallel strands joined by complementary hydrogen bonding between bases.⁵ In duplex DNA, **A** is bound to **T**, and **G** is bound to **C**. These pairings are shown in figure 1.3 a). The double helical structure generates two grooves - the wide major groove, and the narrow minor groove. The structure of B-DNA is also shown in figure 1.3 b).

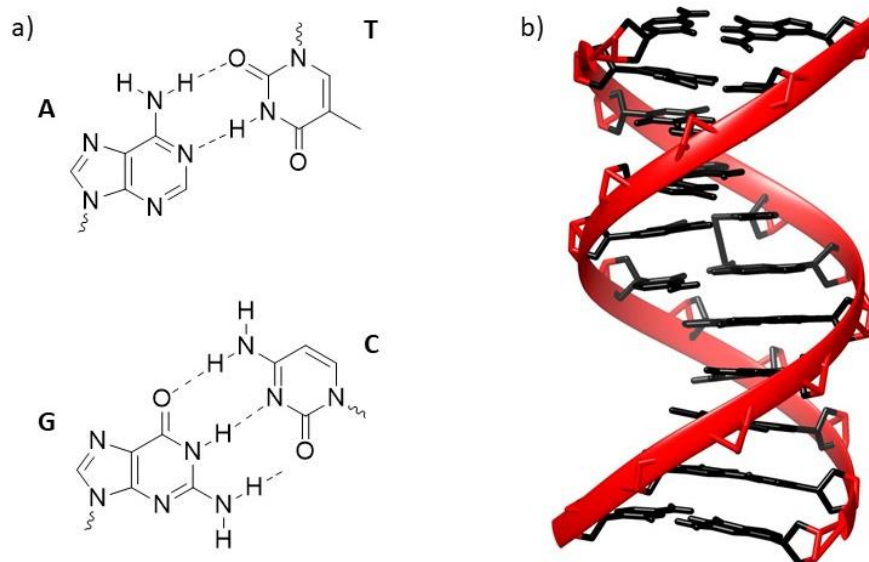


Figure 1.3 a) Complementary hydrogen bonding between base pairs. b) Solution NMR structure of B-DNA duplex (PDB ID: 1KB1)²

1.3 DNA binding

The interaction of molecules with DNA is of huge importance, both in terms of naturally occurring biomolecules, and artificially introduced molecules such as drugs or dyes. Understanding the binding modes available to these molecules is therefore useful in terms of being able to tune the properties of a binding molecule.

Small molecule binding to DNA can be split into two overarching categories – irreversible and reversible binding.

1.3.1 Irreversible Binding

Irreversible binding involves the formation of one or more covalent bonds between the binding agent and one of the structural elements of DNA. Irreversible binding can often prevent enzymes from passing the point at which the agent is bound on the DNA, either due to directly blocking, or permanently altering the secondary structure by introducing kinks. This, in turn, can trigger programmed cell death by apoptosis.

Cisplatin (*cis*-[PtCl₂(NH₃)₂]) (structure shown in figure 1.4 a)) was the first metal complex discovered to be used as a chemotherapeutic agent. First described in 1845 by Peyrone,⁶ its biological activity was never considered until Rosenberg accidentally found the electrolysis of Pt electrodes inhibited cell division in *E. coli* in 1965.⁷ Further work showed cisplatin's efficacy as an anti-tumour agent,⁸ before the drug's eventual approval for use against testicular and ovarian cancers by the FDA in 1978.

Cisplatin is preserved as the dichloride when administered due to the high extracellular chloride concentration. The lower chloride concentration inside cells allows aquation of the chloride ligands, leaving an electrophilic Pt (II) complex, shown in figure 1.4 b). This can then form covalent bonds with nucleophiles, such as the nitrogen-rich nucleotides of DNA. It is believed 1,2-intrastrand ApG and GpG crosslinks are largely responsible for the cytotoxicity of cisplatin.⁹ The formation of these lesions causes significant structural changes to the structure of DNA, as can be seen in figure 1.4 c). If unrepaired, these can prevent cellular processes such as transcription and replication, and can lead to cell death.

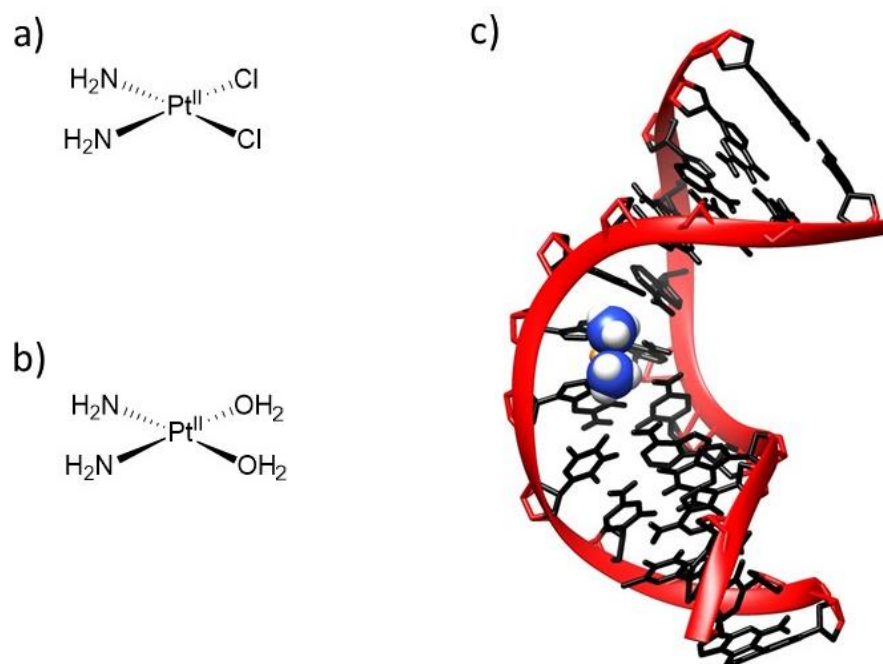


Figure 1.4 a) Structure of cisplatin. b) Structure of active, aquated species. c) Solution NMR structure of cisplatin bound to DNA through a 1,2-intrastrand crosslink (PDB ID: 1A84)¹⁰

Although cisplatin has been highly successful as a chemotherapeutic agent, it has several drawbacks, including poor selectivity towards cancerous cells over healthy cells, high nephro- and gastrointestinal toxicity, relatively low aqueous solubility and low oral bioavailability.¹¹ Furthermore, several cancers can develop cisplatin resistance. Attempts to address these limitations led to the development of several second generation Pt-based drugs, with the general structure *cis*-[PtX₂(NH₂R)₂], where X is a labile leaving group. As of 2010, 24 Pt-based drugs had entered clinical trials, with three gaining worldwide clinical approval, and a further three with approval in individual countries.¹² Carboplatin, shown in figure 1.5 a), which replaces the chloride leaving groups with a more inert 1,1-cyclobutanedicarboxylate, attempts to limit the side effects of cisplatin by lowering the aquation rate (from $\sim 10^{-5} \text{ s}^{-1}$ to $\sim 10^{-8} \text{ s}^{-1}$), thereby reducing the concentration of the highly

toxic active agent, $cis\text{-[Pt(OH}_2\text{)(NH}_3\text{)}_2\text{]}^{2+}$. However, this also reduces the potency of the drug, and means it is only active in the same cancer strains as cisplatin. Oxaliplatin, shown in figure 1.5 b), overcomes cisplatin resistance by introducing a bulky 1*R*,2*R*-cyclohexanediamine ligand, which is thought to project into the major groove when the drug is bound to DNA, blocking the binding of DNA repair proteins.¹³

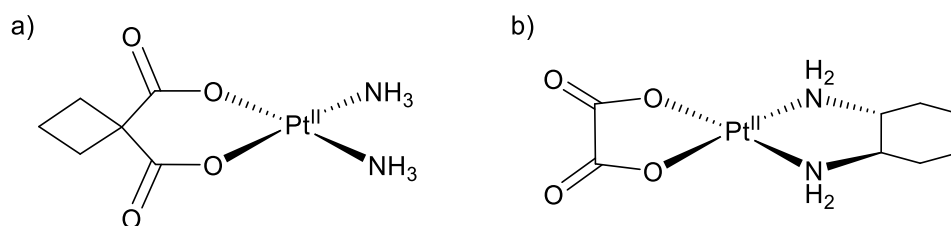


Figure 1.5 a) Structure of carboplatin. b) Structure of oxaliplatin.

1.3.2 Electrostatic Binding

Small molecules can also interact with DNA through several different reversible processes. The simplest of these is electrostatic binding. As DNA is polyanionic, cations can therefore bind to DNA. Under normal conditions, cations such as Mg^{2+} bind to DNA as a counter-ion.

Although electrostatic interactions contribute to other binding modes, as purely electrostatic binding is only between the anionic backbone and the cation, the interaction is generally non-specific – i.e. there is no interaction with the bases, and therefore no sequence selectivity. This is shown in figure 1.6 a), with spermine, a polyamine that is protonated under physiological conditions, and resides close to the phosphodiester backbone.

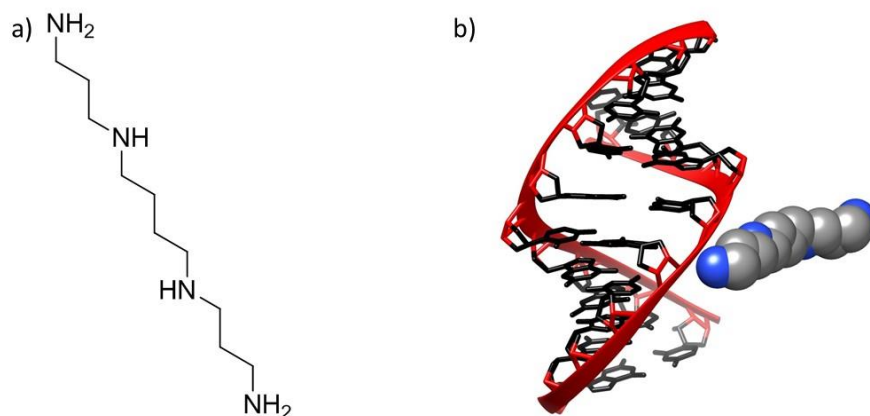


Figure 1.6 a) The structure of spermine. b) Spermine bound to DNA electrostatically (PDB ID: 100D)¹⁴

1.3.3 Groove Binding

Another possible reversible binding mode is groove binding. This involves a small molecule that is either crescent shaped, or appropriately flexible, inserting into one of the major or minor grooves. Groove binding is energetically favourable due to a combination of hydrogen bonding, van der Waals forces, hydrophobic contacts, and electrostatic interactions.

Groove binders have a range of applications. Several, including the Hoechst stains,¹⁵ and DAPI¹⁶ are frequently used as DNA stains in fluorescence microscopy. Netropsin, another groove binder, is a polyamide with antibiotic and antiviral activity, and is shown bound to DNA in figure 1.7.¹⁷

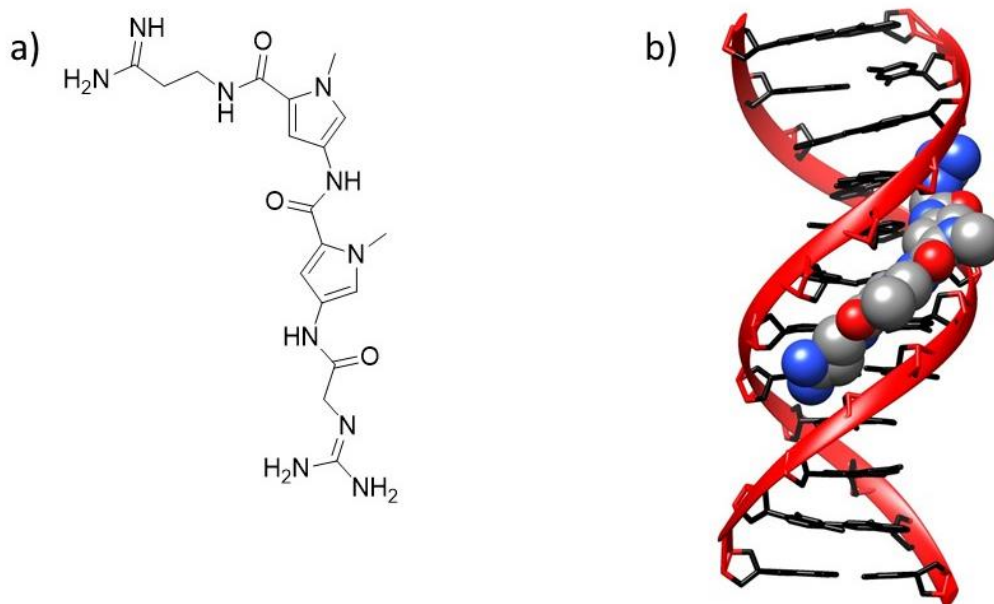


Figure 1.7 a) Structure of netropsin. b) Netropsin bound to the minor groove of a B-DNA duplex (PDB ID: 1D86)¹⁸

1.3.4 Intercalation

Intercalation occurs when a planar aromatic region of a compound inserts between adjacent base pairs in a DNA duplex. Intercalation is favourable due to π -stacking between the intercalator and the nuclear bases, as well as hydrophobic and electrostatic contributions.

In order for intercalation to occur, the DNA duplex must partially unwind; the degree of unwinding varies with different intercalators. This causes separation of the base pairs, creating an opening for intercalation. This local alteration of DNA secondary structure can lead to inhibition of cellular processes like transcription, replication and repair. Doxorubicin (structure shown in figure 1.7 a)), daunorubicin (structure shown in figure 1.7 b)) and dactinomycin are all chemotherapeutic agents that are thought to act at least partially through DNA intercalation.^{19–21}

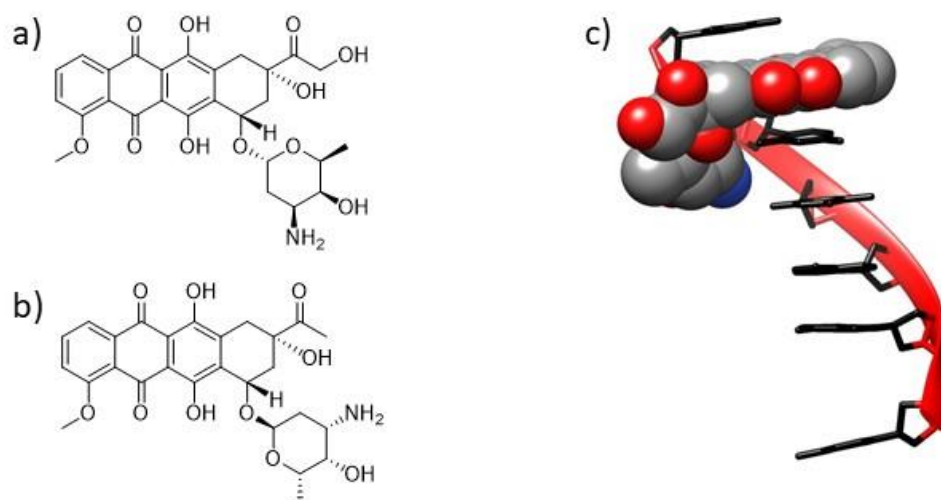


Figure 1.8 a) Structure of doxorubicin. b) Structure of daunorubicin. c) X-ray crystal structure of daunorubicin intercalated into duplex DNA (single strand shown only, PDB ID: 1D12)²²

1.4 Transition Metal Complexes

1.4.1 Metallo-intercalation

1.4.1.1 Early examples

The first example of metallo-intercalators were $[\text{Pt}(\text{terpy})\text{X}]^+$ (terpy = 2,2',2''-terpyridine) complexes developed by the Lippard group. Although preliminary studies with $[\text{Pt}(\text{terpy})\text{Cl}]^+$ suggested intercalation, the lability of the chloride ion was thought to also allow covalent interactions with DNA, in an analogous manner to cisplatin. Substitution of the chloride with 2-mercaptoethanol circumvented this problem due to the much slower rate of substitution.²³ Several techniques were used to determine the binding mode in the initial study – competitive binding assays against ethidium bromide, a known intercalator; relative viscosity changes (the unwinding and lengthening of the DNA

duplex upon intercalation causes an increase in relative viscosity), and monitoring DNA melting temperature (intercalation stabilises the duplex, increasing melting temperature). Later work using X-ray fibre diffraction showed that electron dense Pt atoms could be detected every 10.2 Å along the duplex, indicating binding at every other interbase site.²⁴

1.4.1.2 [Ru(phen)₃]²⁺

The first work on octahedral metal complexes binding to DNA was carried out by the Barton group on the tris-phen (phen = 1,10-phenanthroline) complexes of several transition metals. Of particular interest was [Ru(phen)₃]²⁺, which was initially stated to intercalate with ct-DNA (ct = calf thymus). The binding constant was found to be $6.2 \times 10^3 \text{ M}^{-1}$. Several of the techniques used, including fluorescence quenching, unwinding studies and luminescence measurements, showed greater changes for the Δ isomer than for the Λ , suggesting binding was enantioselective.²⁵ The enantioselectivity was thought to be due to unfavourable steric clashes between the non-intercalating phen ligands of the Λ isomer with the DNA backbone, as shown in figure 1.9. Later work by Barton then suggested a second binding mode – “surface binding” - was available, in which two of the phen ligands partially insert into minor groove, stabilised through hydrophobic and electrostatic interactions. This binding mode would still be sensitive to stereochemistry, but the bound complex would be free to move throughout the groove. Photophysical²⁶ and proton NMR²⁷ experiments, suggested that the intercalative binding mode had a strong preference for the Δ enantiomer, whereas the surface bound mode had a weak preference for the Λ isomer.

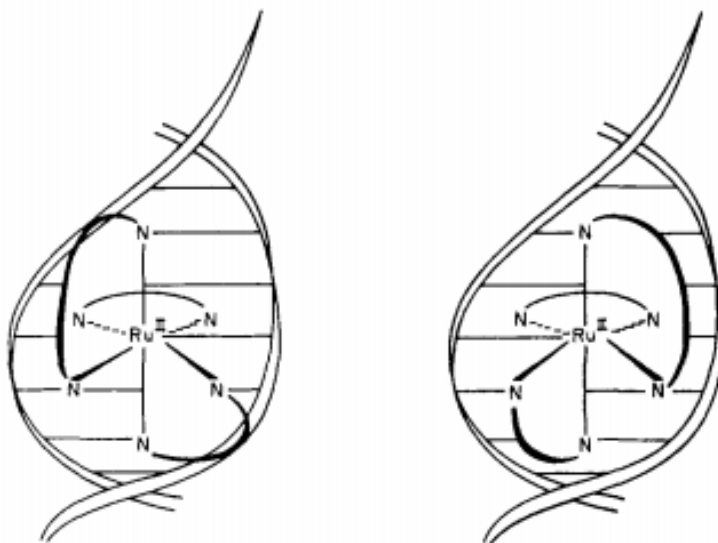


Figure 1.9. Schematic comparing steric interactions between the ancillary ligands and the backbone for Λ -[Ru(N[^]N)₃]²⁺ (left) and Δ -[Ru(N[^]N)₃]²⁺ (right) complexes. Figure taken from reference 25.

In 1990, the binding of [Ru(phen)₃]²⁺ was studied further by the Rodger group, who, using LD (linear dichroism) and CD (circular dichroism), demonstrated each enantiomer did have its own binding mode, but neither were intercalative. Instead, both resided in the major groove with differing geometries dependent upon steric clashes.²⁸ It was proposed that the Δ enantiomer was bound with two phen ligands projecting into the major groove, whereas the Λ enantiomer only had one phen ligand bound, lying parallel to the base pairs. This was supported by work from the Chaires group, who showed that there was a strong dependence of the binding constants for both isomers on the concentration of sodium ions, suggested binding was heavily driven by electrostatic contributions. Relative viscosity experiments were used to further rule out intercalation as a possible binding mode for either isomer – the Λ isomer showed no change in relative viscosity on binding, whereas the Δ isomer showed a decrease. This was attributed to the Δ isomer bending the DNA duplex, which would decrease its length, and therefore the viscosity.²⁸

1.4.1.3 [Ru(bpy)₂(dppz)]²⁺

In order to allow intercalation to occur, the length of the intercalating ligand must be increased. In 1990, the Barton group showed that [Ru(bpy)₂(dppz)]²⁺ (dppz = dipyrido[3,2-a:2',3'-c]phenazine) (structure shown in figure 1.10 a)) was capable of binding to DNA through intercalation.²⁹ Not only is the binding constant for this complex significantly enhanced ($K_b > 10^6 \text{ M}^{-1}$) with respect to [Ru(phen)₃]²⁺, but the complex switches from being non-emissive to emissive upon binding. This is represented in figure 1.10 in both graphical and visual form. Although [Ru(phen)₃]²⁺ showed a luminescent enhancement upon binding, this was the first example of a metallo-intercalator with off-on switching of emission. Previous work had shown that the complex was emissive in non-aqueous media, and that the deactivation of the excited state in water was likely due to protonation of the phenazine nitrogen atoms in the dppz ligand. It was therefore suggested that the “DNA light-switch effect” was due to shielding of these nitrogen atoms by the DNA duplex.

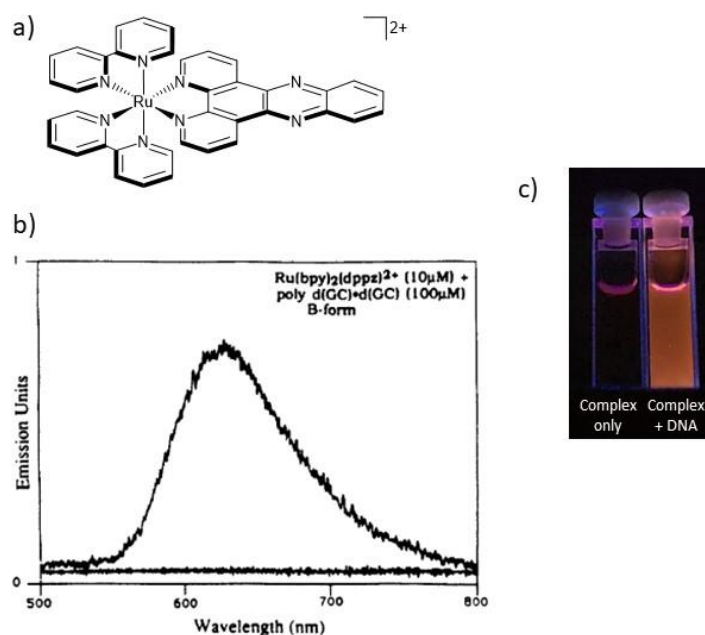


Figure 1.10 a) Structure of $[\text{Ru}(\text{bpy})_2(\text{dppz})]^{2+}$ b) Graphical representation of the DNA “light-switch” effect. Graph from reference 29. c) Visual representation of the DNA “light-switch” effect. $[\text{Ru}(\text{bpy})_2(\text{dppz})]^{2+}$ in the absence (L) and presence (R) of ct-DNA

The excited state responsible for the luminescence had been previously determined by the Sauvage group to be a metal-to-ligand charge transfer (MLCT).³⁰ They found that $[\text{Ru}(\text{bpy})_2(\text{dppz})]^{2+}$ could essentially be considered as having two electronically independent units – a $[\text{Ru}(\text{phen})_3]^{2+}$ -like chromophore, and a phenazine-like electron acceptor. The initial photoexcitation involves electron transfer from the ruthenium centre to an excited state localised on the phen section of the dppz ligand, forming a ¹MLCT excited state. This then decays by intersystem crossing to a ³MLCT located predominately on the phenazine section of the dppz ligand. The excited state can decay to the ground state either non-radiatively, through hydrogen bonding of the phenazine nitrogens to solvent, or through radiative decay. These processes are shown in a simplified Jablonski diagram in figure 1.11.

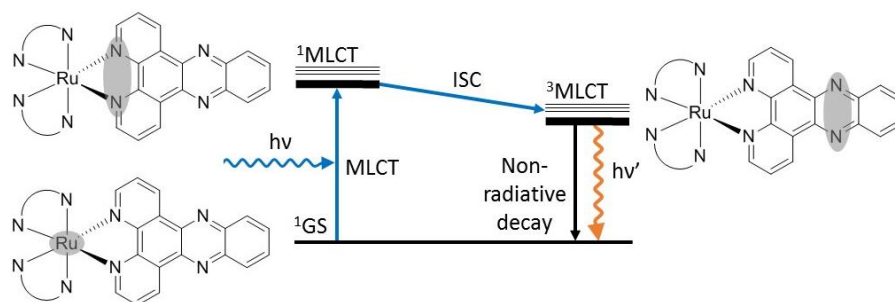


Figure 1.11 Simplified Jablonski diagram representing the excited states and processes involved the DNA “light-switch” effect of $[\text{Ru}(\text{N}^{\wedge}\text{N})_2(\text{dppz})]^{2+}$ complexes. Shaded regions represent the primary regions of electron density in each state. GS = ground state, MLCT = metal-to-ligand charge transfer, ISC = intersystem crossing, $h\nu$ = incident photon, $h\nu'$ = emitted photon.

In order to probe the exact nature of the binding mode of Ru-dppz complexes, the Lincoln group resolved $[\text{Ru}(\text{phen})_2\text{dppz}]^{2+}$ into its Λ and Δ enantiomers. They found that although each enantiomer bound with similar strength ($K_b \approx 10^8 \text{ M}^{-1}$), the relative quantum yield for bound Δ was 6-10 times larger than for bound Λ .³¹ They also found that for each enantiomer, there were two distinct luminescent lifetimes, indicating two possible binding modes. The relative intensity of each lifetime could be varied by changing the mixing ratio of Ru/DNA – the shorter lifetime was favoured at lower mixing ratios (i.e. small amounts of ruthenium complex compared with DNA). LD experiments suggested both binding modes were intercalative in nature. Together with work from the Barton group,³² it was hypothesised that there are two binding modes, differing in the orientation of the dppz ligand relative to the base pairs. Both modes involved binding from the major groove - one with the long axis of the dppz ligand lying perpendicular to the long axis of the base pairs, and the other more side-on, with a more parallel alignment. The difference in lifetimes could be explained through one of the binding modes exposing the phenazine nitrogens to the bulk solvent, thereby increasing the rate of non-radiative decay.

In 2012, the Cardin group reported crystal structures of Λ -[Ru(phen)₂dppz]²⁺ bound to a short DNA oligomer containing either a **TA/TA** or **AT/AT** central step.³³ When the oligomer with the **TA/TA** step was used, it was found the complex bound perpendicular to the base pairs, from the minor groove. For the oligomer containing the **AT/AT** step, the complex was bound asymmetrically, more side on to the base pair long axis. The sequence selectivity of the binding mode was rationalised by examining close contacts between the ancillary phen ligands, hydrogen atoms from the DNA backbone sugars, and heteroatoms of adjacent base pairs. These binding modes are shown in figure 1.12. The triangles between the two backbone phosphorous atoms and the ruthenium (shown in figure 1.12 a) (ii) and b) (ii)) highlights the differences between the two binding modes.

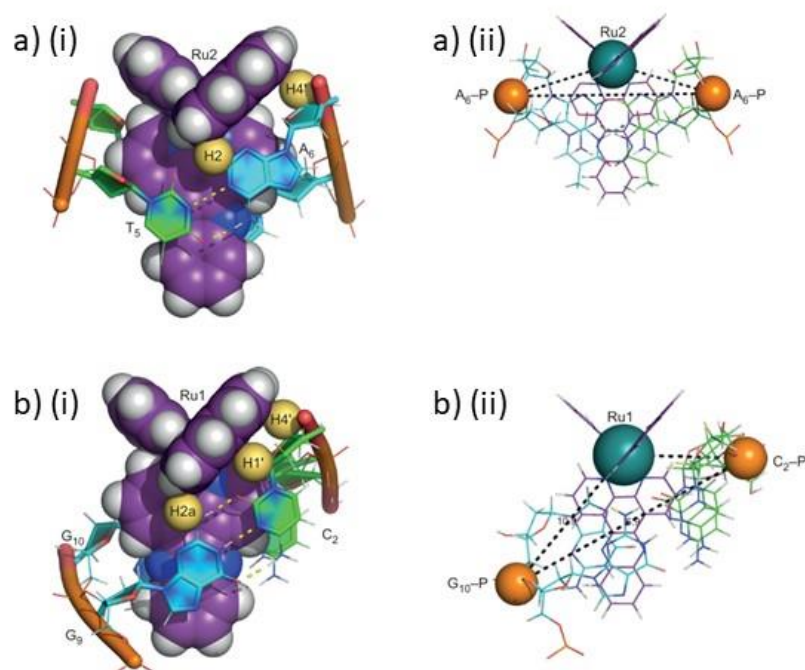


Figure 1.12 Crystal structures of Λ -[Ru(phen)₂dppz]²⁺ intercalated to DNA in both a) symmetric and b) asymmetric binding modes. (i) shows the Ru complexes in as a space filling diagram, whereas (ii) shows the intercalating ligand as a wire frame. Figure adapted from reference 33.

Later work then showed that when racemic $[\text{Ru}(\text{phen})_2(\text{dppz})]^{2+}$ was crystallised with a DNA hexamer, one each of the Λ and Δ enantiomers was found to intercalate at internal **TG/CA** steps, from the minor groove.³⁴ The Δ enantiomer was found to bind in the side on mode described above, with the dppz axis at 65° to the base pair long axis, whereas the Λ enantiomer was bound head on, at 87° . Analysis of the ordered water molecules generated by bases in the major groove found one of the phenazine nitrogen atoms in close contact for the Δ enantiomer, and none for Λ . Although this seems at odds with Lincoln's earlier finding that the bound Δ enantiomer has the higher relative quantum yield, it is worth noting that the crystal structure shows the other phenazine nitrogen of the Δ enantiomer is fully shielded by the backbone, whereas both nitrogens are accessible in the Λ enantiomer. This finding suggests that both phenazine nitrogens require close contact with water for efficient deactivation, and in solution, as water molecules are more disordered, these contacts are more likely to be made.

1.4.2 Structural derivatives of the prototype “light-switch” complex

Due to the interest in, and utility of, Ru complexes of dppz, many other complexes with related structures have been investigated. One of the major advantages of an inorganic scaffold is the relative ease with which any of the intercalating ligand, metal centre, or ancillary ligands can be selectively altered.

1.4.2.1 Intercalating ligand

As a part of their investigations into the exact binding mode of $[\text{Ru}(\text{phen})_2\text{dppz}]^{2+}$, the Barton group synthesised a series of dppz analogues.³⁵ One of the complexes, $[\text{Ru}(\text{phen})_2\text{dppn}]^{2+}$ (dppn = benzo[i]dipyrido[3,2-a:2',3'-c]phenazine), was found to have

weak emission, and show little enhancement upon binding to DNA. As a result, little further interest was shown. Later research by the Yam group revealed that related Re complexes of dppz and dppn ($[\text{Re}(\text{dppz})(\text{CO})_3(\text{py})]^+$ and $[\text{Re}(\text{dppn})(\text{CO})_3(\text{py})]^+$) were capable of photocleaving plasmid DNA – the dppz complex through direct G oxidation, and the dppn complex through generation of reactive oxygen species such as hydroxyl radicals and superoxide radical anions.^{36,37} This eventually led to further investigations into $[\text{Ru}(\text{phen})_2\text{dppn}]^{2+}$, which found that the extension of the π -system in dppn meant that the excited state was a long-lived $\pi\pi^*$ triplet state, rather than the $^3\text{MLCT}$ of the dppz complex.³⁸ It was also found that the dppn complex generated $^1\text{O}_2$ in high yields, providing a potential explanation for its relatively high cytotoxicity in comparison to $[\text{Ru}(\text{bpy})_3]^{2+}$ and $[\text{Ru}(\text{bpy})_2\text{dppz}]^{2+}$.³⁹

Another compound of interest is the dinuclear $[\{\text{Ru}(\text{phen})_2\}\text{tpphz}\{\text{Ru}(\text{phen})_2\}]^{4+}$ (tpphz = tetrapyrido[3,2-a:2',3'-c:3'',2''-h:2''',3'''-j]phenazine), which was found to bind to duplex DNA with similar affinity compared to $[\text{Ru}(\text{phen})_2\text{dppz}]^{2+}$ ($K_b \approx 10^7$), and display a “light-switch effect” upon binding.⁴⁰ It also binds to quadruplex DNA with slightly increased affinity compared with duplex DNA. Quadruplex DNA is an alternative DNA secondary structure composed from four strands, which are typically G rich. Quadruplex DNA does not use the Watson-Crick hydrogen bonding patterns typically observed in duplex DNA, instead, four G residues are arranged around a central metal ion. When bound to quadruplex DNA, the emission maximum was blue-shifted compared to duplex binding ($\lambda_{\text{em}}(\text{duplex}) = 658 \text{ nm}$, $\lambda_{\text{em}}(\text{quadruplex}) = 631 \text{ nm}$). The complex is taken up into cells, and acts as DNA stain for both luminescence and transition electron microscopy. It was found that when cell lines known to be rich in quadruplex DNA were stained, emission from both duplex and quadruplex binding could be observed, meaning

the complex could act as a probe for the structure of cellular DNA.⁴¹ The complex has also found use as a stain for other cellular targets, such as mitochondria, and due to its high photostability, can be used as a stain in several super-resolution microscopy techniques.⁴² These findings were of interest, as although $[\text{Ru}(\text{phen})_2\text{dppz}]^{2+}$ and related complexes have many favourable properties for cellular imaging when compared with conventional organic dyes (for example, low photobleaching, greater Stokes shift, lower energy excitation^{43,44}), they typically have low cell membrane permeability, severely limiting their applications for cellular targets.

1.4.2.2 Metal Centre

Several studies have investigated the effect of changing the metal centre of “light-switch” style complexes. Although there has been some research into first row transition metals, such as chromium⁴⁵ and copper⁴⁵ dppz complexes, most work has focussed on second and third row metals close to ruthenium in the periodic table – rhodium, rhenium, osmium and iridium.

The Barton group have investigated a series of rhodium complexes with bulky intercalating ligands. These ligands are too wide to be easily accommodated in a normal intercalative mode, and instead preferentially bind mismatch sites in DNA duplexes, often with ejection of the mismatched base pair.^{46–48} When studying the cytotoxicity of these complexes, they found that lipophilic complexes preferentially accumulated in the mitochondria, whereas hydrophilic complexes targeted the nucleus. Nuclear targeting compounds were found to show increased cytotoxicity to cell lines that were deficient in mismatch repair (MMR) proteins.⁴⁹ Several types of cancers are known to be associated with MMR deficiency,⁵⁰ and many common chemotherapeutic agents have less effectiveness against MMR deficient cancer cells.⁵¹

The photophysical properties and DNA binding of $[\text{Os}(\text{phen})_2\text{dppz}]^{2+}$ was investigated by the Barton group. As osmium is below ruthenium in the periodic table, the complex behaved in a similar fashion to the original ruthenium complex, maintaining the light-switch effect.⁵² The emission was red-shifted to 740 nm for the osmium complex, compared to 630 nm for the ruthenium complex. Red light generally has greater penetration of living tissue than shorter wavelength light, and due to its heavier nuclei, osmium can also be used as a stain for TEM. There appears to be little work on the cellular imaging properties of $[\text{Os}(\text{phen})_2\text{dppz}]^{2+}$, presumably due to poor uptake (as is the case for the original ruthenium complex), however, dinuclear Os-tpphz complexes have found use as imaging agents for confocal microscopy and TEM.⁵³

1.4.2.3 Ancillary ligands

Alteration of the ancillary ligands can be used to modify the physical properties of the complex, as well as the binding affinity or sequence selectivity to DNA. For instance, the Barton group synthesised a series of Ru-dppz complexes, with a range different ancillary ligands, allowing them to tune the charge, size and lipophilicity of each complex. They found that only the DIP (DIP = 4,7-diphenyl-1,10-phenanthroline) complex was taken up by HeLa cells in significant quantity, indicating that increasing lipophilicity was more important than decreasing charge for cell membrane penetration.⁵⁴

In order to determine how the sterics of the ancillary ligands can affect DNA binding, the Ji group synthesised a pair of Ru-dppz complexes with dmb and dmp (dmb = 4,4'-dimethyl-2,2'-bipyridine, dmp = 2,9-dimethyl-1,10-phenanthroline, structures shown in figure 1.13).⁵⁵ Although the photophysics were almost unaffected, differences in methyl orientation cause significant differences in binding affinity. As the methyl groups of dmp point towards the intercalating ligand, the binding affinity for this complex was reduced

with respect to the parent bpy complex, due to steric clashes with the backbone and base pairs. For the dmb complex, binding affinity was unchanged, however, the emission quantum yield was decreased by a factor of three compared to the parent complex; this was attributed to additional vibrational deactivation due to the flexibility of the bpy ligands.

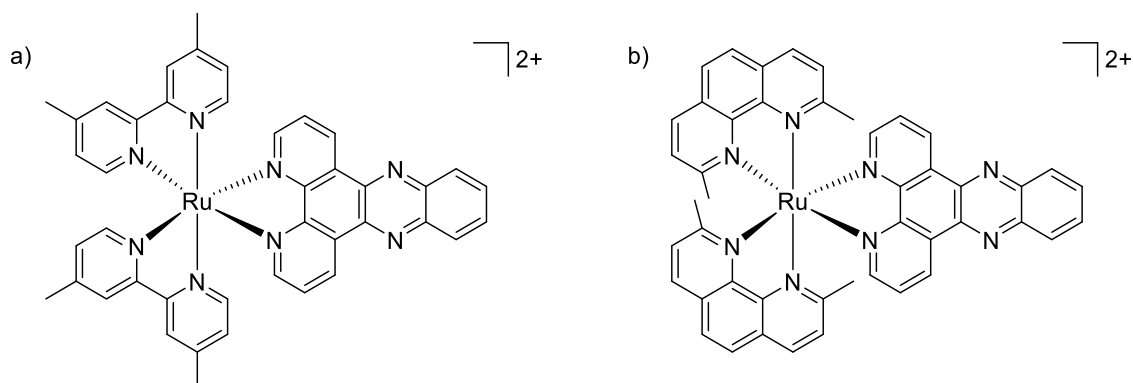


Figure 1.13 a) Structure of $[\text{Ru}(\text{dmb})_2(\text{dppz})]^{2+}$ b) Structure of $[\text{Ru}(\text{dmp})_2(\text{dppz})]^{2+}$

Small changes in substitution pattern can have large effects on binding affinity. A series of complexes based upon the achiral $[\text{Ru}(\text{tpm})(\text{dppz})(\text{py})]^{2+}$ (tpm = trispyrazolemethane) complex have been synthesised by the Thomas group. The axial pyridine has been shown by DFT experiments to be orientated parallel to the dppz axis.⁵⁵ Substitution in the 3 position of the pyridine has little effect on DNA binding, whereas 4-substitution can reduce binding affinity. This is particularly pronounced in the case of 4-aminopyridine (structure shown in figure 1.14), as the amine protons project directly into the base pair below the binding site. This effect appears to prevent intercalation entirely, as the expected “light-switch” effect was not observed for this complex. Relative viscosity measurements suggested the complex was instead groove bound. Later work showed the binding mode of this complex was temperature controlled.⁵⁶ At higher

temperatures, no intercalation was observed. As the temperature was lowered below 10 °C, the emission was switched on, indicating the complex had switched to an intercalative binding mode (this was confirmed by relative viscosity). Interestingly, after the complex was intercalated, it did not switch back to groove binding, even when the temperature was raised for an extended time.

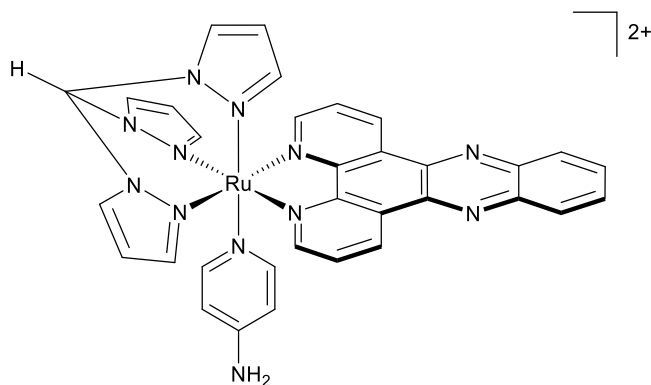


Figure 1.14 Structure of temperature switchable DNA binding probe $[\text{Ru}(\text{tpm})(\text{dppz})(4\text{-NH}_2\text{Py})]^{2+}$

When the ancillary ligand is altered to significantly change their electronic properties, there can be substantial effects to the luminescence characteristics. $[\text{Ru}(\text{TAP})_2(\text{dppz})]^{2+}$ (TAP = 1,4,5,8-tetraazaphenanthrene, structure shown in figure 1.15) is isostructural with $[\text{Ru}(\text{phen})_2\text{dppz}]^{2+}$, but has substantially different properties. The TAP complex is luminescent in water, however, this is partially quenched upon addition to ct-DNA. To investigate the reason for this reverse “light-switch” effect, the Kirsch-DeMesmaeker group studied the binding of $[\text{Ru}(\text{TAP})_2(\text{dppz})]^{2+}$ with a variety of polynucleotide sequences.⁵⁷ They found that the emission intensity upon binding was dependent on the percentage of **G/C** base pairs. At one extreme, binding to poly(**dA-dT**) was found to show a twofold increase in emission intensity, whereas at the other, binding to poly(**dG-dC**) showed almost complete quenching. As the reduction potential of $[\text{Ru}(\text{TAP})_2(\text{dppz})]^{2+}$ is

close to the one-electron oxidation potential of guanosine monophosphate, it was determined that the quenching was due to photo-oxidation of G residues in polynucleotides.

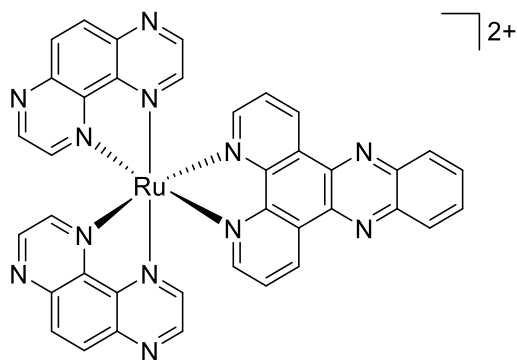


Figure 1.15 Structure of [Ru(TAP)₂(dppz)]²⁺

1.5 Gold Nanoparticles

1.5.1 Overview

Gold nanoparticles (AuNPs) have been widely utilised in biological and medical applications due to their size and shape dependent optoelectronic properties, facile surface functionalisation, biocompatibility and low toxicity. One of their most important physical properties is the surface plasmon resonance (SPR), which is an absorption band arising from resonant excitation of surface conduction electrons by incident photons.⁵⁸ The position of this peak can be altered by changing the size and/or shape of the AuNP – for spherical particles, it generally occurs from 500-550 nm in water, with larger particles absorbing longer wavelengths. If this absorption band overlaps with the luminescent emission of a bound species, AuNPs can be highly efficient quenchers.

AuNPs can be synthesised through a variety of techniques. One of the most common methods was developed by Brust whereby AuNPs are synthesised in a biphasic reaction between HAuCl_4 and NaBH_4 , using tetra-n-octylammonium bromide (TOAB) as a phase transfer agent.⁵⁹ TOAB also acts to stabilise the AuNPs, preventing aggregation. As TOAB binds relatively weakly, it can be efficiently displaced by thiols, which bind strongly to gold. These thiols can then provide a route to attach a substrate of choice. The exact attachment method can be altered to adapt the properties of the conjugate system – a weaker, non-covalent interaction might be favoured for drug delivery applications, whereas a stronger, covalent linker would be more appropriate for an imaging or sensing agent. Common covalent linkages in these systems include coupling amines and carboxylic acids to form amides,⁶⁰ or click reactions such as the azide-alkyne cycloaddition.⁶¹

1.5.2 Therapeutic applications

AuNP based therapeutics can be divided into two broad groups based upon their cell targeting method. Passive targeting involves exploitation of the enhanced permeability and retention (EPR) effect. As tumours are comprised of cells that are malfunctioning, their vasculature is often “leaky”, and so AuNPs can accumulate inside. Lymphatic drainage is often poor, meaning accumulated particles are retained.⁶² Active targeting involves attachment of a ligand with specific affinity for the target.⁶³

There are several available routes for therapeutic action. A common method is utilising the AuNP as a vector for drug delivery, either through covalent attachment, or non-covalent interactions. Covalent attachment typically involves modification of the drug molecule, which can then be released with an appropriate stimulus. In one example,

workers from the Lippard and Mirkin groups used oligonucleotide coated AuNPs as a carrier for inert Pt (IV) pro-drugs, a schematic of which is shown in figure 1.16. Upon intracellular reduction to Pt (II), the axial ligands are liberated, releasing cisplatin as the active drug. They found the Pt-DNA-AuNPs were more active against several cell lines than cisplatin.⁶⁴

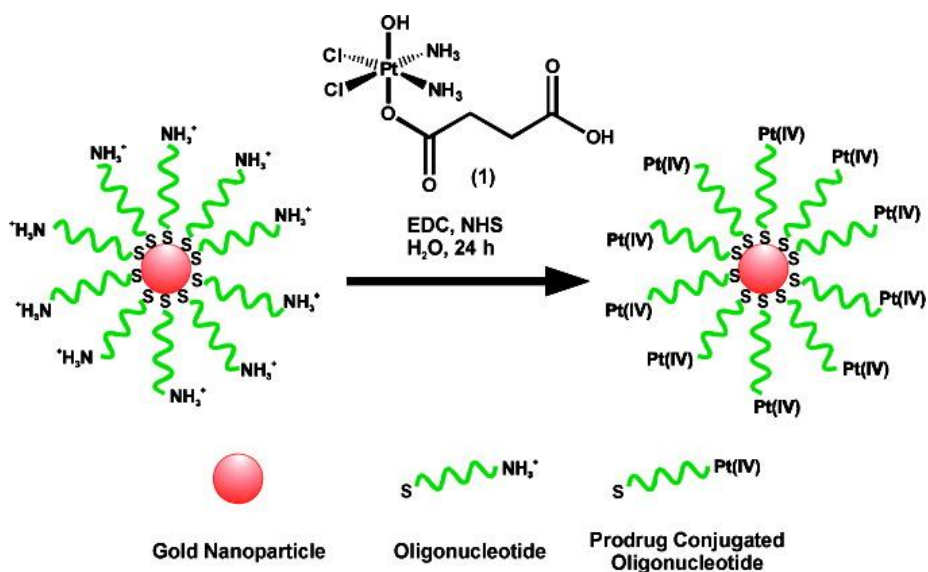


Figure 1.16 Pt(IV)-DNA-AuNP delivery system delivery. Figure taken from reference 64.

Non-covalent attachment means that the drug does not require any modification. It can be of significant advantage in the case of hydrophobic drugs, which are likely to have relatively poor aqueous solubility. Photodynamic therapy (PDT) is a technique where irradiation of a sensitizer is used to generate reactive oxygen species. However, many sensitizers for PDT are hydrophobic, meaning simple intravenous injection is not possible.⁶⁵ For some PDT sensitizers in clinical use, such as Photofrin, patients must wait between 24 and 72 hours between administration of the drug and administration of light.⁶⁶ Patients must avoid direct sunlight in this period, so techniques to improve delivery and clearance are of great importance. The Burda group used PEG (PEG = polyethylene

glycol) coated AuNPs to encapsulate silicon phthalocyanine 4, a hydrophobic PDT sensitiser.⁶⁷ The drug was released by passively diffusing into hydrophobic regions of the cell. *In vivo* studies showed sufficient localisation for treatment after six hours.

The AuNP itself can also be therapeutically active. Photothermal therapy (PTT) typically uses nanomaterials that absorb in the near-infrared region, due to the high transmissivity of living tissue in this region. Absorbed photons are then converted to thermal energy, causing damage to the cellular target. The Borghs group used branched AuNPs functionalised with nanobodies that have high affinity to HER2 antigens, which are heavily expressed on breast and ovarian cancer cells.⁶⁸ They found that the AuNP conjugates were highly specific for HER2-rich cells only, and that both laser light and AuNPs were required for cell damage, showing the damage was from PTT, rather than any other effects.

1.5.3 Sensing applications

An effective sensor requires two components – one to provide recognition of the target analyte, and the other to generate a signal upon recognition. The ease with which AuNPs can be surface functionalised, combined with their optical properties, makes them ideal scaffolds for the design of sensors.

1.5.3.1 Colourimetric-based sensing

One of the most common AuNP sensing techniques is through colourimetric detection. Upon aggregation, the surface plasmon can couple between particles, resulting in a red shift of the absorption band. Therefore induction of aggregation provides a simple route for detection of a target analyte. When sensing metal ions, the most common route is attachment of a chelating agent to the AuNP surface. For example, the Chen group

designed a colourimetric potassium ion sensor based on AuNPs modified with 15-crown-5 chelators.⁶⁹ On addition of potassium ions, a 2:1 sandwich complex is formed, resulting in AuNP aggregation, and the solution colour changed from red to blue. The sensor showed micromolar sensitivity to K^+ only; this was retained even in the presence of other group one and two cations. Incorporation of lipoic acid increased the rate of recognition fourfold, which was attributed to pre-organisation of the crown ether by the carboxylate group.⁷⁰

AuNP-chelate conjugates have also been used for sensing heavy metal ions, which pose a significant risk to public health. Hupp and co-workers reported a system for detection of Cd^{2+} , Pb^{2+} and Hg^{2+} , utilising 11-mercaptoundecanoic acid functionalised AuNPs, shown in figure 1.17.⁷¹ These cations could be detected at concentrations above 400 μM using standard colourimetric detection, although when the intensity of hyper-Rayleigh scattering (which is very sensitive to aggregate formation) was measured, Pb^{2+} could be detected at 25 μM . The limit of detection for Hg^{2+} was further enhanced to 100 nM by the Chang group through careful optimisation of monolayer structure and buffer composition.⁷²

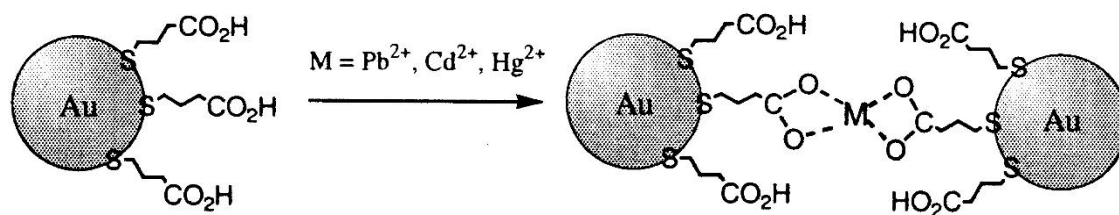


Figure 1.17 AuNP-carboxylate system for detection of heavy metal ions in solution. Figure taken from reference 71.

AuNPs have also been used for polynucleotide detection. Much of the early work in this area came from the Mirkin group, who attached thiol-terminated DNA strands to 13 nm AuNPs. These strands contained non-complementary sticky ends, and so remained disperse. Upon addition a strand complementary to each sticky end, the AuNPs aggregated.⁷³ The system was found to be highly selective and sensitive towards the target oligonucleotide, detecting 10 fmol even under unoptimised conditions.⁷⁴ DNA melting transitions in these systems were very sharp; this allowed discrimination between the full complementary oligonucleotide, and oligonucleotides modified with small deletions or mismatches. Use of larger AuNPs, which have a larger molar extinction coefficient, whilst maintaining the same level of surface coverage, increased the limit of detection to 50 pM.⁷⁵

1.5.3.2 Fluorescence-based sensing

AuNPs have found to be useful quenchers in Förster resonance energy transfer (FRET) based assays. The efficiency of FRET-based quenching is dependent on the overlap between the emission of the donor and the absorption of the quencher. FRET efficiency also decreases sharply as the distance between donor and quencher increases. These systems typically involve a fluorophore that is held close to the AuNP by a loose interaction. Competitive displacement by an analyte releases the fluorophore, thereby switching on the emission.

The Libchaber group used a FRET-based assay for the detection of oligonucleotides. They used a single-stranded hairpin sequence with a thiol at the 5' end and a fluorophore at the 3' end. When the strand was held in the hairpin conformation, the emission was quenched, however, addition of a complementary single strand resulted in duplex formation, allowing the fluorophore to move away from the AuNP, resulting in up to

1000-fold emission enhancement.⁷⁶ A schematic demonstrating these probes is shown in figure 1.18. The hairpin structure has a much smaller number of base pairs bound compared with the complementary strand, allowing for effective displacement, and therefore efficient signalling.

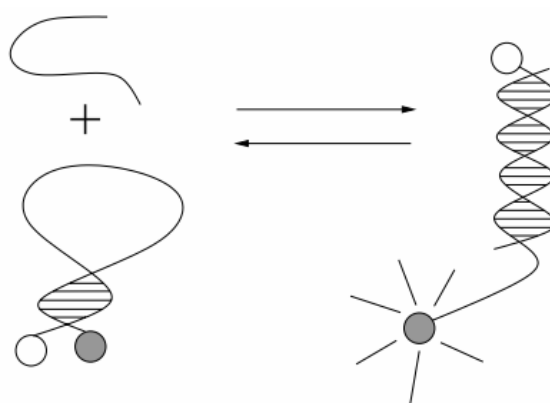


Figure 1.18 Schematic to show FRET-AuNP based assay for polynucleotides. In the hairpin conformation, the fluorophore (dark circle) is held in close proximity to the AuNP (light circle). Upon hybridisation with the target oligonucleotide, the hairpin is released, increasing the fluorophore-AuNP distance, switching on emission. Figure taken from reference 76.

FRET-based probes have also been used to detect and quantify mRNA in living cells. So-called “nano-flares” are oligonucleotide functionalised AuNPs that are hybridised to a fluorophore with a short oligonucleotide strand. Longer target sequences form a more stable duplex, liberating the fluorophore, which acts as a “flare”. A schematic demonstrating this process is shown in figure 1.19. *In vitro* testing showed a fourfold increase of fluorescence upon binding of a target sequence; no enhancement was observed when non-complementary sequences were used.⁷⁷ In order to test their effectiveness as cellular probes, “nano-flares” were designed with a complementary sequence to the survivin transcript, which is of interest in cancer diagnosis and therapy.⁷⁸ SKBR3 cells,

which are known to heavily express survivin, were treated with survivin “nano-flares” as well as a non-complementary control probe. Flow cytometry revealed a 2.5-fold increase in emission for the survivin probe compared with the control. Neither probe showed any emission enhancement when screened against a cell line known not to express survivin transcript. The utility of “nano-flares” has been demonstrated against several targets, including their ability to regulate mRNA levels in a dose-dependent manner,⁷⁹ as probes for other cellular targets, such as adenosine triphosphate,⁸⁰ and to detect cancer cells in blood samples through identifying genetic markers.⁸¹

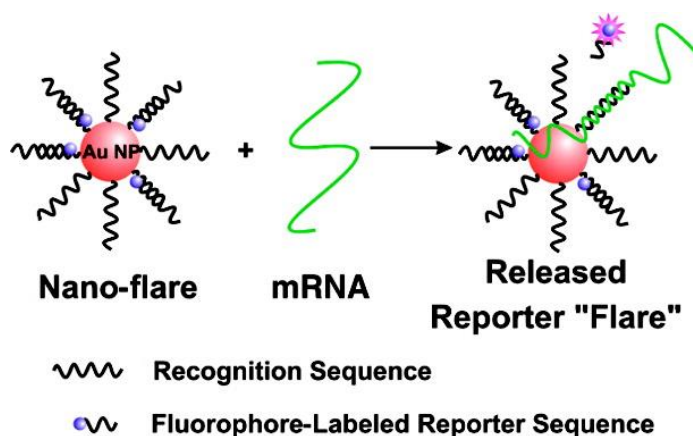


Figure 1.19 Schematic demonstrating AuNP “nano-flares”. Fluorophores are attached to short oligonucleotides, and held in close proximity to AuNPs, quenching emission. Upon binding of the longer target sequence, the fluorophore is released, switching on emission. Figure adapted from reference 77.

1.5.4 Imaging applications

AuNPs have found use in several imaging techniques, including optical coherence tomography,⁸² dark-field light scattering,⁸³ surface enhanced Raman scattering,^{84,85} and computed tomography (CT) scanning. CT imaging uses a series of X-ray scans taken from a range of angles to generate cross sectional images of the scanned object. These

scans can distinguish between different tissues based upon their X-ray attenuation, the ability of matter to extinguish an X-ray beam. High attenuation coefficients are attained with high atomic number and electron density. In order to help distinguish similar tissues, contrast agents with high attenuation coefficients can be used. Most contrast agents in current use are iodine based. Although iodine has high X-ray attenuation, these agents are typically non-specific, as they cannot easily be modified to target biological components or cancer markers. Iodinated contrast agents are also rapidly cleared through the renal system, reducing imaging time.⁸⁶ As gold has a higher atomic number and electron density than iodine, AuNPs are viable alternatives for use as contrast agents. Surface functionalisation can be used to introduce targeting groups or specific biomarkers, and increase circulation time. This can be especially useful for tumour imaging, as the EPR effect can aid accumulation of AuNPs, providing greater contrast. The Kopelman group demonstrated that AuNPs conjugated to an appropriate antibody could selectively enhance the X-ray attenuation of cancer cells expressing the complementary antigen by a factor of 5. Cells not expressing the antigen showed no enhancement.⁸⁷ Several studies have also demonstrated the utility of AuNP CT contrast agents for *in vivo* imaging.^{86,88-90}

1.5.5 Ru-AuNP adducts

There has been a limited amount of research into ruthenium (II) polypyridyl complexes conjugated to AuNPs for cellular imaging or therapeutic purposes. The first example was from the Gunnlaugsson group, who attached a series of simple Ru (II) complexes based on bpy, phen and TAP to small AuNPs.⁹¹ TEM analysis found the diameter of these conjugates to be ~ 4 nm; dynamic light scattering (DLS) measurements showed the hydrodynamic radii of 3-7 nm, showing that there was no aggregation in solution. The

Ru-AuNP conjugates were found to be emissive, although with reduced quantum yield compared with the free Ru complexes. The conjugates were found to bind to DNA with high affinity *in vitro*, and were shown to be non-toxic when taken up by cells. It was claimed that there was accumulation in the cytosol and nucleus, although examination of the confocal microscopy images seems to show that accumulation was predominately around the nuclear membrane, with actual nuclear penetration limited (shown in figure 1.20). A follow up study with the same ruthenium complexes but larger (~ 15 nm) AuNPs found similar photophysical and cellular accumulation properties, with the larger particles also being an effective TEM stain.⁹²

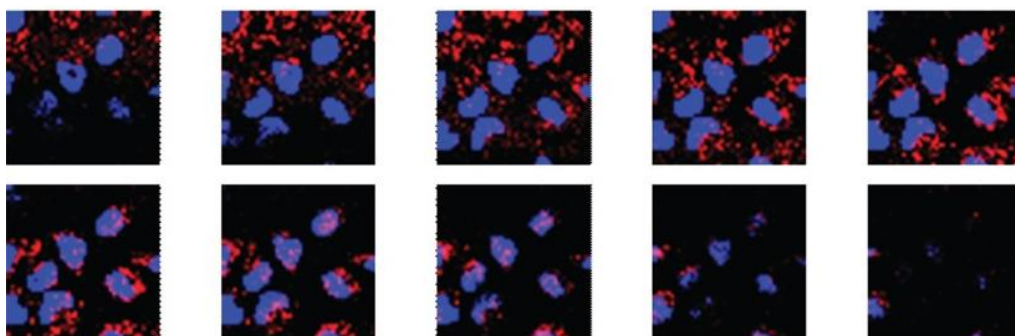


Figure 1.20 Confocal fluorescence Z-stack of Ru-phen-AuNP conjugate (red) with DAPI (blue) as a co-stain. Figure taken from reference 91.

In order to reduce quenching of emission from the ruthenium complexes, the Pikramenou group coated the surface of AuNPs with a fluorinated surfactant, Zonyl 7950, prior to addition of a Ru (II) complex based on $[\text{Ru}(\text{bpy})_3]^{2+}$.⁹³ The luminescence lifetime of the Ru-AuNP conjugates was increased by ~50 % compared with the free complex. The increase in lifetime was attributed to protection of the Ru (II) complex from quenching by oxygen in the solvent, as well as from the AuNPs.⁹⁴ When large, 100 nm

AuNPs were used, the conjugates were found to be effective probes for cellular imaging by confocal luminescence and reflection, as well as TEM. Co-localisation with Hoechst 33258 showed nuclear accumulation, with analysis of TEM images suggesting interaction with chromatin.

Incorporation of more complicated Ru (II) polypyridyl complexes can lead to interesting applications. Spherical AuNPs are more stable than complex AuNP shapes, but typically have poor near infrared (NIR) absorbance, limiting their utility in treatments such as PTT. The Chao group investigates grafting Ru (II) complexes with strong two-photon luminescence to spherical AuNPs to act as sensitisers.⁹⁵ They found that excitation of these conjugates at 808 nm could increase solution temperature by up to 38 °C with a conversion efficiency of 33 %. AuNPs alone only caused a 10 °C increase in temperature, and the free complexes, or laser light alone caused negligible heating. The adducts were tested against HeLa cells, and were found to reduce cell viability under irradiation, however, no damage was observed with either laser light or adduct alone. Finally, the adducts were tested *in vivo*, against HeLa tumours xenografted to mice. On irradiation, the size of xenografted tumours was significantly reduced, or even eliminated in some cases, with no evidence of systemic toxicity after treatment. Again, both the adduct and laser light were required for inhibition. Either used alone allowed the tumours to continue growing.

1.6 Aims

There are a limited number of studies utilising ruthenium polypyridyl complexes with AuNPs. Most of these use complexes based on simple tris-chelates such as $[\text{Ru}(\text{bpy})_3]^{2+}$ or $[\text{Ru}(\text{phen})_3]^{2+}$. This project will aim to incorporate extended planar aromatic ligands

into these Ru-AuNP systems, to allow for a wider range of use, and to include other properties, such as the DNA “light-switch”.

The main aim of this project is to design and synthesise a Ru-dppz complex capable of conjugation to AuNPs. It is hoped that the increased binding affinity for DNA of these intercalating complexes will allow highly sensitive detection of DNA, due to the aggregation-based shift in the SPR band of AuNPs. Furthermore, as these mononuclear intercalators typically have poor cellular uptake, this should be improved on conjugation. Initial attempts will be based on the structures developed by the Gunnlaugsson and Pikramenou groups. This section of the project will be addressed in chapter 2.

A secondary aim of this project is to continue investigations into the effect of changing ancillary ligands on the binding to DNA. Previous work in the Thomas group has shown that for dppz complexes, small changes in the ancillary ligand can alter the binding mode, although binding constants remain relatively unchanged. In the case of dppn complexes, however, it appears that the metal centre is situated further from the duplex, and so changing the ancillary ligand has a much smaller effect. Investigations of other intercalating ligands may allow for further insights into how to selectively modulate binding strength and mode. If these alternative intercalating complexes have suitable optical and DNA binding properties, then they can also be incorporated into the Ru-AuNP systems designed in chapter 2. This section of the project will be addressed in chapter 3.

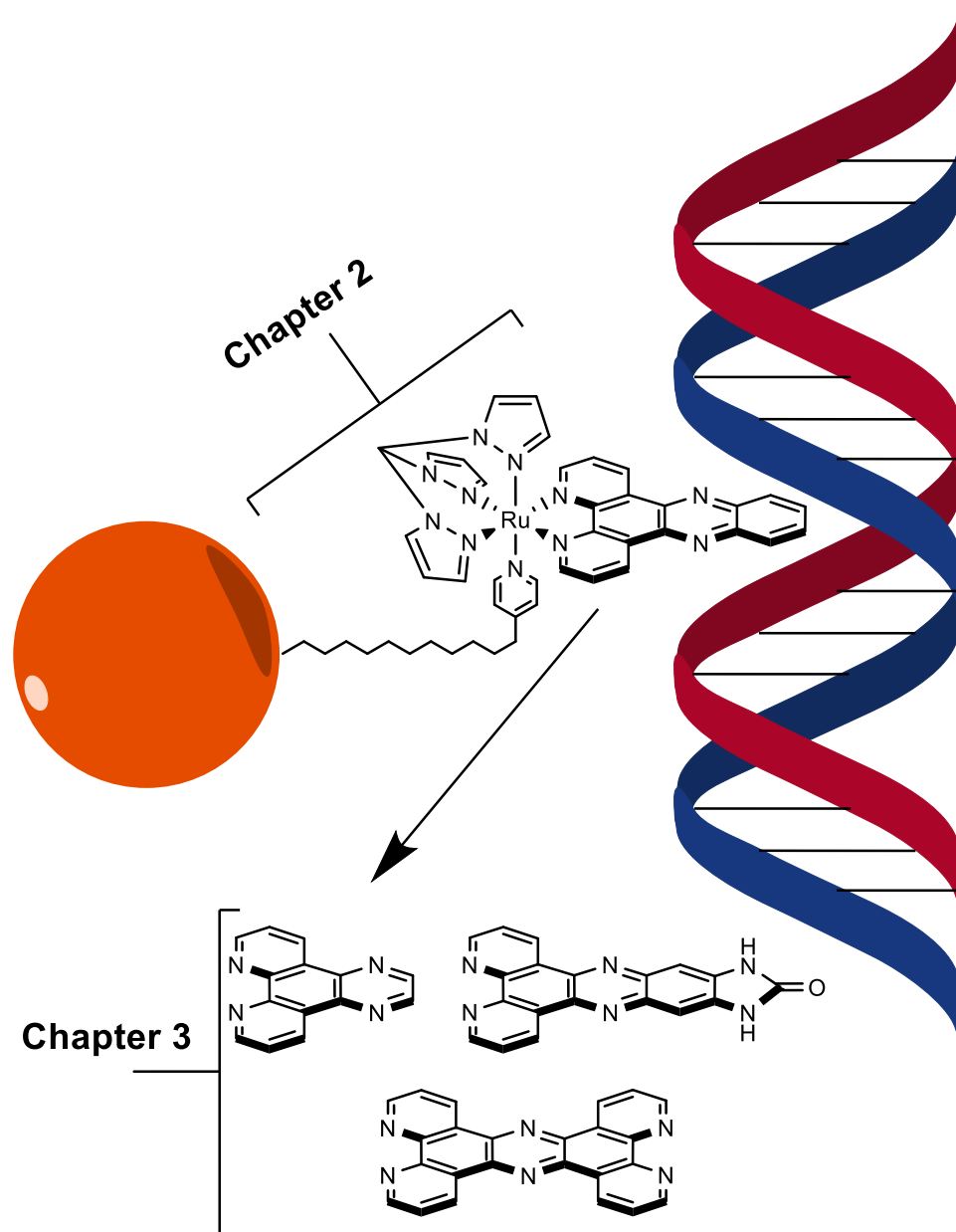


Figure 21 A schematic to show each the work in each chapter. Chapter 2 focusses on the development of a Ru-dppz complex capable of attaching to AuNPs for detection of DNA. Chapter 3 focusses on extending this work with preliminary investigations into alternative intercalating ligands.

1.7 References

- 1 F. H. C. Crick, *Nature*, 1970, **227**, 561–563.
- 2 J. Bohon and C. R. de los Santos, *Nucleic Acids Res.*, 2003, **31**, 1331–1338.
- 3 B. Hingerty, R. S. Brown and A. Jack, *J. Mol. Biol.*, 1978, **124**, 523–534.
- 4 D. B. Lacy, W. Tepp, A. C. Cohen, B. R. DasGupta and R. C. Stevens, *Nat. Struct. Biol.*, 1998, **5**, 898–902.
- 5 J. D. Watson and F. H. C. Crick, *Nature*, 1953, **171**, 737–738.
- 6 M. Peyrone, *Ann. der Chemie und Pharm.*, 1844, **51**, 1–29.
- 7 B. Rosenberg, L. Van Camp and T. Krigas, *Nature*, 1965, **205**, 698–699.
- 8 B. Rosenberg, L. Van Camp, J. E. Trosko and V. H. Mansour, *Nature*, 1969, **222**, 385–386.
- 9 Z. H. Siddik, *Oncogene*, 2003, **22**, 7265–79.
- 10 A. Gelasco and S. J. Lippard, *Biochemistry*, 1998, **37**, 9230–9.
- 11 L. Kelland, *Nat. Rev. Cancer*, 2007, **7**, 573–84.
- 12 N. J. Wheate, S. Walker, G. E. Craig and R. Oun, *Dalt. Trans.*, 2010, **39**, 8113–27.
- 13 J. Kasparikova, M. Vojtiskova, G. Natile and V. Brabec, *Chem. - A Eur. J.*, 2008, **14**, 1330–1341.
- 14 C. Ban, B. Ramakrishnan and M. Sundaralingam, *Nucleic Acids Res.*, 1994, **22**, 5466–5476.
- 15 S. A. Latt, G. Stetten, L. A. Juergens, H. F. Willard and C. D. Scher, *J. Histochem.*

- Cytochem.*, 1975, **23**, 493–505.
- 16 J. Kapuscinski, *Biotech. Histochem.*, 1995, **70**, 220–233.
 - 17 C. Zimmer and U. Wähnert, *Prog. Biophys. Mol. Biol.*, 1986, **47**, 31–112.
 - 18 M. Sriram, G. A. van der Marel, H. L. Roelen, J. H. van Boom and A. H. Wang, *Biochemistry*, 1992, **31**, 11823–34.
 - 19 H. M. Sobell, *Proc. Natl. Acad. Sci. U. S. A.*, 1985, **82**, 5328–31.
 - 20 F. A. Fornari, J. K. Randolph, J. C. Yalowich, M. K. Ritke and D. A. Gewirtz, *Mol. Pharmacol.*, 1994, **45**, 649–56.
 - 21 O. Tacar, P. Sriamornsak and C. R. Dass, *J. Pharm. Pharmacol.*, 2013, **65**, 157–170.
 - 22 C. A. Frederick, L. D. Williams, G. Ughetto, G. A. van der Marel, J. H. van Boom, A. Rich and A. H. Wang, *Biochemistry*, 1990, **29**, 2538–49.
 - 23 K. W. Jennette, S. J. Lippard, G. A. Vassiliades and W. R. Bauer, *Proc. Natl. Acad. Sci. U. S. A.*, 1974, **71**, 3839–43.
 - 24 P. J. Bond, R. Langridge, K. W. Jennette and S. J. Lippard, *Proc. Natl. Acad. Sci. U. S. A.*, 1975, **72**, 4825–9.
 - 25 J. K. Barton, A. Danishefsky and J. Goldberg, *J. Am. Chem. Soc.*, 1984, **106**, 2172–2176.
 - 26 J. K. Barton, J. M. Goldberg, C. V. Kumar and N. J. Turro, *J. Am. Chem. Soc.*, 1986, **108**, 2081–2088.
 - 27 J. P. Rehmann and J. K. Barton, *Biochemistry*, 1990, **29**, 1701–1709.

- 28 C. Hiort, B. Norden and A. Rodger, *J. Am. Chem. Soc.*, 1990, **112**, 1971–1982.
- 29 A. E. Friedman, J. C. Chambron, J.-P. Sauvage, N. J. Turro and J. K. Barton, *J. Am. Chem. Soc.*, 1990, **112**, 4960–4962.
- 30 E. Amouyal, A. Homsy, J.-C. Chambron and J.-P. Sauvage, *J. Chem. Soc. Dalton Trans.*, 1990, 1841.
- 31 C. Hiort, P. Lincoln and B. Norden, *J. Am. Chem. Soc.*, 1993, **115**, 3448–3454.
- 32 R. M. Hartshorn and J. K. Barton, *J. Am. Chem. Soc.*, 1992, **114**, 5919–5925.
- 33 H. Niyazi, J. P. Hall, K. O’Sullivan, G. Winter, T. Sorensen, J. M. Kelly and C. J. Cardin, *Nat. Chem.*, 2012, **4**, 621–8.
- 34 J. P. Hall, D. Cook, S. R. Morte, P. McIntyre, K. Buchner, H. Beer, D. J. Cardin, J. A. Brazier, G. Winter, J. M. Kelly and C. J. Cardin, *J. Am. Chem. Soc.*, 2013, **135**, 12652–12659.
- 35 R. M. Hartshorn and J. K. Barton, *J. Am. Chem. Soc.*, 1992, **114**, 5919–5925.
- 36 V. Wing-Wah Yam, K. Kam-Wing Lo, K.-K. Cheung and R. Yuen-Chong Kong, *J. Chem. Soc. Dalton Trans.*, 1997, **0**, 2067–2072.
- 37 V. W.-W. Yam, K. K.-W. Lo, K.-K. Cheung and R. Y.-C. Kong, *J. Chem. Soc. Chem. Commun.*, 1995, **0**, 1191.
- 38 S. P. Foxon, C. Green, M. G. Walker, A. Wragg, H. Adams, J. A. Weinstein, S. C. Parker, A. J. H. M. Meijer and J. A. Thomas, *Inorg. Chem.*, 2012, **51**, 463–71.
- 39 U. Schatzschneider, J. Niesel, I. Ott, R. Gust, H. Alborzinia and S. Wölfl, *ChemMedChem*, 2008, **3**, 1104–1109.
- 40 C. Rajput, R. Rutkaite, L. Swanson, I. Haq and J. A. Thomas, *Chem. - A Eur. J.*,

- 2006, **12**, 4611–4619.
- 41 M. R. Gill, J. Garcia-Lara, S. J. Foster, C. Smythe, G. Battaglia and J. A. Thomas, *Nat. Chem.*, 2009, **1**, 662–7.
- 42 S. Sreedharan, M. R. Gill, E. Garcia, H. K. Saeed, D. Robinson, A. Byrne, A. Cadby, T. E. Keyes, C. Smythe, P. Pellett, J. Bernardino de la Serna and J. A. Thomas, *J. Am. Chem. Soc.*, 2017, **139**, 15907–15913.
- 43 R. M. Martin, H. Leonhardt and M. C. Cardoso, *Cytom. Part A*, 2005, **67A**, 45–52.
- 44 G. P. Pfeifer, Y.-H. You and A. Besaratinia, *Mutat. Res. Mol. Mech. Mutagen.*, 2005, **571**, 19–31.
- 45 K. D. Barker, B. R. Benoit, J. A. Bordelon, R. J. Davis, A. S. Delmas, O. V. Mytykh, J. T. Petty, J. F. Wheeler and N. A. P. Kane-Maguire, *Inorganica Chim. Acta*, 2001, **322**, 74–78.
- 46 B. M. Zeglis and J. K. Barton, *Nat. Protoc.*, 2007, **2**, 357–71.
- 47 V. C. Pierre, J. T. Kaiser and J. K. Barton, *Proc. Natl. Acad. Sci. U. S. A.*, 2007, **104**, 429–34.
- 48 B. M. Zeglis, V. C. Pierre, J. T. Kaiser and J. K. Barton, *Biochemistry*, 2009, **48**, 4247–53.
- 49 A. C. Komor, C. J. Schneider, A. G. Weidmann and J. K. Barton, *J. Am. Chem. Soc.*, 2012, **134**, 19223–33.
- 50 I. I. Arzimanoglou, F. Gilbert and H. R. K. Barber, *Cancer*, 1998, **82**, 1808–1820.
- 51 J. M. Carethers, M. T. Hawn, D. P. Chauhan, M. C. Luce, G. Marra, M. Koi and

- C. R. Boland, *J. Clin. Invest.*, 1996, **98**, 199–206.
- 52 R. E. Holmlin and J. K. Barton, *Inorg. Chem.*, 1995, **34**, 7–8.
- 53 A. Wragg, M. R. Gill, C. J. Hill, X. Su, A. J. H. M. Meijer, C. Smythe and J. A. Thomas, *Chem. Commun.*, 2014, **50**, 14494–14497.
- 54 C. A. Puckett and J. K. Barton, *J. Am. Chem. Soc.*, 2007, **129**, 46–7.
- 55 J.-G. Liu, Q.-L. Zhang, X.-F. Shi and L.-N. Ji, *Inorg. Chem.*, 2001, **40**, 5045–5050.
- 56 M. G. Walker, V. Gonzalez, E. Chekmeneva and J. A. Thomas, *Angew. Chemie Int. Ed.*, 2012, **51**, 12107–12110.
- 57 I. Ortmans, B. Elias, J. M. Kelly, C. Moucheron and A. Kirsch-DeMesmaeker, *Dalt. Trans.*, 2004, **0**, 668–676.
- 58 P. K. Jain, K. S. Lee, I. H. El-Sayed and M. A. El-Sayed, *J. Phys. Chem. B*, 2006, **110**, 7238–7248.
- 59 M. Brust, M. Walker, D. Bethell, D. J. Schiffrin and R. Whyman, *J. Chem. Soc., Chem. Commun.*, 1994, **0**, 801–802.
- 60 U. Drechsler, N. O. Fischer, B. L. Frankamp and V. M. Rotello, *Adv. Mater.*, 2004, **16**, 271–274.
- 61 X. Li, J. Guo, J. Asong, M. A. Wolfert and G.-J. Boons, *J. Am. Chem. Soc.*, 2011, **133**, 11147–11153.
- 62 R. Ngoune, A. Peters, D. von Elverfeldt, K. Winkler and G. Pütz, *J. Control. Release*, 2016, **238**, 58–70.
- 63 X. Li, H. Zhou, L. Yang, G. Du, A. S. Pai-Panandiker, X. Huang and B. Yan, *Biomaterials*, 2011, **32**, 2540–2545.

- 64 S. Dhar, W. L. Daniel, D. A. Giljohann, C. A. Mirkin and S. J. Lippard, *J. Am. Chem. Soc.*, 2009, **131**, 14652–14653.
- 65 Y. N. Konan, R. Gurny and E. Allémann, *J. Photochem. Photobiol. B.*, 2002, **66**, 89–106.
- 66 D. E. J. G. J. Dolmans, D. Fukumura and R. K. Jain, *Nat. Rev. Cancer*, 2003, **3**, 380–387.
- 67 Y. Cheng, J. D. Meyers, A.-M. Broome, M. E. Kenney, J. P. Basilion and C. Burda, *J. Am. Chem. Soc.*, 2011, **133**, 2583–2591.
- 68 B. Van de Broek, N. Devoogdt, A. D’Hollander, H.-L. Gijs, K. Jans, L. Lagae, S. Muyldermans, G. Maes and G. Borghs, *ACS Nano*, 2011, **5**, 4319–4328.
- 69 S.-Y. Lin, S.-W. Liu, C.-M. Lin and C. Chen, *Anal. Chem.*, 2002, **74**, 330–335.
- 70 S.-Y. Lin, C. Chen, M.-C. Lin and H.-F. Hsu, *Anal. Chem.*, 2005, **77**, 4821–4828.
- 71 Y. Kim, R. C. Johnson and J. T. Hupp, *Nano Lett.*, 2001, **1**, 165–167.
- 72 C.-C. Huang and H.-T. Chang, *Chem. Commun.*, 2007, 1215–1217.
- 73 C. A. Mirkin, R. L. Letsinger, R. C. Mucic and J. J. Storhoff, *Nature*, 1996, **382**, 607–609.
- 74 R. Elghanian, J. J. Storhoff, R. C. Mucic, R. L. Letsinger and C. A. Mirkin, *Science*, 1997, **277**, 1078–1081.
- 75 R. A. Reynolds, C. A. Mirkin and R. L. Letsinger, *J. Am. Chem. Soc.*, 2000, **122**, 3795–3796.
- 76 B. Dubertret, M. Calame and A. J. Libchaber, *Nat. Biotechnol.*, 2001, **19**, 365–370.

- 77 D. S. Seferos, D. A. Giljohann, H. D. Hill, A. E. Prigodich and C. A. Mirkin, *J. Am. Chem. Soc.*, 2007, **129**, 15477–15479.
- 78 D. C. Altieri, *Oncogene*, 2003, **22**, 8581–8589.
- 79 A. E. Prigodich, D. S. Seferos, M. D. Massich, D. A. Giljohann, B. C. Lane and C. A. Mirkin, *ACS Nano*, 2009, **3**, 2147–2152.
- 80 D. Zheng, D. S. Seferos, D. A. Giljohann, P. C. Patel and C. A. Mirkin, *Nano Lett.*, 2009, **9**, 3258–3261.
- 81 T. L. Halo, K. M. McMahon, N. L. Angeloni, Y. Xu, W. Wang, A. B. Chinen, D. Malin, E. Strelakova, V. L. Cryns, C. Cheng, C. A. Mirkin and C. S. Thaxton, *Proc. Natl. Acad. Sci. U. S. A.*, 2014, **111**, 17104–9.
- 82 C. S. Kim, P. Wilder-Smith, Y.-C. Ahn, L.-H. L. Liaw, Z. Chen and Y. J. Kwon, *J. Biomed. Opt.*, 2009, **14**, 034008.
- 83 W. Qian, X. Huang, B. Kang and M. A. El-Sayed, *J. Biomed. Opt.*, 2010, **15**, 046025.
- 84 C. L. Zavaleta, B. R. Smith, I. Walton, W. Doering, G. Davis, B. Shojaei, M. J. Natan and S. S. Gambhir, *Proc. Natl. Acad. Sci. U. S. A.*, 2009, **106**, 13511–6.
- 85 X. Qian, X.-H. Peng, D. O. Ansari, Q. Yin-Goen, G. Z. Chen, D. M. Shin, L. Yang, A. N. Young, M. D. Wang and S. Nie, *Nat. Biotechnol.*, 2008, **26**, 83–90.
- 86 H. Wang, L. Zheng, C. Peng, R. Guo, M. Shen, X. Shi and G. Zhang, *Biomaterials*, 2011, **32**, 2979–2988.
- 87 R. Popovtzer, A. Agrawal, N. A. Kotov, A. Popovtzer, J. Balter, T. E. Carey and R. Kopelman, *Nano Lett.*, 2008, **8**, 4593–4596.

- 88 C. Alric, J. Taleb, G. Le Duc, C. Mandon, C. Billotey, A. Le Meur-Herland, T. Brochard, F. Vocanson, M. Janier, P. Perriat, S. Roux and O. Tillement, *J. Am. Chem. Soc.*, 2008, **130**, 5908–5915.
- 89 D. P. Cormode, E. Roessl, A. Thran, T. Skajaa, R. E. Gordon, J.-P. Schlomka, V. Fuster, E. A. Fisher, W. J. M. Mulder, R. Proksa and Z. A. Fayad, *Radiology*, 2010, **256**, 774–82.
- 90 N. Manohar, F. J. Reynoso, P. Diagaradjane, S. Krishnan and S. H. Cho, *Sci. Rep.*, 2016, **6**, 22079.
- 91 R. B. P. Elmes, K. N. Orange, S. M. Cloonan, D. C. Williams and T. Gunnlaugsson, *J. Am. Chem. Soc.*, 2011, **133**, 15862–15865.
- 92 M. Martínez-Calvo, K. N. Orange, R. B. P. Elmes, B. la Cour Poulsen, D. C. Williams and T. Gunnlaugsson, *Nanoscale*, 2016, **8**, 563–574.
- 93 N. J. Rogers, S. Claire, R. M. Harris, S. Farabi, G. Zikeli, I. B. Styles, N. J. Hodges and Z. Pikramenou, *Chem. Commun.*, 2014, **50**, 617–9.
- 94 S. A. M. Osborne and Z. Pikramenou, *Faraday Discuss.*, 2015, **185**, 219–231.
- 95 P. Zhang, J. Wang, H. Huang, B. Yu, K. Qiu, J. Huang, S. Wang, L. Jiang, G. Gasser, L. Ji and H. Chao, *Biomaterials*, 2015, **63**, 102–114.

Chapter Two

2 Attempted routes towards tether moieties

2.1 Introduction

The aim of this section of the project is to identify methods by which Ru (II) polypyridyl complexes could be attached to AuNPs. As most of the previous work in this field has utilised simple Ru (II) complexes, such as derivatised versions of $[\text{Ru}(\text{bpy})_3]^{2+}$, $[\text{Ru}(\text{phen})_3]^{2+}$ and $[\text{Ru}(\text{TAP})_3]^{2+}$,¹⁻⁴ this work aims to introduce heteroleptic complexes containing more complicated moieties, such as the intercalating dppz ligand. As the nature of the DNA binding interactions of Ru-dppz complexes is known to be dependent on both chirality⁵ and ancillary ligands,⁶ it is important to consider the structure of the linker between the complex and AuNP. For example, if the linker is too short, then the AuNP itself may interfere with binding sterically.

2.2 Parent Complex

2.2.1 Design

To attach a complex to a nanoparticle, it must be functionalised with a group that has a high affinity for the chosen nanoparticle. Functionalisation can present some challenges, especially with regard to stereoisomers. As the dppz ligand is required for intercalative DNA binding, ancillary ligands are the only viable option for functionalization with a tether.

The functionalisation route used by the Gunnlaugsson group - a phen-based ligand modified with 11-mercaptoundecanoic acid for attachment¹ - would not be appropriate for the targeted Ru(dppz)-AuNP conjugates. The simplest complex to incorporate both a

modified ligand for attachment, and dppz for binding would be $[\text{Ru}(\text{bpy}')_2(\text{dppz})]^{2+}$. Unfortunately, the resultant product would then have many structural isomers (figure 2.1), each of which would likely have a different binding affinity to DNA. Even if a more complicated synthetic procedure were to be used, generating a tris-heteroleptic system such as $[\text{Ru}(\text{bpy})(\text{bpy}')(\text{dppz})]^{2+}$, the enantiomers would still need to be resolved in order to determine the binding affinity.⁷ This would also apply if a symmetrically bi-functionalised bpy analogue was used, such as in the systems developed by the Pikramenou group. Examples of the structures used by the Gunnlaugsson and Pikramenou groups are shown in figure 2.2

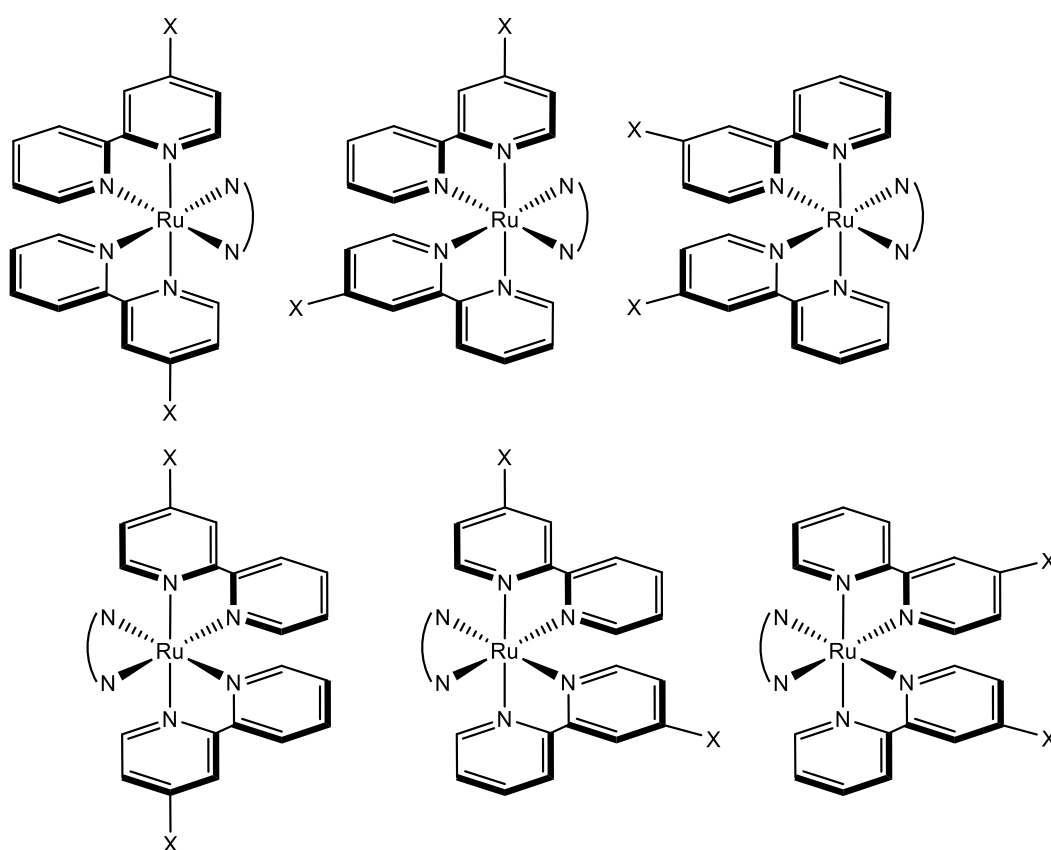


Figure 2.1 The six possible structural isomers of $[\text{Ru}(\text{bpy}')_2(\text{dppz})]^{2+}$. (N^N = dppz, x = AuNP binding group)

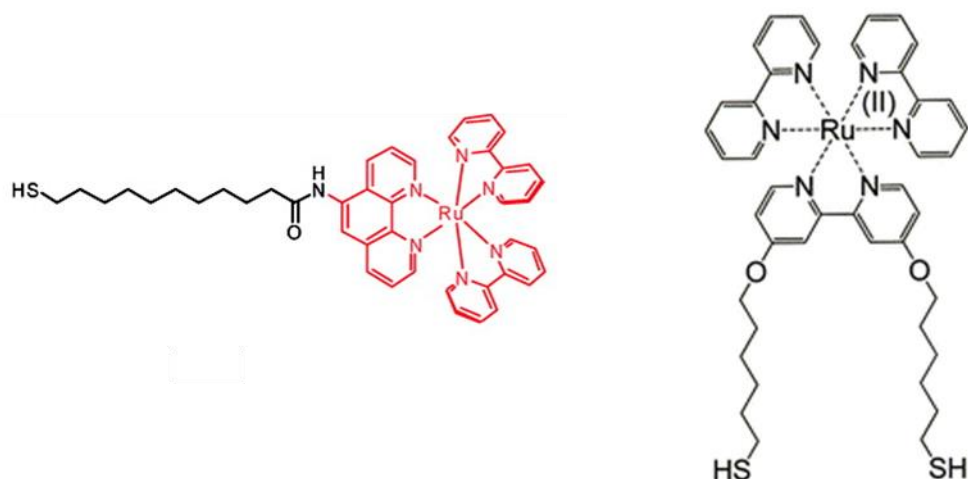


Figure 2.2 Examples of thiol terminated Ru (II) polypyridyl complexes used by the Gunnlaugsson (left) and Pikramenou (right) groups for their studies into Ru-AuNP conjugates. Figure adapted from references 1 and 3.

In order to circumvent these issues, the Thomas group has previously utilised a facially capping “scorpionate” ligand to bind to one face of the complex. This leaves three free co-ordination sites. Two of these are used to bind to dppz, or another intercalator, and the third is free to bind to another ligand. The general structure of these complexes is shown in figure 2.3 a), and the structure of the parent complex, $[\text{Ru}(\text{tpm})(\text{dppz})(\text{py})]^{2+}$ (tpm = tris(1-pyrazole)methane), is shown in figure 2.3 b).

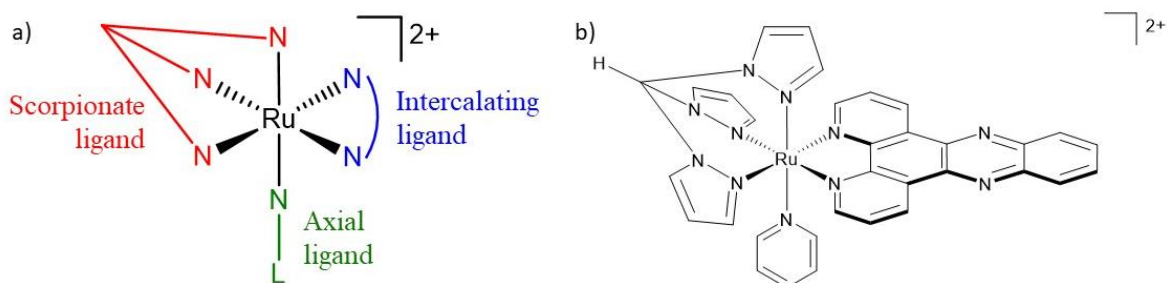


Figure 2.3 a) The general structure of Ru (II) polypyridyl complexes used by the Thomas group. b) The parent $[\text{Ru}(\text{tpm})(\text{dppz})(\text{py})]^{2+}$ complex.

This system allows two routes to functionalisation of the complex, the most explored route being functionalisation of the axial pyridine ligand. To explore how sterics and modulation of hydrogen bonding affect DNA binding, this approach has been explored through the addition of methyls, amines, and more complicated functionalities.^{8,9} In recent work, introduction of a pyridine bearing a pendant di-methoxybenzene group generated a complex that is a ratiometric sensor for DNA¹⁰, and incorporation of a spermine-based linker has allowed synthesis of a dinuclear mixed dppz/dppn theranostic complex, capable of acting both as a DNA “light-switch” and as a ¹O₂ sensitiser.¹¹ The structures of both systems are shown in figure 2.4.

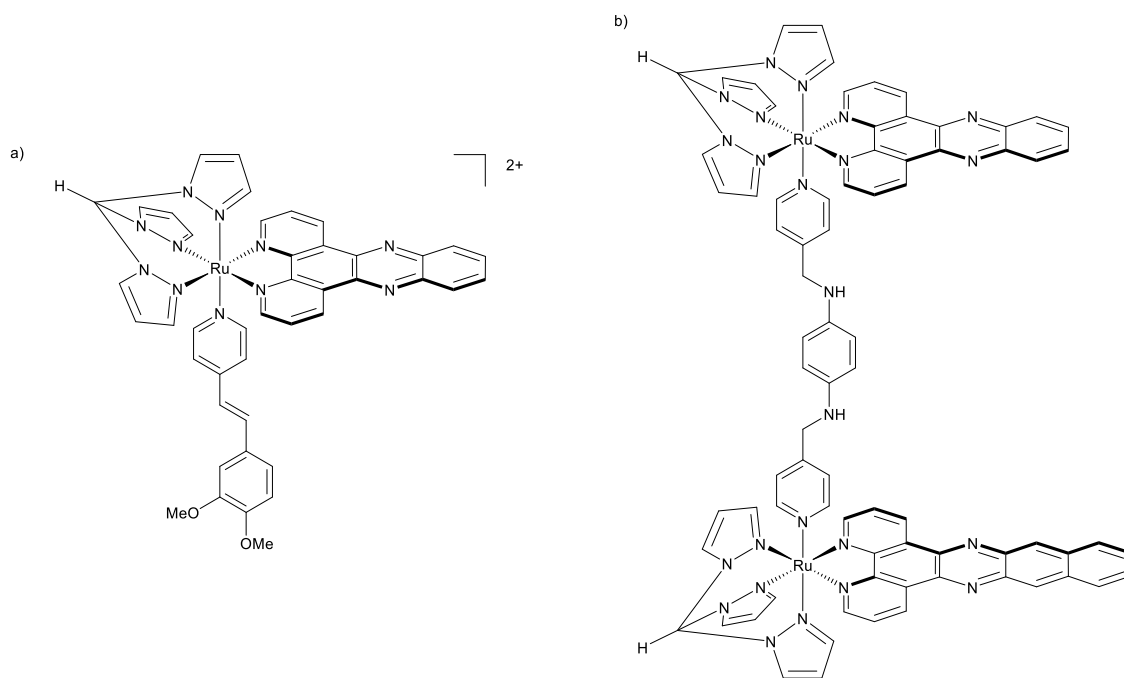


Figure 2.4 a) A Ru-dppz based ratiometric sensor for DNA. b) A dinuclear Ru-dppz/Ru-dppn theranostic compound.

The second route is functionalisation of the tpm ligand. The proton attached to the central carbon is weakly acidic, and can be removed using a strong base such as NaH. The resulting carbanion has been used as a nucleophile to generate functionalised

versions of tpm.¹² Another project in the Thomas, underway concurrently with this work, aimed to attach complexes based on the structure shown in figure 2.2 b) to functionalised gold surfaces, aiming to create systems with enhanced luminescent emission, due to interactions between the surface plasmon of the gold with the emission of the complex. Work in that project primarily focussed on functionalisation through the tpm ligand. However, complexes synthesised have been found to be unstable, regardless of whether the tpm is functionalised pre- or post-coordination. Therefore, work in this project will focus on functionalisation through the axial pyridine.

2.2.1.1 Scorpionate ligands

The Thomas group has previously used tpm as a facially capping “scorpionate” ligand.^{9,13} Tpm is based upon the parent anionic tris(1-pyrazole)borate (Tp) ligand. The structures of Tp and tpm are shown in figure 2.5. Tp was originally designed by Trofimenko in 1966,¹⁴ and the chemistry of the ligand, and many derivatives, has been widely explored.¹⁵⁻¹⁷ Unfortunately, Tp is vulnerable to hydrolysis in aqueous environments, and as such, it is not suitable for biological studies.

Although tpm was originally reported in 1937 by Hückel and Bretschneider,¹⁸ the synthesis was difficult and low yielding, and as such, there were few developments in the chemistry of tpm for several decades. The synthesis of tpm was improved first in 1987 by the Elguero group,¹⁹ who first developed the biphasic synthetic method used today, and again by the Reger group in 2000, who found that simply changing the base from K_2CO_3 to Na_2CO_3 improved both yield and purity.²⁰ As a consequence, metal complexes of tpm and derivatives have since been reported for the majority of metals in the periodic table.²¹

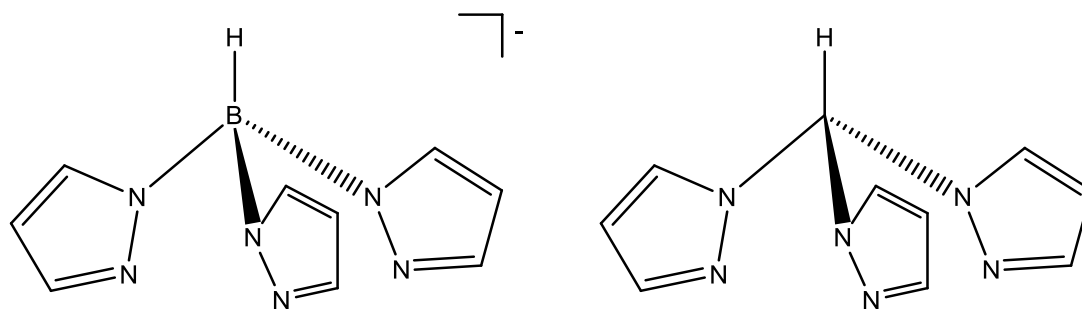
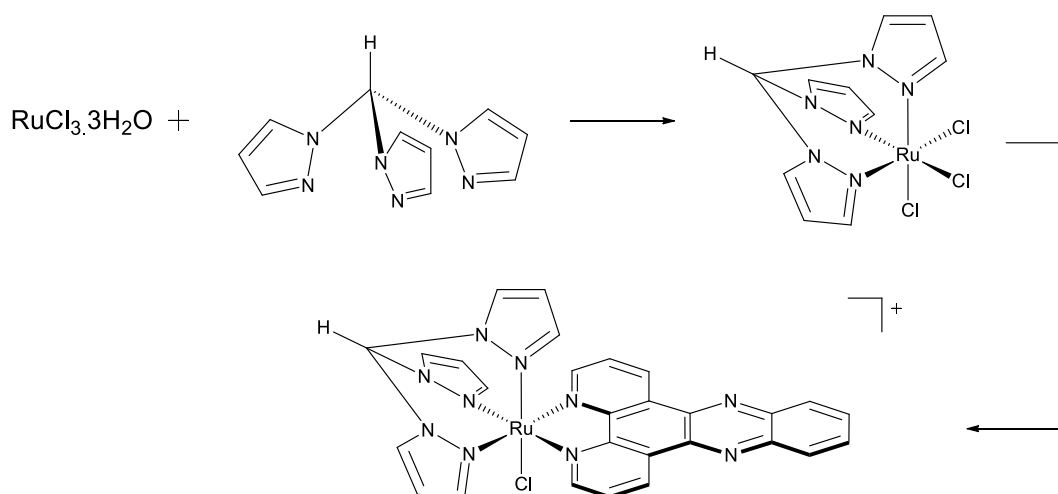


Figure 2.5 The structures of Tp (left) and tpm (right).

The chemistry of tpm complexes is almost identical to that of the analogous Tp complex, except, because tpm is neutral and not an anion like Tp, isostructural complexes display an increase in charge by +1 in the tpm complex.¹⁵ Therefore, due to the polyanionic backbone of DNA, it would be expected that the more cationic tpm complexes should bind to DNA with higher affinities relative to their Tp analogues.

The synthetic route used to synthesise the base complex is shown in scheme 2.1. It has been used extensively in the Thomas group, and was originally adapted from the work of the Meyer group, who produced a series of related complexes, [(tpm)Ru(N[^]N)Cl]Cl, where N[^]N = bpy, 4,4'-Me₂bpy, phen.²²



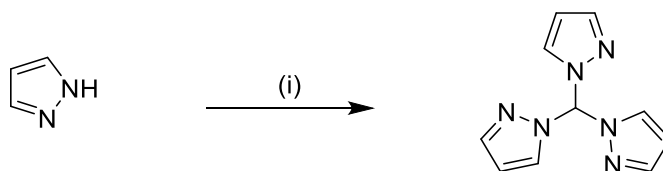
Scheme 2.1 Synthetic route to $[\text{Ru}(\text{tpm})(\text{dppz})(\text{Cl})]^+$, the parent ruthenium complex used in this chapter

From this base complex, an appropriate silver salt can be used to abstract the remaining chloride ligand, followed by subsequent attachment of a ligand to allow easy functionalisation of the system.

2.2.2 Synthesis of $[\text{Ru}(\text{tpm})(\text{dppz})\text{Cl}]^+$

2.2.2.1 Synthesis of tpm

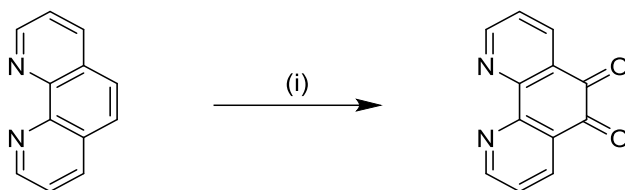
Tpm was synthesised according to the procedure developed by the Reger group,²⁰ as shown in scheme 2.2. Pyrazole is deprotonated by aqueous sodium carbonate, and then reacts with chloroform via tetrabutylammonium bromide (TBAB), which acts as a phase transfer catalyst. Two subsequent substitution reactions afford the desired product. Interestingly, only the tri-substituted product is observed. This is likely due to the central carbon atom being stabilised by substitution of aromatic pyrazole groups, generating a pseudo-benzylic site. This means that the mono-pyrazole substituted intermediate reacts faster with pyrazolyl anions than unreacted chloroform, therefore ensuring that the tri-substituted product is the most favoured.



Scheme 2.2 Synthesis of tris(1-pyrazole)methane. (i) CHCl_3 , Na_2CO_3 , TBAB, H_2O , reflux, 72 hrs

2.2.2.2 Synthesis of 1,10-phenanthroline-5,6-dione (dpq)

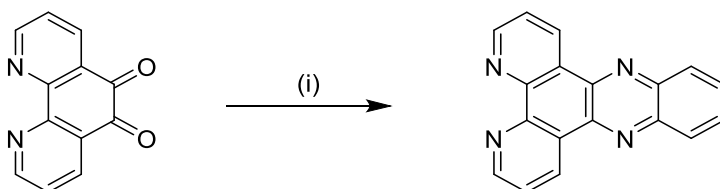
Dpq is an intermediate ligand used in the synthesis of dppz. It is prepared through the oxidation of 1,10-phenanthroline using sulfuric acid and sodium bromate, as shown in scheme 2.3.



Scheme 2.3 (i) 60 % H₂SO₄, NaBrO₃

2.2.2.3 Synthesis of dppz

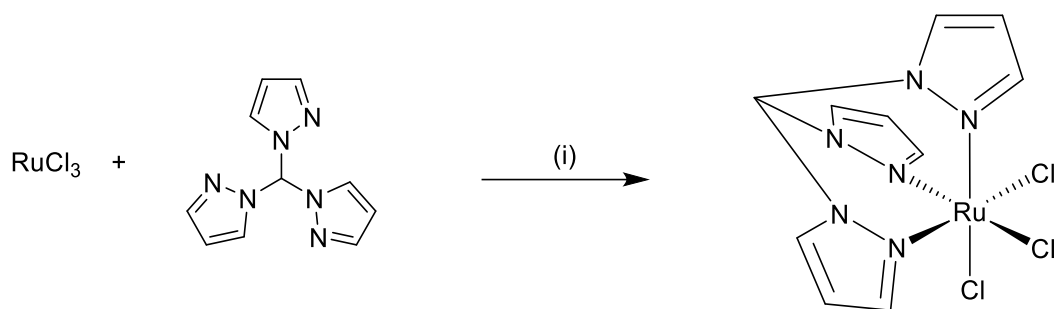
Dppz was synthesised by the condensation reaction of dpq with 1,2-diaminobenzene,²³ as shown in scheme 2.4.



Scheme 2.4 (i) 1,2-diaminobenzene, EtOH, reflux, 20 mins

2.2.2.4 Synthesis of [(tpm)RuCl₃]

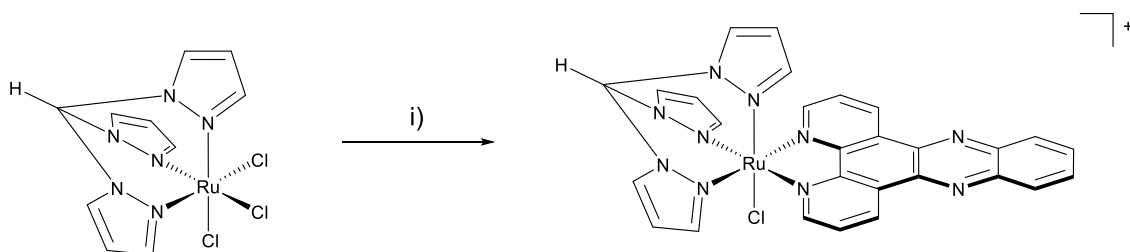
Following the procedure developed by Meyer,²² the tpm complex of Ru (III) was synthesised by refluxing tpm with RuCl₃.3H₂O in EtOH, as shown by scheme 2.5.



Scheme 2.5 (i) EtOH, reflux, 4 hrs

2.2.2.5 Synthesis of $[\text{Ru}(\text{tpm})(\text{dppz})\text{Cl}][\text{PF}_6]$

The synthesis of the parent chloride complex was achieved through refluxing $[(\text{tpm})\text{RuCl}_3]$ with dppz in EtOH:H₂O (3:1) using NEt₃ as a reduction agent. The product was isolated as its PF₆ salt by the addition of excess KPF₆, and purified by column chromatography on neutral alumina with MeCN:toluene (1:1) as the mobile phase. The reaction scheme is shown in scheme 2.6.



Scheme 2.6 (i) dppz, LiCl, EtOH:H₂O (3:1), NEt₃, reflux, 3 hrs

The complex was characterised by ^1H NMR and ESI-MS, and found to be in agreement with previous work.²⁴ The assigned ^1H NMR spectrum is shown in figure 2.6. The ESI-MS showed a singly charged peak at 633 m/z $[\text{M-PF}_6]^+$.

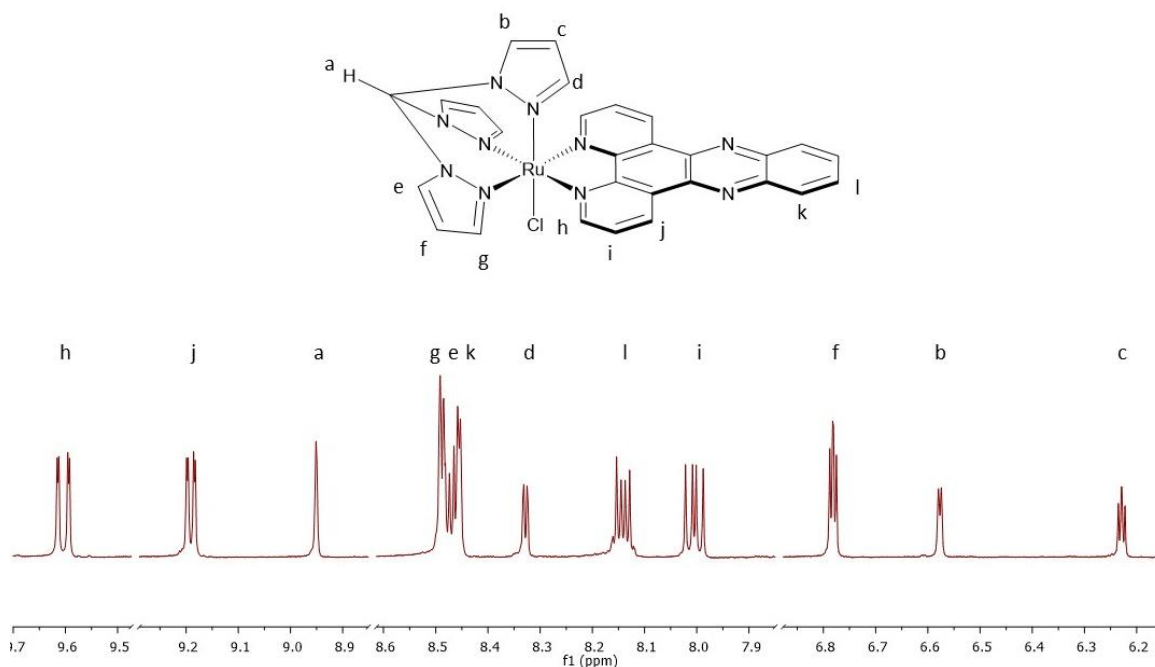


Figure 2.6 The assigned ^1H NMR spectrum of $[\text{Ru}(\text{tpm})(\text{dppz})(\text{Cl})]^+$. Cuts inserted between 6.9-7.8, 8.6-8.8, and 9.3-9.5 ppm for clarity.

2.3 Design of linking ligand

To attach the complex to AuNPs, a linking ligand must be designed that has high affinity for both the complex and the AuNPs. Pyridine and derivatives bind strongly to Ru, and thiols bind strongly to AuNPs. Therefore, a ligand functionalised with each of these groups is the target. A spacer in between the two groups is also necessary, as if the pyridine is too close to the thiol, the AuNP may impede DNA binding. Additionally, an ideal spacer group would be flexible, in order to allow the Ru complex to orientate itself

optimally for DNA binding. Although the nature of the spacer will be likely to affect any electronic or photonic communication between the AuNP and the complex, the initial plan was to design a system as proof of concept before precise tuning could take place.

The synthetic strategies used can be split into two groups. The first involves ruthenium complexes pre-attached to a thiolated ligand, which can then be exchanged directly onto AuNPs. This “all-in-one” method is the route that has been used in systems designed by the Gunnlaugsson and Pikramenou groups. The other, “two-halves” route, involves attachment of an organic linker to AuNPs. This can then be conjugated to a ruthenium complex functionalised with an appropriate reactive group. The “two-halves” route was used by the Lippard and Mirkin groups for their Pt (IV)-AuNP prodrugs (shown previously in figure 1.16),²⁵ and has also been used for attachment of biomolecules such as proteins to AuNPs.²⁶ As both of these examples uses amides to attach the substrate to the AuNP, this provides an obvious starting point for these investigations. These two methods are represented by cartoons in figure 2.8.

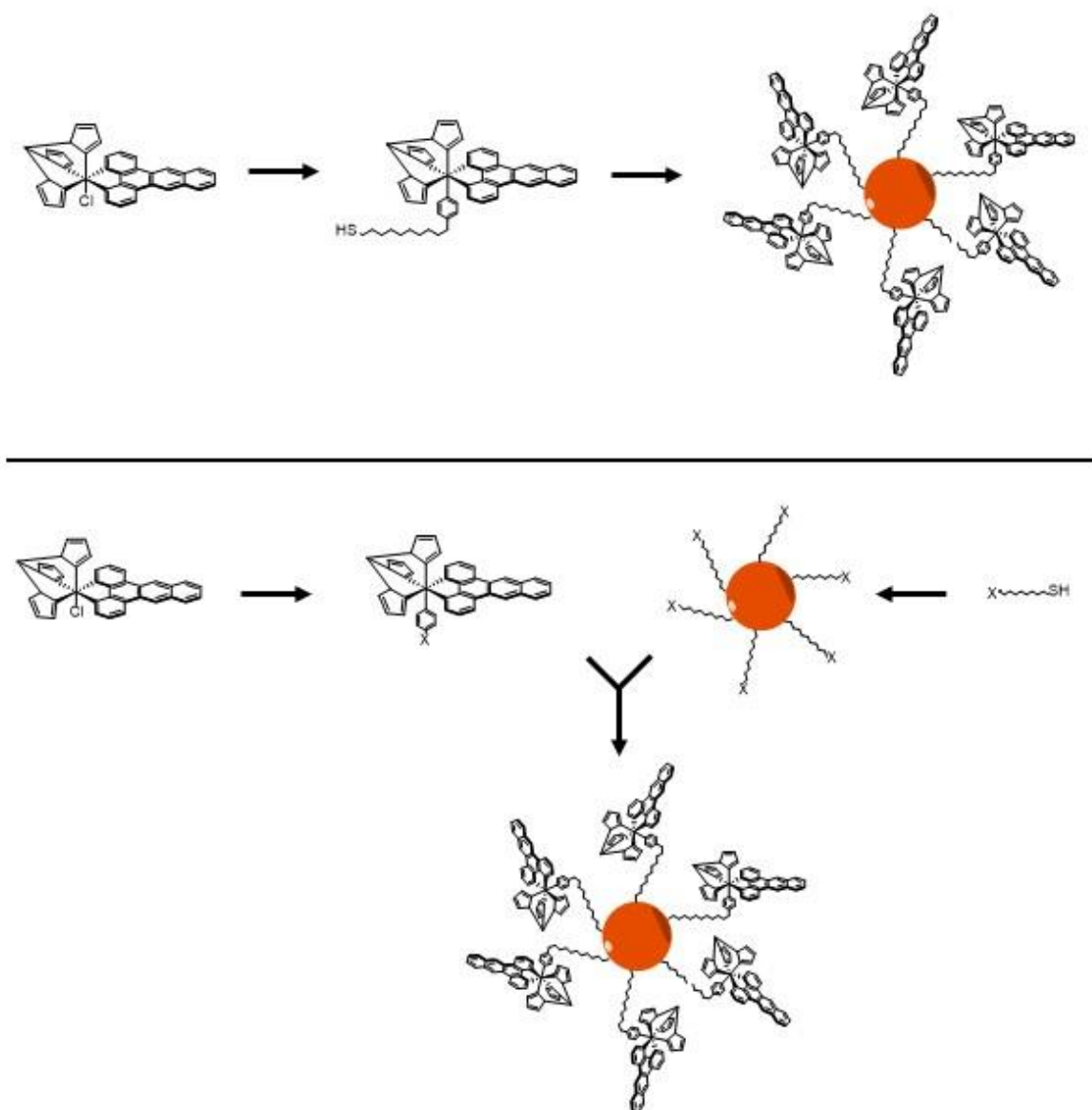


Figure 2.7 Cartoons representing the “all-in-one” (top) and “two-halves” (bottom) methods. Non-essential atom labels omitted for clarity.

2.4 “All-in-one” method

The first route attempted was based on the synthetic chemistry reported by the Gunnlaugsson group, in which racemic Ru (II) complexes were conjugated to AuNPs, by forming the amide of 5-amino-1,10-phenanthroline and 11-mercaptoundecanoic acid, using 1-ethyl-3-(3-dimethylaminopropyl)carbodiimide (EDC) as a coupling reagent. This functionalised phen ligand can then be co-ordinated to the appropriate $[\text{Ru}(\text{N}^{\wedge}\text{N})_2\text{Cl}_2]$ ($\text{N}^{\wedge}\text{N} = \text{bpy}, \text{phen}, \text{TAP}$) precursor. The complexes that were synthesised and the modified phen ligand are shown in figure 2.9.

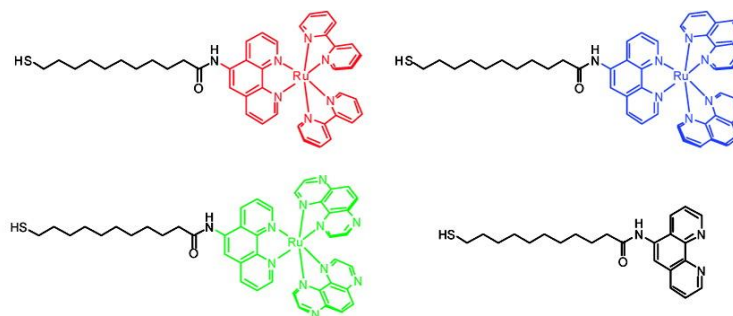


Figure 2.8 The three ruthenium tris-chelate complexes synthesised by the Gunnlaugsson group and the modified phenanthroline used for attachment to AuNPs. Figure adapted from ref. 1.

2.4.1 Gunnlaugsson Route

As discussed in section 1.4.2.3, small changes to the substitution site of ancillary ligands can have large effects on DNA binding affinity and mode. For instance, $[\text{Ru}(\text{tpm})(\text{dppz})(3\text{-NH}_2\text{Py})]^{2+}$ binds to DNA through intercalation, and with similar binding strength to the unsubstituted $[\text{Ru}(\text{tpm})(\text{dppz})(\text{py})]^{2+}$ complex. However, $[\text{Ru}(\text{tpm})(\text{dppz})(4\text{-NH}_2\text{Py})]^{2+}$ binds in the major groove at 25 °C, and binds with an affinity closer to that of $[\text{Ru}(\text{phen})_3]^{2+}$.⁶ Therefore, it was decided to synthesise both the 3- and 4-

substituted ligands, in order to further monitor this effect. The proposed method for the synthesis of the 3-substituted ligand, based upon the route used by the Gunnlaugsson group, is shown in scheme 2.7. The same method was to be used for the 4-substituted ligand.



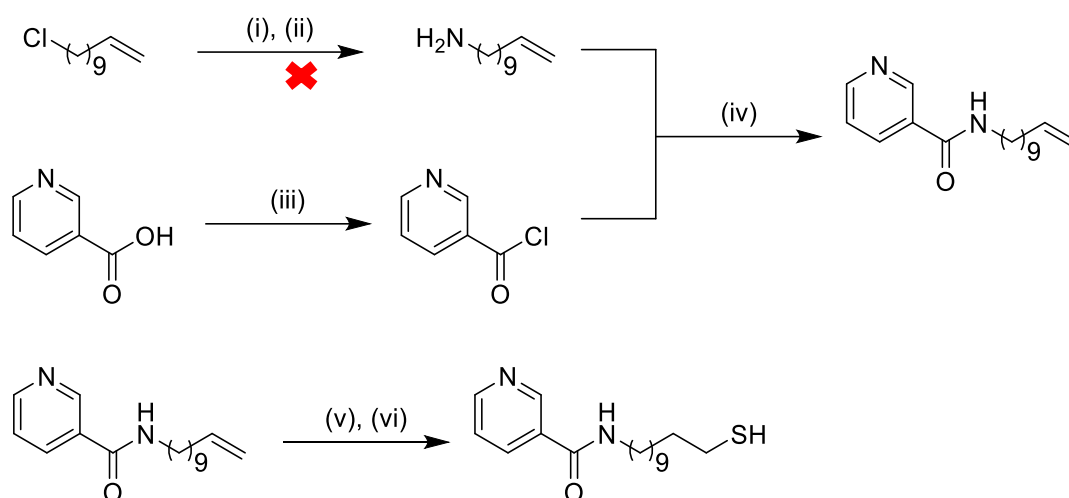
Scheme 2.7 (i) EDC, DMAP, DCM, 0 °C, 1 hr, RT, 24 hrs

Analysis of the solid gathered by NMR and mass spectrometry showed no evidence of product formation. It is possible that some product was generated but did not precipitate. As there are several examples in the literature of successful reactions involving similar substrates, alternative procedures could have been used for the synthesis. For example, the Tron group have shown a general synthetic procedure for synthesis of a combinatorial library of similar pyridines and acids to the one used in this reaction.²⁷

2.4.2 Acid Chloride Route

As the previous route was unsuccessful, it was decided to attempt to synthesise the same ligand, but through a more active acid chloride. From examining available starting materials and reagents, the direction of the amide was reversed (the carbonyl adjacent to the pyridine ring, rather than the nitrogen), for ease of synthesis. The proposed route was to begin with a long chain alkane, functionalised with chloride at one end, and an alkene at the other. The chloride would then be converted to an azide, reduced to an amine using a Staudinger reduction,²⁸ and then reacted on with the acid chloride of nicotinic acid (3-

substituted) and isonicotinic acid (4-substituted) to introduce the pyridine moiety. The alkene was to be conjugated to thioacetic acid using thiol-ene click chemistry.²⁹ Thiol-ene click chemistry uses a thermally activated radical initiator, in this case azobisisobutyronitrile (AIBN), to create a self-propagating radical addition cycle. Thioacetate acts as a protecting group for the thiol, preventing oxidation or formation of disulfides. The thioacetate would then be converted to the thiol using NaOH. The route is shown in scheme 2.8.



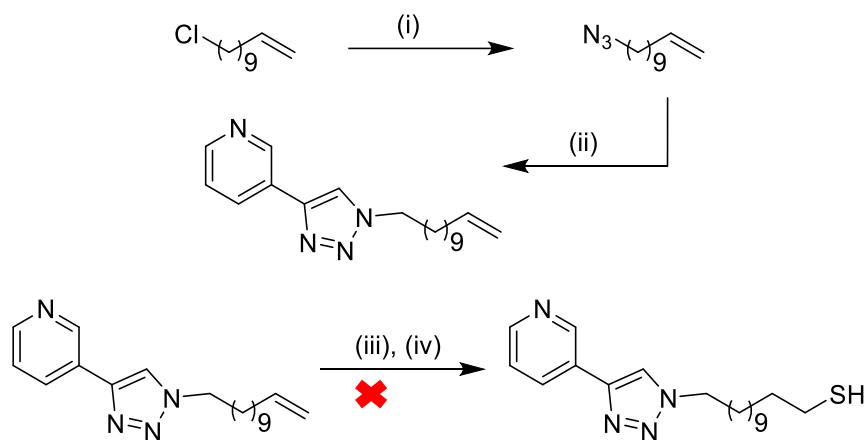
Scheme 2.8 (i) NaN_3 , TBAI, DMF, 50 °C, 14 hrs; (ii) PPh_3 , H_2O , THF, RT, 18 hrs; (iii) SOCl_2 , reflux, 4 hrs; (iv) DCM, dropwise addition, 0 °C \rightarrow RT, 4 hrs; (v) AIBN (cat.), THF, reflux, 24 hrs; (vi) NaOH (10 eq.), EtOH, RT, 4 hrs

When this scheme was attempted experimentally, conversion to the azide was confirmed by NMR and IR, which confirmed the strong IR absorption of azides at around 2000 cm^{-1} . However, both IR and mass spectrometry suggested that the use of the Staudinger reduction to generate the amine was unsuccessful. It is not clear why this was the case. A possible cause is oxidation of triphenylphosphine to triphenylphosphine oxide, however ^{31}P NMR showed that the starting PPh_3 was essentially pure, ruling out this

out. Although the literature shows the Staudinger reduction has been used for a variety of applications, several colleagues working in synthetic organic groups have said they have had mixed experiences with the reaction. It was therefore decided to use the azide synthesised for other routes, rather than trying to deduce the exact problem with the reaction.

2.4.3 Copper-catalysed Azide-Alkyne Click Reaction

As an appropriate azide had been synthesized, the next proposed route utilised this compound in a copper-catalysed azide-alkyne cycloaddition (CuAAC) reaction. This was simply achieved through changing the nicotinic acids for 3-ethynylpyridine. This route is based upon a related procedure used by the Gasser group, in which an azide functionalised peptide is added to a rhenium complex containing a coordinated 3-ethynylpyridine ligand.³⁰ The thiol group could then be introduced as described in section 2.3.2. The proposed reaction scheme is shown in scheme 2.9. Although the click reaction was successful, the thiol-ene click reaction was unsuccessful, as there was no change in the integrals of the alkene peaks relative to the alkane peaks in the ¹H NMR.



Scheme 2.9 (i) NaN_3 , TBAI, DMF, 50 °C, 14 hrs; (ii) 3-ethynylpyridine, CuSO_4 , tris(benzyltriazolylmethyl)amine (TBTA), sodium ascorbate, $\text{H}_2\text{O}:\text{MeCN}$ (1:1), RT, 6 hrs; (iii) AIBN (cat.), THF, reflux, 24 hrs; (iv) NaOH (10 eq.), EtOH, RT, 4 hrs

To determine if the issue was due to the thiol-ene click reaction, the synthetic route was reversed. The thioacetate would be introduced first, followed by the azide, and finally the click reaction to attach the pyridine. This time, although the thiol-ene reaction was successful, the introduction of the azide failed.

The likely cause of problems with this synthetic route is cross-reactivity between the two functionalisation steps. As previously mentioned, thiol-ene click chemistry is driven through free radical chemistry. Azides can be active towards radicals, and so various side reactions become available.³¹ When the thioacetate is introduced first, a possible reason for the failure of the reaction is nucleophilic attack of the carbonyl by the azide. This is a feature of some named organic reactions, such as the Schmidt reaction³².

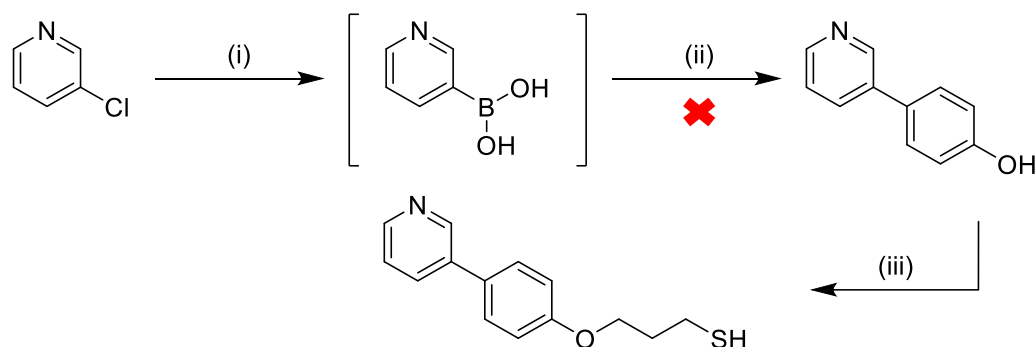
2.4.4 Suzuki-Miyaura Route

Due to the problems posed by the previous synthetic routes, it was decided to design a new route based upon other work on Ru-AuNP conjugates.

The next proposed synthetic route was partially inspired by the ligand used in the work by the Pikramenou group. They began with 4,4'-dihydroxy-2,2'-bipyridine, and then reacted that with alkene-terminated haloalkane, followed by introduction of a thiol using the method previously shown in scheme 2.8 (v) and (vi).

A synthetic route that used Suzuki-Miyaura cross coupling to introduce a pyridine group to 4-chlorophenol was employed. A short chain haloalkane with a thiol group could

then be added through a simple S_N2 reaction; this route is shown below in scheme 2.10. The cross coupling reaction uses a method developed by the Dreher group, using two aryl chlorides in a one-pot reaction.³³ The first aryl chloride is converted *in situ* to the boronic acid, followed by subsequent addition of the second aryl chloride to complete the reaction.



Scheme 2.10 (i) Pd(OAc)₂, 2-dicyclohexylphosphino-2',4',6'-triisopropylbiphenyl, B₂(OH)₄, KOAc, Na^tBu, EtOH, reflux, 2 hrs; (ii) 4-chlorophenol, K₂CO₃, reflux, 15 hrs; (iii) 3-chloropropane-1-thiol, K₂CO₃, EtOH:H₂O, 4 hrs

Although the NMR and mass spectrometry of the crude cross-coupled product suggested the reaction had been successful, purification by either column chromatography or HPLC gave several small fractions, none of which were identifiable as the desired compound. Initially it was thought that the 4-(pyridin-3-yl)phenol intermediate must therefore be unstable, and the route was therefore abandoned, due to the discovery of a viable alternative. However, a recent paper from the Chen group synthesises the desired compound, using a similar procedure, but using a ferrocene based Pd catalyst.³⁴ Future studies could therefore re-start investigations into this route.

2.4.5 Oligoethylene glycol route

2.4.5.1 Linking ligand Synthesis

A survey of the literature led to the discovery of previous work by the Yam group, investigating energy transfer from Ru (II) and Re (I) polypyridyl complexes with AuNPs.³⁵ One of the linkers used in this study was functionalised with a pyridine and a thiol at each end of the ligand, fitting the requirements of our system. Figure 2.10 shows the relevant complexes from in the Yam study, and scheme 2.11 shows the synthetic route to the ligand.

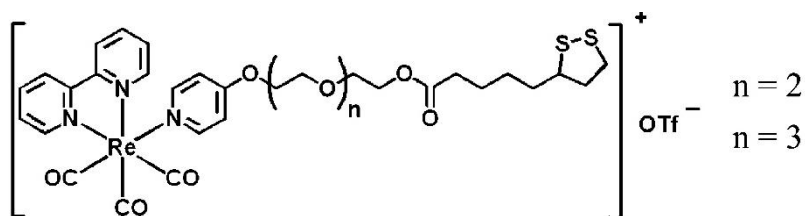
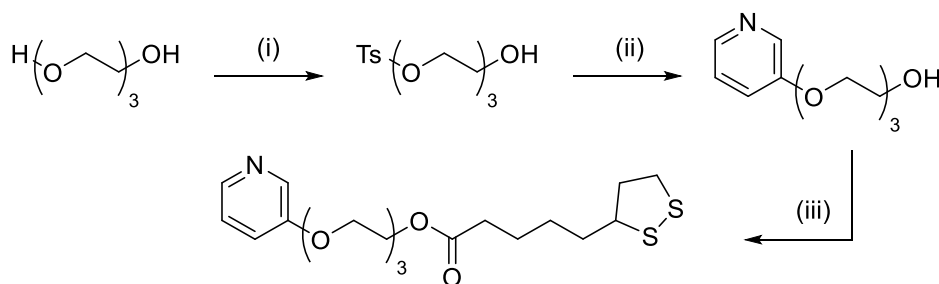


Figure 2.9 The rhenium (I) complexes used the Yam study. Figure adapted from reference 35.



Scheme 2.11 (i) Ag₂O, TsCl, KI_(cat.), DCM, 0 °C, 5 mins; (ii) 3-hydroxypyridine, K₂CO₃, MeCN, reflux, 24 hrs; (iii) lipoic acid, EDC, DMAP, DCM, 0 °C, 1 hr, RT, 24 hrs

The synthesis began with the monotosylation of triethylene glycol, achieved using the procedure developed by the Sauv e group.³⁶ The selectivity is thought to be achieved

through internal hydrogen bonding promoted by the K^+ ions. This leaves a single proton available for abstraction by Ag_2O , which is a weak base.

The monotosylate is then reacted with 3-hydroxypyridine, in the presence of a mild base, in order to selectively introduce the pyridine at a single end of the molecule. The thiol is then introduced by addition of lipoic acid, a naturally occurring carboxylic acid containing a 1,2-dithiolane group. EDC is used as the coupling reagent.

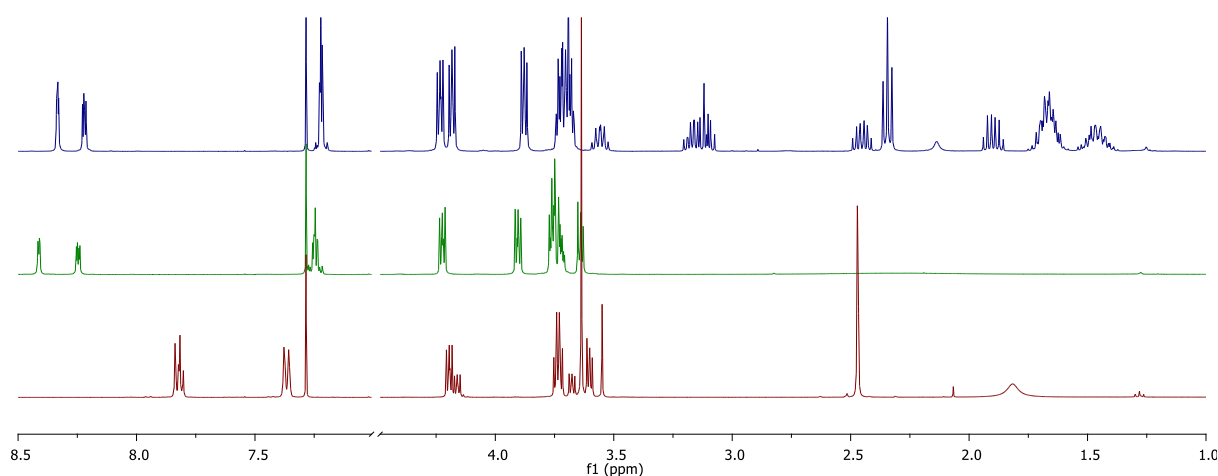


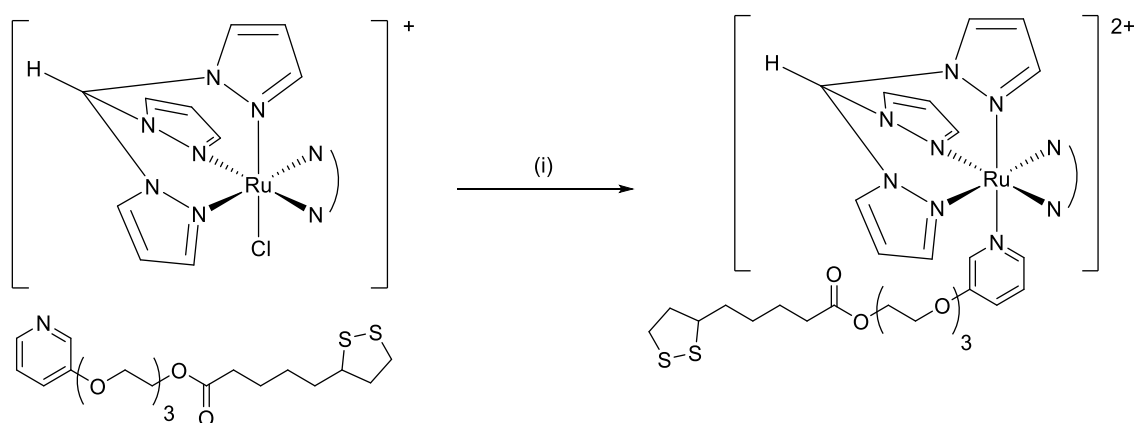
Figure 2.10 Stacked 1H NMR spectra of candidate linker. Red = TsO—OH; green = 3-Py—OH; blue = 3-Py—1,2-dithiolane

The product was characterised by 1H NMR and ESI-MS. In the 1H NMR spectra, there is a central grouping of protons from the ethylene groups. After tosylation, a signal representing the protons adjacent to this functionality move downfield from the central group. Additionally, a pair of doublets appear in the aromatic region of the spectrum, as well as a singlet at around 2.5 ppm from the methyl group. When the pyridine is introduced, these signals are removed, and there are several new peaks in the aromatic region. Two of these are more deshielded than the others, and can be attributed to the

protons adjacent to the pyridine nitrogen. The other two protons are represented by a multiplet at 7.2 ppm. Following attachment of the dithiolane, several peaks appear upfield from the central group which can be attributed to the methylene groups of lipoic acid. ESI-MS showed a singly charged peak at 416 m/z $[M+H]^+$.

2.4.5.2 Complex synthesis

The next step was to co-ordinate the ligand to the complex. This was attempted by refluxing in acetone using silver triflate to abstract the axial chloride, as shown in scheme 2.12.



Scheme 2.12. (i) AgOTf, acetone, reflux, 8 hrs ($N^N = dppz$)

LC-MS showed a peak at 506.6 m/z, corresponding to the doubly charged target complex with loss of counter ions. The 1H NMR spectrum of the crude product suggested the presence of several $[Ru(tpm)(dppz)(L)]$ -based species. Following purification by column chromatography, two ruthenium containing bands were obtained. Analysis of the fractions revealed that neither were the target compound. One of the fractions contained only $[Ru(tpm)(dppz)(Cl)]^+$, confirmed by 1H NMR and LC-MS. The other fraction

showed shifts in the aromatic peaks, however, no additional signals were present, as shown in figure 2.12. LC-MS showed a mono-cation with mass of 641.1 m/z (compared with 633.1 m/z for the starting material). The change in LC-MS signals suggests degradation of the target complex, followed by co-ordination of an NMR silent cation in the axial site, however, examination of the masses of obvious candidates, such as OTf^- from the reaction, and NO_3^- from the column, as well as solvents involved in the synthesis and purification, did not provide any matches. Similar loss of product, and resultant spectra were observed when other purification methods, such as charge separation chromatography were attempted. Use of other solvent mixes, such as EtOH:H₂O mixes, or DMF, as well as other silver salts, such as AgNO₃, also did not noticeably improve the synthesis of the product.

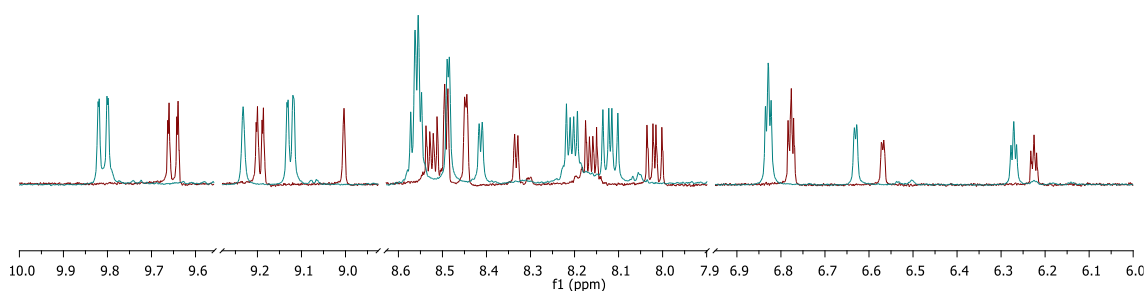


Figure 2.11 ¹H NMR spectra of the starting material fraction (red) and the second, unidentified fraction (blue). Cuts inserted between 7.0-7.9, 8.7-9.0, 9.3-9.6 ppm for clarity.

2.5 “Two-halves” method

As several synthetic routes from the “all-in-one” method had been attempted, and problems were found in both synthesis and co-ordination of the linker, it was decided to attempt a new synthetic method using the “two-halves” method. There were two advantages to this method that seemed immediately apparent. Firstly, the co-ordination

of small, simply functionalised pyridines had been more extensively explored in previous work within the group. Secondly, the potential for steric hindrance during coordination from the long, flexible tails of the “all-in-one” style ligands would be removed.

2.5.1 Amide route

As amide coupling is frequently used for attachment to AuNPs, the first synthetic route investigated involved the co-ordination of pyridines functionalised with carboxylic acids. A linker functionalised with an amine at one end, and a thiol at the other could then be attached to AuNPs. The synthetic route towards the linker would be based on procedures developed by the Wandrey group for the synthesis of heterobifunctional poly(ethylene glycol) derivatives.³⁷

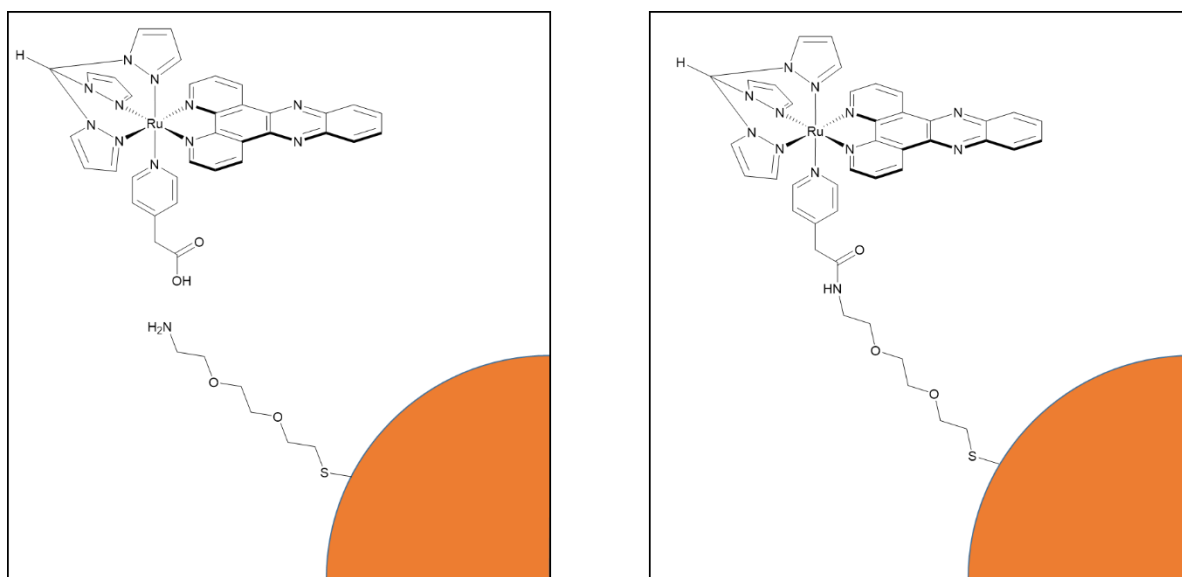
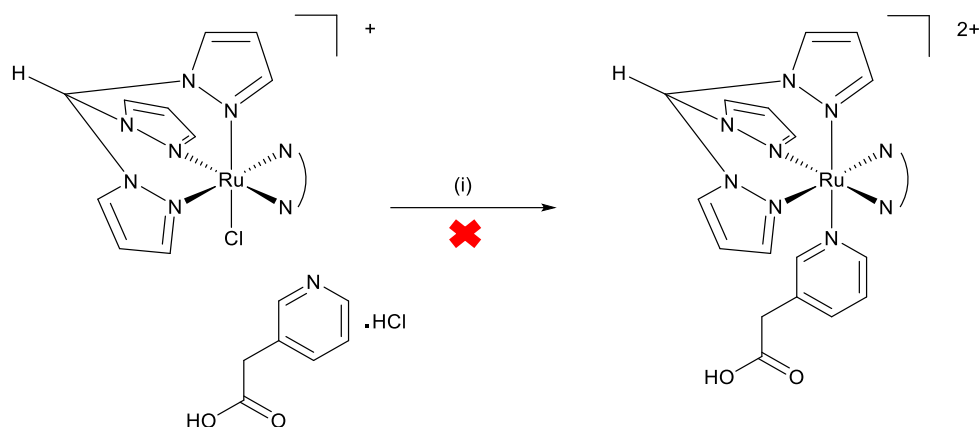


Figure 2.12 Diagram to show the components required to assemble the amide linked system (left), and the proposed final Ru-AuNP conjugate (right).

2.5.1.1 Complex syntheses

3- and 4-pyridyl acetic acid hydrochloride were refluxed with $[\text{Ru}(\text{tpm})(\text{dppz})(\text{Cl})][\text{PF}_6]$ and AgNO_3 in $\text{EtOH}:\text{H}_2\text{O}$ (3:1) for six hours, as shown in scheme 2.13. Triethylamine was used as a base to neutralise the HCl salt.



Scheme 2.13 (i) AgNO_3 , $\text{EtOH}:\text{H}_2\text{O}$ (3:1), reflux, 6 hrs ($\text{N}^{\wedge}\text{N} = \text{dppz}$)

In the case of the 3-substituted pyridine, no reaction was observed. LC-MS showed two major peaks - one singly charged at 633.1 m/z, corresponding to the starting material, and another doubly charged at 299.0 m/z, corresponding to $[\text{Ru}(\text{tpm})(\text{dppz})]^{2+}$. No peaks that could be attributed to the product ($[\text{M}-2\text{PF}_6]^{2+} = 367$ m/z; $[\text{M}-2\text{PF}_6-\text{H}]^+ = 734$ m/z) could be observed. As previously, a range of other solvents and silver salts were tried, with no improvement. It is not clear why the reaction was unsuccessful. The methylene bridge between the carboxylic acid and the pyridine should insulate most, if not all, of any electron withdrawing effects, regardless, pyridines with amides directly attached to the ring have been previously co-ordinated to the same ruthenium precursor complex.³⁸

In the case of the 4-substituted pyridine, in addition to the peaks attributed to starting material with and without chloride, there was another peak at 345.0. This peak matched the mass of $[\text{Ru}(\text{tpm})(\text{dppz})(\text{pic})]^{2+}$, (pic = picoline), where the picoline was generated *in situ* by decarboxylation of the pyridine. Methyl groups are electron donating, picoline will be better able to co-ordinate to the ruthenium centre. As decarboxylation is typically thermally driven, the reaction was tried at lower temperatures, however, no reaction was observed.

It was not initially apparent why only the 4-picoline was observed, until a literature search found a journal article from 1971 investigating the thermal and photo-decarboxylation of 2-,3- and 4-pyridyl acetic acids.³⁹ It was found that 2- and 4-pyridyl acetic acids were easily decarboxylated at elevated temperatures, whereas for 3-pyridyl acetic acid, no decarboxylation was observed. This difference in reactivity was attributed to resonance stabilisation of intermediate, as shown in figure 2.14.

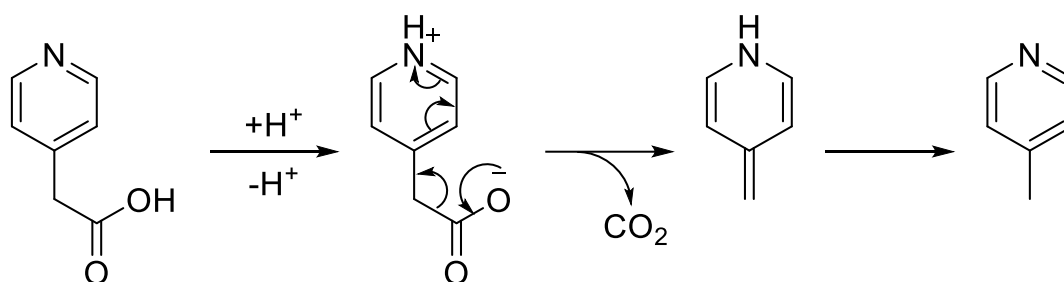


Figure 2.13 Resonance stabilised thermal decarboxylation of 4-pyridyl acetic acid

2.5.2 Reductive amination route

As it did not seem possible to attach the required carboxyl functionalised pyridines to the parent ruthenium complex, other alternatives were explored. Co-ordination of pyridines functionalised with aldehydes had already been achieved in previous work in the group, therefore, imine chemistry was proposed as a candidate.³⁸ Formation of imines has been used in functionalisation of nanomaterials.⁴⁰ Imine formation is reversible, but can be trapped in a reductive amination using a mild reducing agent such as sodium triacetoxyborohydride or sodium cyanoborohydride.

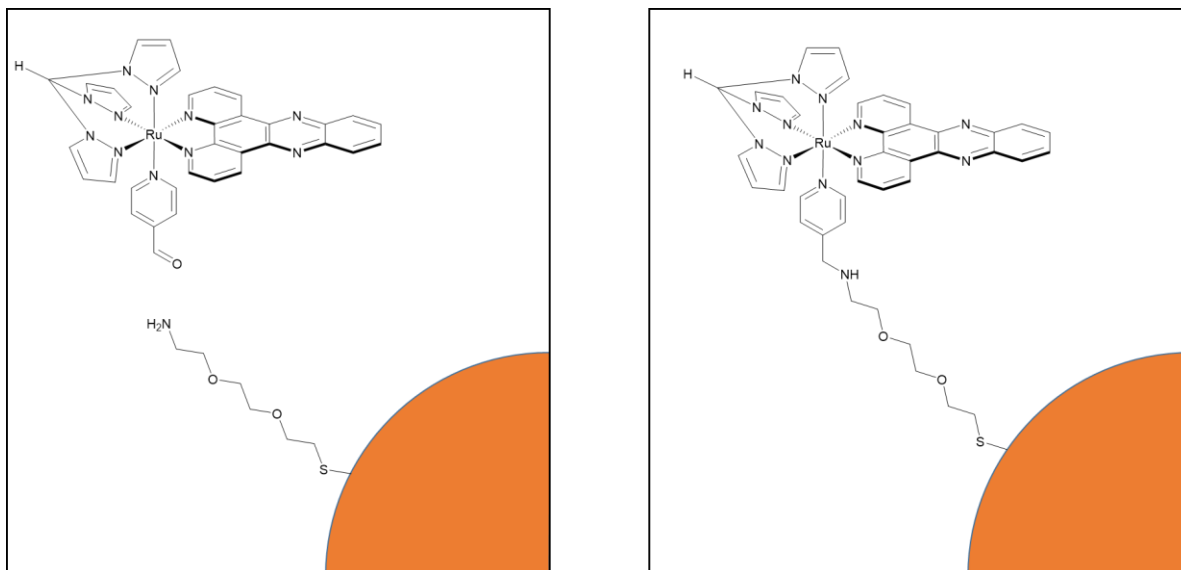
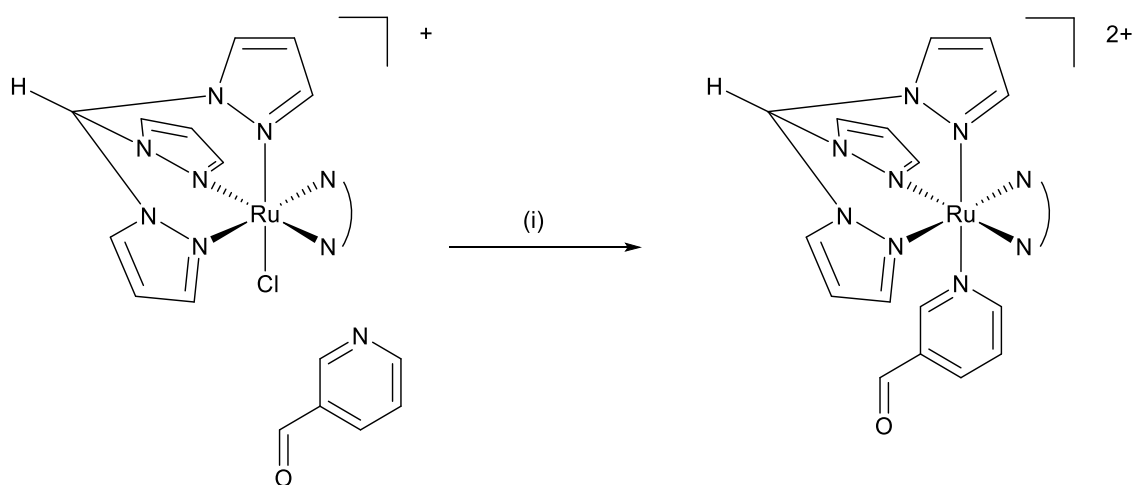


Figure 2.14 Diagram to show the components required to assemble the amine linked system (left), and the proposed final Ru-AuNP conjugate (right).

2.5.2.1 Complex synthesis

$[\text{Ru}(\text{tpm})(\text{dppz})(3\text{-CHOpy})][\text{PF}_6]^{2+}$ and $[\text{Ru}(\text{tpm})(\text{dppz})(4\text{-CHOpy})][\text{PF}_6]^{2+}$ were synthesised by refluxing the parent ruthenium complex with 3- or 4-pyridinecarboxylaldehyde and AgNO_3 in $\text{EtOH}:\text{H}_2\text{O}$ (3:1), and, following purification by column chromatography over silica gel, the ^1H NMR spectrum and mass

spectrometry data were in accordance with previous work.³⁸ The yields from this work were lower than in previous work (29 % cf. 56 % for the 3-substituted and 36 % cf. 90 % for the 4-substituted). The reduction in yield can be explained by the need for additional purification in this work, however, yields of between 30 % and 50 % are typical for reactions of this sort, based upon experience in the group.



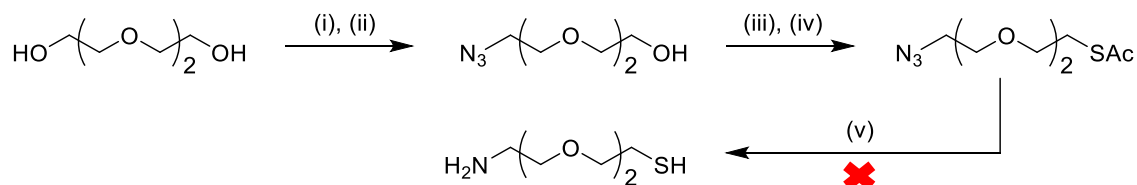
Scheme 2.14 (i) AgNO_3 , $\text{EtOH:H}_2\text{O}$ (3:1), reflux, 6 hrs ($\text{N}^{\wedge}\text{N}$ = dppz)

2.5.2.2 Amino-thiol linker

The amino-thiol linker was to be synthesised using an adapted version of the procedure developed by the Wandrey group for the synthesis of heterobifunctional poly(ethylene glycol) derivatives.³⁷ The alterations were necessary due to the original methods being designed for long poly(ethylene glycol) polymers ($\text{MW} \sim 1500 \text{ g mol}^{-1}$). Many of the steps to isolate and purify the products involved precipitation and washing, which would not be possible with the short chain used for this reaction.

Triethylene glycol would be selectively mono-tosylated using the method described in section 2.4.5.1. An azide could then be introduced through a simple $\text{S}_{\text{N}}2$ substitution.

The other end of the molecule could then be tosylated, followed by a second substitution to introduce a thioacetate. The azide would then be reduced to the amine using PPh_3 in a Staudinger reduction. The synthetic route is shown in scheme 2.15.



Scheme 2.15 (i) Ag_2O , TsCl , $\text{KI}_{(\text{cat.})}$, DCM , $0\text{ }^\circ\text{C}$, 5 mins; (ii) NaN_3 , DMF , $90\text{ }^\circ\text{C}$, 18 hrs; (iii) TsCl , NEt_3 , DCM , $0\text{ }^\circ\text{C}$, 1 hr \rightarrow RT, 18 hrs; (iv) HSAc , NEt_3 , EtOAc , $0\text{ }^\circ\text{C}$, 1 hr \rightarrow RT, 24 hrs; (v) NaOH (10 eq.), EtOH , RT, 4 hrs

All synthetic steps up to the final reduction were successful, and were characterised by ^1H NMR and ESI-MS. The ^1H NMR spectra are shown in figure 2.16. The main ethylene protons are found in the multiplets between 3.6-3.8 ppm. In the spectrum shown in red, the protons adjacent to the azide are represented by the triplet at 3.4 ppm. After tosylation, a pair of doublets appear at 7.4 and 7.8 ppm - see the spectrum shown in green - as well as a singlet at around 2.5, which can be attributed to the methyl group of the tosylate. A triplet also moves downfield from the main ethylene group, which are the protons adjacent to the tosylate group. When the thioacetate is introduced, the tosylate protons are then removed, and the triplet adjacent shifts upfield, as sulfur is less electron withdrawing than oxygen. The methyl group from the thioacetate can also be observed at around 2.3 ppm. Although all attempts at the Staudinger reduction were unsuccessful, the synthetic route developed to the azide will be used in later strategies.

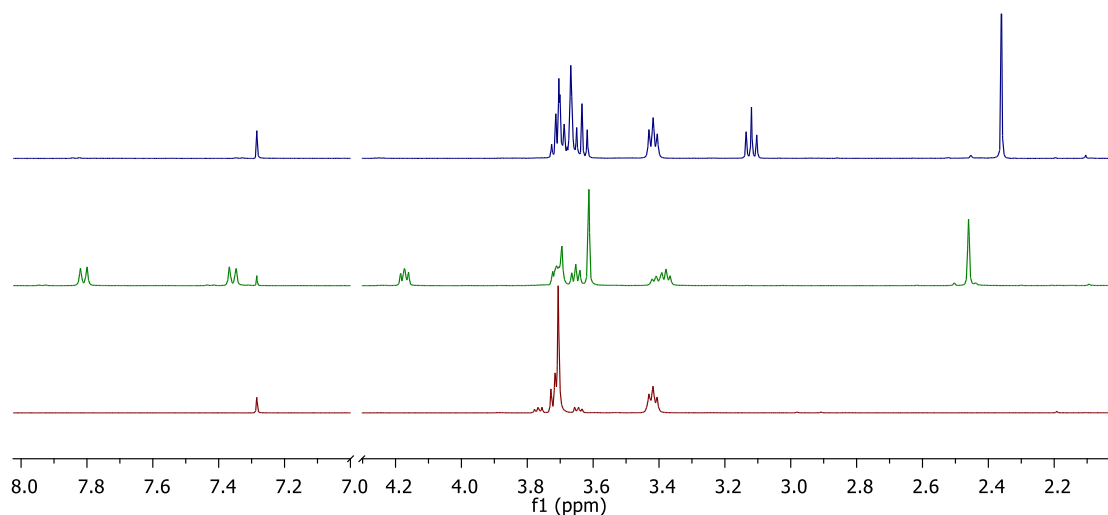


Figure 2.15 Stacked ^1H NMR spectra of intermediates in attempted synthesis of amino-thiol terminated linker. Red = $\text{N}_3\text{—OH}$, green = $\text{N}_3\text{—OTs}$, blue = $\text{N}_3\text{—SAc}$. Cut inserted between 4.3-7.0 ppm for clarity.

2.5.3 Copper catalysed azide-alkyne click route

As the route to azide-thiol terminated linker had already been developed in the previous route, the next step was to co-ordinate alkyne substituted pyridines to the parent ruthenium complex, shown in figure 2.17. Synthesis of both the 3- and 4- substituted pyridines were attempted by refluxing with the $[\text{Ru}(\text{tpm})(\text{dppz})(\text{Cl})][\text{PF}_6]$ and AgNO_3 in $\text{EtOH}:\text{H}_2\text{O}$ (3:1) as shown in scheme 2.16.

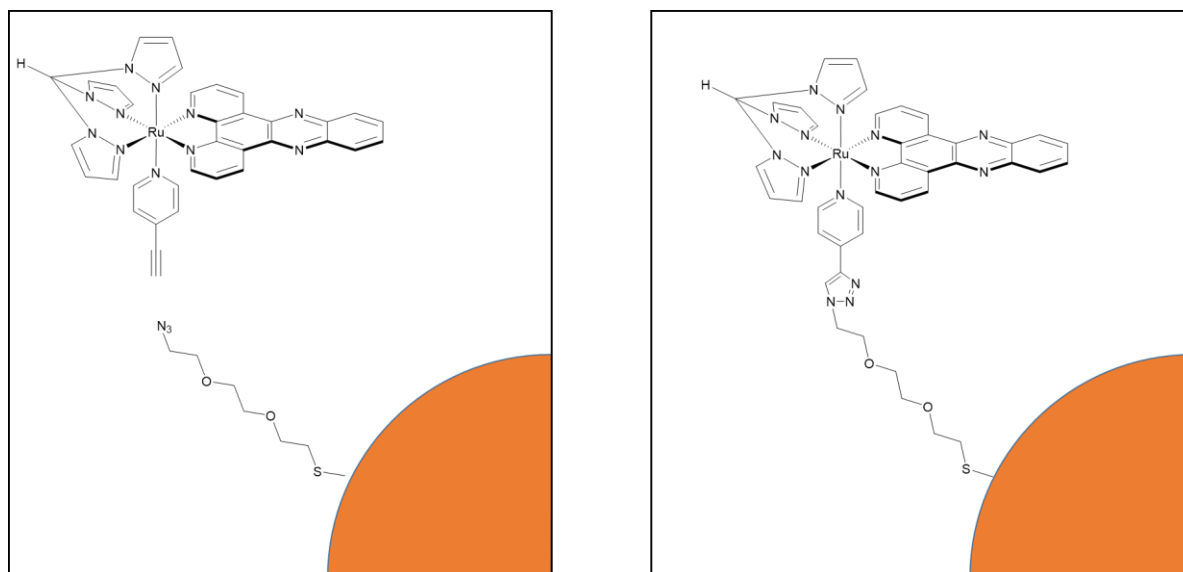
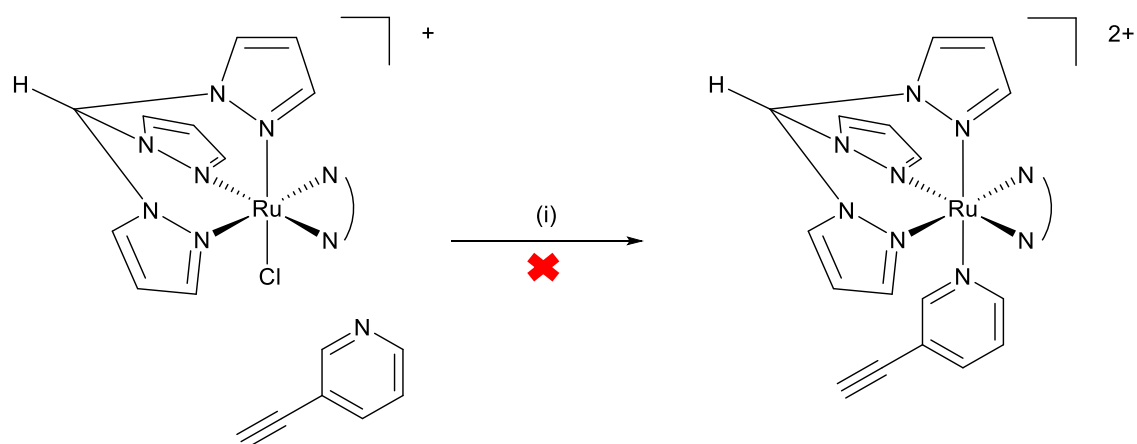


Figure 2.16 Diagram to show the components required to assemble the azide-alkyne click coupled system (left), and the proposed final Ru-AuNP conjugate (right).



Scheme 2.16 (i) AgNO_3 , $\text{EtOH:H}_2\text{O}$ (3:1), reflux, 6 hrs ($\text{N}^{\wedge}\text{N}$ = dppz)

No product was observed in either case, although, when 4-ethynyl pyridine was used, a singly charged peak was observed in the LC-MS at 205 m/z. This matched the mass of the protonated, homocoupled bisacetylene, shown in figure 2.18. Glaser coupling is a

versatile reaction which uses catalytic Cu (I) to generate 1,3-diynes,⁴¹ and some work has shown that silver nitrate based catalysts can also be used to achieve these products.⁴²

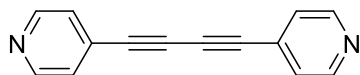
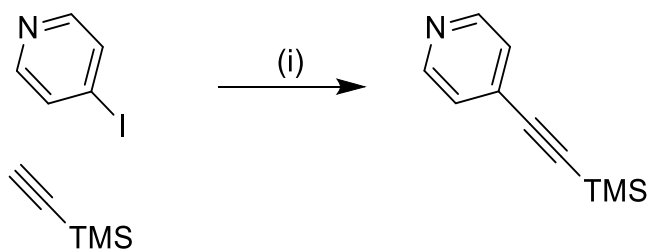


Figure 2.17 Homocoupled reaction by-product observed in the LC-MS

The reaction proceeds through formation of an acetylide complex, therefore, protection of the terminal proton should prevent dimerisation. TMS-protected 4-ethynylpyridine was therefore synthesised by a Sonogashira coupling between 4-iodopyridine and ethynyltrimethylsilane, as shown in scheme 2.17.



Scheme 2.17 (i) $[\text{Pd}(\text{PPh}_3)_4]$, CuI, DIPEA, THF, RT, 72 hrs

Synthesis of the protected product was confirmed by ^1H NMR and ESI-MS. Coordination to $[\text{Ru}(\text{tpm})(\text{dppz})(\text{Cl})][\text{PF}_6]$ was, however, still unsuccessful. To try to force the reaction, microwave synthesis was also attempted. Microwave reactors can achieve much higher temperatures and pressures than conventional synthesis, and so the

likelihood of passing any kinetic or thermodynamic barriers is greatly increased. Even under microwave irradiation, however, the reaction was still unsuccessful.

2.5.4 Second amide route

2.5.4.1 Complex synthesis

A new synthetic route was devised, in which a carboxylic acid functionalised thiol would be coupled to a ruthenium complex with an amino-pyridine in the axial position. Co-ordination of the pyridine will reduce electron density, and so should help to mitigate the problems found with the route described in section 2.4.1. Additionally, a methylene group would be added between the pyridine and amine to break any electronic conjugation. The anticipated route is shown in figure 2.19.

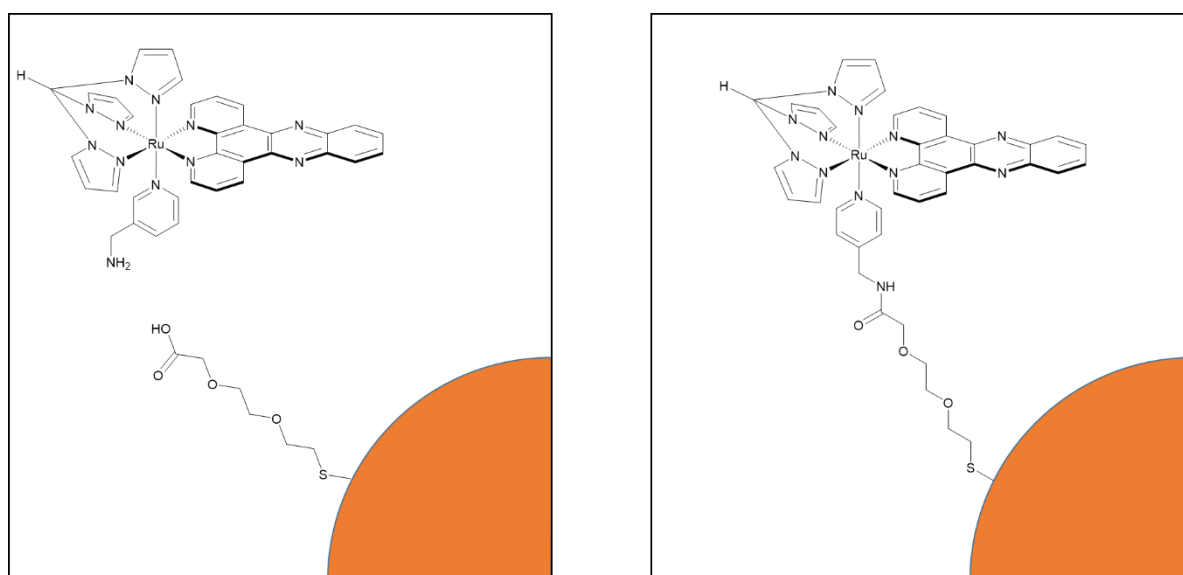
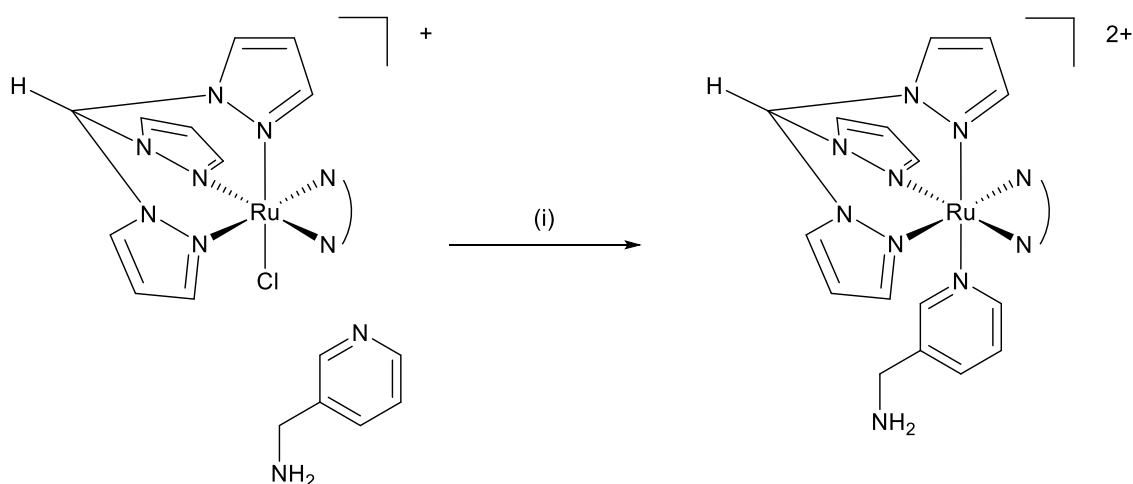


Figure 2.18 Diagram to show the components required to assemble the second amide linked system (left), and the proposed final Ru-AuNP conjugate (right).

The ruthenium complex was synthesised by refluxing 3-picoylamine with [Ru(tpm)(dppz)(Cl)][PF₆] and AgNO₃ in EtOH:H₂O (3:1), as shown in scheme 2.18. ESI-

MS analysis of the crude product showed that there were two doubly charged peaks with 352.6 m/z, matching the expected molecular mass of the product. This is likely due to the axial ligand binding through either of the amine or pyridine ends. After purification, the two peaks were separated. They could be identified by comparison of their ^1H NMR spectra with that of the free ligand. The protons adjacent to the binding site should see a large upfield shift, due to the loss of electron density on the co-ordinated nitrogen. For the first band to elute, although it was not fully separated from the band that followed, there was clear loss of the peak corresponding to the methylene protons, indicating that this species was amine bound. The second showed large upfield shifts in the two protons adjacent to the pyridine nitrogen, and so was the desired product. The fully assigned ^1H NMR is shown in figure 2.20.



Scheme 2.18 (i) AgNO_3 , $\text{EtOH}:\text{H}_2\text{O}$ (3:1), reflux, 6 hrs ($\text{N}^{\wedge}\text{N}$ = dppz)

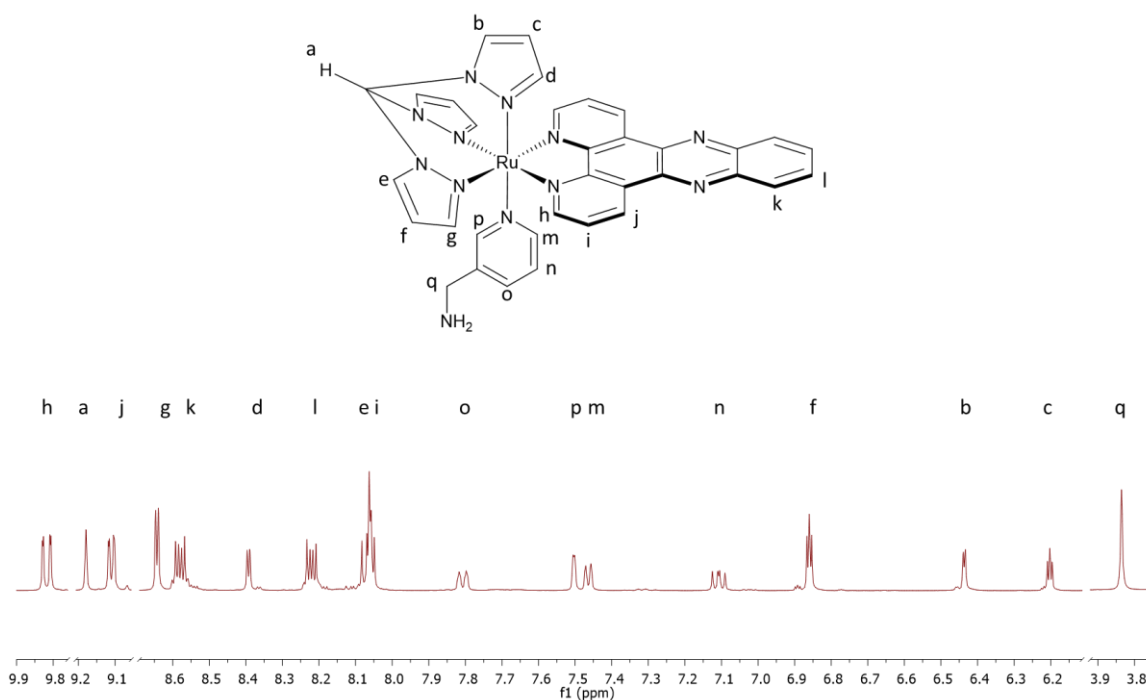
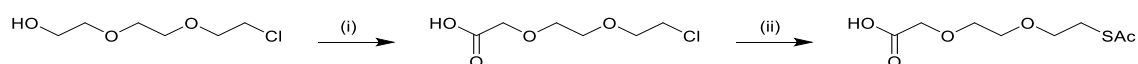


Figure 2.19 The assigned ^1H NMR of $[\text{Ru}(\text{tpm})(\text{dppz})(3\text{-NH}_2\text{MePy})]^{2+}$. Cuts inserted between 3.9-6.1, 8.7-9.1, 9.2-9.8 ppm for clarity.

2.5.4.2 Carboxylic acid-thiol linker

The linker was synthesised using 2-(2-(2-chloroethoxy)ethoxy)ethan-1-ol as the starting material. Firstly, the hydroxyl terminus was oxidised to the carboxylic acid, followed by substitution of the chloride terminus with a thioacetate to introduce a protected thiol. The thiol can be deprotected using $\text{NaOH}_{(\text{aq})}$ as a base. The synthetic route is shown in scheme 2.19.



Scheme 2.19 (i) TCCA, $\text{TEMPO}_{(\text{cat.})}$, NaBr , $\text{Na}_2\text{CO}_{3(\text{aq.})}$, acetone, $0\text{ }^\circ\text{C}$, 1 hr \rightarrow RT, 18 hrs; (ii) HSAc, K_2CO_3 , DMF, RT, 18 hrs

The oxidation step was initially performed using CrO_3 as the oxidising agent, however, this typically gave a distribution of unreacted alcohol, intermediate aldehyde and product that proved difficult to separate. Oxidation was instead performed using a method developed by the Porcheddu group, which uses trichloroisocyanuric acid (TCCA) with catalytic 2,2,6,6-tetramethyl-1-piperidinyloxy (TEMPO) and sodium bromide in acetone/water at room temperature. The reaction gave the desired product in 68 % yield, and no purification required post-workup. The thioacetate was then introduced by reaction with thioacetic acid and potassium carbonate, followed by purification by column chromatography over silica gel. The product was analysed by ^1H NMR and ESI-MS.

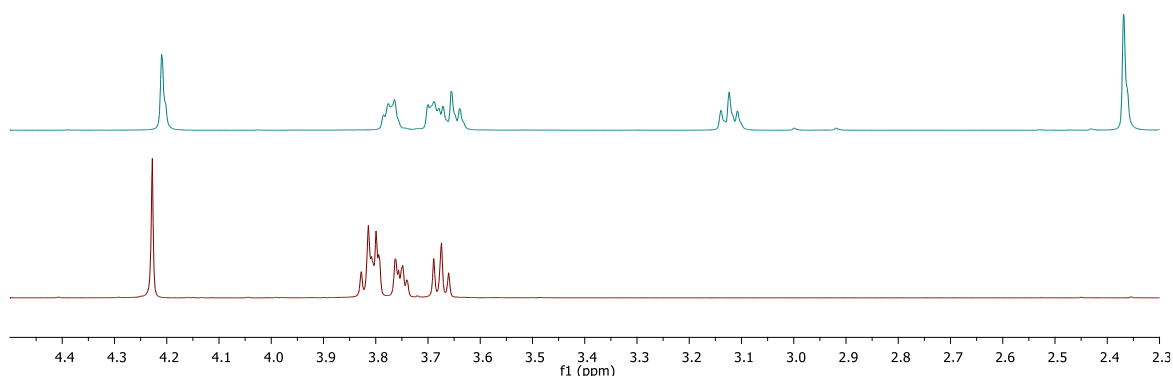
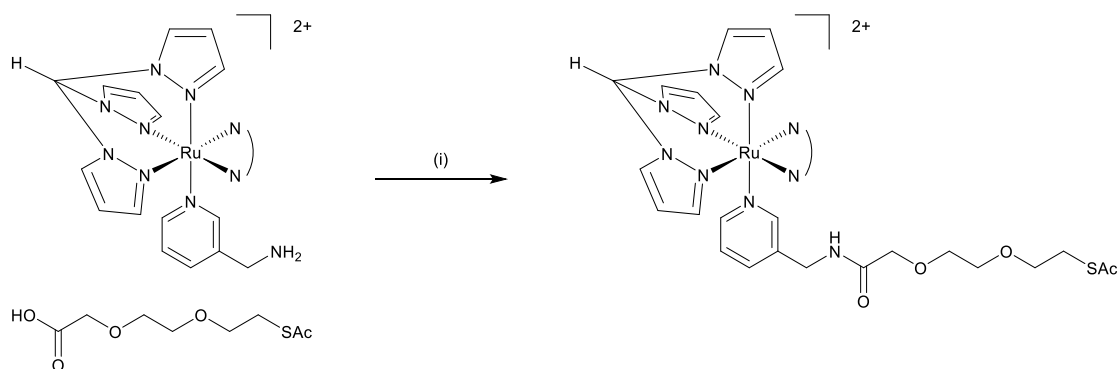


Figure 2.20 ^1H NMR spectra of COOH-Cl (red) and COOH-SAc (blue) linkers.

As with the linker described in section 2.5.2.2, there is a group of peaks in the ^1H NMR spectra around 3.8 ppm corresponding to the ethylene protons. On oxidation of the terminal hydroxide, a singlet appears downfield from the central group of protons. The singlet, and the lack of signals in the deshielded region of the spectrum confirm that no aldehyde is present. Introduction of the thioacetate group again shifted a triplet upfield, and also produced the singlet at 2.3 ppm corresponding to the methyl group. Analysis of

the ESI-MS spectrum gives two signals that could be assigned to the product, one at 223 m/z $[M+H]^+$, and 245 m/z $[M+Na]^+$.

An initial experiment to evaluate the connecting chemistry between $[Ru(tpm)(dppz)(3NH_2-MePy)]^{2+}$ and 2-(2-(2-(acetylthio)ethoxy)ethoxy)acetic acid was performed under standard amide coupling conditions, using EDC as the coupling reagent, and DIPEA as the base. The activated carboxylic acid was detected by mass spectrometry, however, there was no evidence of linkage to the terminal amine of the metal complex. Further work should aim to optimise this reaction. It could be beneficial to initially test the coupling before aminopyridine ligand is co-ordinated to the metal complex.



Scheme 2.20 (i) EDC, DIPEA, MeCN, RT, 18 hrs

It was also important to measure the photophysical and DNA-binding properties of the complex, in order to ensure the suitability of the system for use as a probe for DNA.

2.6 Characterisation

2.6.1 Crystallographic studies

Single crystals of $[\text{Ru}(\text{tpm})(\text{dppz})(3\text{-NH}_2\text{MePy})][\text{PF}_6]_2$ for X-ray diffraction were grown by slow diffusion of Et_2O into MeCN. Although the final refinement of the structure was 0.143, meaning that discussion of bond length or angles is not possible, the data shows that the final product has the expected, pyridine bound structure. The crystal structure of $[\text{Ru}(\text{tpm})(\text{dppz})(3\text{-NH}_2\text{MePy})]^{2+}$ is shown in figure 2.22.

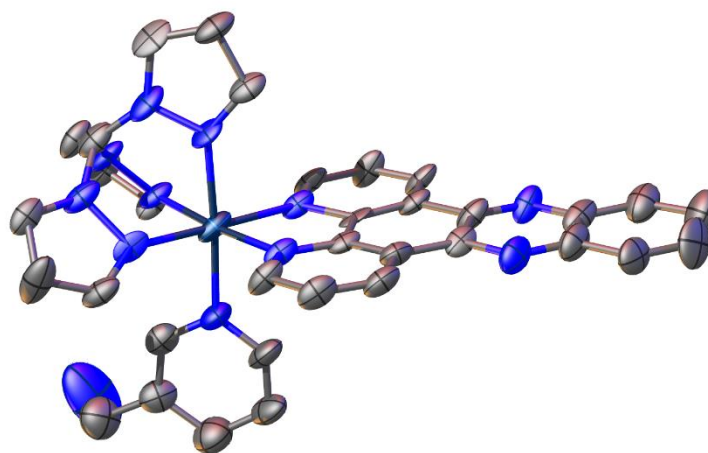


Figure 2.21 ORTEP diagram of $[\text{Ru}(\text{tpm})(\text{dppz})(3\text{-NH}_2\text{MePy})][\text{PF}_6]_2$. Hydrogen atoms, solvent molecules and counter ions omitted for clarity. Black = ruthenium, grey = carbon, blue = nitrogen.

$[\text{Ru}(\text{tpm})(\text{dppz})(3\text{-NH}_2\text{MePy})]^{2+}$ crystallised in a triclinic P-1 space group with two complexes, four counter ions, two Et_2O and one MeCN per asymmetric unit. The two complexes pack with the dppz long axis perpendicular to each other. This packing is shown in figure 2.23. Crystallographic data is provided in the appendix.

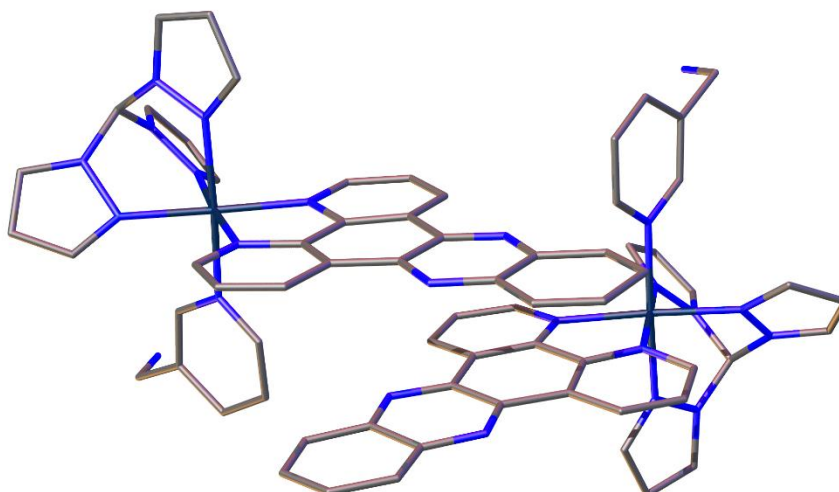


Figure 2.22 Wireframe diagram of 2 $[\text{Ru}(\text{tpm})(\text{dppz})(3\text{-NH}_2\text{MePy})]^{2+}$ units showing perpendicular packing of the dppz ligands. Hydrogen atoms, solvent molecules and counter ions omitted for clarity. Black = ruthenium, grey = carbon, blue = nitrogen.

2.6.2 UV-visible absorption

The extinction coefficient for $[\text{Ru}(\text{tpm})(\text{dppz})(3\text{-NH}_2\text{MePy})]^{2+}$ was measured at room temperature in both MeCN as its PF_6^- salt, and in water as its Cl^- salt, shown in figure 2.24.

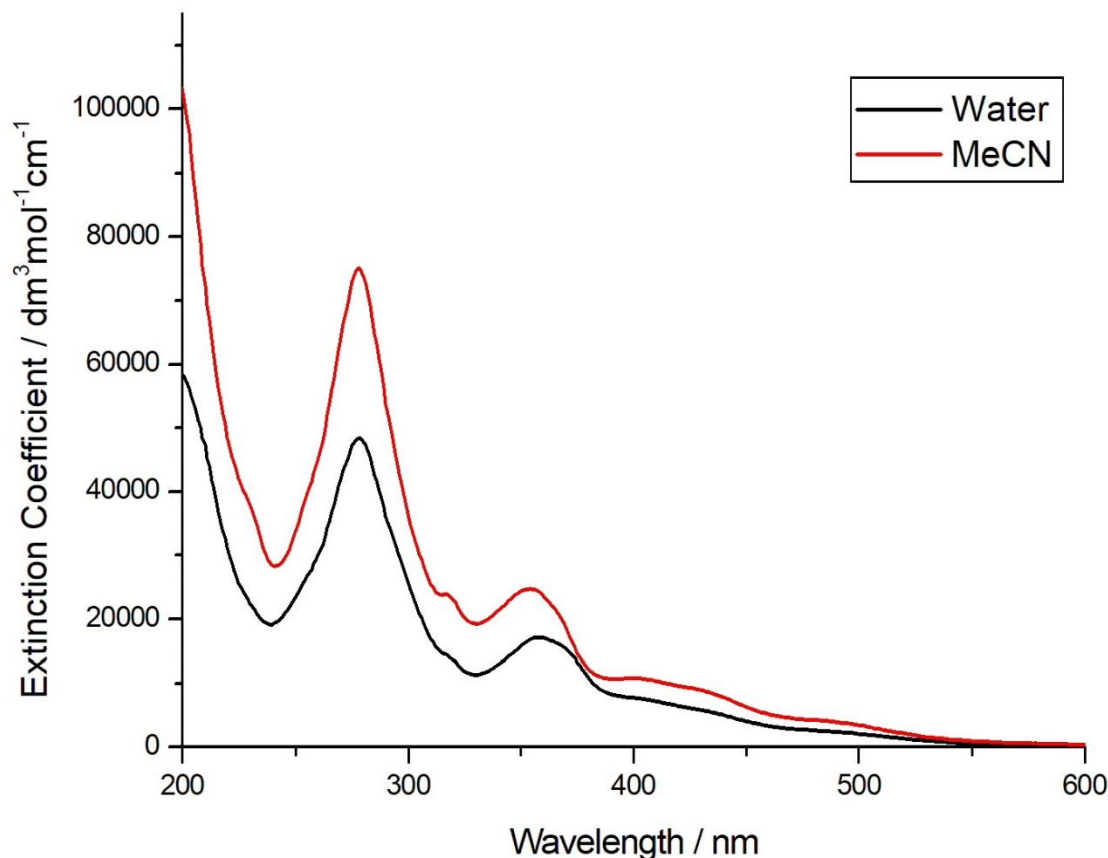


Figure 2.23 Extinction coefficients for $[\text{Ru}(\text{tpm})(\text{dppz})(3\text{-NH}_2\text{MePy})]^{2+}$ in both MeCN and H_2O .

The high energy bands centred at <200 nm and 275 nm can be assigned to $\pi \rightarrow \pi^*$ transitions in the aromatic donor ligands. When dissolved in DMF, free dppz shows structured absorption bands between 340-380 nm, assigned to $\pi \rightarrow \pi^*$ transitions.⁴³ The unstructured band centred at ~ 360 nm can therefore be assigned to the same transition in the complex. The small red-shift in this band in the water spectrum compared with acetonitrile suggests that this is a charge transfer state, as these are typically stabilised in more polar solvents. The broad absorption from around 400-500 nm can be attributed to the MLCT transition. The MLCT maximum is found at 425 nm, which is a similar

wavelength to the related compounds containing 3-aminopyridine (415 nm) and 3-picoline (424 nm) in the axial position.³⁸

2.6.3 Luminescence

The emission spectrum of $[\text{Ru}(\text{tpm})(\text{dppz})(3\text{-NH}_2\text{MePy})]^{2+}$ was measured in MeCN as its PF_6^- salt, and in water at 25 °C as its Cl^- salt, with excitation at the MLCT maximum, 425 nm. The complex has a broad emission in MeCN, centred on 665 nm, but is not emissive in water. This behaviour is typical of “light-switch” style complexes, with the excited state decaying through non-radiative pathway via hydrogen bonding in aqueous solvent. The normalised emission spectrum in MeCN is shown in figure 2.25.

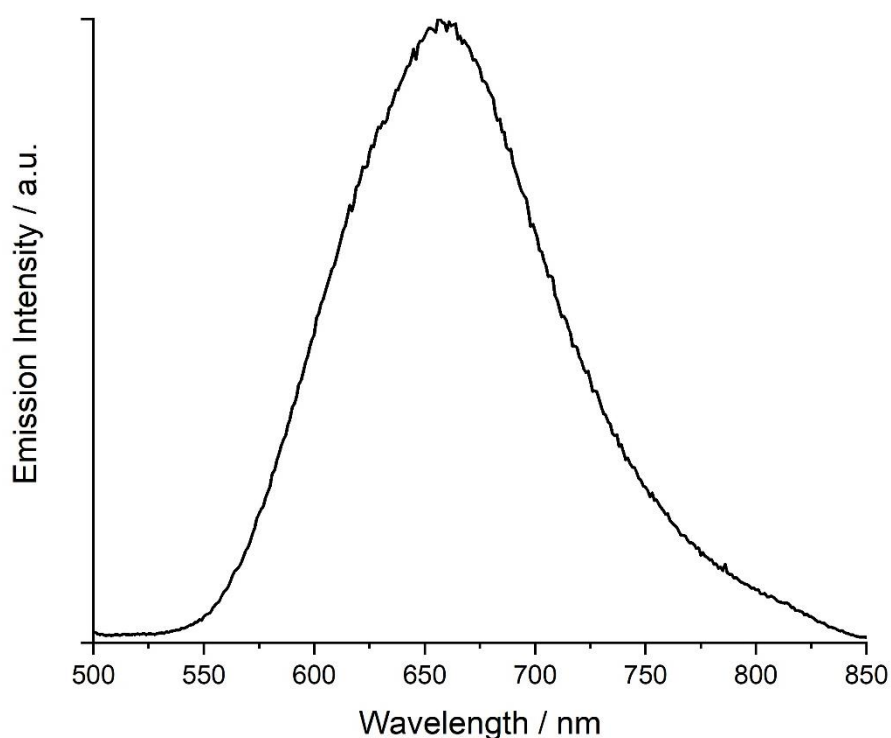


Figure 2.24 The normalised emission spectrum of $[\text{Ru}(\text{tpm})(\text{dppz})(3\text{-NH}_2\text{MePy})]^{2+}$ in MeCN.

2.6.4 Relative viscosity

In the absence of detailed binding information from techniques such as NMR and crystallisation of bound complexes in DNA, one of the most effective methods for probing the binding mode of DNA ligands is measuring the changes in relative viscosity.⁴⁴ This is because of the deformation of the structure of DNA upon binding. On intercalation, the DNA strand lengthens and partially unwinds, increasing the relative viscosity of the solution. Electrostatic binders cause the duplex to compact and kink around the ligand, reducing the length of the strand, and therefore causing a decrease in viscosity. Groove binders cause minimal disruption to the secondary structure, and so the relative viscosity does not change significantly. The use of known DNA binders as reference compounds allows comparative analysis of the binding mode of novel compounds. Ethidium bromide is usually used as an intercalating standard, Hoechst 33258 or DAPI are used as groove binding standards, and polyamines such as spermine or spermidine are frequently used as electrostatic binding standards.

Relative viscosity is calculated using the following formula, where η is the relative viscosity, t_0 is the flow time taken for the solvent, and t is the flow time for the sample.

$$\eta = \frac{t - t_0}{t_0}$$

Monitoring the change in η against η_0 (relative viscosity of DNA solution) as analyte is added then allows the binding mode to be investigated. As analyte is added to the DNA solution, the mixing ratio is measured as R^{-1} , where R is $[\text{DNA}]/[\text{analyte}]$. The results for $[\text{Ru}(\text{tpm})(\text{dppz})(3\text{-NH}_2\text{MePy})]^{2+}$, as well as ethidium bromide and Hoechst 33258 as intercalating and groove binding standards, are shown in figure 2.26.

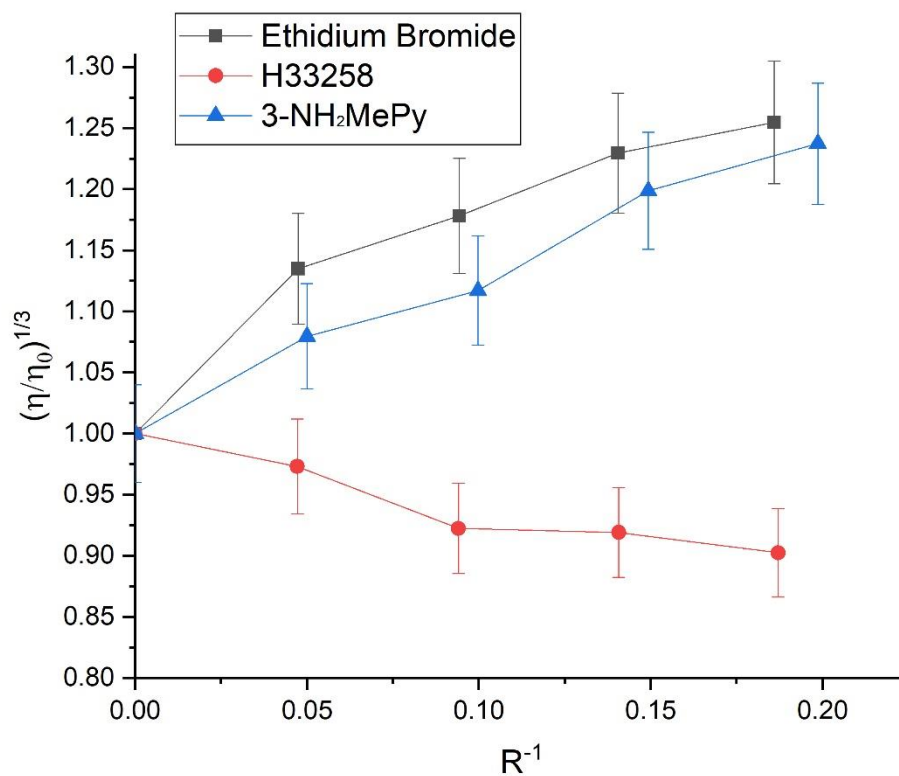


Figure 2.25 Change in relative viscosity of 0.5 mM ct-DNA solution on addition of ethidium bromide, Hoechst 33258 and $[\text{Ru}(\text{tpm})(\text{dppz})(3\text{-NH}_2\text{MePy})]^{2+}$.

Addition of $[\text{Ru}(\text{tpm})(\text{dppz})(3\text{-NH}_2\text{MePy})]^{2+}$ to ct-DNA causes the relative viscosity of the solution to increase in a similar fashion to ethidium bromide. This shows the complex binds to DNA by intercalation, as is typically the case for Ru-dppz complexes of this type.

2.6.5 DNA binding affinity

The binding of $[\text{Ru}(\text{tpm})(\text{dppz})(3\text{-NH}_2\text{MePy})]^{2+}$ to ct-DNA was measured by luminescence titration. On addition of ct-DNA to a solution of the complex, the

luminescence increased, due to the DNA “light-switch” effect. This is demonstrated in figure 2.27.

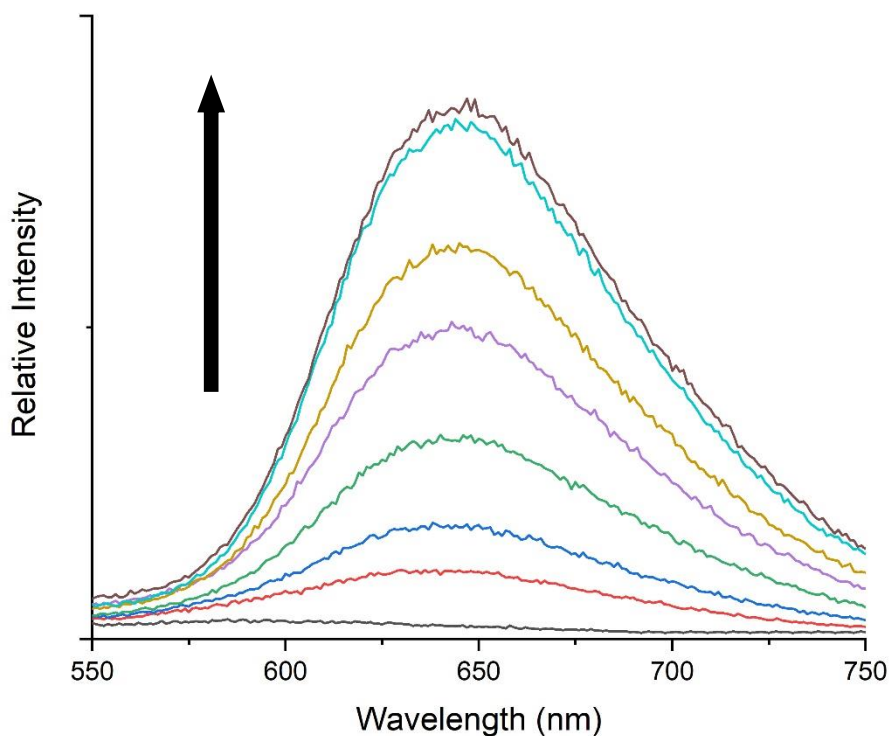


Figure 2.26 Change in emission of $[\text{Ru}(\text{tpm})(\text{dppz})(3\text{-NH}_2\text{MePy})]^{2+}$ on addition of ct-DNA, every 10th spectra shown. $\lambda_{\text{ex}} = 414 \text{ nm}$

The maximum of each curve can then be converted to the binding ratio, X , using the following formula, where I_{obs} is the measured intensity, I_{b} is the fully bound intensity, and I_{f} is the intensity of the free complex.

$$X = \frac{I_{\text{obs}} - I_{\text{f}}}{I_{\text{b}} - I_{\text{f}}}$$

The binding curve for the titration of ct-DNA with $[\text{Ru}(\text{tpm})(\text{dppz})(3\text{-NH}_2\text{MePy})]^{2+}$ is shown in figure 2.28.

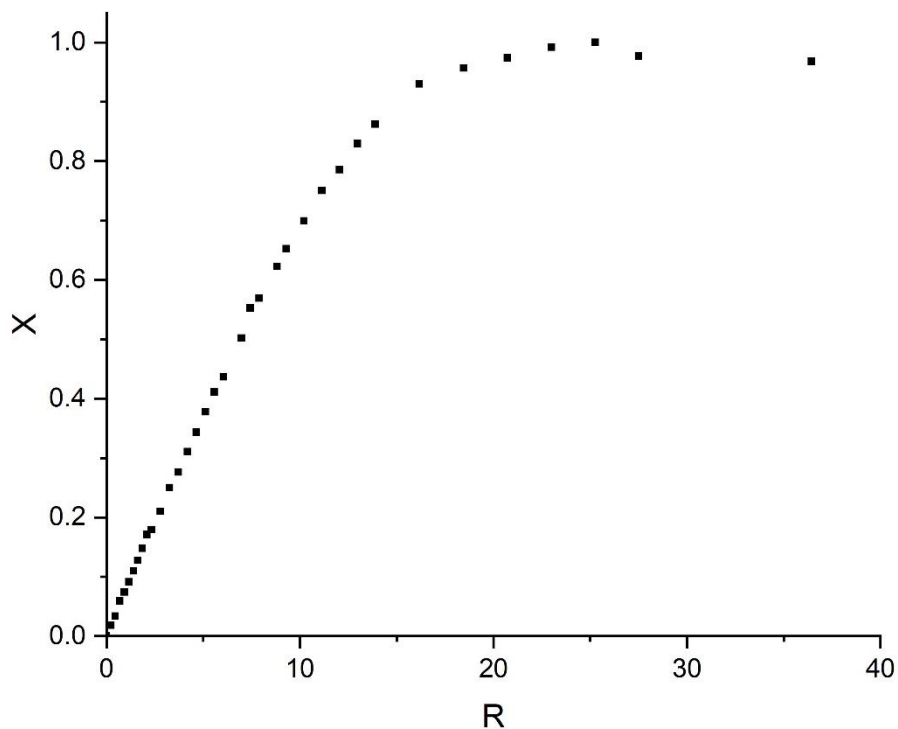


Figure 2.27 Binding curve for titration of ct-DNA with $[\text{Ru}(\text{tpm})(\text{dppz})(3\text{-NH}_2\text{MePy})]^{2+}$, where R is $[\text{DNA}]/[\text{analyte}]$ and X is the fraction bound.

From the initial concentration of analyte, C_i , and the fraction bound, the concentration of bound complex, C_b , can be calculated as follows:

$$C_b = C_i X$$

This allows us to calculate the binding ratio, r, as follows:

$$r = \frac{C_b}{[\text{DNA}]}$$

The concentration of free complex (C_f) can be found by simple subtraction:

$$C_f = C_i - C_b$$

Scatchard plots are traditionally used for studying the interactions of small molecule with proteins.⁴⁵ The graph can be constructed from the Scatchard equation below by

plotting r against r/C_f . K_i is the intrinsic binding constant, and n is the number of binding sites.

$$\frac{r}{C_f} = K_i(n - r)$$

The Scatchard equation is a simple model that assumes binding sites are discrete and isolated from one-another. This is not the case for DNA, as binding sites can overlap, and so binding of an analyte may block or reduce access to adjacent binding sites. The McGhee-von Hippel model treats DNA as a one-dimensional isotropic lattice, i.e. all binding sites are equivalent.⁴⁶ If binding is non-cooperative, then as saturation is approached, the number of available binding sites that are greater than n residues in length decreases, causing the plot to convex towards the origin. The equation used in the non-cooperative binding model is shown below.

$$\frac{r}{C_f} = K(1 - nr) \left[\frac{(1 - nr)}{1 - (n - 1)r} \right]^{n-1}$$

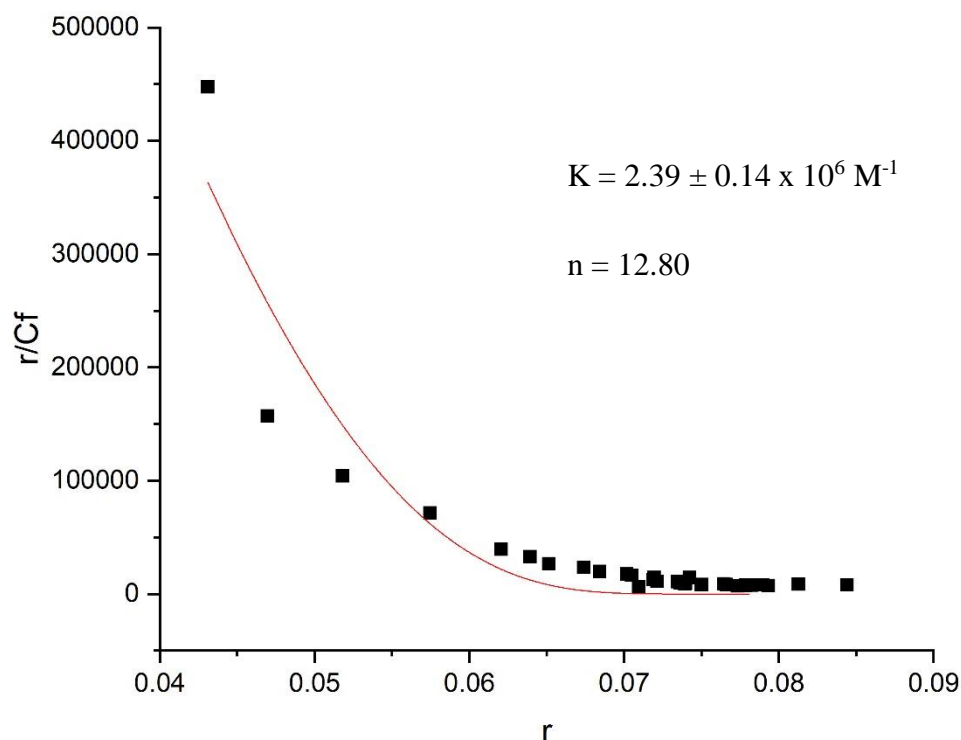


Figure 2.28 Scatchard plot for the binding of $[\text{Ru}(\text{tpm})(\text{dppz})(3\text{NH}_2\text{MePy})]^{2+}$ to ct-DNA. Data fitted using the McGhee-von Hippel model for non-cooperative binding. $R^2 = 0.89$

The Scatchard plot shown in figure 2.29 was obtained by plotting the binding data collected, and fitting to the McGhee-von Hippel model. The quality of the fit was good with $R^2 = 0.97$. The complex has a binding constant of $2.39 \pm 0.14 \times 10^6 \text{ M}^{-1}$ and a site size of 12.80 (error was negligible). Although the binding constant was in expected value for this range of compounds, the site size was much larger. For reference, the related $[\text{Ru}(\text{tpm})(\text{dppz})(3\text{NH}_2\text{py})]^{2+}$ complex has a similar binding constant ($K = 4.7 \pm 0.32 \times 10^6 \text{ M}^{-1}$), but a site size around one order of magnitude lower ($n = 1.5 \pm 0.02$).³⁸ Attempts to fix the site size during fitting to expected values, such as 1 and 3, did not produce a fit. Any factors that disfavour binding, such as electrostatic repulsion from ruthenium centres or the protonated amine could cause other complexes to bind further apart, thus increasing the site size. It may be that the hydrogen bonding moiety of this complex is interacting

with DNA residues to create binding to specific sequences, certainly such effects have been observed before in related, purely groove binding, complexes.

2.7 Conclusions and Future Work

There have been a small number of recent studies which have attached simple ruthenium (II) polypyridyl complexes to AuNPs, however, most of these have utilised simple structures such as bpy and phen.^{1,3} We proposed extending this area of research by incorporating more complicated complexes, such as those based on the intercalating $[\text{Ru}(\text{tpm})(\text{dppz})(\text{py})]^{2+}$. Initial attempts were based on an “all-in-one” method, in which the axially co-ordinated ligand was terminated with a thiol group for AuNP attachment. Synthetic routes investigated as a part of this method were unsuccessful, generally due ligand synthesis, or co-ordination, or problems with purification. Problems with co-ordination were attributed to the steric demands of the long, flexible ligands. In order to simplify this, a new “two-halves” method was derived, in which a functionalised pyridine ligand would be co-ordinated to the ruthenium centre; a heterobifunctional linker with a complementary reactive group at one end, and a thiol at the other, could then be attached to AuNPs. A Ru-dppz complex bearing a pendant amine was synthesised, along with a carboxylic acid/thiol functionalised oligoethylene glycol. An initial attempt to couple the two groups was unsuccessful, although the activated carboxylic acid was detected by mass spectrometry. The ruthenium complex was characterised through several techniques, including x-ray crystallography, which confirmed the connectivity. Relative viscosity showed the complex bound to ct-DNA by intercalation. Luminescence titration of the complex with ct-DNA showed a large increase in emission, as is expected for these

Ru-dppz “light-switch” complexes. The complex was found to bind to ct-DNA strongly, with a binding constant of $2.39 \pm 0.14 \times 10^6 \text{ M}^{-1}$.

Moving forwards with this project, the next step would be to optimise the amide coupling reaction between $[\text{Ru}(\text{tpm})(\text{dppz})(3\text{NH}_2\text{-MePy})]^{2+}$ and the carboxylic acid-thiol linker. Although the initial attempt at the reaction was unsuccessful, the activated acid was detected. A worthwhile first would be to test the unco-ordinated pyridine in the reaction, to determine if the problem is with either the complex as a whole, or the pyridine itself. If the reaction is successful, then assembly of the Ru-AuNP conjugates can take place, followed by characterisation as above. Comparison of the photophysical and DNA binding properties with the free complex will be valuable, in order to determine if attachment of the AuNP inhibits DNA binding, or interferes significantly with the light-switch effect.

2.8 References

- 1 R. B. P. Elmes, K. N. Orange, S. M. Cloonan, D. C. Williams and T. Gunnlaugsson, *J. Am. Chem. Soc.*, 2011, **133**, 15862–15865.
- 2 M. Martínez-Calvo, K. N. Orange, R. B. P. Elmes, B. la Cour Poulsen, D. C. Williams and T. Gunnlaugsson, *Nanoscale*, 2016, **8**, 563–574.
- 3 N. J. Rogers, S. Claire, R. M. Harris, S. Farabi, G. Zikeli, I. B. Styles, N. J. Hodges and Z. Pikramenou, *Chem. Commun.*, 2014, **50**, 617–9.
- 4 S. A. M. Osborne and Z. Pikramenou, *Faraday Discuss.*, 2015, **185**, 219–231.
- 5 J. P. Hall, D. Cook, S. R. Morte, P. McIntyre, K. Buchner, H. Beer, D. J. Cardin, J. A. Brazier, G. Winter, J. M. Kelly and C. J. Cardin, *J. Am. Chem. Soc.*, 2013, **135**, 12652–12659.
- 6 P. Waywell, V. Gonzalez, M. R. Gill, H. Adams, A. J. H. M. Meijer, M. P. Williamson and J. A. Thomas, *Chem. - A Eur. J.*, 2010, **16**, 2407–2417.
- 7 C. S. Burke and T. E. Keyes, *RSC Adv.*, 2016, **6**, 40869–40877.
- 8 P. Waywell, V. Gonzalez, M. R. Gill, H. Adams, A. J. H. M. Meijer, M. P. Williamson and J. A. Thomas, *Chem. - A Eur. J.*, 2010, **16**, 2407–2417.
- 9 M. G. Walker, V. Gonzalez, E. Chekmeneva and J. A. Thomas, *Angew. Chemie Int. Ed.*, 2012, **51**, 12107–12110.
- 10 M. G. Walker, V. Ramu, A. J. H. M. Meijer, A. Das and J. A. Thomas, *Dalt. Trans.*, 2017, **46**, 6079–6086.
- 11 H. K. Saeed, P. J. Jarman, S. Archer, S. Sreedharan, I. Q. Saeed, L. K. Mckenzie, J. A. Weinstein, N. J. Buurma, C. G. W. Smythe and J. A. Thomas, *Angew. Chemie*

- Int. Ed.*, 2017, **56**, 12628–12633.
- 12 D. L. Reger, J. R. Gardinier, S. Bakbak, R. F. Semeniuc, U. H. F. Bunz and M. D. Smith, *New J. Chem.*, 2005, **29**, 1035.
- 13 S. P. Foxon, C. Green, M. G. Walker, A. Wragg, H. Adams, J. A. Weinstein, S. C. Parker, A. J. H. M. Meijer and J. A. Thomas, *Inorg. Chem.*, 2012, **51**, 463–71.
- 14 S. Trofimenko, *J. Am. Chem. Soc.*, 1966, **88**, 1842–1844.
- 15 S. Trofimenko, *Chem. Rev.*, 1972, **72**, 497–509.
- 16 S. Trofimenko, *Chem. Rev.*, 1993, **93**, 943–980.
- 17 S. Trofimenko, *Scorpionates: The Coordination Chemistry of Polypyrazolylborate Ligands*, Imperial College Press, London, 1st edn., 1999.
- 18 W. Hüchel and H. Bretschneider, *Berichte der Dtsch. Chem. Gesellschaft (A B Ser.)*, 1937, **70**, 2024–2026.
- 19 S. Juliá, J. M. del Mazo, L. Avila and J. Elguero, *Org. Prep. Proced. Int.*, 1984, **16**, 299–307.
- 20 D. L. Reger, T. C. Grattan, K. J. Brown, C. A. Little, J. J. S. Lamba, A. L. Rheingold and R. D. Sommer, *J. Organomet. Chem.*, 2000, **607**, 120–128.
- 21 H. R. Bigmore, S. C. Lawrence, P. Mountford and C. S. Tredget, *Dalt. Trans.*, 2005, 635.
- 22 A. Llobet, P. Doppelt and T. J. Meyer, *Inorg. Chem.*, 1988, **27**, 514–520.
- 23 J. Dickeson and L. Summers, *Aust. J. Chem.*, 1970, **23**, 1023.
- 24 S. P. Foxon, C. Metcalfe, H. Adams, M. Webb and J. A. Thomas, *Inorg. Chem.*,

- 2007, **46**, 409–16.
- 25 S. Dhar, W. L. Daniel, D. A. Giljohann, C. A. Mirkin and S. J. Lippard, *J. Am. Chem. Soc.*, 2009, **131**, 14652–14653.
- 26 U. Drechsler, N. O. Fischer, B. L. Frankamp and V. M. Rotello, *Adv. Mater.*, 2004, **16**, 271–274.
- 27 S. Theeramunkong, U. Galli, A. A. Grolla, A. Caldarelli, C. Travelli, A. Massarotti, M. P. Troiani, M. A. Alisi, G. Orsomando, A. A. Genazzani and G. C. Tron, *Medchemcomm*, 2015, **6**, 1891–1897.
- 28 H. Yun, J. Sim, H. An, J. Lee, H. S. Lee, Y. K. Shin, S.-M. Paek and Y.-G. Suh, *Org. Biomol. Chem.*, 2014, **12**, 7127–35.
- 29 C. E. Hoyle and C. N. Bowman, *Angew. Chem. Int. Ed. Engl.*, 2010, **49**, 1540–73.
- 30 A. Leonidova, V. Pierroz, L. A. Adams, N. Barlow, S. Ferrari, B. Graham and G. Gasser, *ACS Med. Chem. Lett.*, 2014, **5**, 809–814.
- 31 M. Minozzi, D. Nanni and P. Spagnolo, *Chem. - A Eur. J.*, 2009, **15**, 7830–7840.
- 32 P. Desai, K. Schildknecht, K. A. Agrios, C. Mossman, G. L. Milligan and J. Aubé, *J. Am. Chem. Soc.*, 2000, **122**, 7226–7232.
- 33 G. A. Molander, S. L. J. Trice and S. D. Dreher, *J. Am. Chem. Soc.*, 2010, **132**, 17701–3.
- 34 S. Fu, W. Xiang, J. Chen, L. Ma and L. Chen, *Chem. Biol. Drug Des.*, 2017, **89**, 815–819.
- 35 F. C.-M. Leung, A. Y.-Y. Tam, V. K.-M. Au, M.-J. Li and V. W.-W. Yam, *ACS Appl. Mater. Interfaces*, 2014, **6**, 6644–53.

- 36 A. Bouzide and G. Sauvé, *Org. Lett.*, 2002, **4**, 2329–2332.
- 37 R. Mahou and C. Wandrey, *Polymers (Basel)*., 2012, **4**, 561–589.
- 38 V. G. González, PhD Thesis, University of Sheffield, 2006.
- 39 F. R. Stermitz and W. H. Huang, *J. Am. Chem. Soc.*, 1971, **93**, 3427–3431.
- 40 S. Wu, S. Y. Tan, C. Y. Ang, K. T. Nguyen, M. Li and Y. Zhao, *Chem. Commun.*, 2015, **51**, 11622–11625.
- 41 W. Shi and A. Lei, *Tetrahedron Lett.*, 2014, **55**, 2763–2772.
- 42 G. Fang and X. Bi, *Chem. Soc. Rev.*, 2015, **44**, 8124–8173.
- 43 J. Fees, W. Kaim, M. Moscherosch, W. Matheis, J. Klima, M. Krejcik and S. Zalis, *Inorg. Chem.*, 1993, **32**, 166–174.
- 44 L. S. Lerman, *J. Mol. Biol.*, 1961, **3**, 18–30.
- 45 G. Scatchard, *Ann. N. Y. Acad. Sci.*, 1949, **51**, 660–672.
- 46 J. D. McGhee and P. H. von Hippel, *J. Mol. Biol.*, 1974, **86**, 469–489.
- 47 A. Ghosh, P. Das, M. R. Gill, P. Kar, M. G. Walker, J. A. Thomas and A. Das, *Chem. - A Eur. J.*, 2011, **17**, 2089–2098.

Chapter Three

3 Tuning DNA binding affinity of metallointercalators through modulation of hydrogen bonding and steric interactions

3.1 Introduction

3.1.1 General

Several studies have shown that, both in solution and solid state, the ancillary ligands of intercalating complexes are in close contact with adjacent base pairs and the phosphodiester backbone of DNA.¹⁻⁵ Therefore, variations in the structure of the ancillary ligands can have large effects on both binding affinity and mode. Understanding how these variations can be tuned will allow the design of more selective DNA-binding molecules. For example, the Barton group designed a series of rhodium complexes containing ancillary ligands functionalised with amine, amide or guanidinium groups. The length of the linker was also varied.⁶ An example structure is shown in figure 3.1. They found that, especially in the case of methyl-guanidinium functionalised complexes, there was strong sequence selectivity with differences observed between the Λ - and Δ -enantiomers. Binding affinities were affected when the binding step or base pairs up to three steps away were altered, indicating that both the central complex and the guanidinium groups were influencing binding affinity.

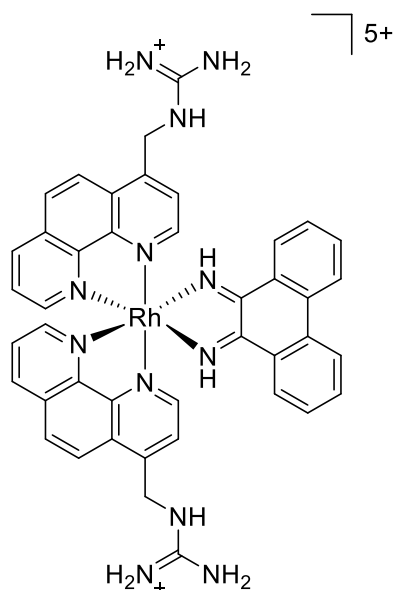


Figure 3.1 Structure of Λ -[Rh(MGP)₂(phi)]⁵⁺ (MGP = 4-(guanidylmethyl)-1,10-phenanthroline, phi = phenanthrene-9,10-diimine)

3.1.2 Previous Work

Previous work in the Thomas group has investigated the effect of varying the structure of ancillary ligands.⁷ Use of the achiral [Ru(tpm)(dppz)(Cl)][PF₆] as a precursor allowed easy synthesis of a series of compound through co-ordination of substituted pyridine ligands. The pyridines chosen were a mixture of hydrogen bond acceptors and/or donors. Methyl-substituted pyridines were also included to control for effects simply due to bulk. Additionally, both the 3- and 4-substituted pyridines were used to investigate the effect of regiochemistry on binding. The pyridines used were nicotinamide (**nic**, 3-amidopyridine), 3-aminopyridine (**3-NH₂py**), 3-pyridinecarboxyaldehyde (**3-CHOpy**), 3-picoline (**3-pic**, 3-methylpyridine), and their 4-substituted counterparts, isonicotinamide (**isonic**, 4-amidopyridine), 4-aminopyridine (**4-NH₂py**), 4-pyridinecarboxyaldehyde (**4-CHOpy**) and 4-picoline (**4-pic**, 4-methylpyridine). The structures are shown in table 3.1.

Structure				
Name	nic	3-NH ₂ py	3-CHOpy	3-pic
Structure				
Name	isonic	4-NH ₂ py	4-CHOpy	4-pic

Table 3.1 Structures of pyridine derivatives used to probe the effects of hydrogen bonding and sterics on DNA binding affinity.

The binding of these complexes to DNA was investigated through a range of techniques, including relative viscosity, absorption and luminescence titrations, and isothermal calorimetry (ITC). Relative viscosity measurements suggested that all complexes bind through intercalation, with the exception of the **4-NH₂py** complex, which appeared to groove bind. Absorption and luminescence titrations showed all complexes bound to ct-DNA with only small variations in binding affinity, again with the exception of the **4-NH₂py** complex, which displayed reduced binding strength in the UV-visible titration, and no luminescent enhancement on binding. As discussed in section 1.4.2.3, these observations are due to the orientation of the pyridyl ligand. DFT calculations suggest the lowest energy conformation has the pyridine aligned parallel to the dppz axis.⁸ This causes the amine protons to also project down the long dppz axis, and therefore they clash with the base pair below the intercalation site. This means intercalation is

disfavoured, and consequently the complex is a groove binder. Examination of the temperature dependence of relative viscosity measurements and thermodynamic properties from ITC measurements revealed that the complex groove binds at higher temperatures, however, at lower temperatures, the binding mode switches to intercalation. Raising the temperature again does not cause reversion to groove binding.⁹

Subsequent work investigated the binding of **nic** and **4-NH₂py** dppn complexes found that both complexes bound to ct-DNA by intercalation with essentially the same affinity. The lack of selectivity in these complexes was attributed to the longer intercalating ligand. This meant the ruthenium centre, and therefore the co-ordinated pyridine, could be situated further from the duplex, and so any steric clashes could be reduced.

3.1.3 This work – aims

In order to further investigate how different intercalating ligands affect the ability of ancillary ligands to alter DNA binding affinity, three new series of complexes were proposed. The first intercalating ligand is pyrazino-1,10-phenanthroline (pzp), which is similar to dppz, but one ring shorter. The second is dipyridophenazine-imidazolone (dppz-izdo), which is similar length to dppn, but contains an imidazolone group instead of the final aromatic ring. The third is 4,5,9,18-tetraazaphenanthrotriphenylene (taptp), which is a wider intercalating ligand. The structures of each parent chloride complex are shown in figure 3.2.

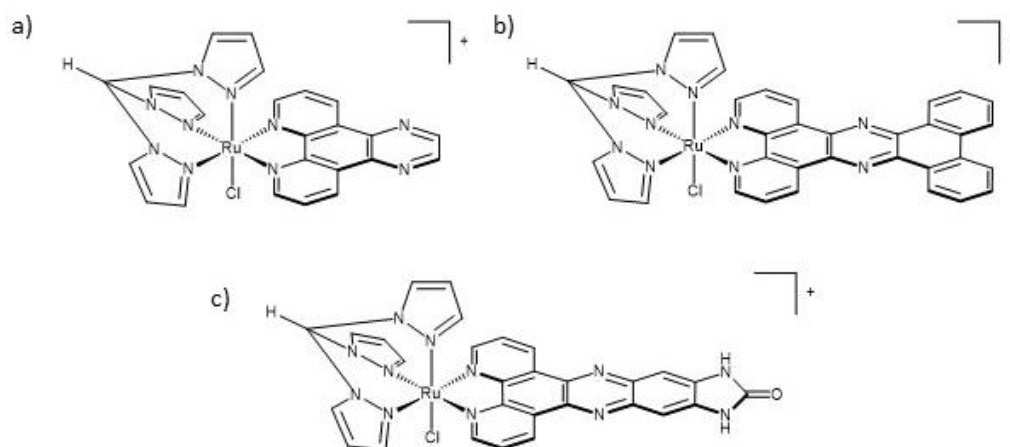


Figure 3.2 Structures of the parent $[\text{Ru}(\text{tpm})(\text{N}^{\wedge}\text{N})(\text{Cl})]^+$ ($\text{N}^{\wedge}\text{N} = \text{pzp}$ (a), tapt (b), dppz-izdo (c)) complexes designed for this study.

The interactions of ruthenium complexes containing pzp has been studied by several groups. ^1H NMR studies have shown that the complex binds through intercalation from the minor groove, albeit generally with reduced affinity compared with dppz complexes ($\sim 10^4 \text{ M}^{-1}$ for pzp, $\sim 10^6 \text{ M}^{-1}$ for dppz).^{10,11} Although Ru-pzp complexes are typically luminescent in both organic and aqueous solvents, and therefore do not display a DNA “light-switch” effect, substitutions at the pyrazine ring can induce switchable luminescence.^{12,13}

Dppz-idzo was first synthesised in 2013 by the Yao group, who found that $[\text{Ru}(\text{bpy})_2(\text{dppz-idzo})]^{2+}$ bound to quadruplex DNA with comparable affinity to the original dppz complex, however, the luminescent enhancement was significantly larger (~ 300 -fold for dppz-idzo compared with ~ 80 -fold for dppz), providing a limit-of-detection of 6 nM.¹⁴ G-quadruplexes are important biological targets, as they are thought to inhibit telomere elongation by blocking telomerase, and so compounds that can act as either probes or therapeutics for these structures are in demand.^{15–17}

Ruthenium complexes of taptp, whilst still binding through intercalation, and displaying a “light-switch” effect, typically bind to ct-DNA with reduced affinity compared with the original dppz complex ($\sim 10^5 \text{ M}^{-1}$ for taptp), presumably due to the increased width of the ligand.¹⁸ There has been a limited amount of work on ruthenium complexes of taptp, although recent work in the Thomas group has shown that $[\text{Ru}(\text{phen})_2(\text{taptp})]^{2+}$ is cytotoxic towards A2780 human ovarian cancer cells.¹⁹

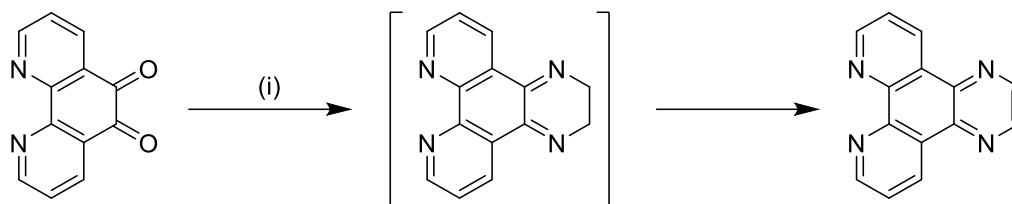
Although initially, all three series of complexes would be compared to their dppz analogues, due to synthetic challenges, this chapter largely amounts to a comparative study between the dppz and pzp complexes, with some preliminary investigations into viable synthetic routes towards the dppz-izdo and taptp complexes.

3.2 Pzp complexes

3.2.1 Synthesis

3.2.1.1 Synthesis of pyrazino-1,10-phenanthroline

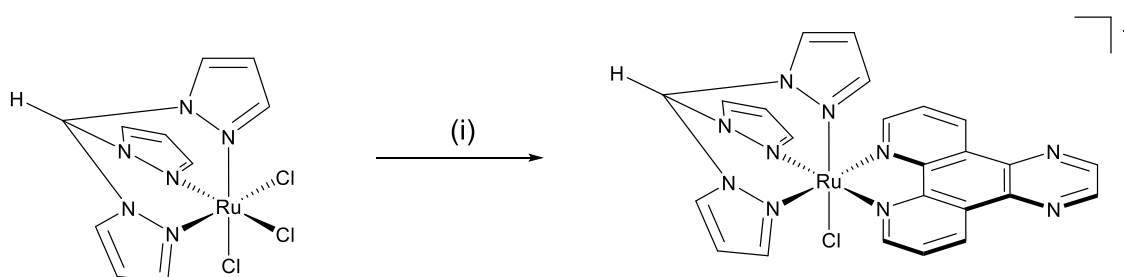
Pzp was synthesised through the condensation of ethylene diamine with dpq in EtOH. Formation of the partially saturated intermediate was rapid, with the solution changing from the yellow of dpq to a deep red. Over time, the solution reverted back to yellow, indicating formation of a larger conjugated system by oxidation of the final ring. Following recrystallisation, analysis by both ^1H NMR and ESI-MS showed only the oxidised final product.



Scheme 3.21 (i) Ethylene diamine, EtOH, reflux, 4 hrs

3.2.1.2 Synthesis of $[\text{Ru}(\text{tpm})(\text{pzp})(\text{Cl})][\text{PF}_6]$

Although $[\text{Ru}(\text{tpm})(\text{pzp})(\text{Cl})][\text{PF}_6]$ has not been previously reported, its synthesis was achieved using the same method as for the dppz complex, as shown in scheme 3.2.



Scheme 3.22 (i) pzp, LiCl, EtOH:H₂O (3:1), NEt₃, reflux, 3 hrs

The complex was characterised by analysis of ¹H NMR and ESI-MS spectra. The assigned ¹H NMR spectrum is shown in figure 3.3; assignment of the peaks was made through comparison with the dppz complex. Most peaks have only minor changes in chemical shift, with the obvious changes being the loss of signals associated with the final ring of dppz, and the appearance of a downfield singlet corresponding to the protons adjacent to the pyrazine nitrogens. Mass spectrometry showed a singly charged peak at 583 m/z, which represents $[\text{M}-\text{PF}_6]^+$.

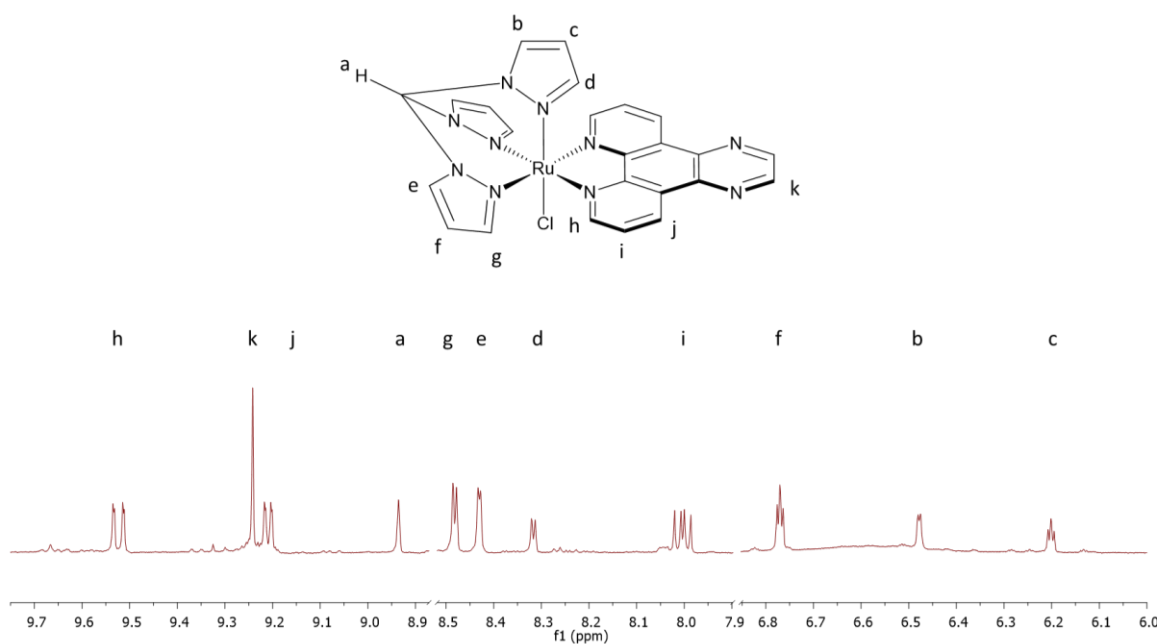


Figure 3.3 The assigned ^1H NMR spectrum of $[\text{Ru}(\text{tpm})(\text{pzp})(\text{Cl})]^+$. Cuts inserted between 6.9-7.9 and 8.6-8.9 ppm for clarity.

3.2.1.3 Synthesis of $[\text{Ru}(\text{tpm})(\text{pzp})(\text{L})][\text{PF}_6]_2$

The complexes to be investigated were synthesised by refluxing the appropriate pyridyl ligand with the parent chloride complex in EtOH:H₂O (3:1), using AgNO₃ to abstract the axial chloride. The complex could then be precipitated through addition of excess KPF₆. Unlike the dppz complexes, which were obtained pure after precipitation, the pzp complexes required extensive purification by both flash column chromatography over silica and charge separation chromatography using SP-Sephadex as the mobile phase. The complexes were analysed by ^1H NMR and ESI-MS. Spectra representative of the 3- and 4-substituted complexes are shown in figure 3.4. All complexes showed a doubly charged peak representing their respective $[\text{M}-2\text{PF}_6]^{2+}$ cations when analysed by mass spectrometry. The complexes were synthesised in low yields (typically single figures). A significant (~20 %) amount of the starting complex was recovered with the

axial chloride abstracted. Attempts to increase the yield by increasing equivalents of the substituted pyridine ligands, increasing reaction time, or reaction temperature made little difference. However, the complexes could be synthesised consistently at these low yields, and the amounts required for the analysis were low (~20 mg is typically sufficient for photophysical analysis, DNA binding titrations and relative viscometry).

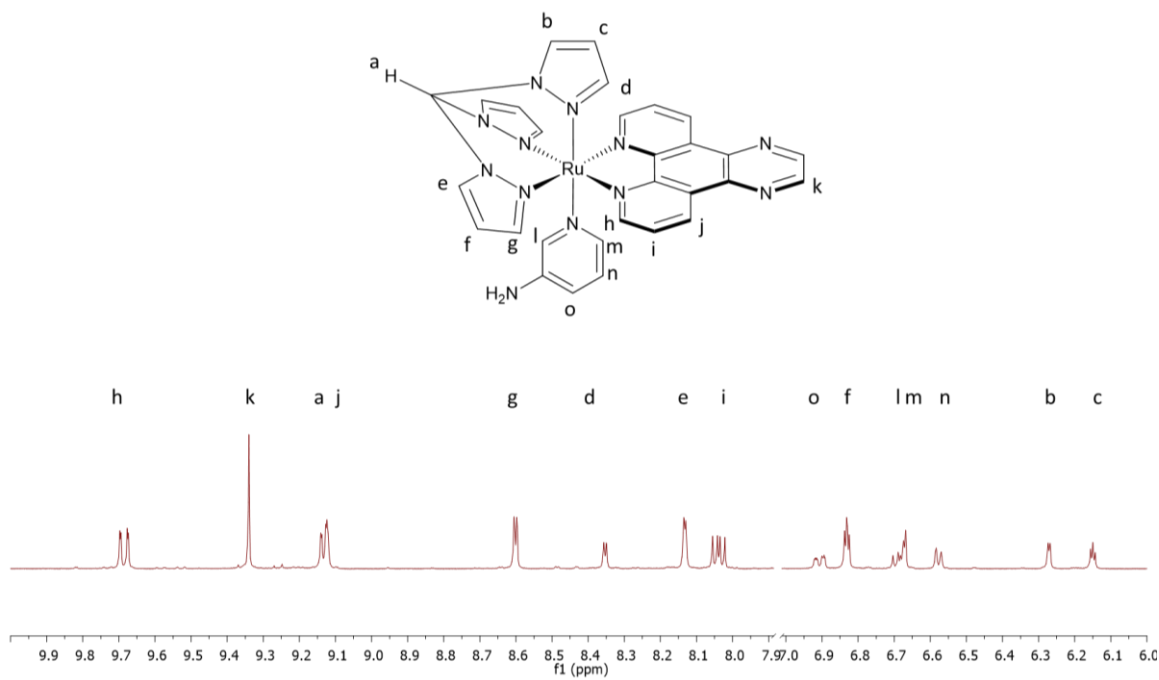
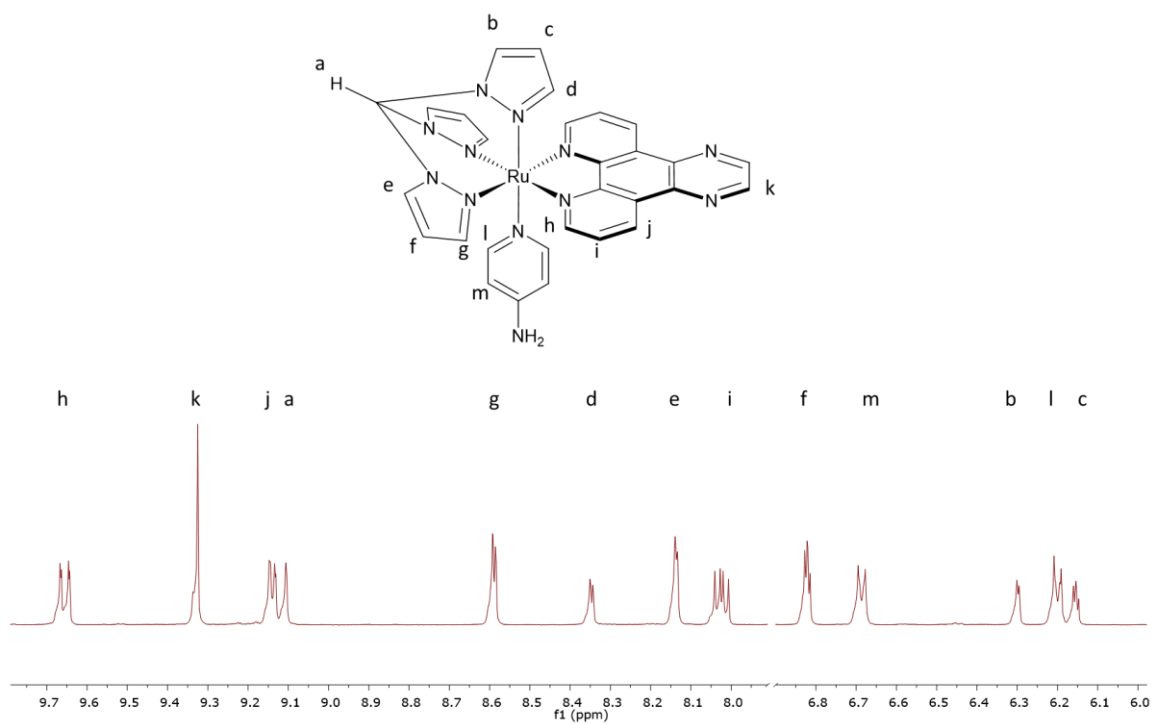


Figure 3.4 Assigned ¹H NMR spectra of $[\text{Ru}(\text{tpm})(\text{pzp})(4\text{-NH}_2\text{py})]^{2+}$ (top) and $[\text{Ru}(\text{tpm})(\text{pzp})(3\text{-NH}_2\text{py})]^{2+}$ (bottom)

The only exceptions were the **3-** and **4-CHOpy** complexes, which could not be obtained pure. The product could be observed by mass spectrometry of the crude precipitate, however, there was a significant amount of the aldehyde hydrate also present. Attempts to separate the two by column chromatography over silica or alumina, charge separation chromatography over SP-Sephadex, or recrystallisation were unsuccessful, and generally led to an increased amount of the hydrate. Additionally, as subsequent analysis would be carried out in aqueous solution, it would be hard to determine that there was no further conversion of aldehyde to hydrate. Therefore, further attempts to synthesise the aldehyde substituted complexes were not undertaken. The six compounds synthesised are shown in table 3.2.

[3.1]	[3.3]	[3.5]
$[\text{Ru}(\text{tpm})(\text{pzp})(\text{nic})]^{2+}$	$[\text{Ru}(\text{tpm})(\text{pzp})(3\text{-NH}_2\text{py})]^{2+}$	$[\text{Ru}(\text{tpm})(\text{pzp})(3\text{-pic})]^{2+}$
[3.2]	[3.4]	[3.6]
$[\text{Ru}(\text{tpm})(\text{pzp})(\text{isonic})]^{2+}$	$[\text{Ru}(\text{tpm})(\text{pzp})(4\text{-NH}_2\text{py})]^{2+}$	$[\text{Ru}(\text{tpm})(\text{pzp})(4\text{-pic})]^{2+}$

Table 3.2 The structures of the complexes investigated in this section. The labels in bold are used to refer to them from herein.

3.2.2 UV-vis

The UV-visible absorption spectra of complexes **[3.1]**-**[3.6]** in both MeCN as their PF₆⁻ salts and in H₂O as their Cl⁻ salts are shown in figures 3.5-3.10, and the peaks reported in tables 3.3 and 3.4. All complexes show high energy bands centred around 200 nm and 256-7 nm that can be assigned to $\pi \rightarrow \pi^*$ transitions in the aromatic donor ligands. Free pzp shows an absorption band centred at 330 nm in MeCN that has been previously assigned to an $n \rightarrow \pi^*$ intra-ligand transition.²⁰ The bands at around 290 nm can therefore be attributed to these transitions. It is worth noting that this band is significantly blue-shifted with respect to the analogous band in the spectra of the dppz analogues of these complexes (as shown in figure 2.22). This is presumably due to the reduced conjugation from the loss of the terminal ring. All the complexes also have a broad MLCT-based transition, generally between 350 nm and 550 nm, with local maxima around 400-425 nm.

Both the pzp based and MLCT transitions are red shifted in H₂O compared to the spectra in MeCN, although the shift is much larger for the MLCTs. As discussed in the previous chapter, this is indicative of charge transfer based transitions, as the more polar solvent stabilises the excited state. The magnitude of this red-shift varies substantially between complexes. The largest shift of the MLCT is observed for **[3.2]**, which shows a 32 nm decrease in the position of the local maximum. The smallest is observed for **[3.4]**, which only has a 5 nm decrease. Both **[3.2]** and **[3.4]** are functionalised in the 4 position, which means the substituent can affect the Ru-N bond through resonance. **[3.2]** is amide substituted; this π withdrawing moiety reduces electron density on the ruthenium centre. This effect increases the energy of MCLT excitement, which involves a formal oxidation of the metal. Complex **[3.4]** is amine substituted, and this π donating functional group

stabilises the MLCT. As the ruthenium centre is more electron rich, the charge difference in the MLCT excited state is therefore reduced, and so the solvent stabilisation has less of an effect.

The intensity of each absorption band varies significantly when the solvents are changed. Broadly speaking, the intensity of a band is related to the size of the dipole moment for its associated transition, and therefore changes in solvent polarity can have large effects. However, exploring the exact nature of these effects is not necessary for studying the interactions of these complexes with DNA. Additionally, due to their complexity, explanations without detailed theoretical work are unlikely to be of great quality.

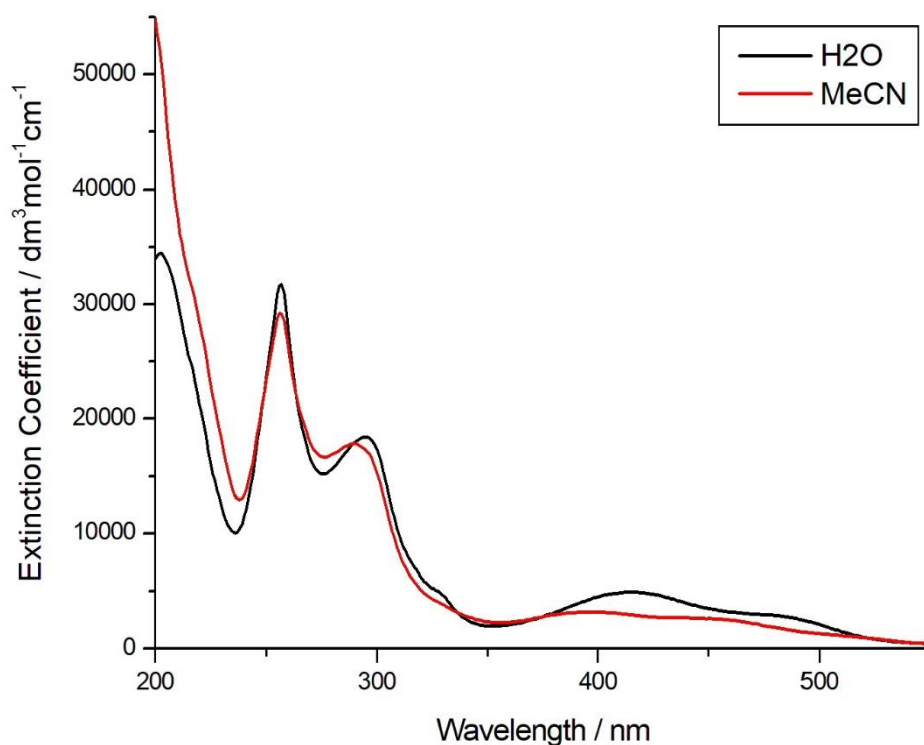


Figure 3.5 UV-vis absorption of [3.1] in both H₂O and MeCN.

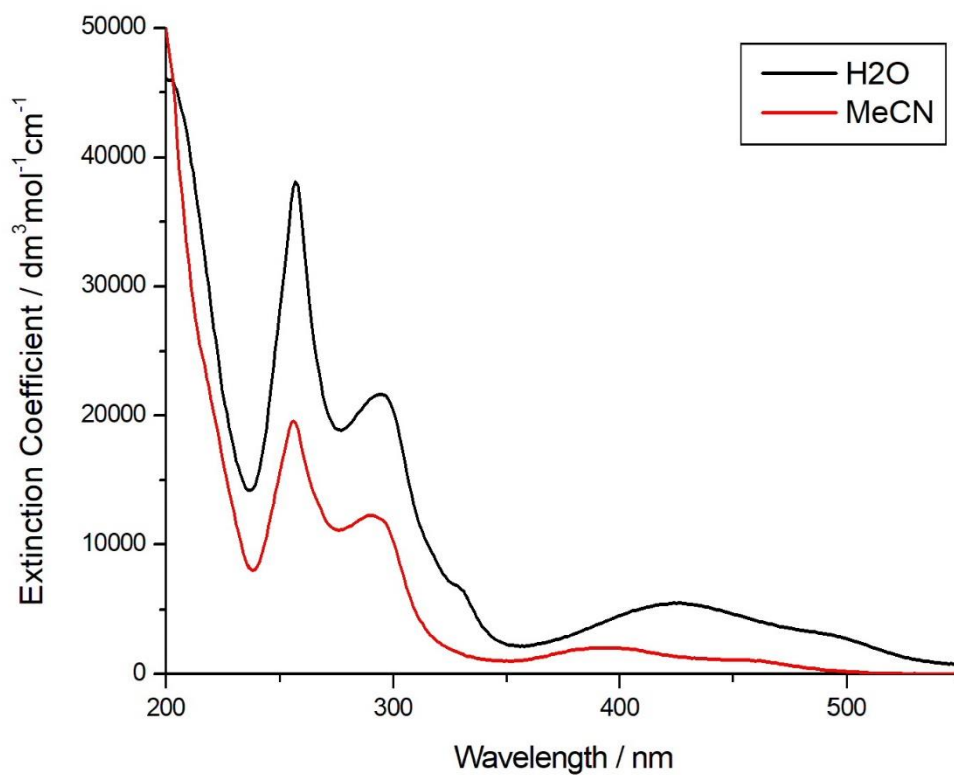


Figure 3.6 UV-vis absorption of [3.2] in both H₂O and MeCN.

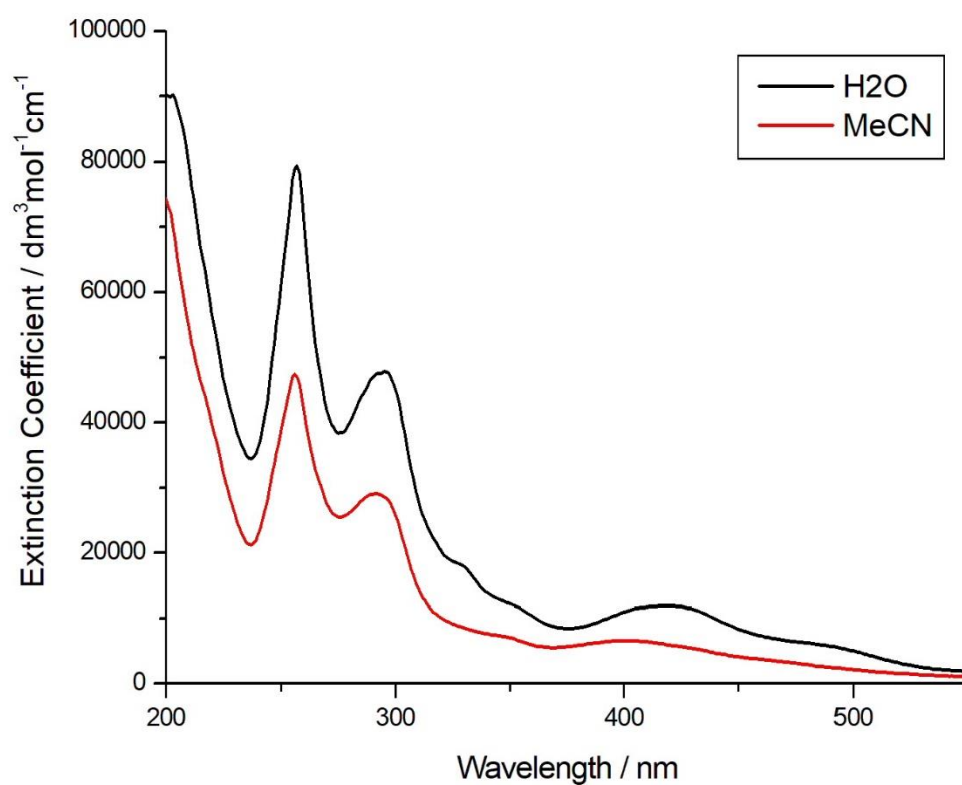


Figure 3.7 UV-vis absorption of [3.3] in both H₂O and MeCN.

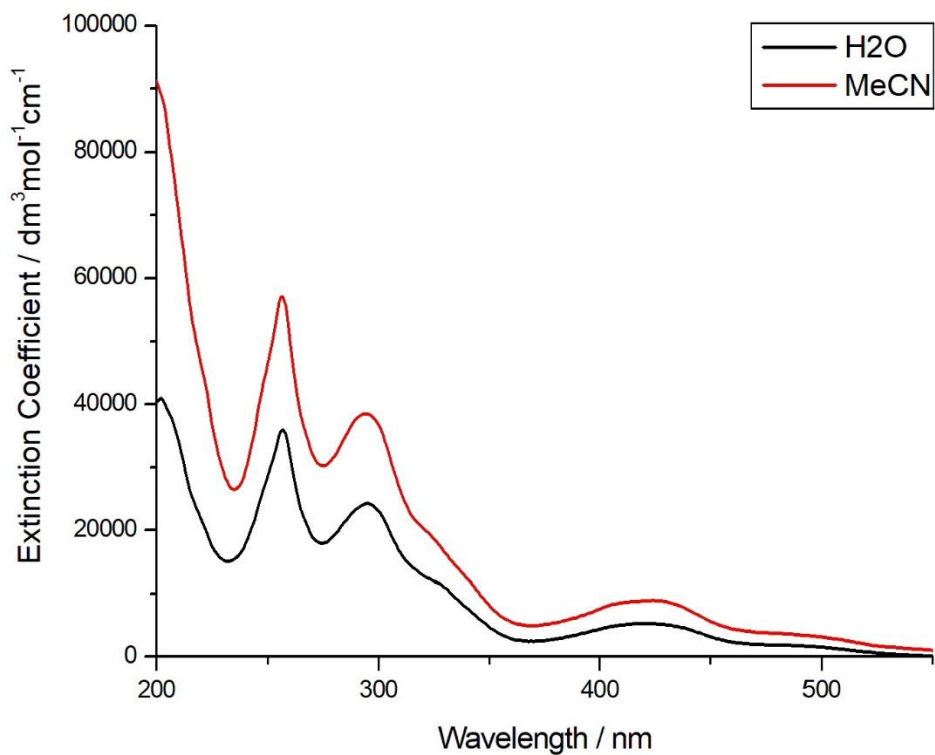


Figure 3.8 UV-vis absorption of [3.4] in both H₂O and MeCN.

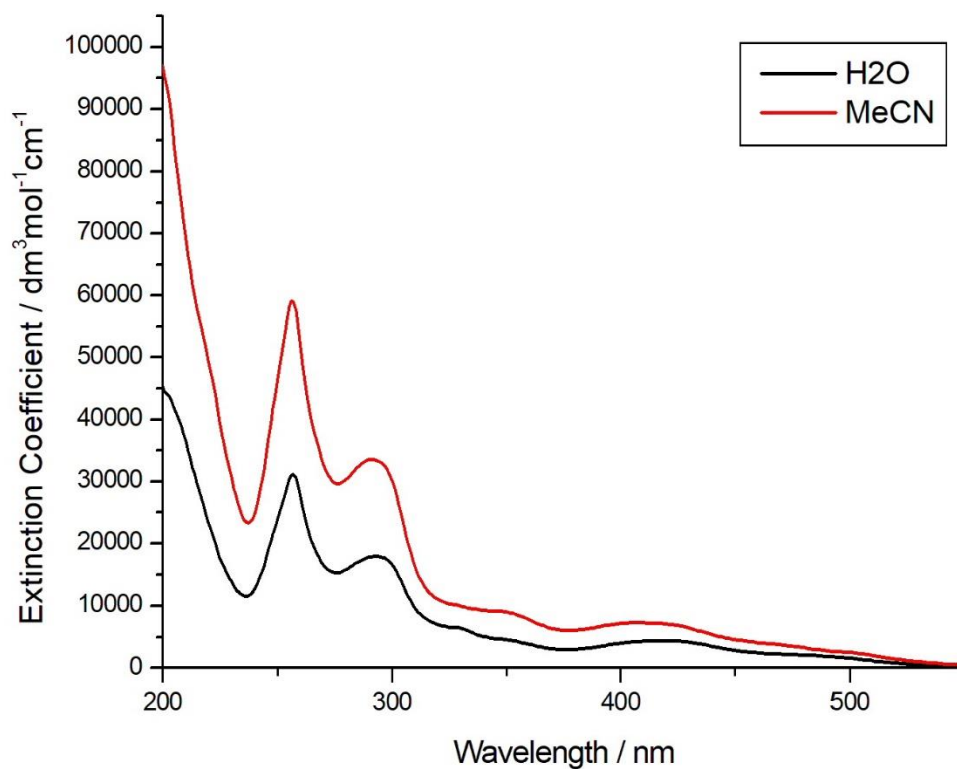


Figure 3.9 UV-vis absorption of [3.5] in both H₂O and MeCN.

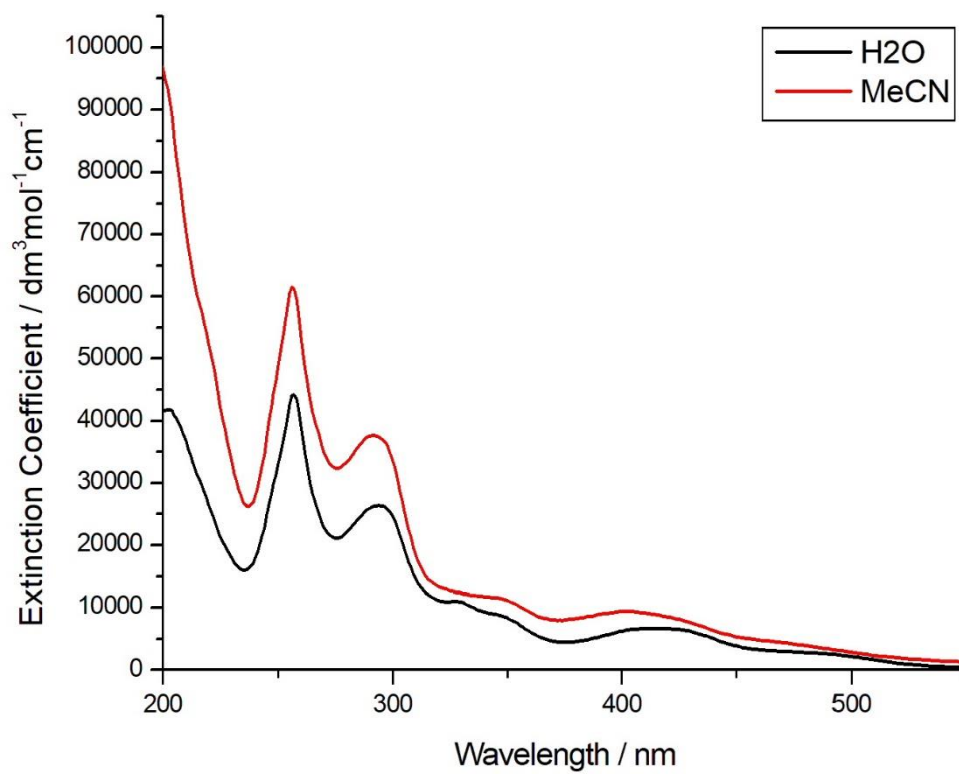


Figure 3.10 UV-vis absorption of [3.6] in both H₂O and MeCN.

Compound	λ_{\max} / nm	ϵ / M ⁻¹ cm ⁻¹	Assignment
[3.1]	256	29206 ± 420	$\pi \rightarrow \pi^*$
	288	17788 ± 300	$n \rightarrow \pi^*$
	400	3207 ± 30	MLCT
	455	Sh	MLCT
[3.2]	256	19575 ± 243	$\pi \rightarrow \pi^*$
	290	12247 ± 247	$n \rightarrow \pi^*$
	394	2050 ± 306	MLCT
	458	Sh	MLCT
[3.3]	256	47454 ± 259	$\pi \rightarrow \pi^*$
	292	29076 ± 189	$n \rightarrow \pi^*$
	400	6645 ± 123	MLCT
[3.4]	256	57092 ± 623	$\pi \rightarrow \pi^*$
	294	38511 ± 457	$n \rightarrow \pi^*$
	414	8954 ± 158	MLCT
	500	Sh	MLCT
[3.5]	256	59085 ± 322	$\pi \rightarrow \pi^*$
	292	33534 ± 197	$n \rightarrow \pi^*$
	351	Sh	
	407	7371 ± 37	MLCT
[3.6]	256	61463 ± 1073	$\pi \rightarrow \pi^*$
	291	37652 ± 750	$n \rightarrow \pi^*$
	348	Sh	
	401	9442 ± 403	MLCT

Table 3.S UV-Vis data for compounds [3.1] – [3.6] recorded in MeCN (Sh = shoulder)

Compound	λ_{\max} / nm	ϵ / M ⁻¹ cm ⁻¹	Assignment
[3.1]	257	31712 ± 216	$\pi \rightarrow \pi^*$
	295	18416 ± 127	$n \rightarrow \pi^*$
	414	4933 ± 37	MLCT
	484	Sh	MLCT
[3.2]	257	25857 ± 574	$\pi \rightarrow \pi^*$
	295	21659 ± 377	$n \rightarrow \pi^*$
	426	5512 ± 164	MLCT
	493	Sh	MLCT
[3.3]	257	79486 ± 280	$\pi \rightarrow \pi^*$
	295	47828 ± 203	$n \rightarrow \pi^*$
	420	11943 ± 63	MLCT
	485	Sh	MLCT
[3.4]	257	35915 ± 2507	$\pi \rightarrow \pi^*$
	295	24245 ± 1623	$n \rightarrow \pi^*$
	419	5260 ± 384	MLCT
	500	Sh	MLCT
[3.5]	257	21103 ± 238	$\pi \rightarrow \pi^*$
	293	17935 ± 134	$n \rightarrow \pi^*$
	330	Sh	
	418	4431 ± 44	MLCT
[3.6]	257	44202 ± 215	$\pi \rightarrow \pi^*$
	294	26401 ± 353	$n \rightarrow \pi^*$
	330	Sh	
	350	Sh	
	413	6726 ± 413	MLCT
	493	Sh	MLCT

Table 3.3 UV-Vis data for compounds [3.1] – [3.6] recorded in H₂O (Sh = shoulder)

3.2.3 Luminescence

Luminescence spectra were recorded for [3.1]-[3.6] in both H₂O and MeCN, with excitation at the MLCT maxima previously determined. All complexes displayed a broad,

unstructured emission between approximately 550-800 nm. The emission maxima for each complex are recorded in table 3.5.

Compound	λ_{ex} (MeCN) / nm	λ_{em} (MeCN) / nm	λ_{ex} (H ₂ O) / nm	λ_{em} (H ₂ O) / nm
[3.1]	400	652	414	N/E
[3.2]	394	599	426	600
[3.3]	400	650	420	620, w
[3.4]	414	692	419	660, w
[3.5]	407	652	418	649
[3.6]	401	653	413	650

Table 3.4 Excitation and emission maxima for compounds [3.1] – [3.6] (N/E = non-emissive, w = weak)

Although all the compounds are emissive in MeCN, several show no or weak emission in H₂O, suggesting that they may show “light-switch” behaviour. For those that do show aqueous emission, the wavelength of emission in both solvents shows only small changes. This is to be expected, as there is not generally time for the solvent shell to re-organise on excitation of the complex, meaning changes in solvent will have a decreased effect on the excited state stability.

3.2.4 Computational Studies

The emission characteristics of [3.1] to [3.6] were studied through computational analysis. Calculations were performed by Prof. Anthony Meijer of the University of Sheffield Department of Chemistry, who also helped with the analysis.

The calculated emission wavelengths are shown in table 3.6.

Compound	λ_{em} (MeCN) / nm	λ_{em} (H ₂ O) / nm
[3.1]	621	641
[3.2]	605	614
[3.3]	630	641
[3.4]	684	655
[3.5]	622	641
[3.6]	630	641

Table 3.5 Calculated emission wavelengths for complexes [3.1]-[3.6].

Geometry optimizations in both the singlet ground state (S_0) and the triplet ground state (T_1) were carried out. From the calculated electronic energies (with added zero-point energy contributions) the 0-0 emission frequencies were calculated. These are reported in table 3.5 with the experimental data. Comparison of theory with experiment shows a qualitative agreement between the absolute wave lengths. The agreement is much better, if the relative changes in the emission wave lengths are considered for sets of structural isomers. For [3.5]/[3.6] the calculations show little difference between the isomers, whereas the difference is larger for [3.3]/[3.4]. The differences between the excited states of [3.3] and [3.4] were therefore considered in larger detail. Figure 3.11 shows the spin densities for the T_1 state for both isomers.

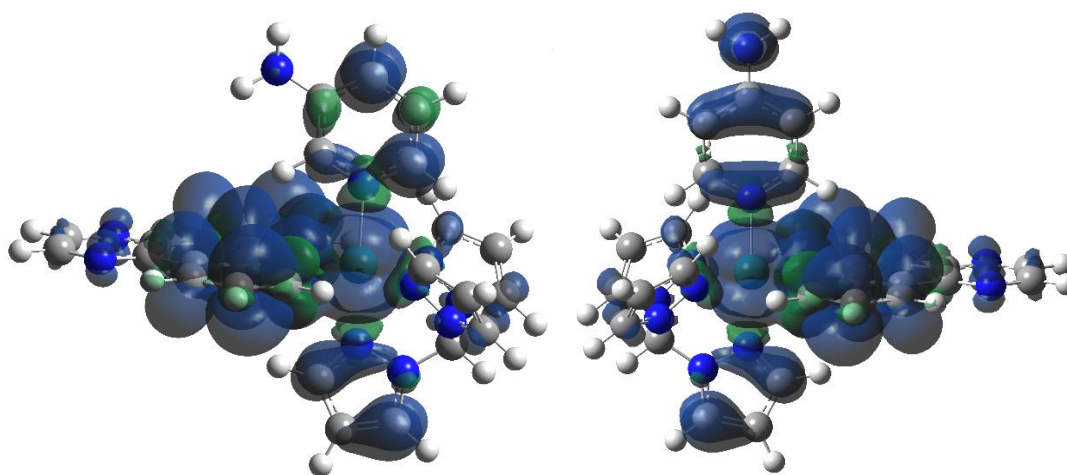


Figure 3.11 Spin density for the T_1 state of [3.3] (left panel) and [3.4] (right panel).

The figure does not show major differences between the states for the two isomers. However, it does show that for [3.4] the NH_2 group is involved in the excited state, whereas for [3.3] this is not the case. On the pzp-side of the complex there is no difference between the two isomers. However, this does mean that the T_1 state for [3.4] is more extensive, leading to a stabilisation of the excited state. The red-shift of the emission wavelength for [3.4] is consistent with this.

Comparing the water-based emission with the MeCN-based one shows for the calculations that there is a clear red-shift for all transitions. This is caused by the fact that the water coordinating to the pzp nitrogen atoms shift electron density on to that part of the complex, again resulting in a more delocalized (and therefore stabilised) triplet state (see figure 3.12). This shift is more pronounced than for the experimental results. In particular, the obvious blue-shift for [3.3]/[3.4] is not observed. The polarisable continuum model used to model solvent effects cannot account for specific interactions, therefore, four water molecules were introduced to include specific hydrogen bonds. Two

were positioned adjacent to the phenazine nitrogen atoms, and a further two were positioned near the substituted section of the pyridine ligand. Although in previous work these four water molecules were sufficient,²¹ in this case, it appears a more extensive investigation is needed to resolve this discrepancy.

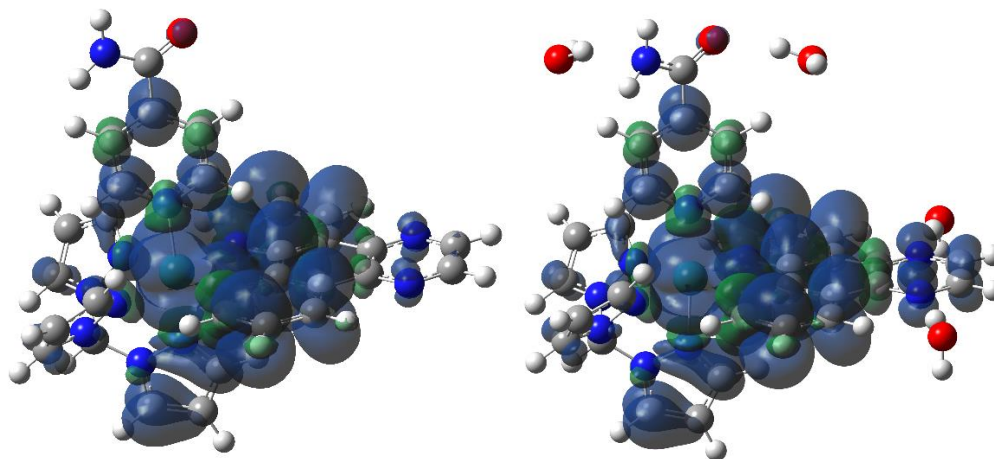


Figure 3.12 Spin density for the T_1 state of [3.6] in MeCN (left panel) and [3.6] in water (right panel).

3.2.5 Relative Viscosity

As previously discussed in chapter 2, changes in relative viscosity provide a highly effective method for probing the binding mode of analytes to DNA. Figure 3.13 shows the change in relative viscosity of ct-DNA solutions on addition of [3.1]-[3.6], as well as ethidium bromide and Hoechst 33258 as intercalating and groove binding references.

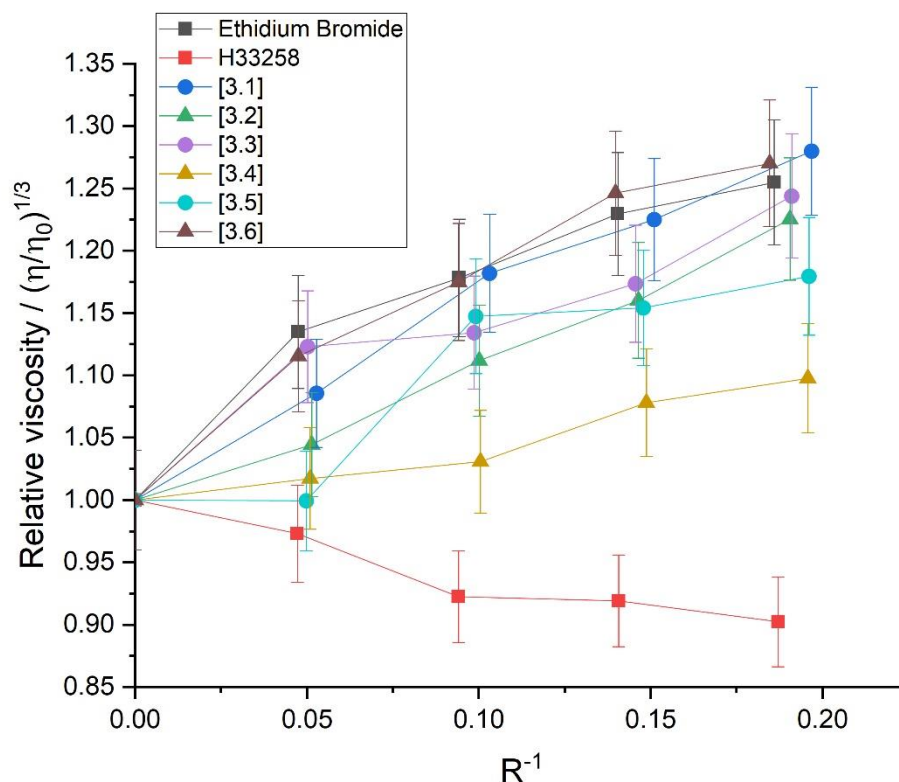


Figure 3.13 Change in relative viscosity of ct-DNA solutions at 25 °C on addition of [3.1]-[3.6], ethidium bromide and Hoechst 33258.

All complexes except for [3.4] and [3.5] show a large, roughly constant increase in relative viscosity, and are within error, the same as for ethidium bromide, indicative of an intercalative binding mode. [3.5] does also show a large increase, although only for one addition, suggesting that the overall binding interaction may be more complicated than simply just intercalation.

[3.4] shows a small increase – not as large as for ethidium bromide, but the relative viscosity is higher than observed for Hoechst 33258. There are two possible explanations for this. The first is that [3.4] does not intercalate as deeply as the other complexes, causing a smaller lengthening of the duplex on binding as a result. The second is that the

complex behaves similar to $[\text{Ru}(\text{tpm})(\text{dppz})(4\text{NH}_2\text{py})]^{2+}$, which groove binds at higher temperatures, but then switches to intercalation at lower temperatures. To investigate this, the change in relative viscosity of **[3.4]** was recorded at 16 °C and 35 °C. The data is shown in figure 3.14.

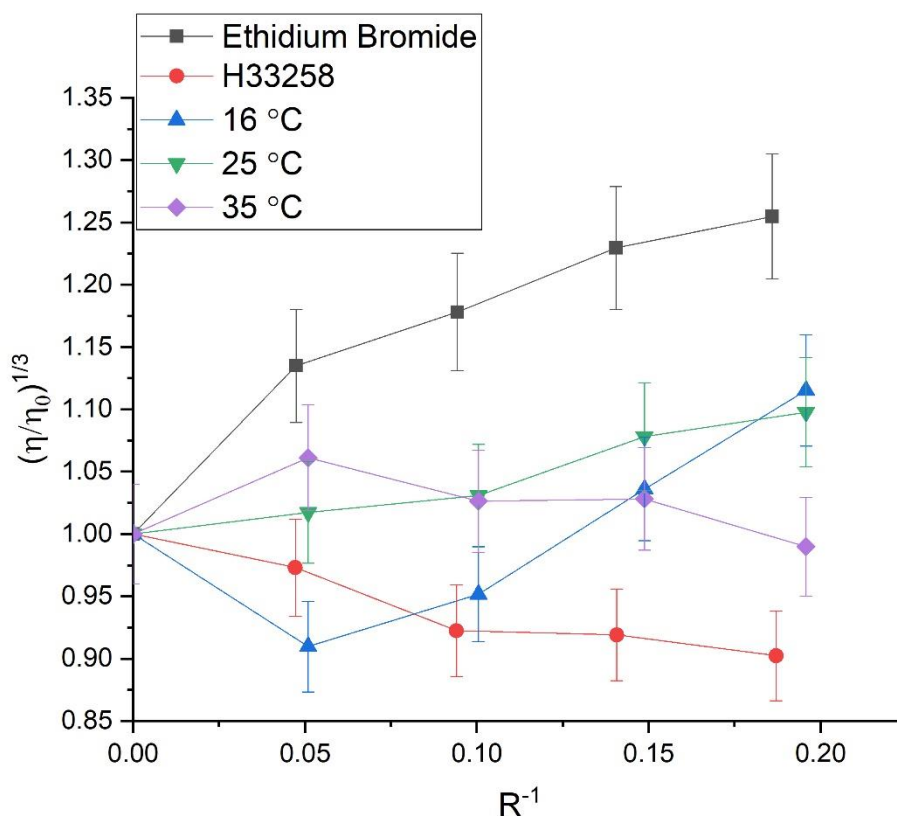


Figure 3.14 Change in relative viscosity of ct-DNA solutions on addition of **[3.4]** at 16 °C, 25 °C, and 35 °C, as well as ethidium bromide and Hoechst 33258.

Comparing 25 °C and 35 °C, at lower mixing ratios, both show a very slight increase in relative viscosity, and then begin to diverge at higher mixing ratios, with 25 °C continuing to increase slowly, and 35 °C decreasing slightly. However, broadly speaking, both seem to show similar behaviour. This is in contrast to the measurements at 16 °C, which shows an initial decrease at low mixing ratios, followed by a rapid increase,

eventually reaching a similar relative viscosity to 25 °C measurement. The rate of increase is greater than that of ethidium bromide, perhaps indicating that at lower temperatures, multiple binding modes are in competition. This preliminary study does indicate that the DNA binding properties of this complex do display temperature dependent changes that could be further explored.

3.2.6 DNA binding titrations

The binding of [3.1]-[3.6] to ct-DNA were investigated by luminescence spectroscopy using the same method as chapter 2. The luminescence data, binding curve, and Scatchard plots where possible are shown below for each complex. UV-visible titrations were attempted, however, consistent changes were not observed, instead, there were small oscillations around each of the major peaks. A possible explanation is the weaker binding of these compounds relative to their dppz analogues means that there is a smaller change in the absorbance of each peak on binding, therefore leaving them more susceptible to interference from noise. Luminescence data of sufficient quality for fitting could not be collected for some complexes. In the case of [3.1], which is essentially non-emissive in water, a small enhancement was observed on binding, however, the emission was very noisy, meaning changes were difficult to monitor accurately. Increasing the concentration did not decrease the relative amount of noise in the emission, and so no binding constant could be derived. For [3.6], an initial small decrease in the emission was observed after the first addition of ct-DNA, and then no further changes were observed. Decreasing the concentration of DNA, as well as the addition volume, yielded the same result, so again, no binding constant could be extracted for this compound.

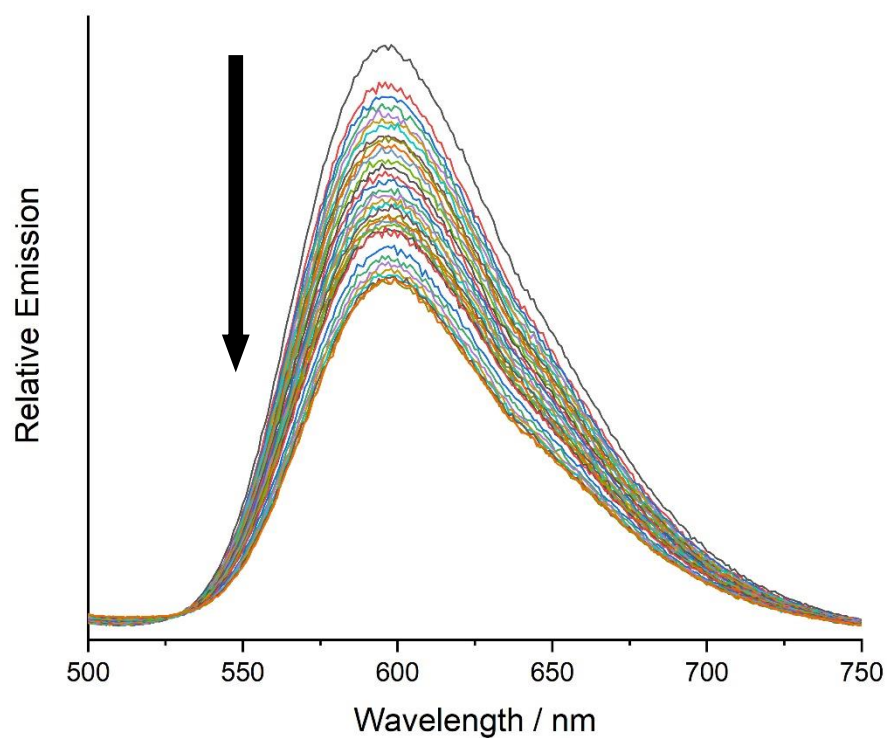


Figure 3.15 Luminescence titration of [3.2] with ct-DNA. $\lambda_{\text{ex}} = 426 \text{ nm}$. [Complex] = $28 \mu\text{M}$. Stock [DNA] = 16 mM . Total DNA addition volume = $70 \mu\text{L}$. Final [DNA] = $365 \mu\text{M}$

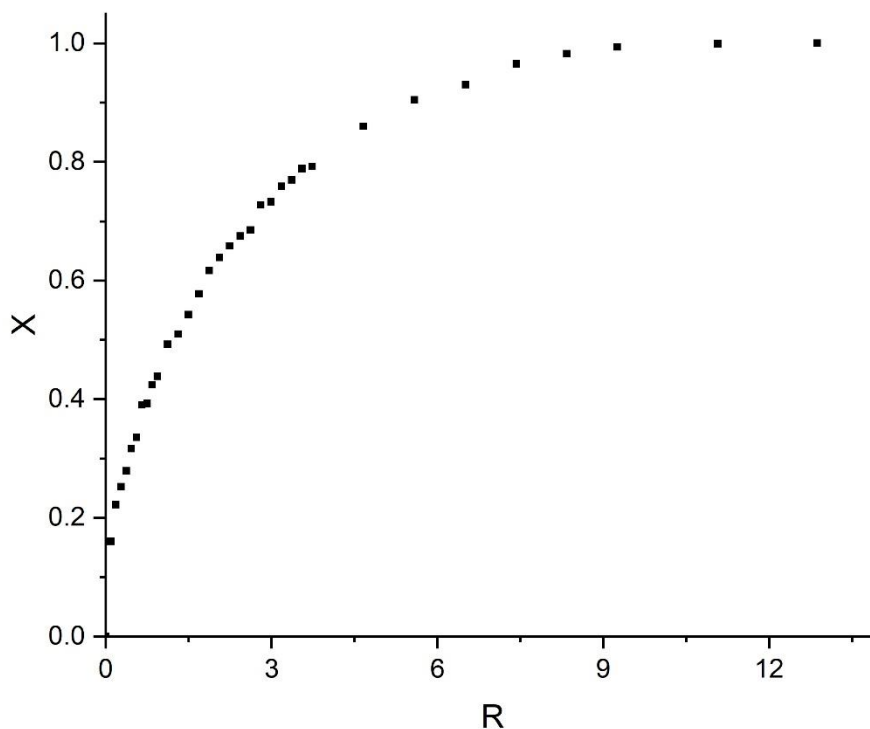


Figure 3.16 Binding curve from titration of [3.2] with ct-DNA, where R is [DNA]/[analyte] and X is the fraction bound.

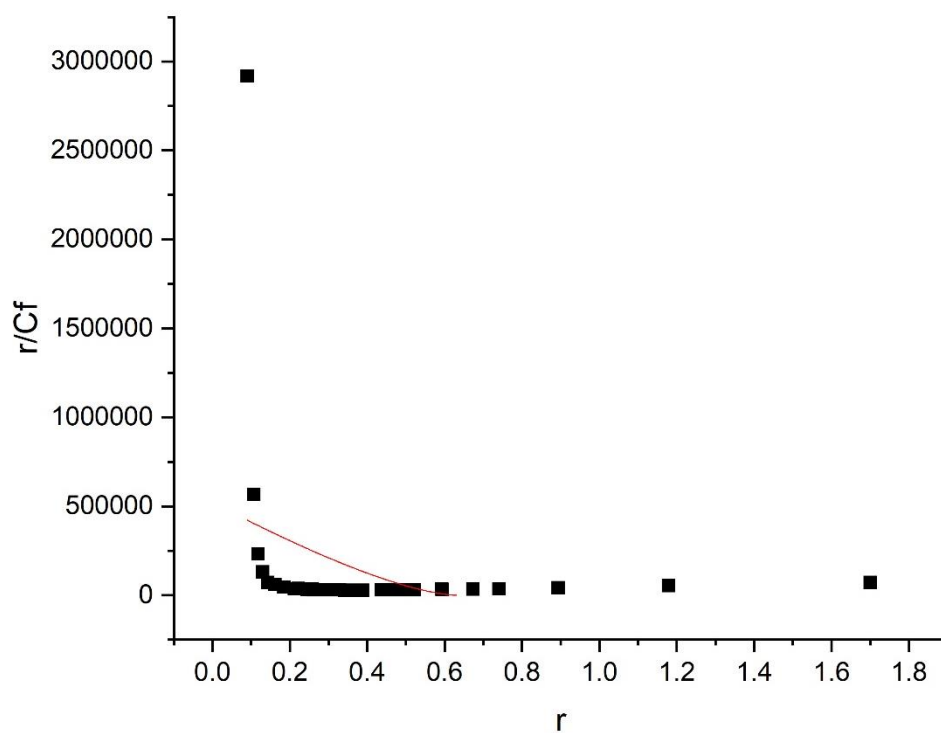


Figure 3.17 Scatchard plot for binding of [3.2] to ct-DNA. Data fitted using the McGhee-von Hippel model for non-cooperative binding. $R^2 = 0.12$

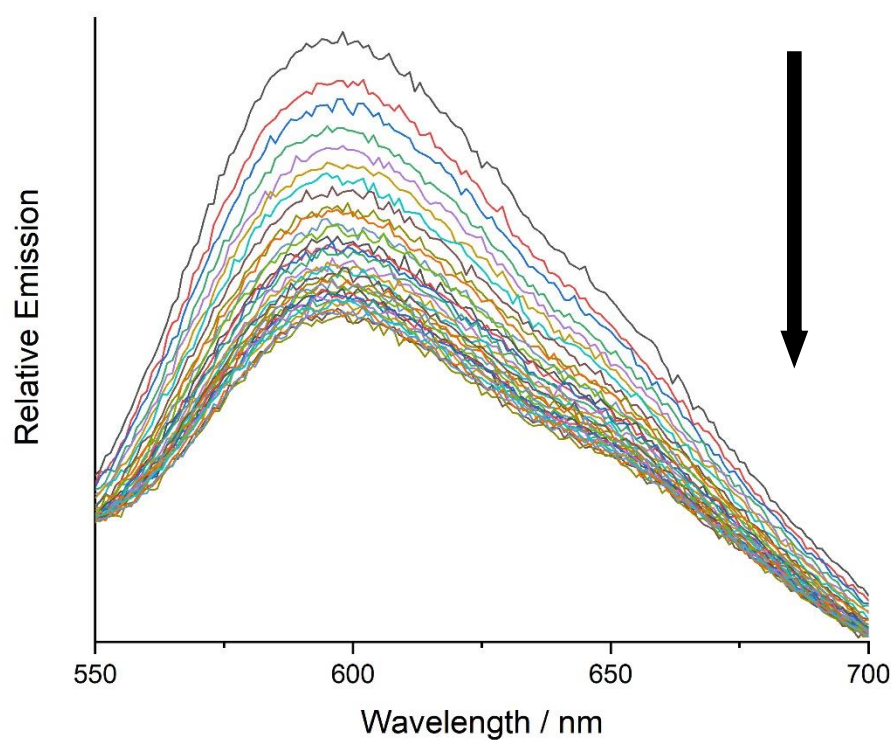


Figure 3.18 Luminescence titration of [3.3] with ct-DNA. $\lambda_{ex} = 420$ nm. [Complex] = 16 μ M. Stock [DNA] = 16 mM. Total addition volume = 50 μ L. Final [DNA] = 262 μ M

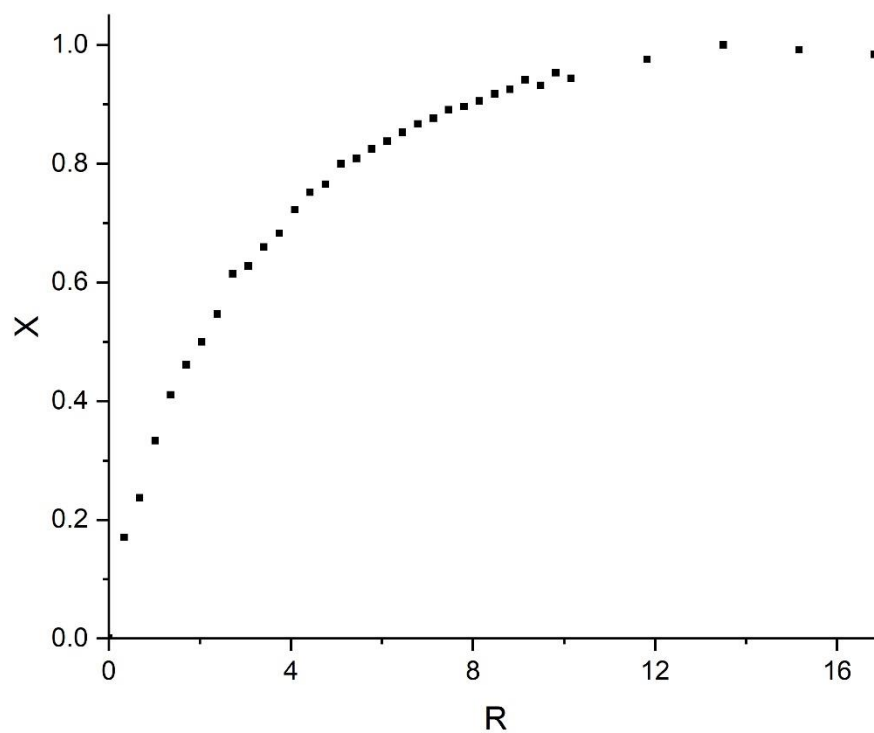


Figure 3.19 Binding curve from titration of [3.3] with ct-DNA, where R is [DNA]/[analyte] and X is the fraction bound.

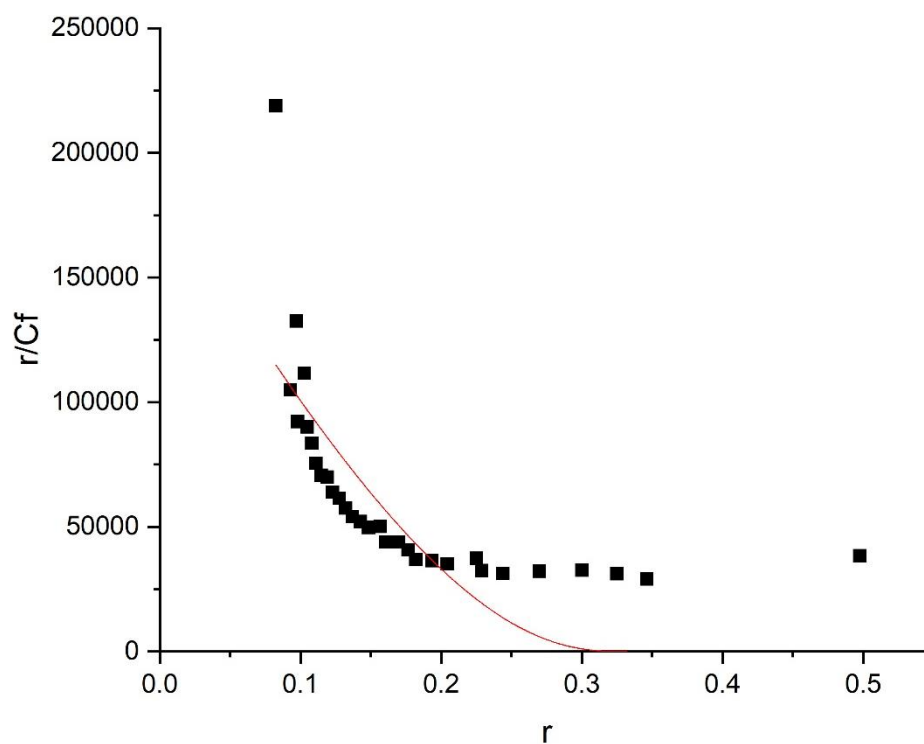


Figure 3.20 Scatchard plot for binding of [3.3] to ct-DNA. Data fitted using the McGhee-von Hippel model for non-cooperative binding. $R^2 = 0.55$

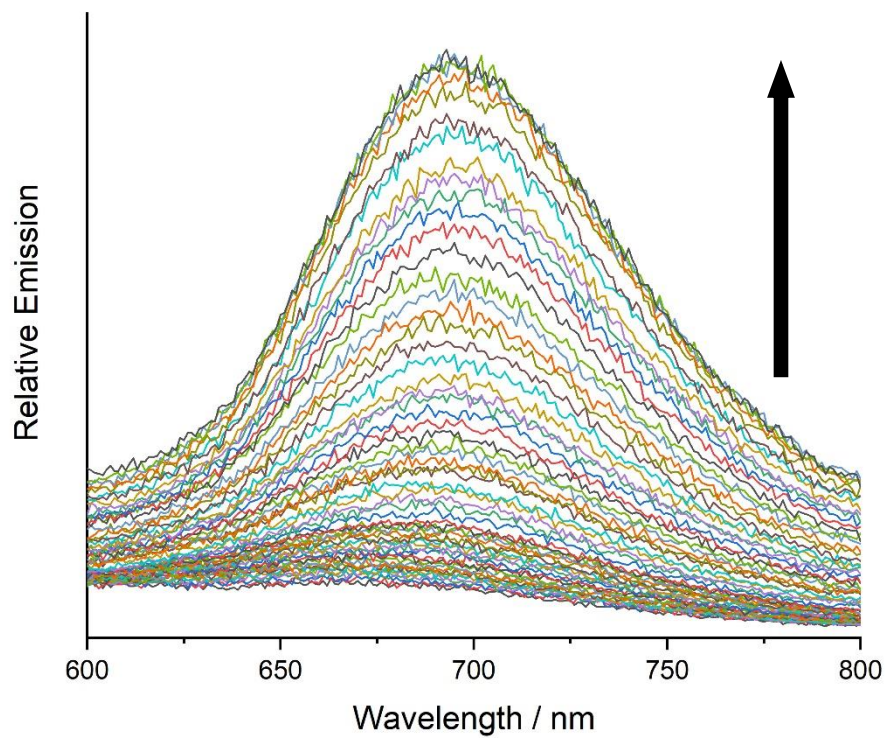


Figure 3.21 Luminescence titration of [3.4] with ct-DNA. $\lambda_{\text{ex}} = 419 \text{ nm}$. [Complex] = $38 \mu\text{M}$. Stock [DNA] = 16 mM . Total addition volume = $600 \mu\text{L}$. Final [DNA] = 2.67 mM

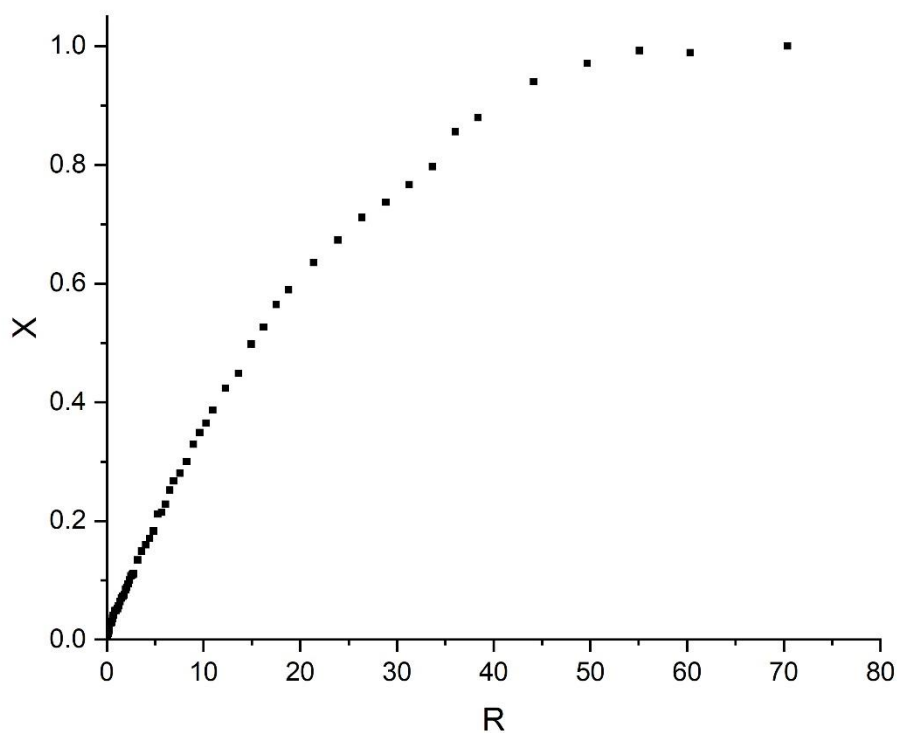


Figure 3.22 Binding curve from titration of [3.4] with ct-DNA, where R is [DNA]/[analyte] and X is the fraction bound.

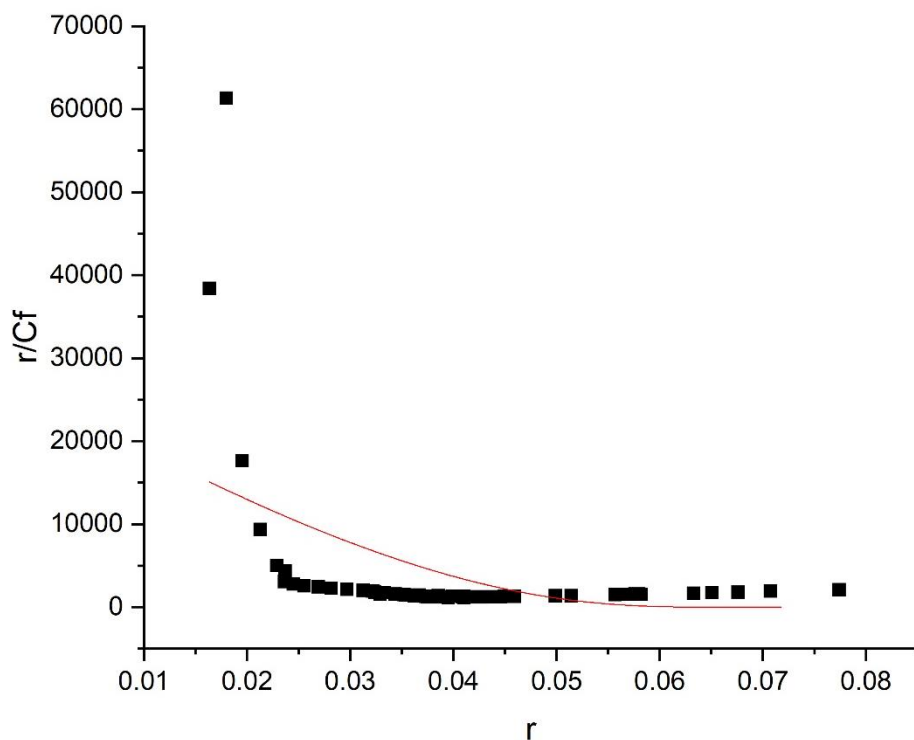


Figure 3.23 Scatchard plot for binding of [3.4] to ct-DNA. Data fitted using the McGhee-von Hippel model for non-cooperative binding. $R^2 = 0.29$

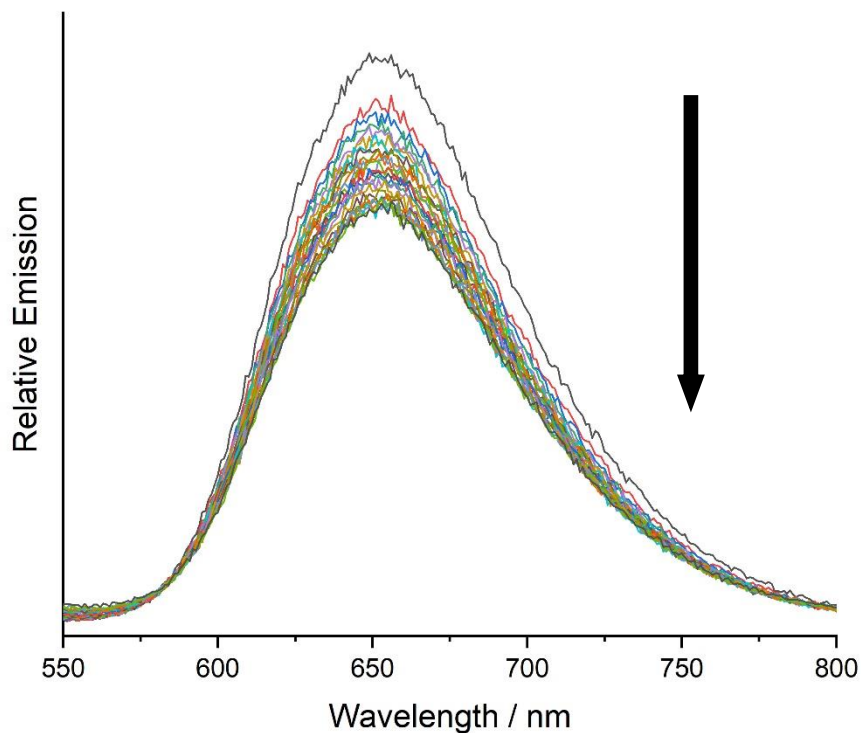


Figure 3.24 Luminescence titration of [3.5] with ct-DNA. $\lambda_{\text{ex}} = 418 \text{ nm}$. $[\text{Complex}] = 47 \mu\text{M}$, $[\text{DNA}] = 16 \text{ mM}$. Total addition volume = $26 \mu\text{L}$. Final $[\text{DNA}] = 25.8 \mu\text{M}$.

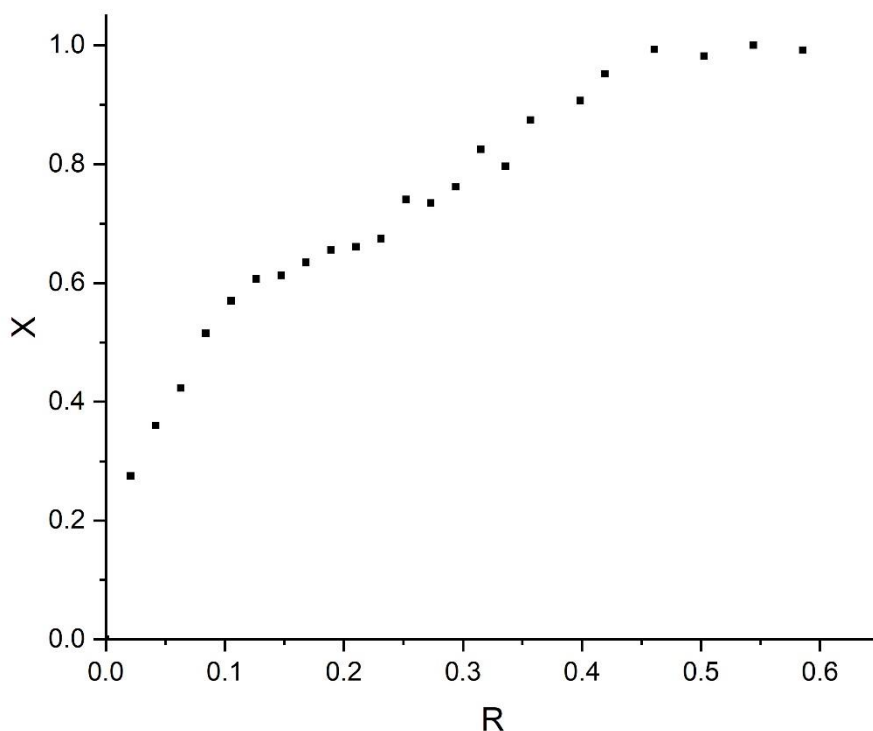


Figure 3.25 Binding curve from titration of [3.5] with ct-DNA, where R is [DNA]/[analyte] and X is the fraction bound.

In the case of [3.5], binding parameters could not be calculated, due to data of insufficient quality. The binding parameters that could be collected are summarised in table 3.7.

Compound	K_b / M^{-1}	n	R^2
[3.2]	$5.21 \pm 1.91 \times 10^5$	1.58	0.12
[3.3]	$1.88 \pm 0.13 \times 10^5$	3.00	0.55
[3.4]	$2.56 \pm 0.42 \times 10^4$	13.9	0.29

Table 3.6 Binding parameters collected for compounds [3.2]-[3.4]. In all cases, the error in the site size was negligible.

The quality of the fit for all three complexes is relatively poor, with the highest R^2 value being only 0.55. This means drawing any firm conclusions or comparisons from

these binding data is not possible. This could be due the McGhee-von Hippel model not accurately describing the binding of these molecules, however, as the model has been used previously to fit the binding of other, related complexes, such as $[\text{Ru}(\text{bpy})_2(\text{pzp})]^{2+}$, this is unlikely.¹¹ Instead, it may be that measuring the change in luminescence is not an effective way of studying the binding of these complexes. It is noticeable that in all binding curves displayed above for which fitting could be performed (figures 3.16, 3.19, 3.22), there is quite a lot of noise around the “perfect” binding curve. It may be more appropriate to use a more direct technique, such as isothermal calorimetry (ITC), to study the binding of these complexes. ITC allows measurement of the binding constant through measurement of heat changes, and so should avoid previously encountered problems with optical data. Additionally, the entropic and enthalpic contributions to binding can be measured, which can allow more detailed study of the binding processes.

[3.5] appears to show two steps in the binding curve shown in figure 3.25. There is an initial binding interaction that appears to begin to saturate, followed by a second curve. The greater noise in the second curve suggests a weaker, less specific interaction. Neither the full data, nor the initial “saturation” could be fitted to the McGhee-von Hippel model. Rather than a two-step binding mode, which would be unusual behaviour for compounds of this type, it is more likely that this apparent “two-step” binding mode is simply generated by noise and is unlikely to be reproducible.

The apparent fraction bound reaches 1.0 at mixing ratios around 0.5, meaning the complex is in twofold excess of the number of base pairs, suggesting a normal intercalative binding mode is unlikely. Referring back to the relative viscometry, [3.5] did show an increase, although only for a single addition, with all others remaining near

constant. In order to attempt to shed further light on the binding of [3.5] to ct-DNA, a continuous variation plot was constructed. The plot is shown in figure 3.26.

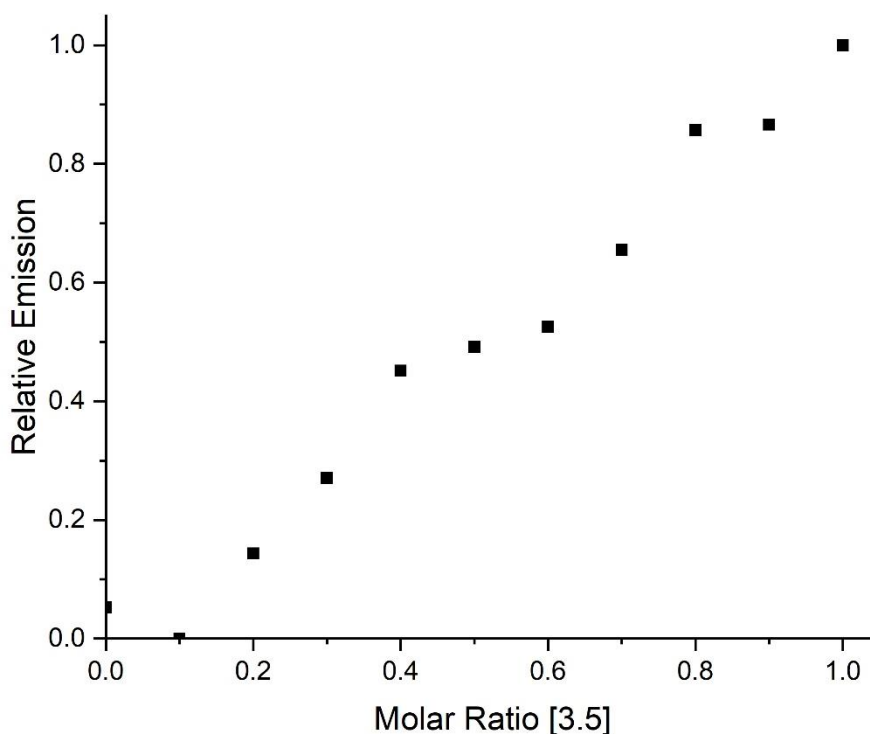


Figure 3.26 Continuous variation plot of the binding of [3.5] to ct-DNA.

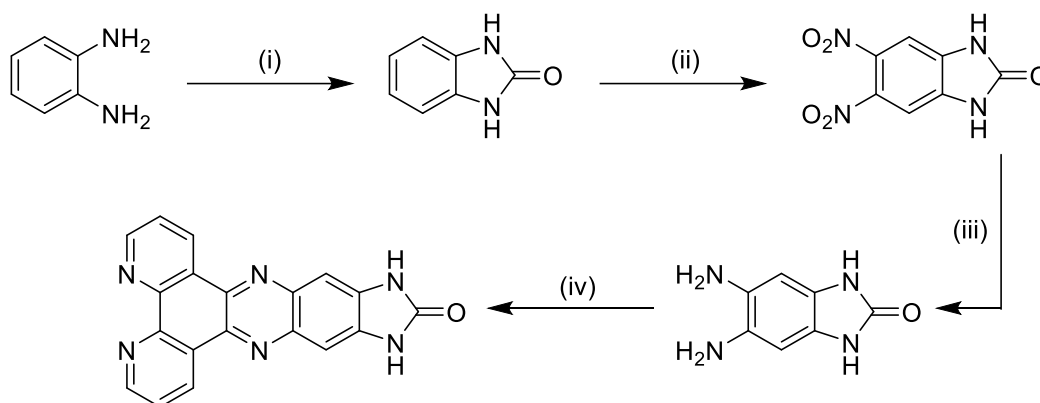
If no binding between [3.5] and the DNA was occurring, then the plot would simply show a dilution of the complex, and therefore a linear reduction of the relative emission intensity. Although the reduction is not perfectly linear, it scatters above and below the line, which seems to suggest binding has little effect on emission intensity. This could be due to either binding simply being so weak that it cannot affect the emission, or that there is no “light-switch” analogue effect. As above, it may be that emission spectroscopy is not the most effective way to probe the binding of these complexes, and the another technique, such as ITC, may be more appropriate.

3.3 Towards other Ru complexes

3.3.1 Synthesis – ligands

3.3.1.1 Synthesis of dppz-idzo

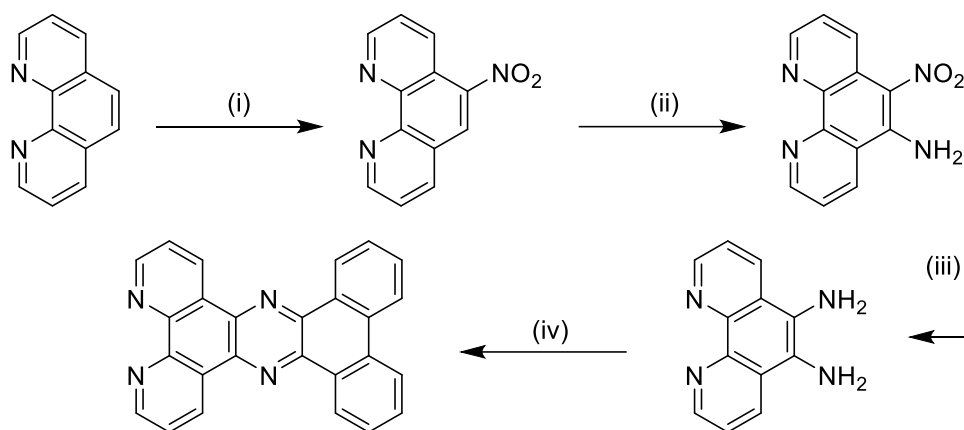
5,6-diaminobenzimidazol-2-one was synthesised using the procedure developed by the Liu group.²² 1,2-diaminobenzene was heated to 130 °C with urea in ethylene glycol to give benzimidazol-2-one as the product. Di-nitration was achieved using nitrating mixture, although fuming nitric acid was required to prevent mono-nitration. The desired diamine was then synthesised by catalytic hydrogenation using N₂H₄ and Pd/C. Condensation with dpq then gave dppz-idzo.¹⁴ The synthetic route is shown in scheme 3.3.



Scheme 3.23 (i) Urea, ethylene glycol, 130 °C, 1 hr → 170 °C, 7 hrs; (ii) HNO₃ (fuming), H₂SO₄, 0 °C; (iii) N₂H₄·H₂O, Pd/C, MeOH:H₂O (1:2), reflux, 18 hrs; (iv) dpq, EtOH, reflux, 15 mins.

3.3.1.2 Synthesis of taptp

Taptp can be synthesised by the condensation reaction of 5,6-diamino-1,10-phenanthroline with phenanthrene-9,10-dione. 5,6-diaminophenanthroline was synthesised by nitration of phen with HNO_3 and H_2SO_4 , followed by amination through a vicarious nucleophilic substitution with NH_2OH . The desired diamine was then produced by reducing with N_2H_4 and Pd/C. Finally, condensation with dpq gave taptp. The synthetic route is shown in scheme 3.4.



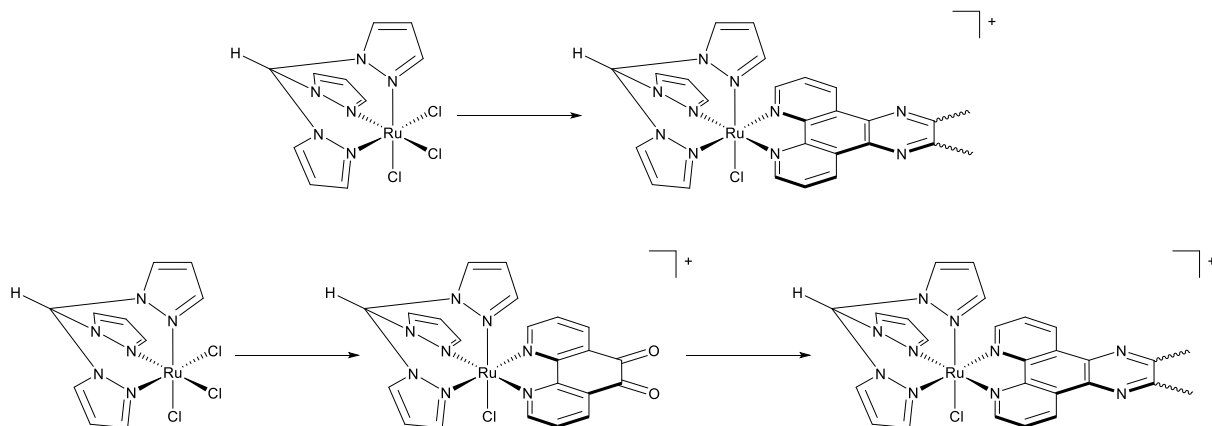
Scheme 3.24 (i) HNO_3 , H_2SO_4 , $160\text{ }^\circ\text{C}$, 1.5 hrs; (ii) $\text{NH}_2\text{OH}\cdot\text{HCl}$, $\text{KOH}_{(\text{MeOH})}$, EtOH:dioxane (3:2), $-5\text{ }^\circ\text{C}$, 1 hr \rightarrow RT, 1hr; (iii) $\text{N}_2\text{H}_4\cdot\text{H}_2\text{O}$, Pd/C, MeOH, reflux, 2 hrs; (iv) dpq, EtOH, reflux, 3 hrs.

3.3.2 Synthesis of chloride complexes

3.3.2.1 Standard route

Initial attempts to synthesise $[\text{Ru}(\text{tpm})(\text{dppz-izdo})(\text{Cl})][\text{PF}_6]$ and $[\text{Ru}(\text{tpm})(\text{taptp})(\text{Cl})][\text{PF}_6]$ through the conventional route previously described for the dppz and pzp complexes were unsuccessful. This is likely due to the limited solubility of these large, planar aromatic ligands in solvents like EtOH and H_2O . Exploration of other commonly used solvents for reactions of this sort, such as DMF and ethylene glycol, also

showed no reaction. It was therefore decided to attempt a “building-block” style synthetic route, involving the synthesis of $[\text{Ru}(\text{tpm})(\text{dpq})(\text{Cl})][\text{PF}_6]$, followed by subsequent condensation of the appropriate diamines. The two methods are shown in scheme 3.5.



Scheme 3.25 The two initial routes to $[\text{Ru}(\text{tpm})(\text{N}^{\wedge}\text{N})(\text{Cl})]^+$. Top – Conventional route involving coordination of planar aromatic ligand to $[\text{Ru}(\text{tpm})(\text{Cl})_3]$. Bottom – “Building-block” route involving synthesis of $[\text{Ru}(\text{tpm})(\text{dpq})(\text{Cl})]^+$ as intermediate, followed by subsequent condensation with a diamine.

The synthesis of $[\text{Ru}(\text{tpm})(\text{dpq})(\text{Cl})][\text{PF}_6]$ by reaction of $[\text{Ru}(\text{tpm})\text{Cl}_3]$ with dpq was unsuccessful under all conditions tried. This is likely caused by the fact that both dpq and $[\text{Ru}(\text{tpm})\text{Cl}_3]$ are relatively electron deficient. A similar problem has been previously encountered in the Thomas group when attempting to synthesise $[\text{Ru}(\text{TAP})_2(\text{dpq})]^{2+}$ from $[\text{Ru}(\text{TAP})_2\text{Cl}_2]$ and dpq. In this case, it was solved through use a microwave reactor, however, the small scale required for microwave synthesis means this would not be an appropriate route for this work. Another alternative that would be worth exploring is use of toluene as either the solvent or as a co-solvent. Large planar aromatics such as dppz-ido and taptp could be forming π -stacked aggregates in solution, preventing coordination. Toluene would help to break up these aggregates.

3.3.2.2 New route

Instead, a new synthetic route adapted from the Keyes group was used.²³ The original work was used to synthesise tris-heteroleptic Ru (II) polypyridyl complexes, however, recent work in the Thomas group has adapted it for synthesis of Ru(tpm)-based complexes.²⁴ The route used is shown in scheme 3.6. $[\text{Ru}(\text{DMSO})_4\text{Cl}_2]$ was synthesised by refluxing DMSO with $\text{RuCl}_3 \cdot 3\text{H}_2\text{O}$ in $^i\text{PrOH}$. Dpq could then be introduced by refluxing in toluene. The ^1H NMR spectrum showed six peaks that could be attributed to dpq, suggesting that the complex is all *cis*-co-ordinated. Mass spectrometry of $[\text{Ru}(\text{DMSO})_2(\text{dpq})\text{Cl}_2]$ proved challenging, as the DMSO ligands are relatively labile, leading to generation of many species in the spectrum. Confirmation of the product stoichiometry was achieved by reacting with excess phen – analysis of the product distribution of this reaction by mass spectrometry could then give information about the Ru:dpq ratio in the original product. The only ruthenium containing peak observed was a doubly charged peak with 336 m/z, corresponding to $[\text{Ru}(\text{phen})_2(\text{dpq})]^{2+}$. This finding confirms the identity of $[\text{Ru}(\text{DMSO})_2(\text{dpq})\text{Cl}_2]$ (as opposed to a doubly dpq co-ordinated product).

Co-ordination of tpm was achieved by refluxing with $[\text{Ru}(\text{DMSO})_2(\text{dpq})\text{Cl}_2]$ in DMF under an argon atmosphere. The complex was isolated relatively pure after precipitation, however, attempts to further purify by either flash column chromatography over silica or deactivated alumina, or charge separation chromatography using SP-Sephadex were unsuccessful, due to the strong retention of the product. This was presumably caused by strong interaction of the quinoidal moiety with the stationary phase. The complex was therefore used without further purification. The complex was characterised by ^1H NMR

and ESI-MS. The assigned ^1H NMR spectrum is shown in figure 3.28. ESI-MS showed a single charged peak at 561 m/z, which matches the expected mass of the product.

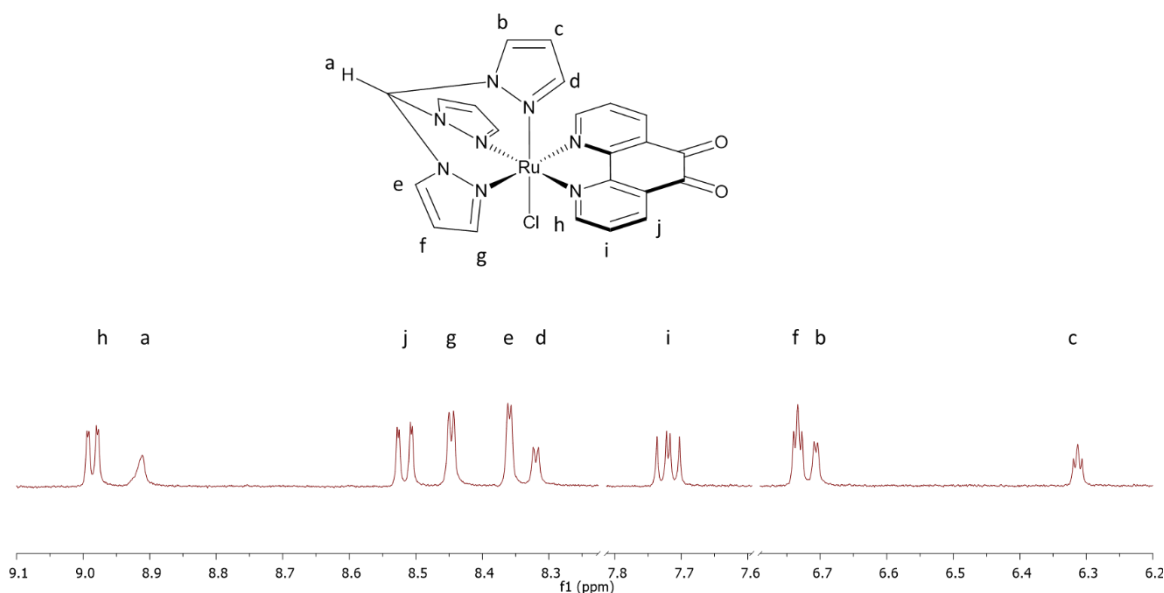
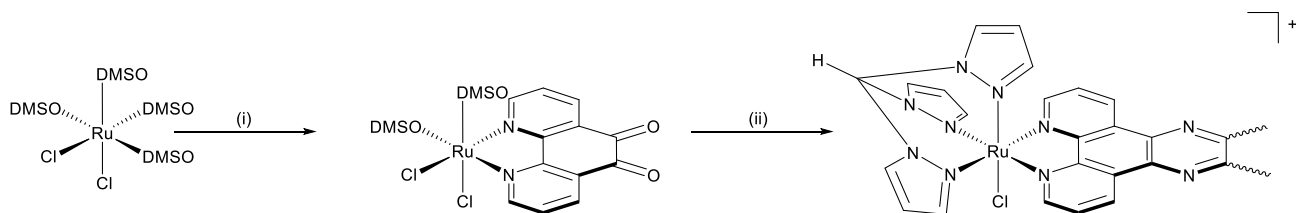


Figure 3.27 The assigned ^1H NMR spectrum of $[\text{Ru}(\text{tpm})(\text{dpq})(\text{Cl})]^+$.

In analogous fashion to other “building-block” strategies of this type, synthesis of the target complexes was achieved by dissolving $[\text{Ru}(\text{tpm})(\text{dpq})(\text{Cl})][\text{PF}_6]$ and the diamine in boiling MeCN and EtOH, respectively, followed by mixing, and reflux for four hours. The products could then be precipitated as their PF_6 salts.



Scheme 3.26 (i) dpq, toluene, reflux, 8 hrs; (ii) tpm, DMF, reflux, 4 hrs.

Initial test reactions suggested both $[\text{Ru}(\text{tpm})(\text{dppz-izdo})(\text{Cl})][\text{PF}_6]$ and $[\text{Ru}(\text{tpm})(\text{taptp})(\text{Cl})][\text{PF}_6]$ can be synthesised by this route. Both products were identified

by ESI-MS. Purification was not attempted, due to the small amount of crude product collected, however, complexes of this type can generally be isolated by column chromatography over neutral alumina, using either MeCN or MeCN:toluene as the mobile phase.

In order for this synthetic route to be fully viable, the yield for synthesis of [Ru(tpm)(dpq)(Cl)]PF₆ requires improvement. Typical yields for this step are around 10-15 %, meaning that very large quantities of starting material would be required to achieve all of the desired taptp and dppz-izdo products.

3.4 Conclusions and future work

A series of Ru-pzp complexes bearing pyridine ligands functionalised with either hydrogen bonding or methyl groups were synthesised. All complexes were found to have broad MCLT-based absorptions around 410-420 nm, and showed broad, unstructured emission in MeCN. Some complexes were non- or weakly emissive in water, suggesting they may be able to act as DNA “light-switches”. Relative viscosity measurements showed all complexes apart from [3.4] bound to ct-DNA by intercalation; [3.4] appears to groove bind. This replicates the room temperature studies for the dppz analogues. At higher temperatures, [3.4] showed similar behaviour to room temperature, however, at lower temperatures, the complex showed an initial decrease at lower mixing ratios, followed by a rapid recovery to similar relative viscosity to higher temperature measurements. This is different to the finding for the dppz analogue, which intercalated at lower temperatures, suggesting the extra energetic stabilisation of the terminal ring of dppz is required to compensate for the negative steric interactions of the meta-amine group.

The DNA binding of complexes [3.1]-[3.6] was studied through luminescence titrations. Binding constants could be determined for three complexes, [3.2], [3.3] and [3.4], although due to the poor quality of the fit, meaningful evaluation of the binding constants, or comparison with related complexes, could not be performed. The binding curves collected are noisy, which may be part of the reason for the poor-quality fit. It would be worthwhile to collect the binding data using a different technique, such as ITC, which directly probes the heat changes on binding, to determine if the problem lies with either model used, or simply with the use of luminescence.

Finally, synthetic routes towards other ruthenium complexes, bearing extended intercalating ligands were explored. One potential route, utilised $[\text{Ru}(\text{tpm})(\text{dpq})(\text{Cl})]^+$ as a building block, with test reactions indicating $[\text{Ru}(\text{tpm})(\text{dppz-izdo})(\text{Cl})][\text{PF}_6]$ and $[\text{Ru}(\text{tpm})(\text{taptp})(\text{Cl})][\text{PF}_6]$ were accessible, however, the total yield of the route is very low, and therefore some optimisation is required before it is fully viable.

3.5 References

- 1 P. Waywell, V. Gonzalez, M. R. Gill, H. Adams, A. J. H. M. Meijer, M. P. Williamson and J. A. Thomas, *Chem. - A Eur. J.*, 2010, **16**, 2407–2417.
- 2 H. Song, J. T. Kaiser and J. K. Barton, *Nat. Chem.*, 2012, **4**, 615–20.
- 3 H. Niyazi, J. P. Hall, K. O’Sullivan, G. Winter, T. Sorensen, J. M. Kelly and C. J. Cardin, *Nat. Chem.*, 2012, **4**, 621–8.
- 4 J. P. Hall, D. Cook, S. R. Morte, P. McIntyre, K. Buchner, H. Beer, D. J. Cardin, J. A. Brazier, G. Winter, J. M. Kelly and C. J. Cardin, *J. Am. Chem. Soc.*, 2013, **135**, 12652–12659.
- 5 J. P. Hall, S. P. Gurung, J. Henle, P. Poidl, J. Andersson, P. Lincoln, G. Winter, T. Sorensen, D. J. Cardin, J. A. Brazier and C. J. Cardin, *Chem. - A Eur. J.*, 2017, **23**, 4981–4985.
- 6 R. H. Terbrueggen, T. W. Johann and J. K. Barton, *Inorg. Chem.*, 1998, **37**, 6874–6883.
- 7 V. G. González, PhD Thesis, University of Sheffield, 2006.
- 8 P. Waywell, V. Gonzalez, M. R. Gill, H. Adams, A. J. H. M. Meijer, M. P. Williamson and J. A. Thomas, *Chem. - A Eur. J.*, 2010, **16**, 2407–2417.
- 9 M. G. Walker, V. Gonzalez, E. Chekmeneva and J. A. Thomas, *Angew. Chemie Int. Ed.*, 2012, **51**, 12107–12110.
- 10 J. G. Collins, A. D. Sleeman, J. R. Aldrich-Wright, I. Greguric and T. W. Hambley, *Inorg. Chem.*, 1998, **37**, 3133–3141.
- 11 S. Delaney, M. Pascaly, P. K. Bhattacharya, K. Han and J. K. Barton, *Inorg. Chem.*,

- 2002, **41**, 1966–1974.
- 12 K. A. O’Donoghue, J. M. Kelly and P. E. Kruger, *Dalt. Trans.*, 2004, **0**, 13.
- 13 A. Ambroise and B. G. Maiya, *Inorg. Chem.*, 2000, **39**, 4264–4272.
- 14 J.-L. Yao, X. Gao, W. Sun, S. Shi and T.-M. Yao, *Dalt. Trans.*, 2013, **42**, 5661.
- 15 K. Suntharalingam, A. J. P. White and R. Vilar, *Inorg. Chem.*, 2009, **48**, 9427–9435.
- 16 J. L. Huppert and S. Balasubramanian, *Nucleic Acids Res.*, 2005, **33**, 2908–2916.
- 17 G. Biffi, D. Tannahill, J. McCafferty and S. Balasubramanian, *Nat. Chem.*, 2013, **5**, 182–186.
- 18 Q.-X. Zhen, B.-H. Ye, Q.-L. Zhang, J.-G. Liu, Hong Li, L.-N. Ji and L. Wang, *J. Inorg. Biochem.*, 1999, **76**, 47–53.
- 19 P. J. Jarman, E. K. Griffiths, H. K. Saeed, J. A. Thomas and C. G. W. Smythe, *submitted*.
- 20 R. Díaz, A. Francois, A. M. Leiva, B. Loeb, E. Norambuena and M. Yañez, *Helv. Chim. Acta*, 2006, **89**, 1220–1230.
- 21 A. B. Wragg, S. Derossi, T. L. Easun, M. W. George, X.-Z. Sun, F. Hartl, A. H. Shelton, A. J. H. M. Meijer and M. D. Ward, *Dalt. Trans.*, 2012, **41**, 10354.
- 22 Z. Yang, J. Wang, L. Li, C. Ye and H. Liu, *J. Heterocycl. Chem.*, 2009, **46**, 788–790.
- 23 C. S. Burke and T. E. Keyes, *RSC Adv.*, 2016, **6**, 40869–40877.
- 24 T. Andrews, PhD Thesis, University of Sheffield, 2018.

Chapter Four

4 Conclusions and Future Work

4.1 Conclusions

There has recently been some interest in the literature into AuNPs conjugated to simple Ru (II) polypyridyl complexes, containing ligands such as bpy, phen and TAP.^{1,2} The aim of this project was to extend this previous work by incorporating ligands with a larger aromatic surface area, as these tend to have interesting photophysical properties, such as the DNA “light-switch” effect of dppz complexes.³ The complexes would be based around an achiral, modular Ru (II) polypyridyl complex developed by the Thomas group, $[\text{Ru}(\text{tpm})(\text{N}^{\wedge}\text{N})(\text{Cl})]^+$, where $\text{N}^{\wedge}\text{N}$ is a bidentate polypyridyl ligand. The axial chloride ligand can be substituted for a modified pyridine ligand, allowing inclusion of a thiol-bearing group, for attachment to AuNPs.

The first strand of this work was based around incorporating dppz into the above system, as the chemistry and photophysical properties of dppz complexes have been widely explored, both in the Thomas group and others. Initial synthetic routes explored were based around the structures used by the Gunnlaugsson¹ and Pikramenou² groups. The general requirements were a ligand bearing a pyridyl group at one end, for Ru coordination, and a thiol at the other, for AuNP attachment. The synthetic route based on the structures used in the Gunnlaugsson group involved attaching a carboxylic acid terminated with a thiol group to aminopyridines via amide coupling. No product was detected, although this may be due to the product remaining in solution, rather than precipitating, and, as the filtrate was not analysed, the product was undetected. Several other routes were explored, including some based around copper-catalysed azide-alkyne click chemistry, Suzuki-Miyaura cross coupling, and oligoethylene glycols. This final

ligand was initially developed by the Yam group, who were investigating the energy transfer between Ru (II) or Re (I) polypyridyl complexes, and AuNPs. Although the ligand was successfully synthesised, it would not co-ordinate to the metal complex. All of the synthetic routes explored above attempted to attach a pyridine to a long tail, terminated with a thiol group. In an effort to explore alternative methods, new routes were designed where the functionalised pyridine was pre-co-ordinated to the Ru complex, and a ligand with a thiol at one end, and a group of complementary reactivity to the pyridine at the other, was pre-attached to the AuNP. Performing the connective chemistry would then create the desired system. A similar concept has been previously developed by the Mirkin group for delivery of Pt (IV) prodrugs to cancerous cells, using AuNPs as a vector.⁴ The connective chemistry explored included amides, reductive aminations, and copper catalysed azide-alkyne click reactions, however, none were successful, due to factors including non-co-ordination of the functionalised pyridines, instability of the complexes generated on co-ordination, or problems with the synthesis of the AuNP ligand. A route was developed which used 3-picolyamine as the functionalised pyridine, and then a short oligoethylene glycol group, terminated with a carboxylic acid at one end, and a thiol at the other. An initial attempt to couple the two via amide coupling was unsuccessful. Although the activated carboxylic acid was detected, the full complex was not. This step, therefore, requires further optimisation. A good starting point would be trying the coupling reaction before co-ordination of the pyridine, to investigate whether the problem lies with the pyridine itself, or the complex. The photophysical and DNA binding properties of the complex were explored, to see if it still retained the DNA “light-switch” effect. The complex was shown to bind through intercalation through relative viscosity measurement, and, when titrated against ct-DNA, its emission increased. The

binding constant was $2.39 \pm 0.14 \times 10^6 \text{ M}^{-1}$, which is a normal value for compounds of this type (around $1-5 \times 10^6 \text{ M}^{-1}$ is typical), although the site size was found to be 12.80, which is significantly larger than expected (1-3 is typical). It was suggested the large site size could be caused by electrostatic repulsion by the pendant amine group.

The second strand of the project involved exploring the photophysical and DNA binding properties of complexes with a range of other intercalating ligands. Previous work in the group had explored a range of $[\text{Ru}(\text{tpm})(\text{dppz})(\text{L})]^{2+}$ complexes, where L represents a range of simple functionalised pyridines with different hydrogen bonding and electronic properties.⁵ This project aimed to use the same set of functionalised pyridines, but with different intercalating ligands. Pzp was chosen, as it is one ring shorter than dppz, and so the functionalised pyridines should be forced closer to the DNA backbone on binding. The other ligands chosen were taptp, which is a wide, long intercalating ligand, and dppz-izdo. These were chosen because it has been shown that changing the pyridine on dppn complexes has little effect on the DNA binding properties, as the metal centre resides further from the backbone, and so interaction with the pyridine were minimised.

For the pzp complexes, six of the eight desired complexes were successfully synthesised. The complexes containing aldehyde-functionalised pyridines could not be obtained pure, as there was a significant amount of the aldehyde hydrate which formed, and could not be separated. The other six complexes were tested for their DNA binding and photophysical properties. The absorption spectra of the complexes were typical for compounds of this type, with some higher energy bands, corresponding to the $\pi-\pi^*$ transitions of the aromatic ligands, and the MLCT band, found between 400-450 nm. The difference in position of the MLCT in water and MeCN was evaluated in terms of the

electronic properties of the axial pyridine. The DNA binding mode of each complex was probed through relative viscosity measurements. It was found that most complexes showed standard intercalative behaviour, except for the complexes bearing 3-picoline and 4-aminopyridine. The 3-picoline complex showed little change in relative viscosity at low mixing ratios, followed by a large jump, and then a consistent increase. This suggests multiple binding modes competing with each other, with the complex perhaps groove binding at lower mixing ratios, before switching to a more standard intercalative binding mode at higher mixing ratio. The 4-aminopyridine complex showed a more intermediate behaviour, with a small increase in relative viscosity, rather than the expected large increase for viscosity, or slight decrease for groove binding. As the dppz analogue showed temperature dependent switching between these two modes, we investigated if the pzp complex had similar behaviour. At higher temperatures, the relative viscosity was similar to that previously measured. At lower temperatures, there was initially a large decrease, followed by a rapid increase, again, suggesting multiple, competing binding modes. Although this investigation did not fully elucidate the binding behaviour of this complex, it did demonstrate the temperature dependent changes to its binding mode.

Attempts to measure the binding strength of these complexes by monitoring changes in luminescence were unsuccessful. In some cases, the luminescence response on addition of DNA was so small it was dominated by noise, and so no binding curve could be generated. In other cases, although a binding curve could be generated, the quality of the fit to the McGhee-von Hippel model was so low that no meaningful evaluation of the binding constant or site size could be performed. This could be either due to the data being of too poor quality, due to noise, or that the McGhee-von Hippel model does not satisfactorily describe the binding of these complexes. This could be tested by using an

alternative method to probe the binding, such as ITC, which directly measure the heat change on binding. We could then determine in the problem lies with using emission changes to measure the binding, or if the binding behaviour is more complex. Another advantage of ITC is it allows calculation of enthalpic and entropic changes, which can also help inform about binding mode.

The chemistry of dppz-izdo⁶ and taptp⁷ Ru (II) complexes has received little attention. Attempts to synthesis the $[\text{Ru}(\text{tpm})(\text{N}^{\wedge}\text{N})(\text{Cl})]^+$ ($\text{N}^{\wedge}\text{N} = \text{dppz-izdo}, \text{taptp}$) parent complexes through the usual route used in the group, where the planar aromatic ligand is reacted with $\text{Ru}(\text{tpm})\text{Cl}_3$, showed no reaction. This was attributed to the limited solubility of these large, planar aromatics. An alternative synthetic route, involving co-ordination of dpq as the $\text{N}^{\wedge}\text{N}$ ligand, followed by subsequent condensation with the appropriate diamine, was developed. This involved first co-ordinating dpq to $\text{Ru}(\text{DMSO})_4(\text{Cl})_2$, followed by co-ordination of tpm. This reaction was shown to work on a small scale, albeit with a low yield, and so requires further optimisation before it can be utilised for synthesis of dppz-izdo and taptp complexes.

4.2 Future work

The first step of future work for the first strand of the project is to find an effective method for the amide synthesis to allow attachment of the Ru complex to the AuNP. A range of amide coupling reagents could be screened against the carboxylic acid and unco-ordinated pyridine, and the successful reactions could then be tested with the complex. This would then allow synthesis of the full Ru-AuNP system.

In the second strand, the DNA binding of the pzp complexes should be measured using an alternative method that does not rely on emission, such as ITC. This would allow either

determination of binding constants, or show that binding behaviour is more complicated than that described by the McGhee-von Hippel model. It could also help to further elucidate the binding modes of some complexes, through measurement of thermodynamic parameters. Finally, the synthetic route towards $[\text{Ru}(\text{tpm})(\text{dppz-izdo})(\text{Cl})]^+$ and $[\text{Ru}(\text{tpm})(\text{taptp})(\text{Cl})]^+$, via $[\text{Ru}(\text{tpm})(\text{dpq})(\text{Cl})]^+$ required further optimisation. If these complexes can be synthesised, then exploring the DNA binding using the same set of functionalised pyridines as for the dppz^5 and pzp complexes. Additionally, if the synthetic route towards $\text{Ru}(\text{dppz})\text{-AuNP}$ system from the first strand is successfully developed, then a range of analogues incorporating all the intercalating ligands described in chapter 3 can be explored.

4.3 References

- 1 R. B. P. Elmes, K. N. Orange, S. M. Cloonan, D. C. Williams and T. Gunnlaugsson, *J. Am. Chem. Soc.*, 2011, **133**, 15862–15865.
- 2 N. J. Rogers, S. Claire, R. M. Harris, S. Farabi, G. Zikeli, I. B. Styles, N. J. Hodges and Z. Pikramenou, *Chem. Commun.*, 2014, **50**, 617–9.
- 3 A. E. Friedman, J. C. Chambron, J.-P. Sauvage, N. J. Turro and J. K. Barton, *J. Am. Chem. Soc.*, 1990, **112**, 4960–4962.
- 4 S. Dhar, W. L. Daniel, D. A. Giljohann, C. A. Mirkin and S. J. Lippard, *J. Am. Chem. Soc.*, 2009, **131**, 14652–14653.
- 5 V. G. González, PhD Thesis, University of Sheffield, 2006.
- 6 J.-L. Yao, X. Gao, W. Sun, S. Shi and T.-M. Yao, *Dalt. Trans.*, 2013, **42**, 5661.
- 7 Q.-X. Zhen, B.-H. Ye, Q.-L. Zhang, J.-G. Liu, Hong Li, L.-N. Ji and L. Wang, *J. Inorg. Biochem.*, 1999, **76**, 47–53.

Chapter Five

5 Experimental

5.1 Materials and Equipment

5.1.1 Chemicals

All chemicals and solvents were purchased from commercial suppliers, and were used as received. Dry solvents were obtained from a Grubbs solvent purification system.

5.1.2 Nuclear Magnetic Resonance (NMR) Spectra

^1H NMR spectra were recorded on a Bruker Avance 400 MHz spectrometer. All chemical shifts are reported in ppm, calibrated to the residual solvent peak.

5.1.3 Mass spectrometry

Electrospray ionisation (ESI) mass spectrometry was performed on a Micromass LCT ES-TOF machine.

5.1.4 Infrared spectroscopy (IR)

IR spectra were obtained using a Perkin-Elmer Spectrum 100 IR spectrometer and were collected using an ATR probe, from 4000 to 600 cm^{-1} .

5.1.5 UV-visible spectroscopy

All UV-visible spectra were collected on a Varian-Carey 50 UV-visible spectrometer, using quartz cells of 10 mm path length at 25 °C. Baselines were corrected using Carey WinUV Scan software.

5.1.6 Luminescence spectroscopy

Luminescence spectra were collected on a Jobin-Yvon FluoroMax-3 spectrophotometer operating in luminescence wavelength scan mode at 25 °C, with excitation and emission slit widths set to 5 nm.

5.1.7 Anion metathesis

Complexes were synthesised and characterised as their hexafluorophosphate (PF₆) salts. Conversion to chloride salts was achieved by stirring in water with Dowex 1x2 anion exchange resin.

5.2 Extinction coefficients

Extinction coefficients were calculated by measuring absorbance at 10 concentrations. 2 mL of solvent was added to the cuvette, and a baseline reading taken. 2 µL of a 1 mM solution of the compound was added, and thoroughly mixed. The absorbance was measured, and the process repeated a further nine times. The extinction coefficient was then calculated for each wavelength using the Beer-Lambert law, and plotted graphically. This process was carried out once per complex. An example spreadsheet is included in the appendix.

5.3 X-ray crystallography

Intensity data was collected at 100 K on either a Bruker SMART APEX-II CCD or Bruker Kappa Apex-II CCD diffractometer operating with a MoK α sealed-tube X-ray source from crystals mounted in fomblin oil on a MiTiGen microloop and cooled in a stream of cold N₂. Data were corrected for absorption using empirical methods (SADABS)¹ based upon symmetry equivalent reflections combined with measurements

at different azimuthal angles.² The crystal structures were solved and refined against F2 values using ShelXT³ for solution and ShelXL⁴ for refinement accessed via the Olex2 program.⁵ Non-hydrogen atoms were refined anisotropically. Hydrogen atoms were placed in calculated positions with idealized geometries and then refined by employing a riding model and isotropic displacement parameters.

5.4 Computational Studies

All calculations were performed with Gaussian 09 v. D.01⁶ using density-functional theory. The functional used was B3LYP⁷ with empirical dispersion corrections.⁸ The basis set used consisted of SDD^{9,10} on Ru and 6-311G(d,p)^{11,12} on all other atoms. All bulk solvent was described using the PCM method^{13,14} as implemented in Gaussian using the provided parameters for MeCN and water. For the calculations involving water, additional water molecules were placed around the complexes coordinated to the free nitrogen atoms. In the case of pzp, the initial orientation of the additional waters was chosen randomly, since for those moieties a negligible dependence of the energetics and final electronic structure on the precise orientation of the water molecules can be expected. For all optimised structures frequencies were calculated in the harmonic approximation. No imaginary frequencies were found, thus these molecules are considered to be true minima. Geometry optimizations were performed for both the singlet and triplet ground states of these complexes. Reported emission frequencies are assumed to be 0-0 transitions between these ground states.

5.5 DNA Binding Studies

5.5.1 Buffer preparation

Tris buffer (pH 7.40) was prepared using Trizma HCl base at 5 mM concentration in 25 mM NaCl. Trizma HCl and NaCl were measured into a volumetric flask and dissolved in deionised water (Millipore HPLC grade). The pH was adjusted using dilute HCl, and additional water added to achieve the correct volume. Solutions were stored in the fridge at 5 °C until required.

5.5.2 DNA preparation

Calf-thymus DNA (ct-DNA) was purchased from Sigma as the lyophilised solid sodium salt, and used without further purification. An average length of 100-250 base pairs was achieved using a modification of the procedure developed by the Chaires group.^{15,16} Stock solutions of ct-DNA were prepared by dissolving ~100 mg of the solid in 20 mL of tris buffer. The stock solution was cooled to 0 °C, and sonicated for 30 minutes using a Sonics Vibra-Cell VCX130, fitted with a 19 mm probe. The quality of the sample and concentration of base pairs was determined by UV-vis absorption. Nucleic acids have an absorbance maximum at 260 nm, whereas contaminants such as proteins have an absorbance maximum at 280 nm. Sample purity was determined by calculating the ratio of the two peaks. $A(260)/A(280) > 1.9$ indicates the sample is of sufficient purity for further use. Base pair concentration can be determined using $\epsilon(260) = 13,200 \text{ M}^{-1} \text{ cm}^{-1}$.

1.

5.5.3 DNA binding titrations

3 ml of buffer was loaded into a 10 mm path length cuvette and allowed to equilibrate inside the spectrometer before a baseline reading was taken. A volume of buffer was removed with a pipette and replaced with the same volume of a stock solution of complex to give a final concentration of around 15-20 μM complex inside the cuvette. After equilibration the spectrum was recorded between 200-600 nm for absorbance spectra, and 500-800 nm for luminescence spectra. 2 μL of a concentrated stock solution of ct-DNA was added to the cuvette and mixed 10 times to ensure homogeneity. The spectrum was recorded after leaving the sample to equilibrate for 5 minutes, checking no bubbles were present. This process was repeated until the absorption/emission became constant, signifying saturation.

5.5.4 Relative Viscometry

Viscosity experiments were performed using a Cannon-Manning semi-micro relative viscometer (size 50) immersed in a 25 °C water bath. 1 mL of previously prepared tris buffer was added to the viscometer, and allowed to stand for 1 hour. Reference measurements were taken, then 50 μL of 1 mM ct-DNA solution was added, and the solution left to equilibrate for 30 minutes. The relative viscosity was measured again, followed by addition of analyte, and a further 20 minutes equilibration. Additions of analyte were made so that the value of r^{-1} ($r = [\text{DNA}]/[\text{analyte}]$) was between 0 and 0.2. Times were recorded in triplicate to within 0.3 s and averaged.

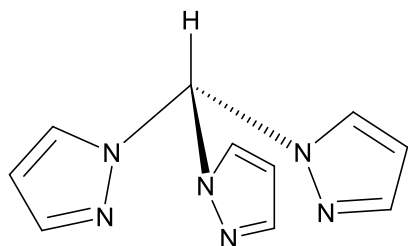
5.5.5 Continuous Variation Analysis

Continuous variation analysis was carried out using a Jobin-Yvon FluoroMax-3 spectrophotometer at 25 °C. The sum of concentrations of the complex and ct-DNA was

maintained at 50 μM , and the molar ratio of complex varied from 0 to 1. The emission intensities were measured, with excitation at the previously determined value.

5.6 Synthesis

5.6.1 Tris(1-pyrazole)methane (tpm)

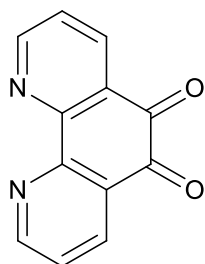


A solution of pyrazole (93.26 g, 1.37 mol) and tetrabutylammonium bromide (21.90 g, 68.5 mmol) was made up in distilled H_2O (1 L). With mechanical stirring, Na_2CO_3 (871.42 g, 8.22 mol) was added slowly. After cooling to room temperature, CHCl_3 (450 mL) was added, and the mixture was heated to reflux for three days. The mixture was cooled to room temperature, and filtered to remove excess base. The organic layer was separated, and the aqueous layer was extracted with Et_2O (3 x 200 mL). The combined organic layers were washed with brine, and dried over MgSO_4 . After filtration, the solvent was removed by rotary evaporation. The crude product was then recrystallised from water to give tris(1-pyrazole)methane (63.87 g, 65 %).

^1H NMR (400 MHz, d_6 -acetone): δ_{H} 8.73 (s, 1H), 7.86 (d, $J = 2.6$ Hz, 3H), 7.62 (d, $J = 1.7$ Hz, 3H), 6.4 (dd, $J = 1.7$ Hz, 2.6 Hz, 3H)

MS ESI+: 147 $[\text{M-pz}]^+$, 215 $[\text{M+H}]^+$

5.6.2 1,10-phenanthroline-5,6-dione (dpq)

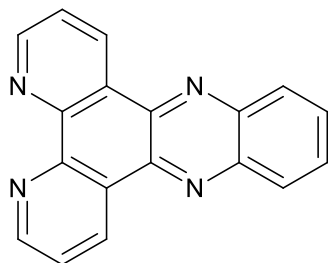


To a rapidly stirred aqueous solution of H_2SO_4 (125 mL, 60 %) was added 1,10-phenanthroline (18.00 g, 100 mmol). Sodium bromate (60.36 g, 400 mmol) was added slowly, and the mixture was then left to cool to room temperature. The reaction mixture was neutralised with a saturated NaOH solution, the temperature was kept below 5 °C at all times. The yellow solid was collected by vacuum filtration, and recrystallised from EtOH to give 1,10-phenanthroline-5,6-dione (10.79 g, 51 %).

$^1\text{H NMR}$ (400 MHz, CDCl_3): δ_{H} 9.13 (dd, $J = 1.8, 4.7$ Hz, 2H), 8.52 (dd, $J = 1.8, 7.9$ Hz, 2H), 7.61 (dd, $J = 4.7, 7.9$ Hz, 2H)

MS ESI+: 211 $[\text{M}+\text{H}]^+$

5.6.3 Dipyrrophenazine (dppz)

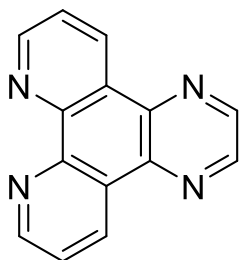


1,10-phenanthroline-5,6-dione (1.00 g, 4.76 mmol) and 1,2-phenylenediamine (0.60 g, 5.46 mmol) were dissolved in EtOH (60 mL) and heated to reflux for 20 minutes. The solvent was removed, and the crude product recrystallised from $\text{H}_2\text{O}:\text{EtOH}$ (1:1). The crystals were washed with ice cold water (30 mL) and ethanol (50 mL) and then dried under vacuum to give dipyrrophenazine (0.73 g, 55 %).

$^1\text{H NMR}$ (400 MHz, $\text{d}_6\text{-acetone}$): δ_{H} 9.50 (dd, $J = 1.8$ Hz, 2H), 9.21 (dd, $J = 1.8, 4.4$ Hz, 2H), 8.37 (dd, $J = 3.4, 6.5$ Hz, 2H), 8.06 (dd, $J = 3.4, 6.5$ Hz, 2H), 7.94 (dd, $J = 4.4, 8.1$ Hz, 2H)

MS ESI+: 283 $[\text{M}+\text{H}]^+$

5.6.4 Pyrazinophenanthroline (pzp)

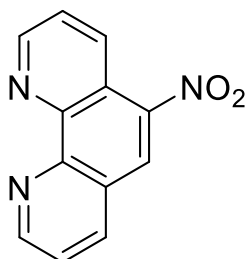


1,10-phenanthroline-5,6-dione (1.50 g, 7.14 mmol) and ethylene diamine (1.5 mL, 1.35 g, 22 mmol) were dissolved in EtOH (150 mL), and heated to reflux for 4 hours. The solvent was removed under vacuum, and the crude product was recrystallised from EtOH to give pyrazinophenanthroline (1.01 g, 61 %).

¹H NMR (400 MHz, d₆-DMSO): δ 9.45 (dd, J = 8.1, 1.6 Hz, 1H), 9.24 (dd, J = 4.3, 1.6 Hz, 1H), 9.18 (s, 1H), 7.96 (dd, J = 8.1, 4.4 Hz, 1H).

MS ESI+: 233 [M+H]⁺

5.6.5 5-Nitro-1,10-phenanthroline

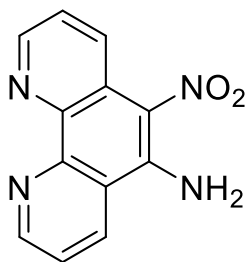


1,10-phenanthroline (10 g, 56 mmol) was dissolved in concentrated H₂SO₄ (40 mL), and heated to 160 °C. HNO₃ (20 mL) was added dropwise and the mixture was heated for a further 1.5 hours. The mixture was poured over ice, and neutralised with concentrated KOH_(aq) taking care to keep the temperature below 10 °C. The pale yellow precipitate was collected by vacuum filtration, washed with copious H₂O and EtOH, and dried under vacuum to give 5-nitro-1,10-phenanthroline (8.79 g, 70 %).

¹H NMR (400 MHz, d₆-DMSO): δ 9.23 (ddd, J = 18.0, 4.3, 1.7 Hz, 2H), 9.09 (dd, J = 4.3, 1.8 Hz, 1H), 8.98 (s, 1H), 8.84 (dd, J = 8.6, 1.6 Hz, 1H), 8.73 (dd, J = 8.1, 1.7 Hz, 1H), 8.47 (dd, J = 8.1, 1.8 Hz, 1H), 7.96 (s, 1H), 7.91 (ddd, J = 12.1, 8.3, 4.3 Hz, 2H), 7.76 (dd, J = 8.1, 4.3 Hz, 1H).

MS ESI+: 226 [M+H]⁺, 248 [M+Na]⁺

5.6.6 5-nitro-6-amino-1,10-phenanthroline

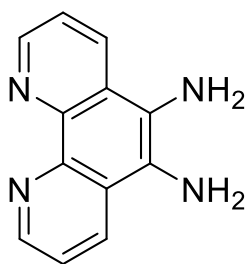


5-nitro-1,10-phenanthroline (3.50 g, 15.5 mmol) was suspended in EtOH:dioxane (100 mL, 3:2), and heated to 60 °C until fully dissolved. The mixture was then cooled to -5 °C, and hydroxylamine hydrochloride (7.00 g, 110 mmol) was added in a single portion. Methanolic KOH (7.30 g, 130 mmol, 100 mL) was added dropwise, taking care to keep the mixture cold. After addition was complete, the mixture was stirred for 1 hour at -5 °C, and then for a further hour at room temperature. The reaction mixture was then poured over ice, and stored at 5 °C overnight. The pale yellow solid was collected by vacuum filtration, washed with MeOH and H₂O, and dried under vacuum to give 5-nitro-6-amino-1,10-phenanthroline (1.12 g, 30 %).

¹H NMR (400 MHz, d₆-DMSO): δ 9.19 (dd, J = 4.3, 1.4 Hz, 1H), 9.06 (dd, J = 8.4, 1.5 Hz, 1H), 8.79 (dd, J = 4.2, 1.5 Hz, 1H), 8.73 (dd, J = 8.6, 1.5 Hz, 1H), 8.64 (s, 2H), 7.86 (dd, J = 8.4, 4.3 Hz, 1H), 7.69 (dd, J = 8.6, 4.2 Hz, 1H).

MS ESI+: 241 [M+H]⁺, 263 [M+Na]⁺

5.6.7 5,6-diamino-1,10-phenanthroline



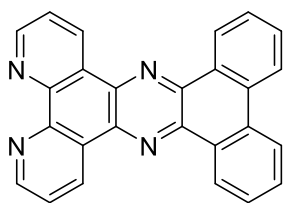
5-nitro-6-amino-1,10-phenanthroline (2.56 g, 10.65 mmol) and Pd/C (10 %, 1.00 g) were suspended in degassed MeOH (25 mL), and heated to reflux under an argon atmosphere. After 30 minutes, hydrazine monohydrate (15 mL) was added dropwise, and the mixture left at reflux for a further 2 hours. The mixture was filtered hot over celite, and the pad washed with boiling MeOH. The solution was concentrated to ~10 % of the original volume under vacuum, poured into 40-60 petroleum ether (200 mL), and left at

-20 °C for 18 hours. The precipitate was collected by vacuum filtration, washed with petroleum ether, and dried under vacuum to give 5,6-diamino-1,10-phenanthroline (1.07 g, 48 %).

¹H NMR (400 MHz, d₆-DMSO): δ 8.79 (dd, J = 1.4, 4.1 Hz, 2H), 8.50 (dd, J = 1.5, 8.4 Hz, 2H), 7.21 (dd, J = 4.2, 8.4 Hz, 2H), 5.25 (s, 4H).

MS ESI+: 211 [M+H]⁺, 233 [M+Na]⁺

5.6.8 4,5,9,18-Tetraazaphenanthrotriphenylene (taptp)

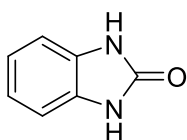


5,6-diamino-1,10-phenanthroline (0.38 g, 1.83 mmol) and phenanthrene-9,10-dione (0.38 g, 1.83 mmol) were dissolved in degassed EtOH (125 mL), and heated to reflux under a nitrogen atmosphere for 3 hours. The precipitate was collected by hot filtration, washed with EtOH and Et₂O, and dried under vacuum to give 4,5,9,18-tetraazaphenanthrotriphenylene (0.54 g, 78 %).

¹H NMR (400 MHz, d-TFA): δ 10.46 (dd, J = 1.1, 8.3 Hz, 2H), 9.90 (d, J = 8.0 Hz, 2H), 9.50 (d, J = 6.3 Hz, 2H), 9.29 (d, J = 4.9 Hz, 2H), 9.09 (d, J = 7.8 Hz, 2H), 8.55 (q, J = 4.5 Hz, 2H), 8.28 (m, J = 4.1 Hz, 2H), 7.71 (td, J = 7.4, 31.0 Hz, 2H).

MS ESI+: 383 [M+H]⁺, 405 [M+Na]⁺

5.6.9 Benzimidazol-2-one



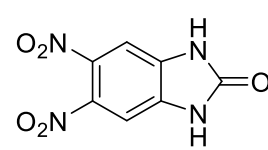
1,2-phenylenediamine (10.0 g, 92 mmol) and urea (6.30 g, 104.9 mmol) were dissolved in ethylene glycol (20 mL) and heated to 130 °C under a nitrogen atmosphere for 1 hour, after which the temperature was increased to 170 °C for 7 hours. The mixture was then cooled to room temperature, EtOH (40 mL) was added,

and followed by stirring for a further 10 minutes. H₂O (100 mL) was added, and the precipitate collected by vacuum filtration. After washing with H₂O and EtOH, the product was dried under vacuum to give benzimidazol-2-one (12.47 g, 97 %)

¹H NMR (400 MHz, d₆-DMSO): δ 10.62 (s, 2H), 6.92 (s, 4H).

MS ESI+: 135 [M+H]⁺, 157 [M+Na]⁺

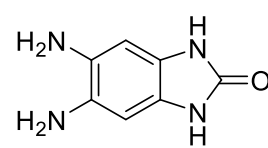
5.6.10 5,6-dinitrobenzimidazol-2-one

 Benzimidazol-2-one (12.47 g, 87 mmol) was dissolved in concentrated H₂SO₄ (60 mL), and cooled to 0 °C. Fuming HNO₃ (9 mL) was mixed with ice cold H₂SO₄ (60 mL), and then added dropwise to the reaction mixture. The solution was then poured over ice, the solid collected by vacuum filtration, and washed with copious cold H₂O. After drying under vacuum, the crude product was recrystallised from EtOH to give 5,6-dinitrobenzimidazol-2-one (17.13 g, 83 %).

¹H NMR (400 MHz, d₆-DMSO): δ 11.81 (s, 2H), 7.66 (s, 2H).

MS ESI+: 225 [M+H]⁺, 247 [M+Na]⁺

5.6.11 5,6-diaminobenzimidazol-2-one

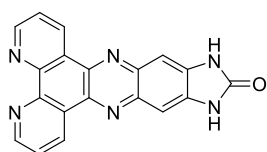
 5,6-dinitrobenzimidazol-2-one (5.00 g, 22.31 mmol) and Pd/C (10 %, 0.60 g) was suspended in MeOH:H₂O (250 mL, 1:2), and heated to reflux under a nitrogen atmosphere. Hydrazine monohydrate (25 mL, 35 eq) was added dropwise, and the mixture was left at reflux for 18 hours. The mixture was filtered over celite, and the pad washed with boiling MeOH. The filtrate was concentrated under vacuum, and the cream precipitate was collected by vacuum filtration. After

washing with cold MeOH, and the precipitate was dried under vacuum to give 5,6-diaminobenzimidazol-2-one (1.31 g, 36 %).

¹H NMR (400 MHz, d₆-DMSO): δ 9.84 (s, 2H), 6.25 (s, 2H), 4.09 (s, 4H).

MS ESI+: 165 [M+H]⁺, 187 [M+Na]⁺

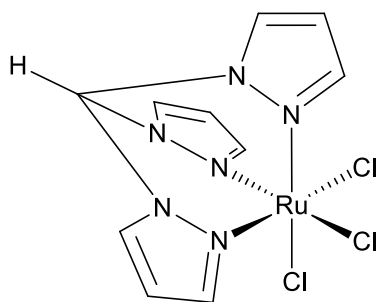
5.6.12 Dipyrrophenazineimidazolone (dppz-izdo)



1,10-phenanthroline-5,6-dione (0.80 g, 3.80 mmol) was dissolved in EtOH (100 mL). After addition of 5,6-diaminobenzimidazol-2-one (0.64 g, 3.80 mmol), the mixture was heated to reflux for 15 minutes. The precipitate was collected by hot filtration, washed with EtOH and Et₂O, and dried under vacuum to give dipyrrophenazineimidazolone (1.27 g, 99 %).

MS ESI+: 339 [M+H]⁺, 361 [M+Na]⁺

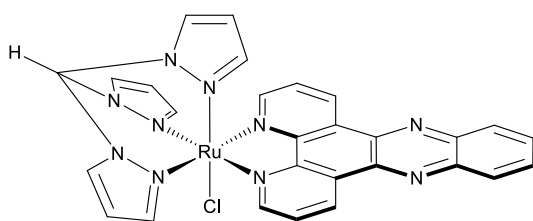
5.6.13 [(tpm)RuCl₃]



RuCl₃·3H₂O (4.00 g, 15.28 mmol) and tpm (3.28 g, 15.28 mmol) were dissolved in MeOH (350 mL), and heated to reflux for 4 hours. The brown solid was collected by vacuum filtration, washed with EtOH, acetone, and Et₂O and then dried under vacuum to give [(tpm)RuCl₃] (1.02 g, 56 %).

MS ESI+: 386 [M-Cl]⁺

5.6.14 [Ru(tpm)(dppz)Cl][PF₆]



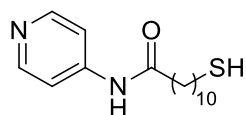
$\text{[Ru(tpm)(dppz)Cl][PF}_6\text{]}^+$ [(tpm)RuCl₃] (1.55 g, 3.21 mmol), dppz (1.00 g, 3.54 mmol) and LiCl (1.23 g, 29.0 mmol) were dissolved in degassed EtOH:H₂O (150 mL, 3:1), and heated to

reflux for 10 minutes. 12 drops of NEt₃ were added, and the mixture refluxed for a further three hours. Upon completion, the mixture was cooled to room temperature, and the solvent removed by rotary evaporation. The residue was dissolved in MeOH (20 mL) and filtered over celite. The complex was precipitated by the addition of aqueous NH₄PF₆. The solid was collected by filtration, and then washed with H₂O (20 mL) and Et₂O (20 mL). The crude product was purified by column chromatography on neutral alumina using MeCN:toluene (50:50) as the mobile phase. The fractions were combined, and the solvent removed by rotary evaporation to give [Ru(tpm)(dppz)Cl][PF₆] (1.33 g, 53 %).

¹H NMR (400 MHz, CD₃CN): 9.56 (dd, J = 8.1 Hz, 1.2 Hz, 2H), 9.19 (dd, J = 5.4 Hz, 1.2 Hz, 2H), 8.95 (s, 1H), 8.49 (d, J = 2.9 Hz, 2H), 8.46 (d, J = 2.1 Hz, 2H), 8.44 (dd, J = 6.6 Hz, 3.4 Hz, 2H), 8.33 (d, J = 2.7 Hz, 1H), 8.12 (dd, J = 6.6 Hz, 3.4 Hz, 2H), 7.99 (dd, J = 8.1 Hz, 5.4 Hz, 2H), 6.79 – 6.77 (m, 2H), 6.58 (d, J = 2.2 Hz, 1H), 6.24 – 6.22 (m, 1H)

MS ESI⁺: 635 [M-PF₆]⁺, 298.5 [M-Cl-PF₆]²⁺

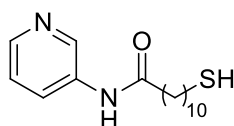
5.6.15 Attempted synthesis of 11-mercapto-N-(pyridine-4-yl)undecamide



4-aminopyridine (0.50 g, 5.30 mmol) was dissolved in dry DCM (100 mL), and the solution was cooled to 0 °C. 11-mercaptoundecanoic acid (1.16 g, 5.30 mmol), 1-ethyl-3-(3-

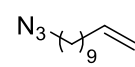
dimethylaminopropyl)carbodiimide (2.90 mL, 2.55 g, 13.25 mmol) and DMAP (0.65 g, 5.30 mmol) were added to the reaction mixture, followed by stirring at 0 °C for 1 hour. The mixture was warmed to room temperature before stirring for a further 24 hours. The solvent was removed by rotary evaporation, and H₂O (50 mL) was added, after which a white solid precipitated, which was collected by centrifugation. The solid was washed with MeCN (10 mL), and centrifuged again, before drying under vacuum. NMR and mass spectrometry showed the white solid was the 11-mercaptoundecanoic acid starting material.

5.6.16 Attempted synthesis of 11-mercapto-N-(pyridine-3-yl)undecamide



3-aminopyridine (0.50 g, 5.30 mmol) was dissolved in dry DCM (100 mL), and the solution was cooled to 0 °C. 11-mercaptoundecanoic acid (1.16 g, 5.30 mmol), 1-ethyl-3-(3-dimethylaminopropyl)carbodiimide (2.90 mL, 2.55 g, 13.25 mmol) and DMAP (0.65 g, 5.30 mmol) were added to the reaction mixture, followed by stirring at 0 °C for one hour. The mixture was warmed to room temperature before stirring for a further 24 hours. The solvent was removed by rotary evaporation, and H₂O (50 mL) was added, after which a white solid precipitated, which was collected by centrifugation. The solid was washed with MeCN (10 mL), and centrifuged again, before drying under vacuum. NMR and mass spectrometry showed the white solid was the 11-mercaptoundecanoic acid starting material

5.6.17 11-azidoundec-1-ene

 11-chloroundec-1-ene (1.88 mL, 1.89 g, 10 mmol), NaN₃ (0.85 g, 13 mmol) and tetrabutylammonium iodide (0.37 g, 1 mmol) were dissolved in DMF (20 mL) at 0

°C. The solution was stirred for 14 hours at 50 °C, after which the reaction was quenched with the addition of 100 mL of H₂O. The solution was extracted with Et₂O (5 x 20 mL), and then the combined organic layers were washed with 1 M aqueous LiCl solution (5 x 40 mL) to remove the excess DMF. The organic layers were then dried over MgSO₄, filtered, and the solvent removed under vacuum to give 11-azidoundec-1-ene (1.64 g, 84 %).

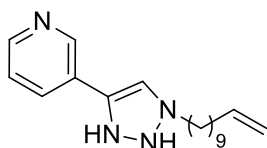
¹H NMR (400 MHz, CDCl₃): δ_H 5.81 (ddt, J = 16.9, 10.2, 6.7 Hz, 1H), 5.02 (dt, J = 3.2, 1.6 Hz, 1H), 4.98 (dt, J = 3.2, 1.6 Hz, 1H), 4.95 (dt, J = 2.3, 1.2 Hz, 1H), 4.92 (dt, J = 2.3, 1.2 Hz, 1H), 3.48 (q, J = 7.0 Hz, 2H), 3.26 (t, J = 7.0 Hz, 2H), 2.10 – 2.00 (m, 2H), 1.66 – 1.55 (m, 2H), 1.39 (dd, J = 21.0, 14.0 Hz, 4H), 1.30 (s, 4H)

FT-IR (ATR): ν_{max} 3077, 2924, 2854, 2090, 1641, 1464, 1348, 1257, 993, 906 cm⁻¹

5.6.18 Attempted synthesis of Undec-10-en-1-amine

 11-azidoundec-1-ene (1.63 g, 8.38 mmol) and triphenylphosphine (2.86 g, 10.89 mmol) were dissolved in THF (10 mL) and H₂O (2 mL), and were stirred for 18 hours at room temperature. 10 drops of saturated NaHCO_{3(aq)} were added, after which the solution was extracted with EtOAc (3 x 20 mL). The combined organic phases were dried over MgSO₄, and the solvent removed under vacuum. As the IR spectrum still showed a strong azide band, and no evidence of any new signals that could be attributed to an amine, the reaction was unsuccessful.

5.6.19 3-(1-(undec-10-en-1-yl)-1H-1,2,3-triazol-4-yl)pyridine



This method was adapted from earlier work by the Gasser group.¹⁷

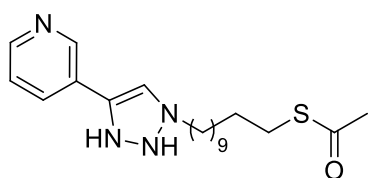
11-azidoundec-1-ene (0.50 g, 2.56 mmol), 3-ethynylpyridine (0.26 g, 2.56 mmol), CuSO₄ (0.041 g, 0.256 mmol),

tris(benzyltriazolylmethyl)amine (TBTA) (0.14 g, 0.256 mmol), sodium ascorbate (0.15 g, 0.768 mmol) were dissolved in H₂O:MeCN (1:1, 10 mL), and stirred for 6 hours at room temperature. The solvent was then removed under vacuum, and the crude product was then dissolved in CHCl₃ (20 mL) and washed with water (10 mL). The organic layer was then dried over MgSO₄, filtered, and the solvent removed under vacuum. The crude product was then purified by flash column chromatography on silica gel, using EtOAc as the mobile phase, to give 3-(1-(undec-10-en-1-yl)-1H-1,2,3-triazol-4-yl)pyridine as a yellow oil (0.48 g, 62 %).

¹H NMR (400 MHz, CDCl₃): δ 8.27 (d, J = 7.1 Hz, 1H), 7.86 (s, 1H), 7.38 (d, J = 6.6 Hz, 1H), 5.82 (ddt, J = 16.9, 10.2, 6.7 Hz, 1H), 5.55 (s, 1H), 5.05 – 4.93 (m, 2H), 4.45 (t, J = 7.2 Hz, 2H), 2.10 – 1.93 (m, 4H), 1.37 (d, J = 4.1 Hz, 6H), 1.30 (s, 7H)

MS ESI+: 299 [M+H]⁺

5.6.20 Attempted synthesis of S-(11-(4-(pyridin-3-yl)-1H-1,2,3-triazol-1-yl)undecyl) ethanethioate



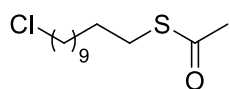
3-(1-(undec-10-en-1-yl)-1H-1,2,3-triazol-4-yl)pyridine

(0.48 g, 1.60 mmol), thioacetic acid (0.61 g, 0.57 mL, 8 mmol) and azobisisobutyronitrile (0.013 g, 0.08 mmol)

were dissolved in 1,2-dichloroethane (20 mL) and heated to 80 °C for 8 hours under a nitrogen atmosphere. The reaction mixture was washed with saturated NaHCO_{3(aq)} solution (5 x 20 mL), dried over MgSO₄, filtered, and the solvent removed under vacuum. Analysis of the ¹H NMR spectrum showed the alkene signals from the starting material still persisted, and no new signal was present for the methyl group of the

thioacetate, suggested the reaction was unsuccessful. Mass spectrometry also showed no evidence of the product.

5.6.21 S-(11-chloroundecyl) ethanethioate



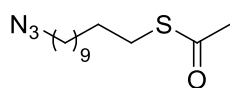
11-chloroundec-1-ene (0.50 g, 0.50 mL, 2.64 mmol), azobisisobutyronitrile (0.043 g, 0.264 mmol) and thioacetic acid (1.00 g, 0.94 mL, 13.18 mmol) were dissolved in 1,2-dichloroethane (15 mL), and heated to 80 °C for 8 hours under a nitrogen atmosphere. The reaction mixture was washed with saturated NaHCO_{3(aq)} solution (5 x 20 mL), dried over MgSO₄, filtered, and the solvent removed under vacuum. The crude product was purified by flash column chromatography on silica gel, using EtOAc as the mobile phase to give S-(11-chloroundecyl) ethanethioate (0.15 g, 22 %).

¹H NMR (400 MHz, CDCl₃): δ 3.52 (t, J = 6.8 Hz, 2H), 2.85 (t, J = 7.6 Hz, 2H), 2.30 (s, 3H), 1.80 – 1.70 (m, 2H), 1.70 – 1.60 (m, 2H), 1.59 – 1.49 (m, 2H), 1.40 (dd, J = 14.5, 7.1 Hz, 4H), 1.36 – 1.20 (m, 8H)

MS ESI+: 265 [M+H]⁺

FT-IR (ATR): ν_{max} 2924, 2853, 1670, 1463, 1353, 1305, 1132, 1107, 951, 722 cm⁻¹

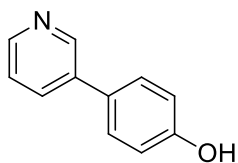
5.6.22 Attempted synthesis of S-(11-azidoundecyl) ethanethioate



S-(11-chloroundecyl) ethanethioate (0.15 g, 0.58 mmol), NaN₃ (0.049 g, 0.76 mmol) and tetrabutylammonium iodide (0.022 g, 0.058 mmol) were dissolved in DMF (20 mL) at 0 °C. The reaction mixture was stirred for 14 hours at 50 °C, after which it was quenched by the addition of 100 mL of H₂O. The solution was extracted with Et₂O (5 x 20 mL), and then the combined organic layers were

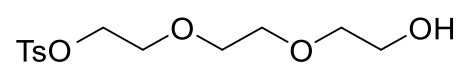
washed with 1 M aqueous LiCl solution (5 x 40 mL) to remove the excess DMF. The organic layers were then dried over MgSO₄, filtered, and the solvent removed under vacuum. Analysis of the NMR spectrum showed only starting material; additionally, no azide band was found in the infrared spectrum, suggesting the reaction was unsuccessful.

5.6.23 Attempted synthesis of 4-(pyridine-3-yl)phenol



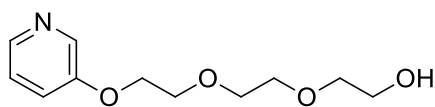
This method is adapted from earlier work by the Dreher group.¹⁸ 2-dicyclohexylphosphino-2',4',6'-triisopropylbiphenyl (0.028 g, 0.058 mmol), Pd(OAc)₂ (6.6 μg, 0.029 mmol), KOAc (0.34 g, 3.50 mmol), B₂(OH)₄ (0.31 g, 3.48 mmol) and NaO^tBu (2.8 μg, 0.029 mmol) and 3-chloropyridine (0.13 g, 0.16 mL, 1.17 mmol) were dissolved in degassed EtOH (20 mL), and heated to reflux for two hours under a nitrogen atmosphere. 1.8 M K₂CO_{3(aq)} (2.0 mL) was added to decompose the remaining B₂(OH)₄, followed by addition of 4-chlorophenol (0.15 g, 0.18 mL, 1.17 mmol). The mixture was then heated to reflux for a further 15 hours. After cooling to room temperature, the mixture was filtered through celite and the pad washed with EtOAc. The solvent was then removed under vacuum, and the crude product dissolved in EtOAc (20 mL). The solution was washed with H₂O (10 mL), dried over MgSO₄, filtered, and the solvent removed under vacuum. NMR and mass spectrometry of the crude product suggested that the reaction had been successful, however, following purification by HPLC, the product had decomposed.

5.6.24 Triethylene glycol monotosylate

 Triethylene glycol (0.44 mL, 0.50 g, 3.33 mmol) was dissolved in DCM (30 mL) and cooled to 0 °C. Ag₂O (1.16 g, 5.00 mmol), TsCl (0.70 g, 3.66 mmol), and KI (0.11 g, 0.67 mmol) were added, and the reaction mixture stirred

for a further five minutes at 0 °C. The mixture was filtered through a pad of silica, and eluted with EtOAc (3 x 20 mL). The solvent was removed by rotary evaporation to give triethylene glycol monotosylate which was used without further purification. Although a small amount of starting material remained, the reaction was assumed to be quantitative for the purpose of the subsequent reactions.

5.6.25 1-(3-Pyridyloxy)-3,6-dioxaoctane-8-ol

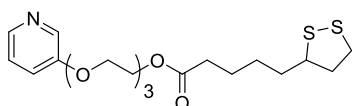


Triethylene glycol monotosylate (1.01 g, 3.33 mmol), 3-hydroxypyridine (0.32 g, 3.33 mmol) and K_2CO_3 (0.92 g, 6.66 mmol) were dissolved in dry MeCN (40 mL), and heated to reflux for 24 hours under a nitrogen atmosphere. The reaction mixture was cooled to room temperature, and the solvent removed under vacuum. H_2O (20 mL) was added, and the solution was extracted with $CHCl_3$ (3 x 50 mL). The combined organic layers were dried over $MgSO_4$, filtered, and the solvent removed under vacuum. The crude product was purified by flash column chromatography on silica gel, using $CHCl_3:MeOH$ (99:1 \rightarrow 9:1) to give 1-(3-pyridyloxy)-3,6-dioxaoctane-8-ol (0.28 g, 37 %).

1H NMR (400 MHz, $CDCl_3$): δ 8.41 (dd, $J = 2.6, 0.8$ Hz, 1H), 8.25 (dd, $J = 4.2, 1.8$ Hz, 1H), 7.28 – 7.21 (m, 2H), 4.25 – 4.20 (m, 2H), 3.94 – 3.88 (m, 2H), 3.79 – 3.74 (m, 4H), 3.72 (ddd, $J = 9.0, 4.4, 2.7$ Hz, 2H), 3.67 – 3.61 (m, 2H)

MS ESI+: 228 $[M+H]^+$

5.6.26 Lipoic acid 1-(4-Pyridyloxy)-3,6-dioxaoctane-8-yl ester (3Py-O₃-LA)



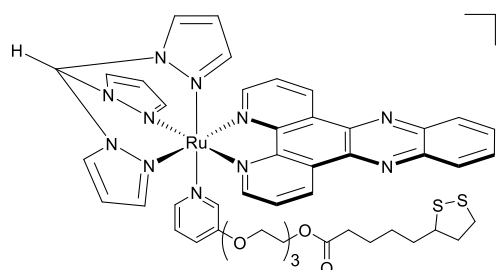
Py3-O₃ (0.66 g, 0.29 mmol), lipoic acid (0.060 g, 0.29 mmol) and DMAP (0.036 g, 0.29 mmol) were dissolved in DCM (10 mL) under a nitrogen atmosphere. The reaction mixture was cooled to 0 °C, after which 1-ethyl-3-(3-dimethylaminopropyl) carbodiimide (0.14 g, 0.16 mL, 0.73 mmol) was added. After stirring for one hour at 0 °C, the mixture was allowed to warm to room temperature, and left for a further 24 hours. Following this, the solvent was removed under vacuum, and the crude product purified by flash column chromatography

on silica gel, using CHCl_3 as the mobile phase to give lipoic acid 1-(4-pyridyloxy)-3,6-dioxaoctane-8-yl ester (0.15 g, 42 %).

$^1\text{H NMR}$ (400 MHz, CDCl_3): δ 8.38 – 8.34 (m, 1H), 8.25 (dd, $J = 3.7, 2.3$ Hz, 1H), 7.26 – 7.21 (m, 2H), 4.28 – 4.23 (m, 2H), 4.23 – 4.19 (m, 2H), 3.93 – 3.88 (m, 2H), 3.80 – 3.68 (m, 6H), 3.38 – 3.26 (m, 1H), 3.26 – 3.05 (m, 3H), 2.65 (t, $J = 7.3$ Hz, 1H), 1.80 – 1.57 (m, 7H), 1.20 (q, $J = 6.9$ Hz, 1H)

MS ESI+: 416 $[\text{M}+\text{H}]^+$

5.6.27 Attempted synthesis of $[\text{Ru}(\text{tpm})(\text{dppz})(3\text{Py-O}_3\text{-LA})][\text{PF}_6]_2$

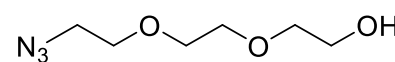


$[\text{Ru}(\text{tpm})(\text{dppz})\text{Cl}][\text{PF}_6]$ (0.061 g, 0.078 mmol), 3py-O₃-LA (0.32 g, 0.78 mmol) and AgOTf (0.022 g, 0.086 mmol) were dissolved in acetone (20 mL), and heated to reflux under

a nitrogen atmosphere for eight hours. After cooling to room temperature, the reaction mixture was filtered over celite, and eluted with acetone. The solvent was removed by rotary evaporation, and the crude product dissolved in the minimum amount of acetone. The complex was precipitated by the addition of 10 equivalents of $\text{NH}_4\text{PF}_6(\text{aq})$, and collected by vacuum filtration. The precipitate was washed with H_2O and Et_2O , and dried under vacuum. Purification was attempted by flash column chromatography over silica gel using $\text{MeCN}:\text{H}_2\text{O}:\text{KNO}_3(\text{sat. aq.})$ (95:4:1 \rightarrow 90:8:2) as the mobile phase. The product was found to be unstable.

MS ESI+: 506.6 $[\text{M}-2\text{PF}_6]^{2+}$

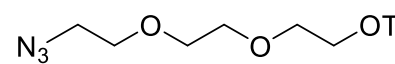
5.6.28 2-(2-(2-azidoethoxy)ethoxy)ethan-1-ol

 Triethylene glycol monotosylate (3.04 g, 10 mmol) and sodium azide (3.25 g, 50 mmol) were dissolved in DMF (20 mL) and heated to 90 °C under an argon atmosphere for 18 hours. The mixture was cooled to room temperature, and brine (100 mL) was added. The product was extracted with EtOAc (3 x 100 mL), and the organic layers combined, dried over MgSO₄, filtered, and the solvent removed under vacuum. The crude oil was purified by flash column chromatography over silica gel using 40-60 petroleum ether:EtOAc (1:2) as the mobile phase. The fractions were combined, and the solvent removed to give 2-(2-(2-azidoethoxy)ethoxy)ethan-1-ol (1.05 g, 61 %).

¹H NMR (400 MHz, CDCl₃): δ 3.78 – 3.74 (m, 2H), 3.73 – 3.67 (m, 6H), 3.66 – 3.61 (m, 2H), 3.42 (t, *J* = 5.0 Hz, 2H).

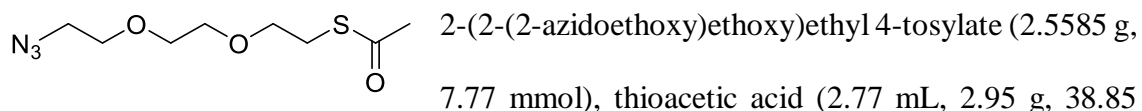
MS ESI+: 176 [M+H]⁺, 198 [M+Na]⁺

5.6.29 2-(2-(2-azidoethoxy)ethoxy)ethyl 4-tosylate

 2-(2-(2-azidoethoxy)ethoxy)ethan-1-ol (0.37 g, 2.12 mmol), TsCl (0.44 g, 2.33 mmol) and NEt₃ (0.88 mL, 1.21 g, 6.36 mmol) were dissolved in DCM (50 mL) and cooled to 0 °C under a nitrogen atmosphere. The mixture was stirred for 1 hour, and then left to warm to room temperature, followed by stirring for a further 18 hours. The reaction mixture was washed with saturated NH₄Cl_(aq) (3 x 30 mL), dried over MgSO₄, filtered, and the solvent removed under vacuum. The crude oil was purified by flash column chromatography over silica gel using 40-60 petroleum ether:EtOAc (2:1 → 0:1) as the mobile phase. The fractions were combined, and the solvent removed to give 2-(2-(2-azidoethoxy)ethoxy)ethyl 4-tosylate (0.39 g, 55 %).

¹H NMR (400 MHz, CDCl₃): δ 7.82 (d, *J* = 8.3 Hz, 2H), 7.37 (d, *J* = 8.1 Hz, 2H), 4.21 – 4.17 (m, 2H), 3.75 – 3.71 (m, 2H), 3.68 – 3.64 (m, 2H), 3.63 (s, 4H), 3.43 – 3.34 (m, 2H), 2.47 (s, 3H).

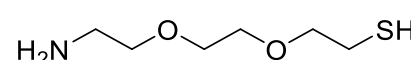
5.6.30 S-(2-(2-(2-azidoethoxy)ethoxy)ethyl) ethanethioate



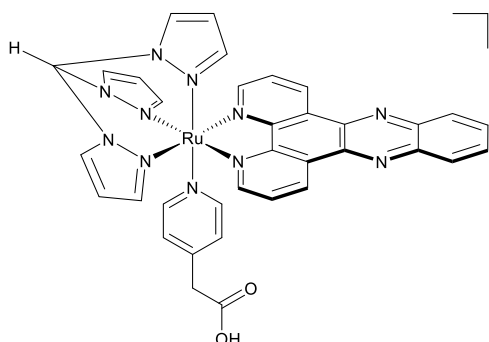
¹H NMR (400 MHz, CDCl₃): δ 3.74 – 3.60 (m, 8H), 3.42 (t, *J* = 5.1 Hz, 2H), 3.12 (t, *J* = 6.4 Hz, 2H), 2.36 (s, 3H).

MS ESI⁺: 234 [M+H]⁺

5.6.31 Attempted synthesis of 2-(2-(2-aminoethoxy)ethoxy)ethane-1-thiol

 S-(2-(2-(2-azidoethoxy)ethoxy)ethyl) ethanethioate (0.080 g, 0.39 mmol) and triphenylphosphine (0.20 g, 0.78 mmol) were dissolved in dry MeOH (50 mL), and the mixture was heated to reflux under a nitrogen atmosphere for 18 hours. After cooling to room temperature, the solvent was removed by rotary evaporation. Analysis by ¹H NMR and ESI-MS only showed starting materials.

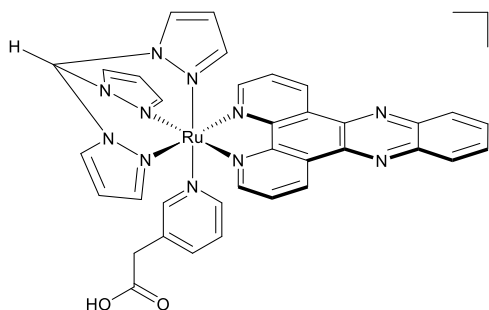
5.6.32 Attempted synthesis of $[\text{Ru}(\text{tpm})(\text{dppz})(4\text{-Py-MeCOOH})][\text{PF}_6]_2$



$[\text{Ru}(\text{tpm})(\text{dppz})\text{Cl}][\text{PF}_6]$ (0.10 g, 0.13 mmol), 4-pyridylacetic acid hydrochloride (0.22 g, 1.3 mmol), AgNO_3 (0.046 g, 0.27 mmol) and NEt_3 (0.36 mL, 0.26 g, 2.6 mmol) were dissolved in $\text{EtOH}:\text{H}_2\text{O}$ (50 mL, 3:1),

and heated to reflux under a nitrogen atmosphere for 6 hours. After cooling to room temperature, the solution was filtered over celite, and the pad washed with MeOH. The solution was treated with 1 M HCl until acidified, concentrated under vacuum, and the complex precipitated with addition by addition of aqueous KPF_6 . The solid was collected by vacuum filtration, washed with H_2O and Et_2O .

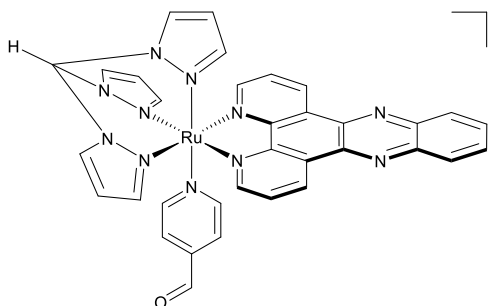
5.6.33 Attempted synthesis of $[\text{Ru}(\text{tpm})(\text{dppz})(3\text{-Py-MeCOOH})][\text{PF}_6]_2$



$[\text{Ru}(\text{tpm})(\text{dppz})\text{Cl}][\text{PF}_6]$ (0.10 g, 0.13 mmol), 3-pyridylacetic acid hydrochloride (0.22 g, 1.3 mmol), AgNO_3 (0.046 g, 0.27 mmol) and NEt_3 (0.36 mL, 0.26 g, 2.6 mmol) were dissolved in $\text{EtOH}:\text{H}_2\text{O}$ (50 mL, 3:1)

and heated to reflux under a nitrogen atmosphere for 6 hours. After cooling to room temperature, the solution was filtered over celite, and the pad washed with MeOH. The solution was treated with 1 M HCl until acidified, concentrated under vacuum, and the complex precipitated with addition by addition of aqueous KPF_6 . The solid was collected by vacuum filtration, washed with H_2O and Et_2O .

5.6.34 **[Ru(tpm)(dppz)(4-CHOPy)][PF₆]₂**



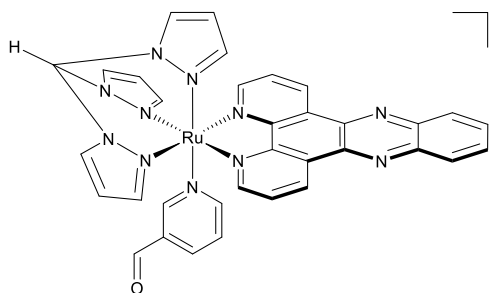
$[Ru(tpm)(dppz)(Cl)]^{2+}$ (0.10 g, 0.13 mmol), 4-pyridinecarboxaldehyde (1 mL) and $AgNO_3$ (0.046 g, 0.27 mmol) were dissolved in EtOH:H₂O (50 mL, 3:1), and heated to reflux under a nitrogen atmosphere

for 6 hours. After cooling to room temperature, the solution was filtered over celite, and the pad washed with MeOH. The solution was concentrated under vacuum, and the product precipitated by addition of aqueous KPF_6 . The solid was collected by vacuum filtration, and washed with H₂O and Et₂O. The crude product was purified by flash column chromatography over silica gel using MeCN:H₂O: KNO_3 (sat. aq.) (95:4:1 → 90:8:2) as the mobile phase. The fractions were combined, and the solvent removed under vacuum. The solid was dissolved in H₂O, and precipitated by addition of aqueous KPF_6 . The precipitate was collected by vacuum filtration, washed with H₂O and Et₂O, and dried under vacuum to give $[Ru(tpm)(dppz)(4-CHOPy)][PF_6]_2$ (0.046 g, 36 %).

¹H NMR (400 MHz, CD₃CN): δ 10.50 (s, 1H), 9.96 (s, 1H), 9.84 (dd, *J* = 8.2, 1.3 Hz, 2H), 9.08 (dd, *J* = 5.4, 1.2 Hz, 2H), 8.78 (d, *J* = 2.9 Hz, 2H), 8.60 (dd, *J* = 6.6, 3.4 Hz, 2H), 8.53 (d, *J* = 2.7 Hz, 1H), 8.23 (dd, *J* = 6.6, 3.4 Hz, 2H), 8.08 – 8.03 (m, 4H), 7.76 – 7.73 (m, 2H), 7.37 (dd, *J* = 5.3, 1.4 Hz, 2H), 6.85 – 6.82 (m, 2H), 6.47 (d, *J* = 2.3 Hz, 1H), 6.23 – 6.17 (m, 1H).

MS ESI+: 352.5 $[M-2PF_6]^{2+}$

5.6.35 **[Ru(tpm)(dppz)(3-CHOPy)][PF₆]₂**



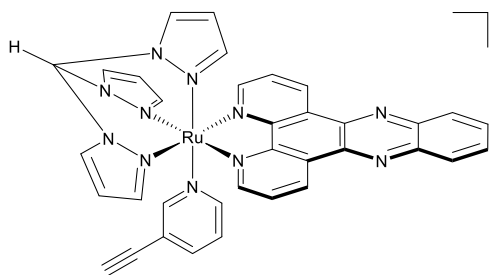
$^{2+}$ [Ru(tpm)(dppz)(Cl)][PF₆]₂ (0.10 g, 0.13 mmol), 3-pyridinecarboxaldehyde (1 mL) and AgNO₃ (0.046 g, 0.27 mmol) were dissolved in EtOH:H₂O (50 mL, 3:1), and

heated to reflux under a nitrogen atmosphere for 6 hours. After cooling to room temperature, the solution was filtered over celite, and the pad washed with MeOH. The solution was concentrated under vacuum, and the product precipitated by addition of aqueous KPF₆. The solid was collected by vacuum filtration, and washed with H₂O and Et₂O. The crude product was purified by flash column chromatography over silica gel using MeCN:H₂O:KNO₃(sat. aq.) (95:4:1 → 90:8:2) as the mobile phase. The fractions were combined, and the solvent removed under vacuum. The solid was dissolved in H₂O, and precipitated by addition of aqueous KPF₆. The precipitate was collected by vacuum filtration, washed with H₂O and Et₂O, and dried under vacuum to give [Ru(tpm)(dppz)(3-CHOPy)][PF₆]₂ (0.038 g, 29 %).

¹H NMR (400 MHz, CD₃CN): δ 10.62 (s, 1H), 9.83 (dd, *J* = 8.2, 1.2 Hz, 2H), 9.67 (s, 1H), 9.12 (dd, *J* = 5.4, 1.1 Hz, 2H), 8.81 (d, *J* = 2.8 Hz, 2H), 8.59 (dd, *J* = 6.6, 3.4 Hz, 2H), 8.54 (d, *J* = 2.7 Hz, 1H), 8.22 (dd, *J* = 6.6, 3.4 Hz, 2H), 8.13 (d, *J* = 7.9 Hz, 1H), 8.10 (d, *J* = 2.2 Hz, 2H), 8.06 (dd, *J* = 8.2, 5.4 Hz, 2H), 7.98 – 7.93 (m, 1H), 7.66 (d, *J* = 5.3 Hz, 1H), 7.18 (dd, *J* = 7.8, 5.9 Hz, 1H), 6.86 – 6.75 (m, 2H), 6.45 (d, *J* = 2.3 Hz, 1H), 6.23 – 6.15 (m, 1H).

MS ESI+: 352.5 [M-2PF₆]²⁺

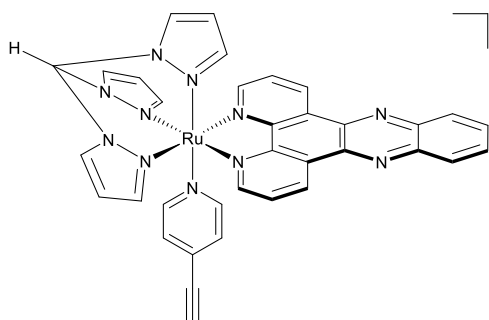
5.6.36 Attempted synthesis of $[\text{Ru}(\text{tpm})(\text{dppz})(3\text{-}\equiv\text{-Py})][\text{PF}_6]_2$



$[\text{Ru}(\text{tpm})(\text{dppz})(\text{Cl})][\text{PF}_6]_2$ (0.080 g, 0.10 mmol), 3-ethynylpyridine (0.050 g, 0.51 mmol) and AgNO_3 (0.040 g, 0.24 mmol) were dissolved in EtOH:H₂O (50 mL, 3:1),

and heated to reflux under a nitrogen atmosphere for 6 hours. After cooling to room temperature, the solution was filtered over celite, and the pad washed with MeOH. The solution was concentrated under vacuum, and the complex precipitated by addition of aqueous KPF_6 . The solid was collected by vacuum filtration, and washed with H₂O and Et₂O.

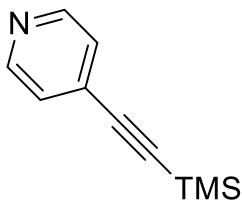
5.6.37 Attempted synthesis of $[\text{Ru}(\text{tpm})(\text{dppz})(4\text{-}\equiv\text{-Py})][\text{PF}_6]_2$



$[\text{Ru}(\text{tpm})(\text{dppz})(\text{Cl})][\text{PF}_6]_2$ (0.08 g, 0.10 mmol), 4-ethynylpyridine hydrochloride (0.070 g, 0.51 mmol), AgNO_3 (0.040 g, 0.24 mmol) and NEt_3 (5 drops) were dissolved in EtOH:H₂O (50 mL, 3:1), and heated to reflux

under a nitrogen atmosphere for 6 hours. After cooling to room temperature, the solution was filtered over celite, and the pad washed with MeOH. The solution was concentrated under vacuum, and the complex precipitated by addition of aqueous KPF_6 . The solid was collected by vacuum filtration, and washed with H₂O and Et₂O.

5.6.38 4-((Trimethylsilyl)ethynyl)pyridine

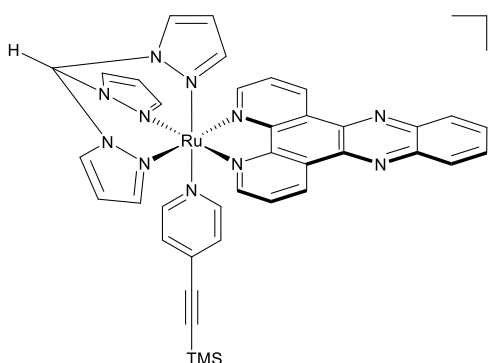


4-iodopyridine (1.00 g, 4.88 mmol), ethynyltrimethylsilane (0.57 g, 0.81 mL, 5.85 mmol), $[\text{Pd}(\text{PPh}_3)_4]$ (0.282 g, 0.244 mmol), CuI (0.0465 g, 0.244 mmol) and DIPEA (15 mL) were stirred at room temperature in degassed THF (45 mL) under an argon atmosphere for 3 days. The solution was filtered over celite, and the pad washed with DCM (3 x 30 mL). The organic layer was washed with saturated $\text{NH}_4\text{Cl}_{(\text{aq})}$ (2 x 30 mL), and H_2O (2 x 30 mL), dried over MgSO_4 , filtered, and the solvent removed under vacuum. The crude product was purified by flash column chromatography over silica gel using 40:60 petroleum ether:EtOAc (9:1) as the mobile phase. The fractions were combined, and the solvent was removed under vacuum to give 4-((trimethylsilyl)ethynyl)pyridine (0.55 g, 64 %).

$^1\text{H NMR}$ (400 MHz, CDCl_3): δ 8.54 (d, $J = 5.8$ Hz, 2H), 7.29 (d, $J = 5.8$ Hz, 2H), 0.25 (s, 9H).

MS ESI^+ : 176 $[\text{M}+\text{H}]^+$

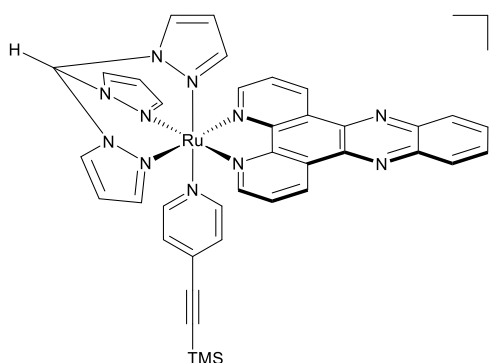
5.6.39 Attempted synthesis of $[\text{Ru}(\text{tpm})(\text{dppz})(4\text{-TMS-}\equiv\text{-Py})][\text{PF}_6]_2$ (a)



$[\text{Ru}(\text{tpm})(\text{dppz})(\text{Cl})][\text{PF}_6]_2$ (0.10 g, 0.13 mmol), 4-((trimethylsilyl)ethynyl)pyridine (0.11 g, 0.64 mmol) and AgNO_3 (0.052 g, 0.31 mmol) were dissolved in EtOH: H_2O (50 mL, 3:1), and heated to reflux under a nitrogen atmosphere for 6 hours. After cooling to room temperature, the solution was filtered over celite, and the pad washed with MeOH. The solution was concentrated under

vacuum, and the product precipitated by addition of aqueous KPF_6 . The solid was collected by vacuum filtration, and washed with H_2O and Et_2O .

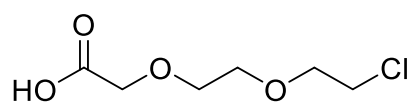
5.6.40 Attempted synthesis of $[\text{Ru}(\text{tpm})(\text{dppz})(4\text{-TMS-}\equiv\text{Py})][\text{PF}_6]_2$ (**b**)



$2+$ $[\text{Ru}(\text{tpm})(\text{dppz})(\text{Cl})][\text{PF}_6]_2$ (0.020 g, 0.026 mmol), 4-((trimethylsilyl)ethynyl)pyridine (0.23 g, 0.13 mmol) and AgNO_3 (0.010 g, 0.062 mmol) were dissolved in $\text{EtOH}:\text{H}_2\text{O}$ (1:1, 10 mL), and heated to $150\text{ }^\circ\text{C}$ under

microwave irradiation for 1 hour. After cooling to room temperature, the solution was filtered over celite, washed with MeOH, and concentrated under vacuum. The product was precipitated by addition of aqueous KPF_6 , collected by vacuum filtration, and washed with H_2O and Et_2O .

5.6.41 2-(2-(2-chloroethoxy)ethoxy)acetic acid



2-(2-(2-chloroethoxy)ethoxy)ethan-1-ol (2.60 mL, 3.00 g, 17.79 mmol) was dissolved in acetone (150 mL),

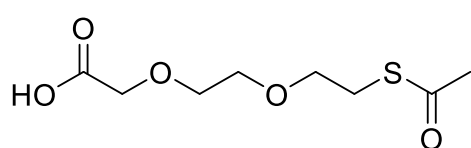
cooled to $0\text{ }^\circ\text{C}$ and then $\text{NaHCO}_{3(\text{aq})}$ (1.60 g, 15 mL), TEMPO (0.056 g, 0.36 mmol) and NaBr (0.37 g, 3.56 mmol) were added. Trichloroisocyanuric acid (8.27 g, 35.58 mmol) was added slowly over 20 minutes. The mixture was warmed to room temperature, and stirred for 18 hours. After addition of $i\text{PrOH}$ (10 mL), the mixture was filtered over celite, and the pad washed with acetone (50 mL). The solvent was removed under vacuum, and the crude oil dissolved in saturated $\text{Na}_2\text{CO}_{3(\text{aq})}$ (50 mL, ~15 g). The aqueous solution was washed with EtOAc (3 x 50 mL), acidified with 1 M HCl, and then extracted with EtOAc

(3 x 50 mL). The organic layers were dried over MgSO₄, and the solvent removed under vacuum to give 2-(2-(2-chloroethoxy)ethoxy)acetic acid (2.21 g, 68 %).

¹H NMR (400 MHz, CDCl₃): δ 4.23 (s, 2H), 3.86 – 3.78 (m, 4H), 3.78 – 3.71 (m, *J* = 6.0, 2.8 Hz, 2H), 3.67 (t, *J* = 5.7 Hz, 2H).

MS ESI-: 181 [M-H]⁻

5.6.42 2-(2-(2-(acetylthio)ethoxy)ethoxy)acetic acid



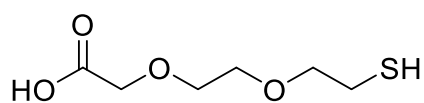
2-(2-(2-chloroethoxy)ethoxy)acetic acid (1.84 g, 10.11 mmol), thioacetic acid (0.92 mL, 1.00 g, 13.14 mmol) and K₂CO₃ (4.19 g, 30.33 mmol)

were dissolved in dry DMF (25 mL) and stirred for 18 hours at room temperature under a nitrogen atmosphere. After acidification with 4 M HCl, H₂O (100 mL) was added, and the solution extracted with EtOAc (4 x 30 mL). The combined organic layers were washed with 1 M LiCl_(aq) (5 x 40 mL), dried over MgSO₄, filtered, and the solvent removed under vacuum. The crude product was purified by flash column chromatography over silica gel, using MeOH:CHCl₃ (1:19 → 1:9) as the mobile phase. The fractions were combined, and the solvent removed under vacuum to give 2-(2-(2-(acetylthio)ethoxy)ethoxy)acetic acid (1.07 g, 47 %).

¹H NMR (400 MHz, CDCl₃): δ 4.21 (s, 2H), 3.82 – 3.71 (m, 2H), 3.71 – 3.57 (m, 4H), 3.12 (t, *J* = 6.3 Hz, 2H), 2.37 (s, 3H).

MS ESI+: 223 [M+H]⁺, 245 [M+Na]⁺

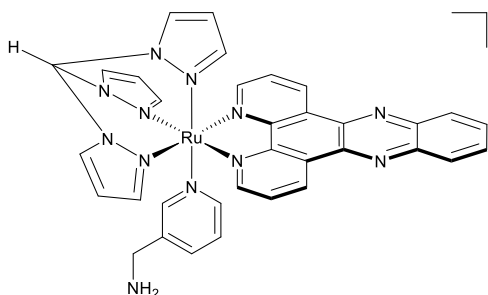
5.6.43 2-(2-(2-mercaptoethoxy)ethoxy)acetic acid



2-(2-(2-(acetylthio)ethoxy)ethoxy)acetic acid (1.34 g, 6.02 mmol) was dissolved in MeOH (15 mL). After

addition of 2 M NaOH_(aq) (15 mL), the mixture was stirred at room temperature for 1 hour. The mixture was neutralised with 1 M HCl, and extracted with EtOAc (3 x 10 mL). The organic layers were combined, dried over MgSO₄, filtered, and the solvent removed under vacuum. The crude oil was used without further purification.

5.6.44 [Ru(tpm)(dppz)(3-NH₂MePy)][PF₆]₂



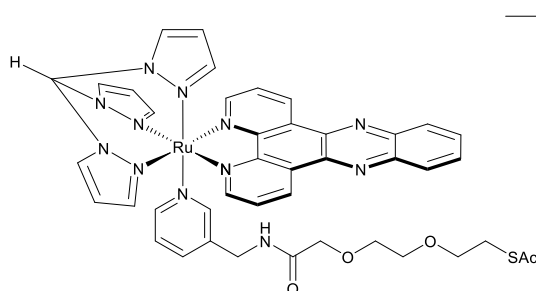
[Ru(tpm)(dppz)Cl][PF₆] (0.30 g, 0.39 mmol), 3-picoylamine (0.40 mL, 0.42 g, 3.87 mmol) and AgNO₃ (0.16 g, 0.93 mmol) were heated to reflux in EtOH:H₂O (50 mL, 3:1)

under a nitrogen atmosphere for 6 hours. After cooling to room temperature, the solution was filtered over celite, and the pad washed with MeOH. The solution was concentrated under vacuum, and precipitated with aqueous KPF₆. After collection by vacuum filtration, the precipitate was purified by flash column chromatography over silica gel using MeCN:H₂O:KNO₃(sat. aq.) (95:4:1 → 90:8:2) as the mobile phase. The fractions were combined, and the solvent removed under vacuum. The solid was dissolved in H₂O, and precipitated by addition of aqueous KPF₆. After collection and conversion to the chloride salt, the product was further purified by charge separation chromatography over SP-Sephadex with elution at 0.3 M NaCl solution. After addition of aqueous KPF₆, the product was extracted with DCM, and the solvent removed under vacuum to give [Ru(tpm)(dppz)(3-NH₂MePy)][PF₆]₂ (0.079 g, 21 %).

$^1\text{H NMR}$ (400 MHz, CD_3CN): δ 9.82 (dd, $J = 8.2, 1.2$ Hz, 2H), 9.18 (s, 1H), 9.11 (dd, $J = 5.4, 1.2$ Hz, 2H), 8.64 (d, $J = 2.9$ Hz, 2H), 8.58 (dd, $J = 6.6, 3.4$ Hz, 2H), 8.39 (d, $J = 2.7$ Hz, 1H), 8.22 (dd, $J = 6.6, 3.4$ Hz, 2H), 8.09 – 8.03 (m, 4H), 7.81 (d, $J = 8.0$ Hz, 1H), 7.50 (d, $J = 1.6$ Hz, 1H), 7.46 (d, $J = 5.6$ Hz, 1H), 7.11 (dd, $J = 7.8, 6.0$ Hz, 1H), 6.89 – 6.83 (m, 2H), 6.44 (d, $J = 2.3$ Hz, 1H), 6.24 – 6.17 (m, 1H), 3.84 (s, 2H).

MS ESI+: 352.6 $[\text{M}-2\text{PF}_6]^+$

5.6.45 Thiol terminated $[\text{Ru}(\text{tpm})(\text{dppz})(3\text{-NH}_2\text{MePy})][\text{PF}_6]_2$

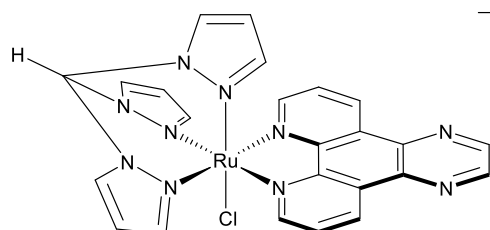


$[\text{Ru}(\text{tpm})(\text{dppz})(3\text{-NH}_2\text{MePy})][\text{PF}_6]_2$

(0.014 g, 0.013 mmol), 2-(2-(2-(acetylthio)ethoxy)ethoxy)acetic acid (0.0029 g, 0.013 mmol), EDC.HCl

(0.0040 g, 0.021 mmol) and DIPEA (0.0042 g, 0.005 mL, 0.0325 mmol) were dissolved in 5 mL of MeCN at 0°C under a nitrogen atmosphere, and stirred for 1 hour. The mixture was left to warm to room temperature, and left to stir overnight. The complex was precipitated by addition of aqueous KPF₆, and collected by centrifugation. Both the solid and crude mixture were submitted for mass spectrometry. Product was not detected, but a mass ion corresponding to the activated carboxylic acid was detected.

5.6.46 $[\text{Ru}(\text{tpm})(\text{pzp})\text{Cl}][\text{PF}_6]$



$[(\text{tpm})\text{RuCl}_3]$ (1.00 g, 2.38 mmol), pzp (0.61 g, 4.62 mmol) and LiCl (0.80 g, 18.96 mmol) were dissolved in degassed EtOH:H₂O (150 mL, 3:1), and heated to reflux for 10 minutes.

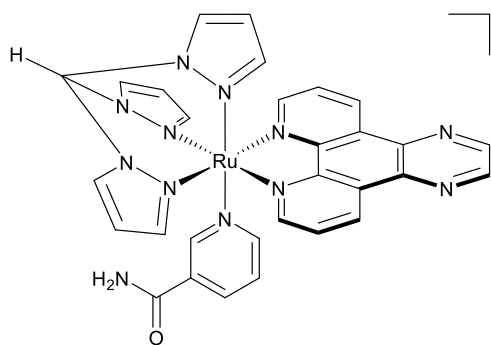
12 drops of NEt₃ were added, and the mixture refluxed for a further three hours. Upon

completion, the mixture was cooled to room temperature, and the solvent removed by rotary evaporation. The residue was dissolved in MeOH (20 mL) and filtered over celite. The complex was precipitated by the addition of aqueous NH_4PF_6 . The solid was collected by filtration, and then washed with H_2O (20 mL) and Et_2O (20 mL). The crude product was purified by column chromatography on neutral alumina using MeCN:toluene (50:50) as the mobile phase. The fractions were combined, and the solvent removed by rotary evaporation to give $[\text{Ru}(\text{tpm})(\text{pzp})\text{Cl}][\text{PF}_6]$ (1.33 g, 53 %).

^1H NMR (400 MHz, CD_3CN): δ 9.52 (dd, $J = 8.2, 1.1$ Hz, 2H), 9.23 (s, $J = 1.9$ Hz, 1H), 9.21 (dd, $J = 5.3, 1.1$ Hz, 2H), 8.96 (s, 1H), 8.48 (d, $J = 2.6$ Hz, 2H), 8.44 (d, $J = 1.7$ Hz, 2H), 8.32 (d, $J = 2.5$ Hz, 1H), 8.04 – 7.96 (m, 2H), 6.83 – 6.74 (m, 2H), 6.48 (d, $J = 1.8$ Hz, 1H), 6.20 (m, 1H).

MS ESI+: 583 $[\text{M}-\text{PF}_6]^+$, 274 $[\text{M}-\text{Cl}-\text{PF}_6]^{2+}$

5.6.47 $[\text{Ru}(\text{tpm})(\text{pzp})(\text{nic})][\text{PF}_6]_2$



$2+$ $[\text{Ru}(\text{tpm})(\text{pzp})\text{Cl}][\text{PF}_6]$ (0.10 g, 0.13 mmol), nicotinamide (0.16 g, 1.3 mmol) and AgNO_3 (0.052 g, 0.31 mmol) were dissolved in degassed EtOH: H_2O (50 mL, 3:1) and heated to reflux for 6 hours. After cooling to room

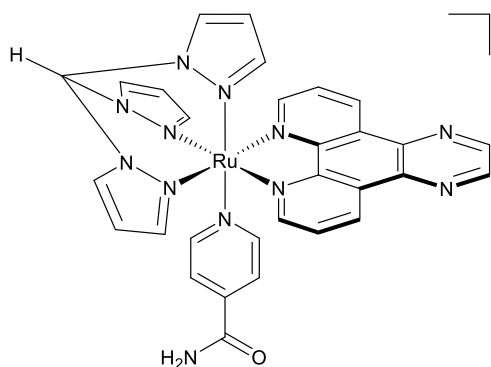
temperature, the reaction mixture was filtered over celite, and the pad was washed with MeOH. The filtrate was concentrated under vacuum, and the product precipitated by addition of aqueous KPF_6 . After collection by vacuum filtration, the precipitate was purified by flash column chromatography over silica gel using MeCN: H_2O : $\text{KNO}_3(\text{sat. aq.})$ (95:4:1 \rightarrow 90:8:2) as the mobile phase. The fractions were combined, and the solvent

removed under vacuum. The solid was dissolved in H₂O, and precipitated by addition of aqueous KPF₆. After collection and conversion to the chloride salt, the product was further purified by charge separation chromatography over SP-Sephadex with elution at 0.3 M NaCl solution. After addition of aqueous KPF₆, the product was extracted with DCM, and the solvent removed under vacuum to give [Ru(tpm)(pzp)(nic)][PF₆]₂ (2.62 mg, 2 %).

¹H NMR (400 MHz, CD₃CN): δ 9.70 (dd, *J* = 8.3, 1.2 Hz, 2H), 9.34 (s, 2H), 9.18 (s, 1H), 9.11 (dd, *J* = 5.4, 1.2 Hz, 2H), 8.63 (d, *J* = 2.9 Hz, 2H), 8.37 (d, *J* = 2.8 Hz, 1H), 8.10 (d, *J* = 2.0 Hz, 2H), 8.08 – 8.00 (m, 3H), 7.80 (s, 1H), 7.42 (d, *J* = 5.7 Hz, 1H), 7.07 (dd, *J* = 7.9, 5.9 Hz, 1H), 6.89 – 6.82 (m, 2H), 6.32 (d, *J* = 2.3 Hz, 1H), 6.20 – 6.14 (m, 1H).

MS ESI+: 335 [M-2PF₆]⁺

5.6.48 [Ru(tpm)(pzp)(isonic)][PF₆]₂



²⁺ [Ru(tpm)(pzp)Cl][PF₆] (0.10 g, 0.13 mmol), isonicotinamide (0.16 g, 1.3 mmol) and AgNO₃ (0.052 g, 0.31 mmol) were dissolved in degassed EtOH:H₂O (50 mL, 3:1) and heated to reflux for 6 hours. After cooling to

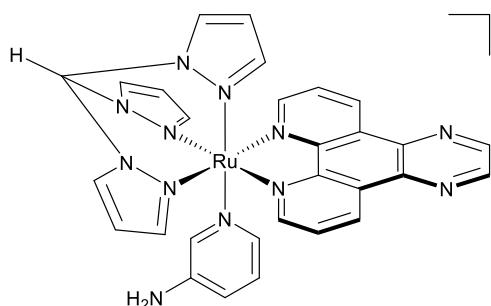
room temperature, the reaction mixture was filtered over celite, and the pad was washed with MeOH. The filtrate was concentrated under vacuum, and the product precipitated by addition of aqueous KPF₆. After collection by vacuum filtration, the precipitate was purified by flash column chromatography over silica gel using MeCN:H₂O:KNO₃(sat. aq.) (95:4:1 → 90:8:2) as the mobile phase. The fractions were combined, and the solvent

removed under vacuum. The solid was dissolved in H₂O, and precipitated by addition of aqueous KPF₆. After collection and conversion to the chloride salt, the product was further purified by charge separation chromatography over SP-Sephadex with elution at 0.3 M NaCl solution. After addition of aqueous KPF₆, the product was extracted with DCM, and the solvent removed under vacuum to give [Ru(tpm)(pzp)(isonic)][PF₆]₂ (7.17 mg, 6 %).

¹H NMR (400 MHz, CD₃CN): δ 9.69 (dd, J = 8.2, 1.1 Hz, 2H), 9.35 (s, 2H), 9.15 (dd, J = 5.3, 1.1 Hz, 2H), 9.11 (s, 1H), 8.62 (d, J = 2.8 Hz, 2H), 8.09 (d, J = 3.0 Hz, 1H), 8.05 (dd, J = 8.3, 5.4 Hz, 2H), 7.51 (d, J = 6.8 Hz, 2H), 7.31 (d, J = 6.8 Hz, 2H), 6.84 (dd, J = 5.6, 3.2 Hz, 2H), 6.54 (d, J = 2.2 Hz, 2H), 6.32 (d, J = 2.2 Hz, 1H), 6.19-6.17 (m, 1H).

MS ESI+: 335 [M-2PF₆]⁺

5.6.49 [Ru(tpm)(pzp)(3-NH₂Py)][PF₆]₂



2+ [Ru(tpm)(pzp)Cl][PF₆] (0.10 g, 0.13 mmol), 3-aminopyridine (0.12 g, 1.3 mmol) and AgNO₃ (0.052 g, 0.31 mmol) were dissolved in degassed EtOH:H₂O (50 mL, 3:1) and heated to reflux for 6 hours. After cooling to

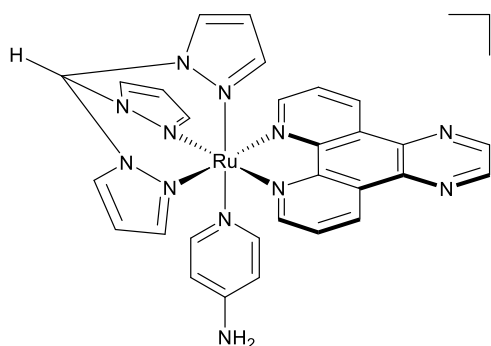
room temperature, the reaction mixture was filtered over celite, and the pad was washed with MeOH. The filtrate was concentrated under vacuum, and the product precipitated by addition of aqueous KPF₆. After collection by vacuum filtration, the precipitate was purified by flash column chromatography over silica gel using MeCN:H₂O:KNO₃(sat. aq.) (95:4:1 → 90:8:2) as the mobile phase. The fractions were combined, and the solvent removed under vacuum. The solid was dissolved in H₂O, and precipitated by addition of

aqueous KPF_6 . After collection and conversion to the chloride salt, the product was further purified by charge separation chromatography over SP-Sephadex with elution at 0.3 M NaCl solution. After addition of aqueous KPF_6 , the product was extracted with DCM, and the solvent removed under vacuum to give $[\text{Ru}(\text{tpm})(\text{pzp})(3\text{-NH}_2\text{Py})][\text{PF}_6]_2$ (9.40 mg, 7 %).

^1H NMR (400 MHz, CD_3CN): δ 9.69 (dd, $J = 8.2, 1.2$ Hz, 2H), 9.34 (s, 2H), 9.14 (d, $J = 1.2$ Hz, 1H), 9.13 (d, $J = 1.3$ Hz, 2H), 8.60 (d, $J = 2.9$ Hz, 2H), 8.35 (d, $J = 2.8$ Hz, 1H), 8.13 (d, $J = 2.1$ Hz, 2H), 8.04 (dd, $J = 8.2, 5.4$ Hz, 2H), 6.91 (dd, $J = 7.8, 1.9$ Hz, 1H), 6.86 – 6.81 (m, 2H), 6.71 – 6.66 (m, 2H), 6.58 (d, $J = 5.5$ Hz, 1H), 6.27 (d, $J = 2.2$ Hz, 1H), 6.17 – 6.13 (m, 1H), 4.19 (s, 2H).

MS ESI+: 321 $[\text{M}-2\text{PF}_6]^{2+}$

5.6.50 $[\text{Ru}(\text{tpm})(\text{pzp})(4\text{-NH}_2\text{Py})][\text{PF}_6]_2$



$[\text{Ru}(\text{tpm})(\text{pzp})\text{Cl}][\text{PF}_6]$ (0.10 g, 0.13 mmol), 4-aminopyridine (0.12 g, 1.3 mmol) and AgNO_3 (0.052 g, 0.31 mmol) were dissolved in degassed EtOH:H₂O (50 mL, 3:1) and heated to reflux for 6 hours. After cooling to

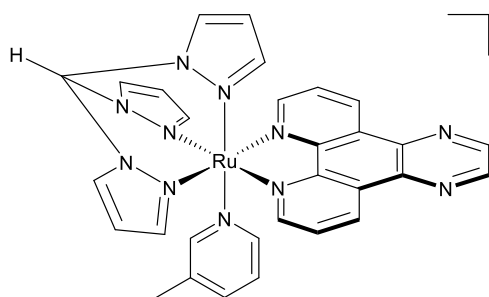
room temperature, the reaction mixture was filtered over celite, and the pad was washed with MeOH. The filtrate was concentrated under vacuum, and the product precipitated by addition of aqueous KPF_6 . After collection by vacuum filtration, the precipitate was purified by flash column chromatography over silica gel using MeCN:H₂O: KNO_3 (sat. aq.) (95:4:1 \rightarrow 90:8:2) as the mobile phase. The fractions were combined, and the solvent removed under vacuum. The solid was dissolved in H₂O, and precipitated by addition of

aqueous KPF_6 . After collection and conversion to the chloride salt, the product was further purified by charge separation chromatography over SP-Sephadex with elution at 0.3 M NaCl solution. After addition of aqueous KPF_6 , the product was extracted with DCM, and the solvent removed under vacuum to give $[\text{Ru}(\text{tpm})(\text{pzp})(4\text{-NH}_2\text{Py})][\text{PF}_6]_2$ (4.98 mg, 4 %).

^1H NMR (400 MHz, CD_3CN): δ 9.66 (dd, $J = 8.2, 1.2$ Hz, 2H), 9.33 (d, $J = 4.8$ Hz, 2H), 9.14 (dd, $J = 5.3, 1.2$ Hz, 2H), 9.11 (s, 1H), 8.59 (d, $J = 2.9$ Hz, 2H), 8.35 (d, $J = 2.9$ Hz, 1H), 8.14 (d, $J = 2.1$ Hz, 2H), 8.02 (dd, $J = 8.2, 5.4$ Hz, 2H), 6.85 – 6.80 (m, 2H), 6.69 (d, $J = 7.1$ Hz, 2H), 6.30 (d, $J = 2.2$ Hz, 1H), 6.23 – 6.18 (m, 2H), 6.18 – 6.13 (m, 1H), 5.19 (s, 2H).

MS ESI+: 321 $[\text{M}-2\text{PF}_6]^{2+}$

5.6.51 $[\text{Ru}(\text{tpm})(\text{pzp})(3\text{-pic})][\text{PF}_6]_2$



$[\text{Ru}(\text{tpm})(\text{pzp})\text{Cl}][\text{PF}_6]$ (0.10 g, 0.13 mmol), 3-picoline (0.11 mL, 0.11 g, 1.3 mmol) and AgNO_3 (0.052 g, 0.31 mmol) were dissolved in degassed EtOH:H₂O (50 mL, 3:1) and

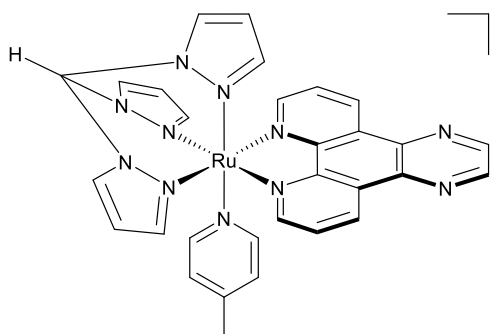
heated to reflux for 6 hours. After cooling to room temperature, the reaction mixture was filtered over celite, and the pad was washed with MeOH. The filtrate was concentrated under vacuum, and the product precipitated by addition of aqueous KPF_6 . After collection by vacuum filtration, the precipitate was purified by flash column chromatography over silica gel using MeCN:H₂O: $\text{KNO}_3(\text{sat. aq.})$ (95:4:1 \rightarrow 90:8:2) as the mobile phase. The fractions were combined, and the solvent removed under vacuum. The solid was dissolved in H₂O, and precipitated by addition of aqueous KPF_6 . After collection and

conversion to the chloride salt, the product was further purified by charge separation chromatography over SP-Sephadex with elution at 0.3 M NaCl solution. After addition of aqueous KPF_6 , the product was extracted with DCM, and the solvent removed under vacuum to give $[\text{Ru}(\text{tpm})(\text{pzp})(3\text{-pic})][\text{PF}_6]_2$ (10.66 mg, 9 %).

^1H NMR (400 MHz, CD_3CN): δ 9.69 (dd, $J = 8.3, 1.2$ Hz, 2H), 9.34 (s, 2H), 9.13 (s, 2H), 9.12 (d, $J = 1.1$ Hz, 1H), 8.61 (d, $J = 2.9$ Hz, 2H), 8.36 (d, $J = 2.8$ Hz, 1H), 8.07 (d, $J = 2.1$ Hz, 2H), 8.04 (dd, $J = 8.3, 5.4$ Hz, 2H), 7.54 (d, $J = 7.8$ Hz, 1H), 7.25 (s, 1H), 7.11 (d, $J = 5.7$ Hz, 1H), 6.92 – 6.80 (m, 3H), 6.28 (d, $J = 2.2$ Hz, 1H), 6.19 – 6.13 (m, 1H), 2.19 (s, 3H).

MS ESI+: 320.6 $[\text{M}-2\text{PF}_6]^{2+}$

5.6.52 $[\text{Ru}(\text{tpm})(\text{pzp})(4\text{-pic})][\text{PF}_6]_2$



$[\text{Ru}(\text{tpm})(\text{pzp})\text{Cl}][\text{PF}_6]$ (0.10 g, 0.13 mmol), 4-picoline (0.11 mL, 0.11 g, 1.3 mmol) and AgNO_3 (0.052 g, 0.31 mmol) were dissolved in degassed $\text{EtOH}:\text{H}_2\text{O}$ (50 mL, 3:1) and heated to reflux for 6 hours. After cooling to

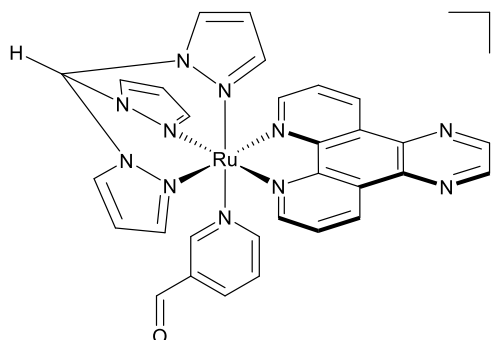
room temperature, the reaction mixture was filtered over celite, and the pad was washed with MeOH. The filtrate was concentrated under vacuum, and the product precipitated by addition of aqueous KPF_6 . After collection by vacuum filtration, the precipitate was purified by flash column chromatography over silica gel using $\text{MeCN}:\text{H}_2\text{O}:\text{KNO}_3(\text{sat. aq.})$ (95:4:1 \rightarrow 90:8:2) as the mobile phase. The fractions were combined, and the solvent removed under vacuum. The solid was dissolved in H_2O , and precipitated by addition of aqueous KPF_6 . After collection and conversion to the chloride salt, the product was

further purified by charge separation chromatography over SP-Sephadex with elution at 0.3 M NaCl solution. After addition of aqueous KPF₆, the product was extracted with DCM, and the solvent removed under vacuum to give [Ru(tpm)(pzp)(4-pic)][PF₆]₂ (13.36 mg, 11 %).

¹H NMR (400 MHz, CD₃CN): δ 9.69 (dd, J = 8.3, 1.2 Hz, 2H), 9.34 (s, 2H), 9.13 (s, 2H), 9.12 (d, J = 1.1 Hz, 1H), 8.61 (d, J = 2.9 Hz, 2H), 8.36 (d, J = 2.8 Hz, 1H), 8.07 (d, J = 2.1 Hz, 2H), 8.04 (dd, J = 8.3, 5.4 Hz, 2H), 7.54 (d, J = 7.8 Hz, 1H), 7.25 (s, 1H), 7.11 (d, J = 5.7 Hz, 1H), 6.92 – 6.80 (m, 3H), 6.28 (d, J = 2.2 Hz, 1H), 6.19 – 6.13 (m, 1H), 2.19 (s, 3H).

MS ESI+: 320.6 [M-2PF₆]²⁺

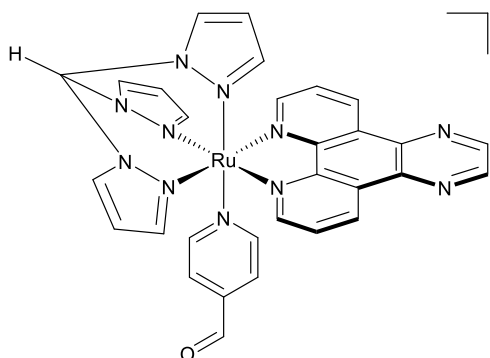
5.6.53 Attempted synthesis of [Ru(tpm)(pzp)(3-CHOPy)][PF₆]₂



²⁺ [Ru(tpm)(pzp)Cl][PF₆] (0.10 g, 0.13 mmol), 3-pyridinecarboxaldehyde (1 mL) and AgNO₃ (0.052 g, 0.31 mmol) were dissolved in degassed EtOH:H₂O (50 mL, 3:1) and heated to reflux for 6 hours. After cooling to

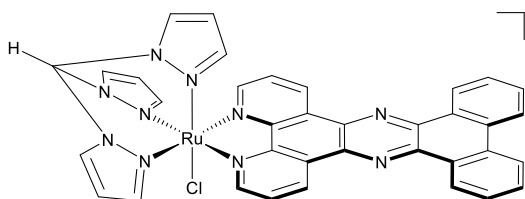
room temperature, the reaction mixture was filtered over celite, and the pad was washed with MeOH. The filtrate was concentrated under vacuum, and the complex precipitated by addition of aqueous KPF₆. After collection by vacuum filtration, the precipitate was purified by flash column chromatography over silica gel using MeCN:H₂O:KNO₃(sat. aq.) (95:4:1 → 90:8:2) as the mobile phase.

5.6.54 Attempted synthesis of $[\text{Ru}(\text{tpm})(\text{pzp})(4\text{-CHOPy})][\text{PF}_6]_2$



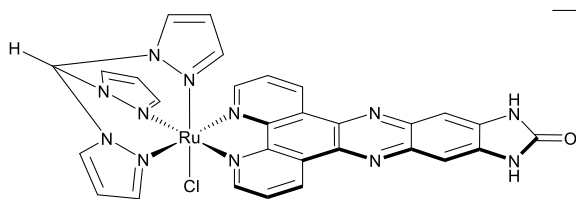
$[\text{Ru}(\text{tpm})(\text{pzp})\text{Cl}][\text{PF}_6]$ (0.10 g, 0.13 mmol), 4-pyridinecarboxaldehyde (1 mL) and AgNO_3 (0.052 g, 0.31 mmol) were dissolved in degassed $\text{EtOH}:\text{H}_2\text{O}$ (50 mL, 3:1) and heated to reflux for 6 hours. After cooling to room temperature, the reaction mixture was filtered over celite, and the pad was washed with MeOH. The filtrate was concentrated under vacuum, and the complex precipitated by addition of aqueous KPF_6 . After collection by vacuum filtration, the precipitate was purified by flash column chromatography over silica gel using $\text{MeCN}:\text{H}_2\text{O}:\text{KNO}_3(\text{sat. aq.})$ (95:4:1 \rightarrow 90:8:2) as the mobile phase.

5.6.55 Attempted synthesis of $[\text{Ru}(\text{tpm})(\text{taptp})(\text{Cl})][\text{PF}_6]$



$[(\text{tpm})\text{RuCl}_3]$ (0.50 g, 1.19 mmol), taptp (0.50 g, 1.30 mmol) and LiCl (0.41 g, 9.52 mmol) were dissolved in degassed $\text{EtOH}:\text{H}_2\text{O}$ (100 mL, 3:1), and heated to reflux for 10 minutes. 5 drops of NEt_3 were added, and the mixture refluxed for a further three hours. Upon completion, the mixture was cooled to room temperature, and the solvent removed by rotary evaporation. The residue was dissolved in MeOH (20 mL) and filtered over celite. The complex was precipitated by the addition of aqueous NH_4PF_6 . The solid was collected by filtration, and then washed with H_2O (20 mL) and Et_2O (20 mL).

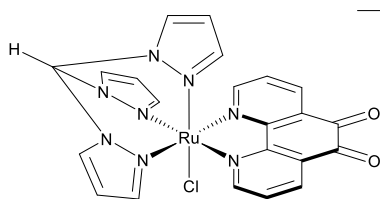
5.6.56 Attempted synthesis of $[\text{Ru}(\text{tpm})(\text{dppz-izdo})(\text{Cl})][\text{PF}_6]$



$[\text{tpm}]\text{RuCl}_3$ (0.20 g, 0.42 mmol),
dppz-izdo (0.16 g, 0.46 mmol) and LiCl
(0.13 g, 3.15 mmol) were dissolved in

degassed EtOH:H₂O (50 mL, 3:1), and heated to reflux for 10 minutes. 5 drops of NEt₃ were added, and the mixture refluxed for a further three hours. Upon completion, the mixture was cooled to room temperature, and the solvent removed by rotary evaporation. The residue was dissolved in MeOH (20 mL) and filtered over celite. The complex was precipitated by the addition of aqueous NH₄PF₆. The solid was collected by filtration, and then washed with H₂O (20 mL) and Et₂O (20 mL).

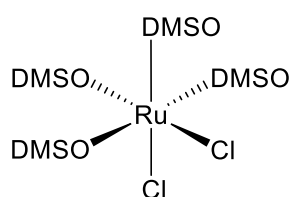
5.6.57 Attempted synthesis of $[\text{Ru}(\text{tpm})(\text{dpq})(\text{Cl})][\text{PF}_6]$



$[\text{tpm}]\text{RuCl}_3$ (0.50 g, 1.19 mmol), dpq (0.27 g, 1.30
mmol) and LiCl (0.41 g, 9.52 mmol) were dissolved in
degassed EtOH:H₂O (100 mL, 3:1), and heated to reflux

for 10 minutes. 5 drops of NEt₃ were added, and the mixture refluxed for a further three hours. Upon completion, the mixture was cooled to room temperature, and the solvent removed by rotary evaporation. The residue was dissolved in MeOH (20 mL) and filtered over celite. The complex was precipitated by the addition of aqueous NH₄PF₆. The solid was collected by filtration, and then washed with H₂O (20 mL) and Et₂O (20 mL).

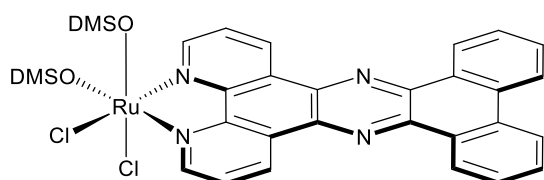
5.6.58 $[\text{Ru}(\text{DMSO})_4\text{Cl}_2]$



RuCl₃ (25.00 g, 261.47 mmol) was dissolved in ⁱPrOH (200 mL) under a nitrogen atmosphere, and DMSO (70 mL) was added dropwise, after which the mixture was heated to 85 °C for 18

hours. The solution was cooled to room temperature, and the yellow solid was collected by vacuum filtration, washed with copious acetone and Et₂O, and dried under vacuum to give [Ru(DMSO)₄Cl₂] (30.39 g, 66 %).

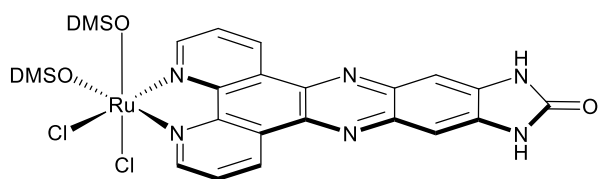
5.6.59 Attempted synthesis of [Ru(taptp)(DMSO)₂Cl₂]



[Ru(DMSO)₄Cl₂] (0.20 g, 0.41 mmol) and taptp (0.16 g, 0.41 mmol) were suspended in dry toluene (50 mL) and heated to reflux for

8 hours under a nitrogen atmosphere. The solid was collected by hot filtration, washed with copious toluene and Et₂O, and dried under vacuum.

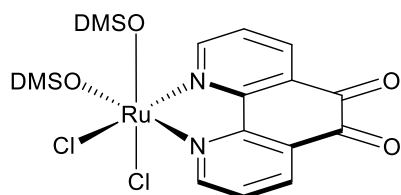
5.6.60 Attempted synthesis of [Ru(dppz-izdo)(DMSO)₂Cl₂]



[Ru(DMSO)₄Cl₂] (0.20 g, 0.41 mmol) and dppz-izdo (0.14 g, 0.41 mmol) were suspended in dry toluene (50 mL) and

heated to reflux for 8 hours under a nitrogen atmosphere. The solid was collected by hot filtration, washed with copious toluene and Et₂O, and dried under vacuum.

5.6.61 [Ru(dpq)(DMSO)₂Cl₂]

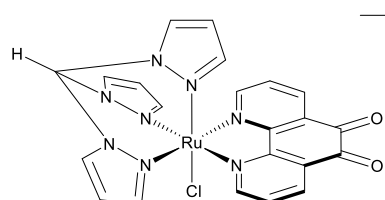


[Ru(DMSO)₄Cl₂] (1.00 g, 2.06 mmol) and dpq (0.43 g, 0.2.06 mmol) were suspended in dry toluene (125 mL) and heated to reflux for 8 hours under a nitrogen

atmosphere. The solid was collected by hot filtration, washed with copious toluene and Et₂O, and dried under vacuum to give [Ru(dpq)(DMSO)₂Cl₂] (0.92 g, 83 %).

^1H NMR (400 MHz, $\text{d}_6\text{-DMSO}$): δ 9.84 (d, $J = 5.1$ Hz, 2H), 9.71 (d, $J = 4.8$ Hz, 2H), 8.64 (d, $J = 7.0$ Hz, 2H), 8.49 (d, $J = 7.3$ Hz, 2H), 8.00 (dd, $J = 7.7, 5.7$ Hz, 2H), 7.83 (dd, $J = 7.7, 5.9$ Hz, 2H), 2.89 (s, 6H).

5.6.62 $[\text{Ru}(\text{tpm})(\text{dpq})(\text{Cl})][\text{PF}_6]$

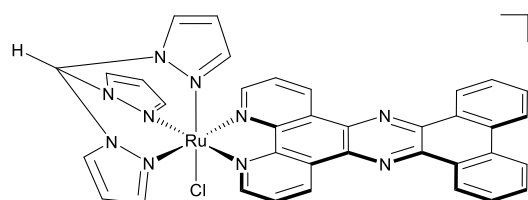


$[\text{Ru}(\text{dpq})(\text{DMSO})_2\text{Cl}_2]$ (0.10 g, 0.19 mmol) and tpm (0.040, 0.186 mmol) were dissolved in dry DMF (10 mL) and heated to reflux under a nitrogen atmosphere for 4 hours. After cooling to room temperature, the product was precipitated by addition of aqueous KPF_6 . The solid was collected by vacuum filtration, washed with copious H_2O and Et_2O , and dried under vacuum to give $[\text{Ru}(\text{tpm})(\text{dpq})(\text{Cl})][\text{PF}_6]$, which was used without further purification. (0.021 g, 16 %).

^1H NMR (400 MHz, CD_3CN): δ 8.99 (d, $J = 4.5$ Hz, 2H), 8.89 (s, 1H), 8.52 (dd, $J = 7.9, 1.2$ Hz, 2H), 8.45 (d, $J = 2.9$ Hz, 2H), 8.36 (d, $J = 1.9$ Hz, 2H), 8.32 (d, $J = 2.9$ Hz, 1H), 7.72 (dd, $J = 7.9, 5.7$ Hz, 2H), 6.73 (t, $J = 2.5$ Hz, 2H), 6.71 (d, $J = 2.1$ Hz, 1H), 6.31 (m, 1H).

MS ESI+: 561 $[\text{M-PF}_6]^+$

5.6.63 $[\text{Ru}(\text{tpm})(\text{taptp})(\text{Cl})][\text{PF}_6]$

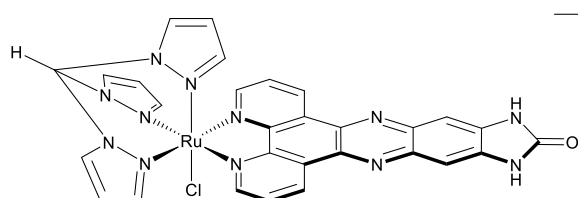


$[\text{Ru}(\text{tpm})(\text{dpq})(\text{Cl})][\text{PF}_6]$ (0.023 g, 0.033 mmol) was dissolved in boiling MeCN (25 mL), and 5,6-diaminophenanthrene (0.0068 g, 0.033 mmol) was suspended in boiling EtOH (25 mL). After dissolution, the solutions were mixed, and refluxed for further 4 hours. The mixture was filtered over celite, and the pad washed with MeOH. The mixture was concentrated under vacuum, and the

product precipitated by addition of aqueous KPF_6 . The solid was collected by vacuum filtration, washed with H_2O and Et_2O , and dried under vacuum.

MS ESI+: 733 $[\text{M-PF}_6]^+$

5.6.64 $[\text{Ru}(\text{tpm})(\text{dppz-izdo})(\text{Cl})][\text{PF}_6]$



$\square +$ $[\text{Ru}(\text{tpm})(\text{dpq})(\text{Cl})][\text{PF}_6]$ (0.023 g, 0.033 mmol) was dissolved in boiling MeCN (25 mL), and 5,6-

diaminobenzimidazol-2-one (0.0054 g, 0.033 mmol) was suspended in boiling EtOH (25 mL). After dissolution, the solutions were mixed, and refluxed for further 4 hours. The mixture was filtered over celite, and the pad washed with MeOH. The mixture was concentrated under vacuum, and the product precipitated by addition of aqueous KPF_6 . The solid was collected by vacuum filtration, washed with H_2O and Et_2O , and dried under vacuum.

MS ESI+: 689 $[\text{M-PF}_6]^+$

References

- 1 Bruker, *SADABS*, Bruker AXS Inc., Madison, Wisconsin, USA, 2016.
- 2 L. Krause, R. Herbst-Irmer, G. M. Sheldrick and D. Stalke, *J. Appl. Crystallogr.*, 2015, **48**, 3–10.
- 3 G. M. Sheldrick, *Acta Crystallogr. Sect. A Found. Adv.*, 2015, **71**, 3–8.
- 4 G. M. Sheldrick, *Acta Crystallogr. Sect. C Struct. Chem.*, 2015, **71**, 3–8.
- 5 O. V. Dolomanov, L. J. Bourhis, R. J. Gildea, J. A. K. Howard and H. Puschmann, *J. Appl. Crystallogr.*, 2009, **42**, 339–341.
- 6 M. J. Frisch, G. W. Trucks, H. B. Schlegel, G. E. Scuseria, M. A. Robb, J. R. Cheeseman, G. Scalmani, V. Barone, B. Mennucci, G. A. Petersson, H. Nakatsuji, M. Caricato, X. Li, H. P. Hratchian, A. F. Izmaylov, J. Bloino, G. Zheng, J. L. Sonnenberg, M. Hada, M. Ehara, K. Toyota, R. Fukuda, J. Hasegawa, M. Ishida, T. Nakajima, Y. Honda, O. Kitao, H. Nakai, T. Vreven, J. A. Montgomery Jr., J. E. Peralta, F. Ogliaro, M. Bearpark, J. J. Heyd, E. Brothers, K. N. Kudin, V. N. Staroverov, R. Kobayashi, J. Normand, K. Raghavachari, A. Rendell, J. C. Burant, S. S. Iyengar, J. Tomasi, M. Cossi, N. Rega, J. M. Millam, M. Klene, J. E. Knox, J. B. Cro, J. Jaramillo, R. Gomperts, R. E. Stratmann, O. Yazyev, A. J. Austin, R. Cammi, C. Pomelli, J. W. Ochterski, R. L. Martin, K. Morokuma, V. G. Zakrzewski, G. A. Voth, P. Salvador, J. J. Dannenberg, S. Dapprich, A. D. Daniels, O. Farkas, J. B. Foresman, J. V. Ortiz, J. Cioslowski and D. J. Fox, 2009.
- 7 A. D. Becke, *J. Chem. Phys.*, 1993, **98**, 5648–5652.
- 8 S. Grimme, S. Ehrlich and L. Goerigk, *J. Comput. Chem.*, 2011, **32**, 1456–1465.

- 9 M. Dolg, *Modern Methods and Algorithms of Quantum Chemistry*, Ju'lich Research Center, Ju'lich, Germany, 2000.
- 10 M. Dolg, U. Wedig, H. Stoll and H. Preuss, *J. Chem. Phys.*, 1987, **86**, 866–872.
- 11 R. Krishnan, J. S. Binkley, R. Seeger and J. A. Pople, *J. Chem. Phys.*, 1980, **72**, 650–654.
- 12 A. D. McLean and G. S. Chandler, *J. Chem. Phys.*, 1980, **72**, 5639–5648.
- 13 J. Tomasi, B. Mennucci and R. Cammi, *Chem. Rev.*, 2005, **105**, 2999–3094.
- 14 M. Cossi, N. Rega, G. Scalmani and V. Barone, *J. Comput. Chem.*, 2003, **24**, 669–681.
- 15 M. Hogan, N. Dattagupta and D. M. Crothers, *Proc. Natl. Acad. Sci.*, 1978, **75**, 195–199.
- 16 J. B. Chaires, N. Dattagupta and D. M. Crothers, *Biochemistry*, 1982, **21**, 3933–3940.
- 17 A. Leonidova, V. Pierroz, L. A. Adams, N. Barlow, S. Ferrari, B. Graham and G. Gasser, *ACS Med. Chem. Lett.*, 2014, **5**, 809–814.
- 18 G. A. Molander, S. L. J. Trice and S. D. Dreher, *J. Am. Chem. Soc.*, 2010, **132**, 17701–3.

Chapter Six

6 Appendix

6.1 X-ray Crystallographic Data

Table 6.1 Crystal Data for [Ru(tpm)(dppz)(3-NH₂MePy)][PF₆]₂

Identification code	IAJ673k_0m
Empirical formula	C ₃₉ H _{39.5} F ₁₂ N _{12.5} OP ₂ Ru
Formula weight	1090.34
Temperature/K	100
Crystal system	triclinic
Space group	P-1
a/Å	15.858(4)
b/Å	16.266(4)
c/Å	20.557(5)
α/°	74.198(10)
β/°	68.618(12)
γ/°	65.702(12)
Volume/Å ³	4453.5(19)
Z	4
ρ _{calc} /cm ³	1.626
μ/mm ⁻¹	0.524
F(000)	2204.0
Crystal size/mm ³	0.05 × 0.04 × 0.04
Radiation	MoKα (λ = 0.71073)
2θ range for data collection/°	2.15 to 52.982
Index ranges	-19 ≤ h ≤ 19, -20 ≤ k ≤ 20, -23 ≤ l ≤ 25
Reflections collected	59081
Independent reflections	18134 [R _{int} = 0.3722, R _{sigma} = 0.5589]
Data/restraints/parameters	18134/1239/1217
Goodness-of-fit on F ²	1.008

Final R indexes [$I \geq 2\sigma(I)$]	$R_1 = 0.1430$, $wR_2 = 0.2705$
Final R indexes [all data]	$R_1 = 0.3971$, $wR_2 = 0.3798$
Largest diff. peak/hole / $e \text{ \AA}^{-3}$	1.35/-0.96

6.2 Example extinction coefficient calculation

Each wavelength from 800-200 nm →

	A	B	C	D	E	F	G
1		Conc	799.98	799.01	798.0396	797.0689	795.959
2	0 uL	0	0.000448	6.43E-05	-0.00023	0.000539	6.18E-05
3	2 uL	9.99028E-07	-0.00081	-0.00016	-0.00079	-0.00043	-0.00094
4	4 uL	1.99606E-06	0.004728	0.004544	0.004138	0.005094	0.004845
5	6 uL	2.99111E-06	0.004399	0.004574	0.00302	0.002496	0.001331
6	8 uL	3.98417E-06	1.39E-05	0.000457	0.000258	7.08E-05	-0.00025
7	10 uL	4.97526E-06	0.000986	0.000649	0.000483	0.001235	0.000573
8	12 uL	5.96438E-06	8.08E-05	0.000522	3.55E-05	0.000894	0.000366
9	14 uL	6.95153E-06	0.006476	0.006853	0.006746	0.007559	0.007082
10	16 uL	7.93672E-06	0.007224	0.007434	0.007036	0.007626	0.006782
11	18 uL	8.91997E-06	0.00743	0.007369	0.007135	0.007689	0.007202
12	20 uL	9.90126E-06	0.008163	0.008218	0.007209	0.008012	0.007661
13							
14			729.9454	750.5465	680.4021	764.9315	685.6533

Absorbance at each wavelength for each concentration

Use function “=SLOPE(Y_values,X_values)” to calculate extinction coefficient at for each wavelength.